UNIVERSITÀ DEGLI STUDI DI PADOVA
Sede amministrativa: UNIVERSITÀ DEGLI STUDI DI PADOVA
DIPARTIMENTO DI ASTRONOMIA

Dottorato di ricerca in Astronomia
Ciclo XIX

Cluster and field star formation in the Magellanic Clouds

Coordinatore: Ch.mo Prof. Giampaolo Piotto
Supervisori: Dott. Antonella Vallenari
Ch.mo Prof. Cesare Chiosi

Dottorando: Emanuela Chiosi

2 febbraio 2009

RIASSUNTO DELLA TESI

Il lavoro presentato nella tesi ha lo scopo di migliorare la comprensione del complesso fenomeno della formazione stellare. Il laboratorio piu' adatto a questo proposito e' quello delle Nubi di Magellano la cui prossimita' alla Galassia permette di risolvere le singole stelle. La prima parte della ricerca ha determinato l'eta' di un campione di 462 ammassi ed associazioni della Piccola Nube di Magellano (SMC) attraverso il metodo del fit delle isocrone nei diagrammi colore-magnitudine. A questi ammassi e' stata inoltre attribuita una stima dell'arrossamento. I dati utilizzati sono stati presi al telescopio 2.2m ESO per una regione di 0.3 sq. deg. intorno a NGC 269 ed inoltre si e' fatto uso dei dati OGLE per una regione di 2.4 sq. deg. che ricopre l'intera barra centrale della SMC. Il cospicuo numero di ammassi ha permesso di determinare il tasso di formazione degli stessi con una buona statistica ma anche di studiarne la correlazione con l'ambiente, in particolare con le regioni di HI e le relative mappe di dispersione di velocita' e con le nubi molecolari di CO. Si sono determinate le rate di formazione stellare di campo nelle aree delle due super-shell 37A e 304A. Gli ammassi risultano essersi formati nel corso dell' ultimo miliardo di anni in maniera continua ma con picchi di formazione a 8, 90, 700 Myr. Le due supershell 37A e 304A rilevate nella distribuzione di HI sono chiaramente visibili nella distribuzione in eta' degli ammassi: un picco nella rate di formazione di ammassi ha avuto luogo dall'epoca di formazione delle shell. Si trova una stretta correlazione fra gli ammassi giovani e le aree di maggiore intensita' di HI. Il grado di correlazione decresce con l'eta' degli ammassi. Ammassi piu' vecchi di 300 Myr sono situati al di fuori dei picchi di HI. Ammassi ed associazioni piu' giovani di 10 Myr sono in relazione con le nubi di CO situate nella regione sud-ovest del disco della SMC. Si deriva una correlazione positiva fra le posizioni degli ammassi giovani ed il campo delle dispersioni di velocita' del gas atomico solo per la shell 304A, fatto che suggerisce che la collisione fra nubi probabilmente non e' il meccanismo principale di formazione di ammassi. Si trovano inoltre prove di episodi di formazione stellare dovuti all'interazione fra SMC ed LMC sia nella distribuzione degli ammassi che in quella del campo.
Successivamente si sono analizzati piu' approfonditamente tre ammassi : NGC 265, K 29 e NGC 290. Per questi ammassi i dati, provenienti dall'archivio dell'ESO, sono stati presi con la WFC di HST. La migliore qualita' dei dati ha permesso di determinare i parametri fisici dei tre ammassi. Inoltre per gli stessi ammassi si sono determinate l'eta', la metallicita', l'arrossamento, i coefficienti della funzione iniziale di massa (IMF) con il metodo del chi-quadro. Quest'ultimo prevede che al variare dei parametri nelle funzioni di luminosita' ottenute dalla sintesi di popolazione stellare si calcoli la soluzione che minimizza il chi-quadro fra la funzione di luminosita' teorica e sperimentale. Anche in questo caso si sono determinate le rate di formazione stellare dei campi associati ai tre ammassi. Per gli ammassi troviamo le seguenti eta' e metallicita': NGC 265 ha $log(Age) = 8.5 \pm 0.3$ e metallicita'

$Z = 0.004 \pm 0.003$, K 29 ha $log(Age) = 8.2 \pm 0.2$ e metallicita' $Z = 0.003 \pm 0.002$, NGC 290 ha $log(Age) = 7.8 \pm 0.5$ e metallicita' $Z = 0.003 \pm 0.002$. La funzione iniziale di massa e' in accordo col modello standard di Kroupa. La rate di formazione stellare della popolazione di campo presenta periodi di maggiore attivita' a 300-400 Myr, 3-4 Gyr ed infine a 6 Gyr. Tuttavia e' relativamente quiescente ad eta' maggiori di 6 Gyr. Questo risultato suggerisce che ad eta' piu' vecchie, l'interazione mareale fra le Nubi di Magellano e la Via Lattea non e' stata in grado di provocare episodi significativi di formazione stellare.
L'ultima parte della tesi analizza una regione di intensa attivita' di formazione stellare nella Grande Nube di Magellano (LMC) denominata N11. Anche in questo caso i dati sono stati presi da archivio. L'analisi dei diagrammi colore-magnitudine ha subito presentato una interessante caratteristica: la presenza di una doppia sequenza principale alle basse magnitudini che e' stata giustificata come costituita da stelle di pre-sequenza. Viene anche discussa l'ipotesi di un arrossamento differenziale. In questa regione sono presenti associazioni ed un ammasso giovane: di questi oggetti viene studiata la presenza di sottostrutture con il metodo dei grafi. Infine si sono confrontati i picchi di formazione stellare con i modelli dinamici di interazione fra la Galassia e le Nubi di Magellano presenti in letteratura trovando che i due, per esempio, sono correlati intorno a 200 Myr(passaggio perigalattico fra le due Nubi di Magellano) e a 1-2 Gyr(passaggio perigalattico con la Via Lattea).

SUMMARY OF THE THESIS

The work presented in the thesis is intended to improve the understanding of the complex star formation phenomenon. Magellanic Clouds represent the ideal laboratory for they proximity to the Galaxy allows us to resolve single stars. The first part of the research determined the age of a sample of 462 clusters and associations in the Small Magellanic cloud (SMC). Adopted method was that of isochrone fitting in the colour-magnitude diagram. An extimate of the reddening has also been given for all these clusters. Data were taken at the telescope 2.2m ESO for a region of 0.3 sq.deg. around NGC 269. Moreover it has been made use of OGLE data for an area of 2.4 sq.deg. that covers the entire SMC bar. The number of considered clusters not only allows for a good statistic in the determination of the cluster star formation rate but also allows to study the correlation with the environment, expecially with HI regions and with the relative velocity dispersion maps and with CO clouds. Finally the field star formation rate were drawn for the areas of the two super-shells 37A and 304A. The cluster age distribution supports the idea that clusters formed in the last 1 Gyr of the SMC history in a roughly continous way with periods of enhancements. The two super-shells 37A and 304A detected in the HI distribution are clearly visible in the age distribution of the clusters: an enhancement in the cluster formation rate has taken place from the epoch of the shell formation. A tight correlation between young clusters and the HI intensity is found. The degree of correlation is decreasing with the age of teh clusters. Clusters older than 300 Myr are located away from the HI peaks. Clusters and associations younger than 10 Myr are related to the CO clouds in the SW region of teh SMC disk. A positive correlation between the location of the young clusters and the velocity dispersion field of the atomic gas is derived only for the shell 304A, suggesting that the cloud-cloud collision is probably not the most important mechanism of cluster formation. Evidence of gravitational triggered episode due to the most recent close interaction between SMC and LMC is found both in the cluster and field star distribution.
Subsequently three clusters in particular were deeper analyzed: NGC 265, K 29, NGC 290. For these clusters data were drawn from the ESO archive. Images were taken with the ACS/WFC of HST. The better quality of the data allows the determination of cluster physical parameters. Moreover for the same clusters were determined the age, the metallicity, the reddening, the slope of the initial mass function (IMF) with the chi-square method. This method varies the parameter of the luminosity functions obtained from stellar population synthesis and finds the solution that best minimize the chi-square between theoretical and experimental luminosity functions. In this case also field star formation rates were drawn from the associated fields. For the clusters we find the following ages and metallicities: NGC 265 has $log(Age) = 8.5 \pm 0.3$ and metallicity $Z = 0.004 \pm 0.003$, K 29 has $log(Age) = 8.2 \pm 0.2$ and metallicity $Z = 0.003 \pm 0.002$, NGC 290 has $log(Age) = 7.8 \pm 0.5$ and metallicity $Z = 0.003 \pm 0.002$. The initial mass function turns out to be in agreement with the

standard Kroupa model. The star formation rate of the field population presents periods of enhancements at 300-400 Myr, 3-4 Gyr and finally 6 Gyr. However it is relatively quiescent at ages older than 6 Gyr. This result suggests that at older ages, the tidal interaction between the Magellanic Clouds and the Milky Way was not able to trigger significant star formation events.
The last part of the thesis analyzes a region of high intensity star formation in the Large Magellanic Cloud (LMC), namely N11. In this case also the data were taken from the archive. The analysis of the colour-magnitude diagrams immediately presented an interesting feature: the presence of a double low-magnitude main sequence. This feature has been interpreted as the presence of pre-main sequence stars (PMSs). The hypothesis of a differential reddening has also been discussed. In this region young clusters and associations are present: for all the observed objects the presence of clustered substructures has been investigated by mean of the graph method. Finally all the enhancements of star formation are compared with dynamical models of the interaction between the Milky Way and the Magellanic Clouds known in literature, finding that they are related, for example, around 200 Myr (perigalactic passage between the Magellanic Clouds) and at 1-2 Gyr (perigalactic passage with the Milky Way).

Contents

List of Tables

List of Figures

Chapter

1 Introduction

Scientific Rationale and Aims. The Milky Way (MW) and the two Magellanic Clouds (MCs) have long been considered as a system made of three mutually interacting galaxies (at least during a significant fraction of the Hubble time). Whether the three galaxies have always been a system of bound objects or they captured each other under suitable circumstances under the effect of the common gravitational potential of the Local Group (LG) is not clear at all. This question can perhaps be clarified by cross-correlating the histories of star formation and chemical enrichment in the triplet. The subject is not entirely new. It has already been addressed several times during the last two decades with no fully convincing conclusions. Therefore it is worth going over it again. In this context we plan to highlight the correlation between the star formation history (SFH) deduced from the stellar content of the MW and MCs (paying major attention to the much less studied case of the Small Magellanic Cloud) and their dynamical interaction. The Small Magellanic Cloud in particular represents a unique environment for studying star formation because of its low metallicity.

On one hand the SFH and companion chemical enrichment in the triplet can be deduced with standard populations synthesis techniques from the Colour-Magnitude Diagrams (CMD) and the Luminosity and Colour Functions of the stellar contents (both field and cluster stars). On the other hand, assuming suitable initial conditions for the present day position and velocities of the Large (LMC) and Small (SMC) MCs with respect to the MW and a reasonable representation of the global gravi-

tational potential (also the other galaxies of the LG should be taken into account), one may reconstruct their orbits and look for significant close encounters. The bottom line is that each close encounter will leave important traces in the star forming efficiency of the triplet members. As the close encounters depend on the dynamical history, their foot-prints in the stellar contents would put important constraints on the dynamical history and vice-versa. In particular it would cast light on the issue of the binary status of the MW amd LMC+SMC. Current understanding of this problem is far from being settled down and new possibilities could perhaps be found.

The MW and MCs, which are believed to be interacting with each other, are ideal laboratories to study the effect of dynamical interaction on the structure, kinematics, star formation, and chemical properties of galaxies. Their proximity offers a unique opportunity to tackle these issues from different perspectives. In this project we will concentrate on star formation in clusters and fields.

The SFH of each galaxy can be traced back in different ways: from the analysis of the CMDs for large assemblies of stars using the population synthesis technique, the study of individual star clusters both by means of their CMDs and their integrated properties (colors, spectra etc..), the study of chemical evolution and abundances of important elemental species such as carbon and silicon that bear very much on extinction and emission properties. Often each diagnostic tells us a different story that on the contrary should be reduced to a self-contained picture. More relevant here, the SFH of the three galaxies seems to be truly different even if some puzzling coincidences can be found. How much of the differences is either due to diagnostic uncertainties or to the intrinsic nature of the problem?

Needless to say that in each galaxy of the triplet the star formation has two components: the internal one driven by the physical properties of a galaxy on its own and the one triggered, modulated by the mutual interactions. Likely the modulation in the MW was less than in the two companion galaxies simply because of the mass difference; roughly in the sequence $\simeq 10^{11}\,M_\odot$ (MW), $10^{10}\,M_\odot$ (LMC), and $10^{9}\,M_\odot$ (SMC).

The question is whether the resulting SFHs in the three galaxies show evidences of mutual correlations that can be univocally ascribed to dynamical interactions, e.g. enhancements in the star formation rate (SFR) at close encounters between LMC and SMC, LMC and MW, SMC and MW, and LMC+SMC and MW. The three galaxies separately show some evidences that alternate periods of major activity did occur. The question is whether interdependence and synchronization can be assessed.

There are numberless questions to be addressed and possibly answered. Among others, is there any solid evidence of a similarity of the SFR in the three galaxies, as expected if at least partially, the SFR is due to an external trigger? Is it possible to find traces of those close encounters in the stellar content of LMC, SMC and MW? Traces of it in the cluster population are by far more difficult to detect as clusters formed in early epoch may have been disrupted by dynamical effects if not massive enough. Field stars offer better chances provided that very deep and accurate CMDs are available. Are the age differences suggested for different stellar fields in the MCs the traces we are looking for? Further question to be addressed is the different behaviour of the two clouds with respect to star formation. In fact, if the LMC and SMC have always been close together (and this is by no means certain), why is the SMC field and star cluster age distribution apparently skewed towards much older ages compared to the LMC? Did the SMC not experience the same perturbation that enhanced the SFR in the LMC?

If those similarities and differences are real, they should of course depend on the past dynamical history, in other words whether the MCs have always been bound to the MW or at least for a very long period of time. What we know about the past dynamical history is very little (despite the efforts) and not univocal. There are indeed many possible solutions all of them compatible with the present day information of the MC positions and velocity components (on which by the way there is no general consensus). Therefore it is worth investing time and resources to seek consistency between the information derived from the stellar and chemical diagnostics and the expectation from dynamical simulations. This would eventually cast light on the most plausible dynamical history of the complex MW+LMC+SMC.

1.1 Magellanic Clouds

The SFH of the MCs is the subject of a long lasting debate. Long ago Tifft and Snell (1971) and Hodge (1973) noted that the LMC has contained a number of distinct active star forming regions over the past 0.1 Gyr. Butcher (1977) and Stryker (1984) found that the LMC appears to have formed the bulk of its stars at some intermediate epoch about 3 to 4 Gyr ago. The pioneer works by Bertelli et al. (1992), Vallenari et al. (1996) studied the SFH of the LMC on the basis of ground-based CMDs. They favoured a predominance of young and intermediate age stars in the LMC field population. Evidences were presented for field to field variations. In particular, it was suggested that West of the Bar towards the SMC, star formation began 2-3 Gyr ago from partially enriched gas. In the regions East and South-East of the Bar the star formation had a sort of enhancement about 6-8 Gyr ago. The result implies that the LMC was quiescent for about 70% of its life. Works based on HST data could not come to a unique solution. On one side a roughly constant

star formation or with evidence of small enhancements of a factor of 2-3 was found by Gallagher et al. (1996), Holtzman et al. (1997), Geha et al. (1998), Olsen (1999). On the other hand Elson et al. (1997) identified two main populations, with ages 1-2 Gyr and 2-4 Gyr. Dolphin et al. (2001), Harris and Zaritsky (2001) derive two main episodes of star formation at epochs younger than 2 Gyr and older than 7 Gyr respectively, with a quiescent period in between. Smecker-Hane et al. (2002) find that the Disk SFR has been relatively smooth and continuous over the last 13 Gyr, while the Bar was dominated by SF episodes at intermediate ages, more precisely from 4 to 6 Gyr and 1 to 2 Gyr ago. Recently Javiel et al. (2005) derive a SFR varying from one region to another. Periods of enhanced star formation at intermediate ages (2-6 Gyr) are found closer to the bar and on the eastern side of the LMC, while a more uniform rate is detected in the NW part of the LMC disk. The observed differences from one field to another, if confirmed, point in favour that the mixing of stellar populations within the LMC is not 100% efficient. On the contrary, it cannot be excluded that coeval stars resulting from the same star formation episode move coherently in the potential of the galaxy. A dynamical model, taking into account typical velocity dispersions and orbital motions is then required to fully understand the star formation process.

The SMC shows an asymmetric appearance with an irregular Bar and an eastern extension. In a photographic plate study Gardiner and Hatzidimitriou (1992) found that the bulk of the stellar population in the SMC is about 10 Gyr old. They observe that the young stellar population is biased toward the eastern LMC -facing side of the SMC. No large differences in age and metallicity are found among the SMC old stars (Tosi et al., 2008). Crowl et al. (2001) find the same trend among the SMC populous clusters: those toward the eastern side tend to be younger and more metal rich than those on the western side. Recently Zaritsky et al. (2000) and Maragoudaki et al. (2001), Cioni et al. (2000) confirmed that the asymmetric structure of the SMC is due exclusively to the distribution of young main sequence stars, while old stars show a rather regular and smooth distribution typical of a spheroidal body. The asymmetric distribution of the young stars is consistent with the patterns of the associations and HII regions (Bica and Schmitt, 1995). This is interpreted as the effect of the perturbations developed by the gravitational interaction of LMC-SMC. This is the kind of reshaping that a low mass disk galaxy should undergo after a few passages around the MW (Pasetto et al., 2003). A few studies are devoted to the determination of the SFR of the field stars in the SMC. No real consensus is reached whether the star formation has proceeded with several periods of enhancements, namely at 400 Myr, 3 Gyr, 9 Gyr as found by Harris and Zaritsky (2004), or in a more continuous way, with a main episode between 5 and 8 Gyr (Dolphin et al., 2001). Glatt et al. (2008) analyzed 6 clusters in the SMC and determined the ages with different sets of isochrones. The clusters result to have intermediate ages (from

6 to 7.5 Gyr) but a noticeable metallicity spread. Concerning the distribution of the clusters, the oldest lie in the northwestern side of the SMC while the youngest in the main body. Piatti et al. (2008) also analyzed seven clusters in the inner region of the SMC. The ages were evaluated through isochrone fitting method and found younger ages from 25 Myr to 1.2 Gyr. Carrera et al. (2008) studied from spectroscopy the metallicity of 350 stars from several fields in different points of the SMC. In this way they determined the metallicity gradient and found that it is related to the age gradient. In fact young metal rich stars are concentrated in the centre of the galaxy.

1.2 Milky Way

In the MW the SFH had a much more complicate behaviour owing to the complex structure of the Galaxy: halo, bulge thick, and thin disc. Limiting ourselves to the disc, it is generally thought that the best representation of the SFR is the one rising to a maximum value back in the past and ever since declining with a time scale of a few Gyr (G-Dwarf problem). The SFR of the disk is derived by several authors using completely different techniques, going from white dwarf luminosity functions (Barry, 1988; Scalo et al., 1987; Noh and Scalo, 1990; Isern et al., 1995; García-Berro et al., 1999), to age-metallicity relation of G dwarfs (Rocha-Pinto and Maciel, 1997), distribution of coronal emission as measured by X-ray luminosities (Micela et al., 1993; Lachaume et al., 1999), Hipparcos data (Bertelli and Nasi, 2001), chromospheric age studies (Rocha-Pinto et al., 2000; Gizis et al., 2002), kinematics of disk stars (Just, 2002, 2003). The vast majority of the authors suggest that the disk of the MW has experienced star formation with several episodes of enhancement. Fluctuations on time scales less than 1 Gyr are found by Hernandez et al. (2000) and by Rocha-Pinto et al. (2000) for the field stars in the solar vicinity. These latter find that, superposed on this short period oscillations, the disk of our Galaxy has experienced enhanced episodes of star formation at 0-1 Gyr, 2-5 Gyr and 7-9 Gyr ago, although the reality of the latter burst is still uncertain. Bertelli and Nasi (2001) discussing Hipparcos data, derive a SFR globally increasing from the past, with an enhancement at a time between 2.5 and 5.5 Gyr. A cyclic behaviour with a period less than 0.4 Gyr is found by de La Fuente Marcos and de La Fuente Marcos (2004) on the basis of the age distribution of the Galactic open clusters younger than 2 Gyr. While a precise coincidence of the SF epochs is difficult to be assessed, it is evident a general agreement of the major episodes of star formation in the disk with the enhancements of the SFR in the MCs, mainly in the LMC. In addition, the oscillatory component with shorter period might be interpreted as a tidally triggered bursts due to the interaction with the Sagittarius and the SMC-LMC. Remarkably, episodes at 0.35 Gyr, 1.1 Gyr,1.5 Gyr are found, in agreement with the prediction of the closest approaches between the SMC and/or LMC and the MW (Oh et al., 1995).

1.3 Cluster formation history of the MCs

Previous studies have pointed out significant differences in the star formation of the two Clouds. The vast majority of LMC clusters is relatively young, with ages < 4 Gyr, while only a small number of objects (about 15) is found having ages > 10 Gyr. Only one is of intermediate age (Olszewski et al., 1996). The age gap among the LMC clusters (van den Bergh, 1991; Girardi et al., 1995; Westerlund, 1997) suggests that a long period of quiescence took place. The rate of cluster formation in the SMC is instead quite continuous. A conspicuous population of clusters younger than 1-2 Gyr is found (Pietrzynski and Udalski, 1999; Chiosi et al., 2004; Rafelski and Zaritsky, 2005). The data seem to suggest that the formation of young clusters took place in bursts (Chiosi et al., 2004; Rich et al., 2000). The SMC is known to have at least six populous clusters of intermediate age, namely in the range 5-9 Gyr, but only one true old object (NGC 121) having an age > 10 Gyr is known in this galaxy (Stryker et al., 1985; Dolphin et al., 2001). Finally, it is quite puzzling to reconcile the SFH of the field stars and clusters of the SMC and LMC.

How old are the oldest GCs of the MCs? Old LMC-SMC clusters are all very similar in age and metallicity to classical Galactic GCs such as M5, with little age spread Brocato et al. (1996); Olsen et al. (1998); Mackey and Gilmore (2004). This finding strongly supports the notion that the LMC formed at the same time as the MW.

1.4 Chemical evolution of the MCs

The age gap in the LMC cluster distribution results as an abundance gap, since old clusters are metal poor ([Fe/H]=–1.74 , Johnson et al 2004) while the clusters younger than 4 Gyr are relatively metal rich ([Fe/H]=-0.45, Smith et al 2002) having a metallicity quite close to the present day abundance in the LMC (Olszewki et al 1991). Recent determination of the age-metallicity relation of field stars is made using different tracers, namely RR Lyrae (Gratton et al., 2004), planetary nebulae (Dopita et al., 1997), red giants (Smith et al., 2002; Cole et al., 2004; Cole, 2005). A very rapid enrichment is found at the oldest times, when the metallicity raised rapidly from [Fe/H]=-3 at the end of the population III phase to about -1 within the first 4 Gyr. The age-metallicity relation (AMR) is almost flat during the period from 5 to 10 Gyr ago. At present the interpretation of those data is not yet clear. Chemical evolution models cannot distinguish between a continuous star formation and a bursting mode (Cole, 2005).

The present-day knowledge of the AMR in the SMC is mainly based on clusters. RR Lyrae star abundances are measured by Smith et al. (1992), while Cepheids metallicity are derived by Harris (1981). The interpretation of the existing SMC AMR

widely varies from author to author. Current data cannot really discriminate among different models. A continuous enrichment from the oldest to the youngest objects is found by Da Costa and Hatzidimitriou (1998) and by Dolphin et al. (2001). On the other hand, Olszewski et al. (1996); Pagel and Tautvaišienė (1999); Piatti et al. (2001) analyses of the data favour a bursting mode of star formation.

It is clear that star formation and chemical enrichment go together. Is the current modelling of chemical evolution consistent with other information, e.g. the extinction and emission curves of the three galaxies? Is the predicted time dependency for the elemental species consistent with the amount and nature of the dust component in the interstellar medium we need to match extinction and emission? Also in this case MW, LMC and SMC are an interesting laboratory as they constitute a natural sequence of decreasing mean metallicity. Along the sequence, the absolute value of the slope and the intensity of 2175 Å bump increases and decreases respectively. This trend is currently attributed to the different percentages of carbon abundance with respect to that of silicon in the three galaxies. Emission contains the features due to the poli-aromatic hydrocarbons (PAH). If PAHs are mainly produced in AGB stars, then one would expect PAH features to arise in galaxies with a minimum metallicity (Dwek, 2005) thus allowing for a metallicity threshold below which PAHs have not yet formed and explaining the absence of the 2175 Å in low metallicity environment. This means that the history of chemical evolution must include also that of dust. But for a few exceptions (e.g. Dwek, 1998) most models in literature simply ignore dust, which is later inserted by hand. This is a point of inconsistency that should be improved. The paradigm should be that the same SFH is at work in the CMDs, chemical evolution and dynamical models.

1.5 The MW+LMC+SMC system

It is tempting to attribute the LMC and SMC star-burst trigger and the suspected enhancement in the SFR in the Galactic Disc to some sort of tidally induced shock caused by a close encounter of the three galaxies.

Starting from the pioneer study of Murai and Fujimoto (1980) the dynamical interaction between the MCs and the MW has been modelled with the aim of explaining the evolution and morphology of the satellite galaxies, casting light on the binary nature of the LMC+SMC system, accounting for the periods of enhanced stellar activity in the three galaxies, explaining and reproducing the Magellanic Stream (narrow band of H emerging from SMC and lying on a Great Circle passing through the South Galactic Pole and the present position of the MC's).

Murai and Fujimoto (1980) found that several close encounters are possible which

should have left traces in the age distribution of the field stars. Assuming that LMC+SMC revolve around the MW with constant rotation velocity of about 250 km/s and that the total mass of the MW within 50 kpc is about $10^{11}\ M_{\odot}$,

(i) several bound orbits for the complex LMC+SMC are possible during the last 10 Gyr if the peri-galactic distance of LMC is > 40 kpc;

(ii) the main characteristics of the Magellanic Stream are reproduced (radial velocity of about 200 km/s at the tip of the stream) if the following conditions are met: (1) orbital plane of LMC is nearly perpendicular to the galactic plane; (2) peri-galactic distance of LMC is about 50 kpc; (3) the revolution about the Galaxy is counter-clockwise; (4) SMC approached LMC as close as 3 kpc about 200 Myr ago.

Over the years the situation has been much improved thanks to studies aimed at reproducing the properties of LMC and SMC by shaping their SFH by means of the mutual dynamical interactions in the triplet LMC+SMC+MW. Among others, two studies are particularly relevant here: Yoshizawa and Noguchi (2003) for the SMC and Bekki and Chiba (2005) for the LMC. Both follow a similar strategy: given the present day position and space velocities UVW of LMC (SMC), the mass of MW, LMC, SMC and the gravitational potential of the MW and the companion satellite (LMC, SMC as appropriate) the orbit of LMC or SMC is reconstructed back to the past and the distances between the MCs and MW, between MW and LMC, and between MW and SMC. The solution is not unique owing to uncertainty in the initial conditions, and furthermore in many cases the MCs cannot keep their binary status for more than about 5-6 Gyr. Chosen a suitable orbit, LMC or SMC (initially approximated to thin disc) are launched on their predetermined orbit and followed down to the present. Under the action of the MW gravitational potential and the companion satellite (reduced to point a suitable source of gravitational potential) the satellite is reshaped, its SFH is affected by the dynamical interaction. The results are as follows:

LMC (Bekki and Chiba, 2005). Tidal interactions between the MCs and MW changed the initial LMC disc into three components: central bar, thick disc and a cinematically hot halo. The bar is made of both old stars and newly formed ones in almost equal proportions. The thick disc has central velocity dispersion of 30 km/s and shows rotationally supported kinematics (V_r/σ_0=2.3). The stellar halo is formed during the interaction and consists mainly of old stars originating from the outer parts of the initial thin disk: it contains relatively young metal-rich stars with total mass fraction of about 2%. Repeated interactions between the MCs and the MW enhances the SFR in the LMC disc. Most of the new stars are formed inside the bar during the last few Gyr. Efficient globular cluster formation occurs only when LMC starts interacting violently and closely with the SMC (about 3 Gyr

ago). About 15-20% of the field stars and gas in the initial thin disk are tidally stripped to form a great circle of relics around the MW.

SMC (Gardiner et al., 1994; Yoshizawa and Noguchi, 2003). The tidal response of the SMC to LMC and MW (in presence of gas dynamics and star formation) yields models in which we note a gas stream with almost no stars, the presence of young stars in agreement with the observations, a tidal tail and bridge for both disc and halo stars. No details on the past SFH are given.

Some recent works (Kallivayalil et al., 2006) measured proper motions of the SMC. These measures together with other previous data on the LMC are compatible with the hypothesis that the Magellanic Clouds could be unbound systems. However the autors say that more constraints would be necessary to check this idea.

1.6 Aim and plan of the thesis

Aim of the thesis is to investigate part of this complex problem. Specifically, we study the cluster and field SFH in the main body of the SMC trying to determine the epochs of dominant activity and quiescence. They could provide important constraints to any theory of the dynamical structure and evolution of the Local Group. To this aim we analyse the stellar content of clusters and field with the aid of the population synthesis technique.

The plan of the thesis is as follows. In Chapter 2 we derive an estimate of the age for a large number of SMC clusters (462 in total) taken from the catalog of Bica and Dutra (2000) We make use of the OGLE data (Udalski et al., 1998) to derive the Colour Magnitude Diagrams (CMDs), which in turn are interpreted with the standard comparison with theoretical isochrones. Owing to the very large number of objects, the interpretation of the CMD is made in a simplified manner which does not fully exploit the potential of the population synthesis technique. Therefore the corresponding age distribution function has to be considered as approaching the true one only in statistical sense. In order to verify how good are the ages derived in this way, in Chapter 3 we check the ages of chapter 2 by studying in detail three clusters of the above list. The two age assignments agree within an acceptable range of uncertainty thus lending support to the age distribution function derived in chapter 2 and ensuring that it can be used for further analysis (at least in statistical sense). In Chapter 4 we investigate whether there is any correlation between the cluster formation efficiency and age distribution with the environment (clouds of HI and CO) and the position of the clusters within the HI and CO clouds. In Chapter 5 we derive the age distribution for the field stars in the so-called HI super-shells. In Chapter 6 the same analysis is made for three fields nearby the three test clusters.

In Chapter 7 we present a study of N11 region in the LMC. We find that there is a pre-main sequence population of stars. We also present some results on young stellar objeccts in the area. In Chapter 8 the two age distributions in the super-shell area of the SMC are compared one to another and to the age distribution derived from the large sample of clusters. In addition to this we compare the age intervals of stellar activity indicated by the three age distribution functions with those found in simulations of the dynamical interactions in the LMC+SMC+MW complex. In each chapter some particular conclusions are drawn for the specific topic under consideration, whereas a summary and several general conclusions are presented in Chapter 9.

Finally, in Chapter 10 (Appendix A) we present the catalog of clusters for which a preliminary estimate of the age (at given mean metallicity and reddening varying from one to another as appropriate) has been obtained.

Chapter 2

Ages of the SMC clusters

2.1 Introduction

In this chapter we aim to derive the age distribution for a large sample of clusters in the SMC and in turn to discuss the star formation on a large scale. Using the data from the OGLE survey we can estimate the ages of quite a conspicuous sample of clusters spread over an area of 2.4 sq.deg. Then we can compare the resulting age distribution with those known in literature (Pietrzynski and Udalski, 1999) getting an idea on the general trend and the way in which star formation occurs.

This is only our starting point because star formation itself is a complex phenomenon involving at the same time several physical processes such as turbulence, gravitational collapse, cooling, gravitational trigger. There are many open questions about star formation in galaxies: is it a continuous process or does it proceed by bursts? Which are the fundamental triggers of star formation and in which measure are they internal or external? The MCs, which are believed to be interacting with each other, are ideal laboratories to study the process of field star and cluster formation.

LMC has been widely studied using both ground based and HST data (Bertelli et al., 1992; Vallenari et al., 1996; Gallagher et al., 1996; Holtzman et al., 1997; Elson et al., 1997; Geha et al., 1998; Harris and Zaritsky, 1999, 2004; Olsen, 1999; Dolphin, 2000b; Javiel et al., 2005; Kumar et al., 2008). The vast majority of the authors suggest that the LMC experienced a continuous star formation with sev-

eral enhancements, roughly at 2-4 Gyr and at 6-7 Gyr although the precise epochs change from field to field.

For the moment we concentrate on the cluster age distribution. The discussion of the relation between cluster star formation and field star formation is delayed to chapters 4 and 5. We think that there are different mechanisms of star formation in the clusters and in the field or that stars are formed in clusters and then released into the surroundings. Each hypothesis can be confirmed or denied by the age determination of clusters and related fields being coeval or subsequent. It is well known that the rich cluster system of the MCs is quite different from that of our own Galaxy where a dichotomy is found between young sparse open clusters and old compact objects. The MCs present a wide distribution of rich cluster ages and constitute an ideal laboratory for testing the star and cluster formation process, either due to global effects, such as gravitational triggers because of tidal interactions, or to internal processes. In fact, the star formation process depends on the cooling and the heating of the interstellar gas which in turn, depend on the presence of metals (Lisenfeld and Ferrara, 1998; Wolfire et al., 1995).

A large population of clusters is found in the SMC. Hodge (1986), comparing the number of clusters found down to B=22 (inner regions) or B=23 (outer regions) in selected regions with the number of known clusters in SMC catalogs at that time, estimated a global population of 900 clusters. Considering incompleteness effects, 2000 clusters are expected if small older clusters were detectable. Pietrzynski and Udalski (2000) catalog includes 238 clusters down to $B\sim$21.1 or $V\sim$21.5. Bica and Dutra (2000) including in the catalog faint and loose systems, find 633 clusters. Considering also the clusters related to emission (NC and CN types) the total number of objects is 719. As pointed out by the authors, the number of clusters in Bica and Dutra (2000) is still far from being complete.

Several catalogs are available in literature. Pietrzynski and Udalski (1999) using isochrone fitting, and Rafelski and Zaritsky (2005) making use of integrated colors derive the age of a limited number of bright clusters, namely 93, and 200 respectively.

Concerning the cluster age distribution, the SMC is known to have at least six populous clusters of intermediate age in the range 5-9 Gyr, but only one true old object (NGC 121) having an age of $>$ 10 Gyr (Stryker et al., 1985; Dolphin et al., 2001; Glatt et al., 2008). Only a few of the clusters in Bica and Dutra (2000) catalog have known ages. Pietrzynski and Udalski (1999) using isochrone fitting, and Rafelski and Zaritsky (2005) making use of integrated colours derive the age of a limited number of bright clusters, namely 93, and 200 respectively. Piatti et al. (2005) discuss the age and metallicity for 36 SMC clusters. The data seem to suggest that the

formation of young clusters took place in bursts (Rafelski and Zaritsky, 2005; Piatti et al., 2001; Rich et al., 2000).

If it is interesting to derive an estimate of the age of a large number of clusters for statistical consideration and to check the correlation with the environment like with CO clouds and HII regions, it is worthy, whenever possible, to make use of smaller samples but with better quality data in order to know more accurately the ages as a check of the previous determination, especially in regions of particular interest such as the HII shells. To this purpose, we make use of the OGLE data for the whole SMC disk, and of better quality data obtained at the ESO 2.2m telescope for a region around NGC 269, located at the SE end of the disk, at the border of the super-shell 37A. Ground based CMDs must avoid the cluster centres and suffer from the effects of the high crowding and serious contamination by field stars. The superior quality of Hubble Space Telescope (HST) data makes it possible to study the central regions of the clusters allowing precise determinations of their ages. For this reason we searched the ESO archive for HST data of SMC regions and we found ACS/WFI data for three clusters in the SMC, namely NGC265, K29 and NGC290. They are located close to the borders of HI shell 37A where star formation seems to have been very active in the recent past (Stanimirović et al., 2004; Chiosi et al., 2006). These data will be discussed in Chapter 3. The quality of this data allows for precise determinations of age, metallicity, reddening and IMF. Among the few other age determinations of SMC clusters based on HST data, we quote Rich et al. (2000) who presented HST/WFPC2 data of 7 clusters.

In section §2.2 the SMC distance, reddening, metallicity, and line of sight depth are given. In section §2.3 the observations and data reduction are described. In section §2.4 the cluster age distribution in the whole disk is derived. Section §2.5 summarizes the results.

2.2 SMC distance modulus, reddening, line of sight depth, metallicity

In this paragraph we discuss some parameters that we will need in the determination of the star formation of our clusters. While distance modulus and line of sight depth are assumed from literature, reddening and metallicity are also confirmed by our determinations. In the case of the OGLE data reddening and metallicity are derived by isochrone fitting of the colour-magnitude diagrams (CMDs) while for the three clusters with HST data we could perform a more precise estimation by means of luminosity functions fitting with synthetic populations.

A distance modulus of $(m-M)_0 = 18.9$ is assumed for the SMC, in agreement with recent determinations by Storm et al. (2004), Weldrake et al. (2004), Caputo et al. (1999) and Sandage et al. (1999).

The extinction map across the SMC was recently determined by Zaritsky et al. (2002) using data from the Magellanic Cloud Photometric surveys. They show that the extinction varies spatially increasing along the SMC ridge from northeast to southwest. In addition, young stars present an average differential extinction 0.3 mag higher than old stars. By comparison, a mean reddening $E(B-V)$=0.08 mag is derived by Rachford et al. (2002) and Hunter et al. (2003). In the following, when possible, we derive the reddening of each cluster by main sequence fitting. Otherwise, a mean value of $E(B-V)$=0.08 mag of the reddening is assumed. In the case of field star population we account for an additional reddening Gaussian dispersion with $\sigma = 0.09$. No differential extinction is included.

The line of sight depth of the SMC is a long-lasting controversial issue. Mathewson et al. (1986) derive a great depth of 30 Kpc by measuring distances and radial velocities of Cepheid stars. Welch et al. (1987) concluded that the SMC does not extend beyond its tidal radius (4-9 Kpc). Groenewegen (2000) using near infrared data of Cepheids derives a depth of 14 Kpc. Crowl et al. (2001) using the magnitudes of the clump stars in clusters derive a depth ranging between 6 and 12 Kpc. The main reasons of those discrepancies can be found in the uncertainties on the extinction and on the relation period-luminosity-metallicity of Cepheid. Stanimirović et al. (2004) point out that the application of the correction for differential reddening derived by Zaritsky et al. (2002) significantly influences the distance determinations bringing the depth of the SMC within its tidal radius (4-9 Kpc). Additionally, while the tidal tails contribute mostly to the elongation of the galaxy, the main body of the SMC does not present a significant elongation ($\sim$ 5 Kpc). A recent determination is made by Lah et al. (2005) who using the P-L relation of OGLE II variables find a very patchy structure with a depth of about 3.2 $\pm$ 1.6 Kpc. In the following discussing the SFR of the field stars, we adopt an intermediate value of 4 Kpc implying a difference in the distance modulus of about 0.14mag.

The present-day knowledge of the age-metallicity relation in the SMC is mainly based on clusters. Only a few determinations based on stars are available. RR Lyrae star abundances are measured by Smith et al. (1992), while Cepheids metallicity are derived by Harris (1981). The interpretation of the existing SMC age-metallicity relation widely varies from author to author. Current data cannot really discriminate among different models. A continuous enrichment from the oldest to the youngest objects is found by Da Costa and Hatzidimitriou (1998) and by Dolphin et al. (2001). Olszewski et al. (1996) suggest that no significant enrichment is

produced from 10 Gyr ago to 1-2 Gyr ago. During that time the metallicity rapidly increases. Olszewski et al. (1996), Pagel and Tautvaišienė (1999) and Piatti et al. (2001) analyses of the data favour a bursting mode of star formation (Harris and Zaritsky, 2004).

2.3 Data, observations, and reduction

2.3.1 NGC 269 region

V,I images were taken with the WFI at the ESO 2.2m telescope on 2000, October 21 under photometric conditions as backup observations for a different project. The field of view is of 34 $\times$33 arcmin^2. It is centered on the cluster NGC 269 at $\alpha = 00^h48^m30.6^s$ and $\delta = -73^0 31' 30''$. The exposure times are 300 sec in V and 300 sec in I. To avoid saturation at the bright magnitude end two images having exposure times of 20 sec were taken. The seeing was 1 arcsec.

Pre-reduction of CCD images was performed within the IRAF environment. Each image was bias-subtracted and flat-fielded using twilight sky flats. After these steps, all images were astrometrically calibrated using the IRAF package MSCRED (Valdes 1998) and the script package WFPRED developed at the Padova Observatory (Rizzi et al., 2003). Photometry was obtained with DAOPHOT (Stetson 1987).The photometric zero points were then set by comparison with secondary standard stars accurately calibrated onto the Landolt (1992) system. The estimated uncertainty of the zero point calibration is 0.03 mag in both V and I. More than 100000 stars are found down to V=24. Fig 2.1 presents the CMD of the whole region. The completeness correction is calculated as usual by means of artificial stars experiments where a small number of artificial stars are injected in the original frames. Then the frames are reduced following the same procedure. The completeness factors in V and I band, Λ_V, and Λ_I respectively, defined as the number of recovered on the added stars are plotted in Fig. 2.2. The data are complete at 50% level for magnitudes brighter than $V = 22$. Photometric errors are derived from artificial stars experiments and are plotted in Fig. 2.3.

2.3.2 OGLE data

An analysis over a wider area of the galaxy is made using Optical Gravitational Lensing Experiment (OGLE II) data (Udalski et al., 1998) to derive cluster and field star age distribution for the regions not covered by our photometry. The data cover 2.4 sq. deg. of the main body of the SMC. The limiting magnitude of the photometry is $V\sim$21.5. Completeness correction is applied following Udalski et al. (1998). Field population data are complete at about 80% level and 89% level down

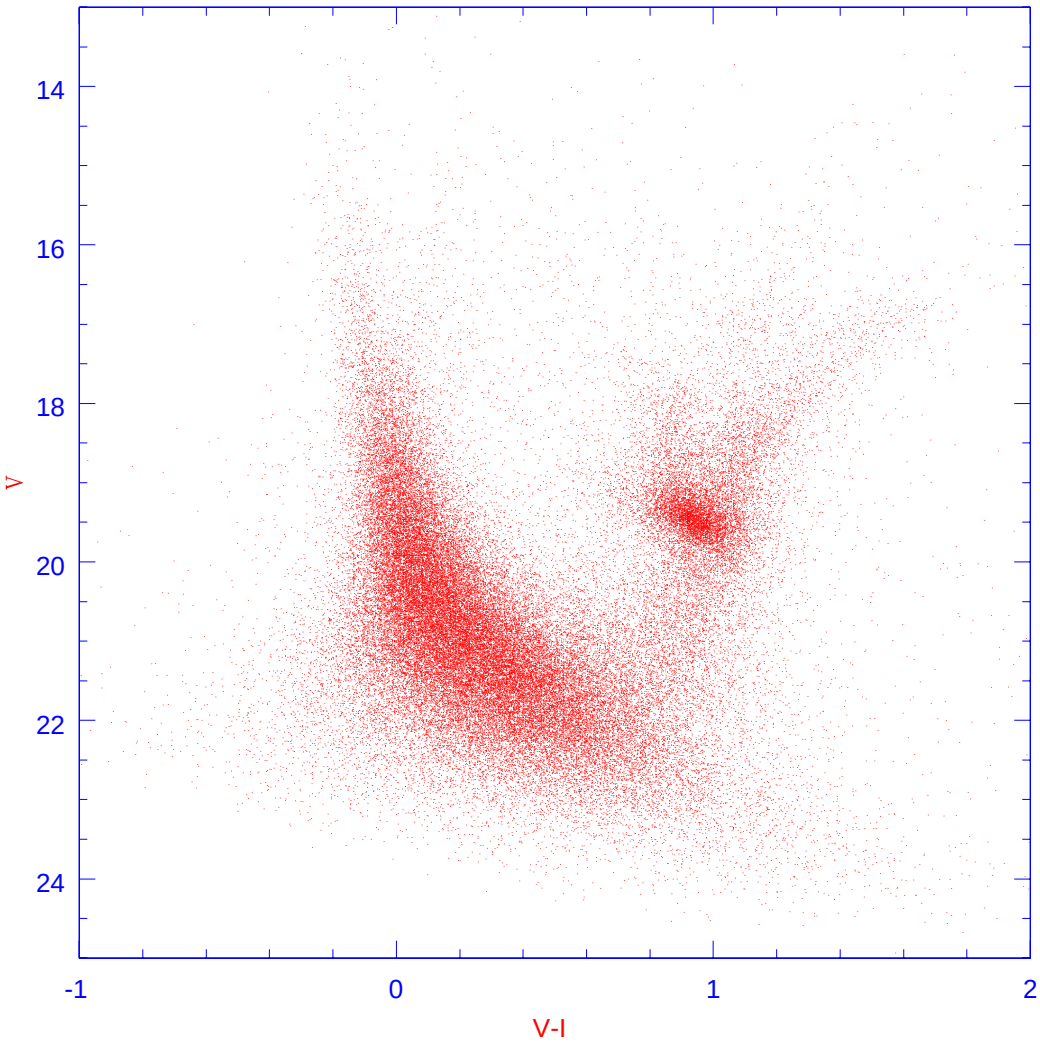

Figure 2.1: The CMD of the observed region around NGC 269

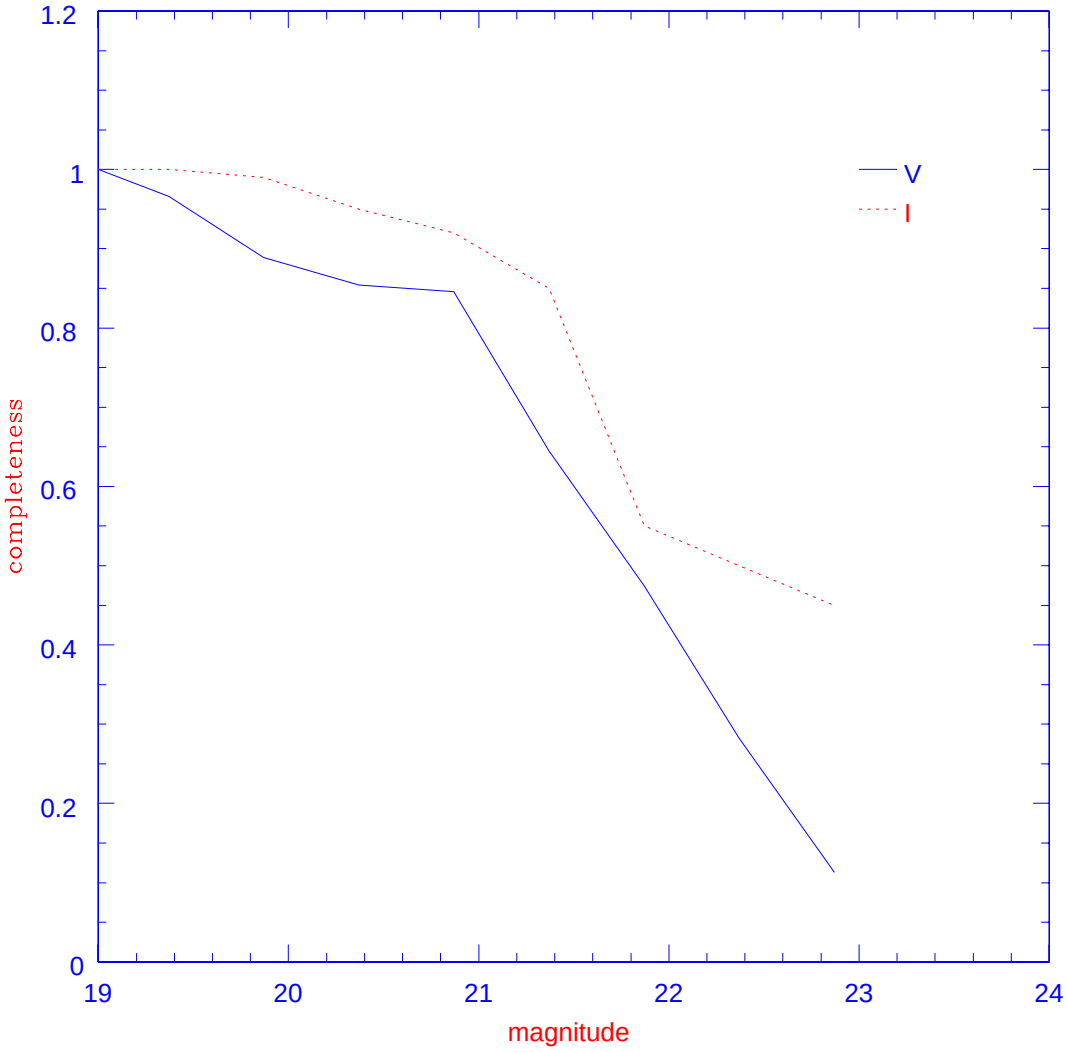

Figure 2.2: Completeness factors Λ in V and I magnitude are plotted as functions of the magnitude

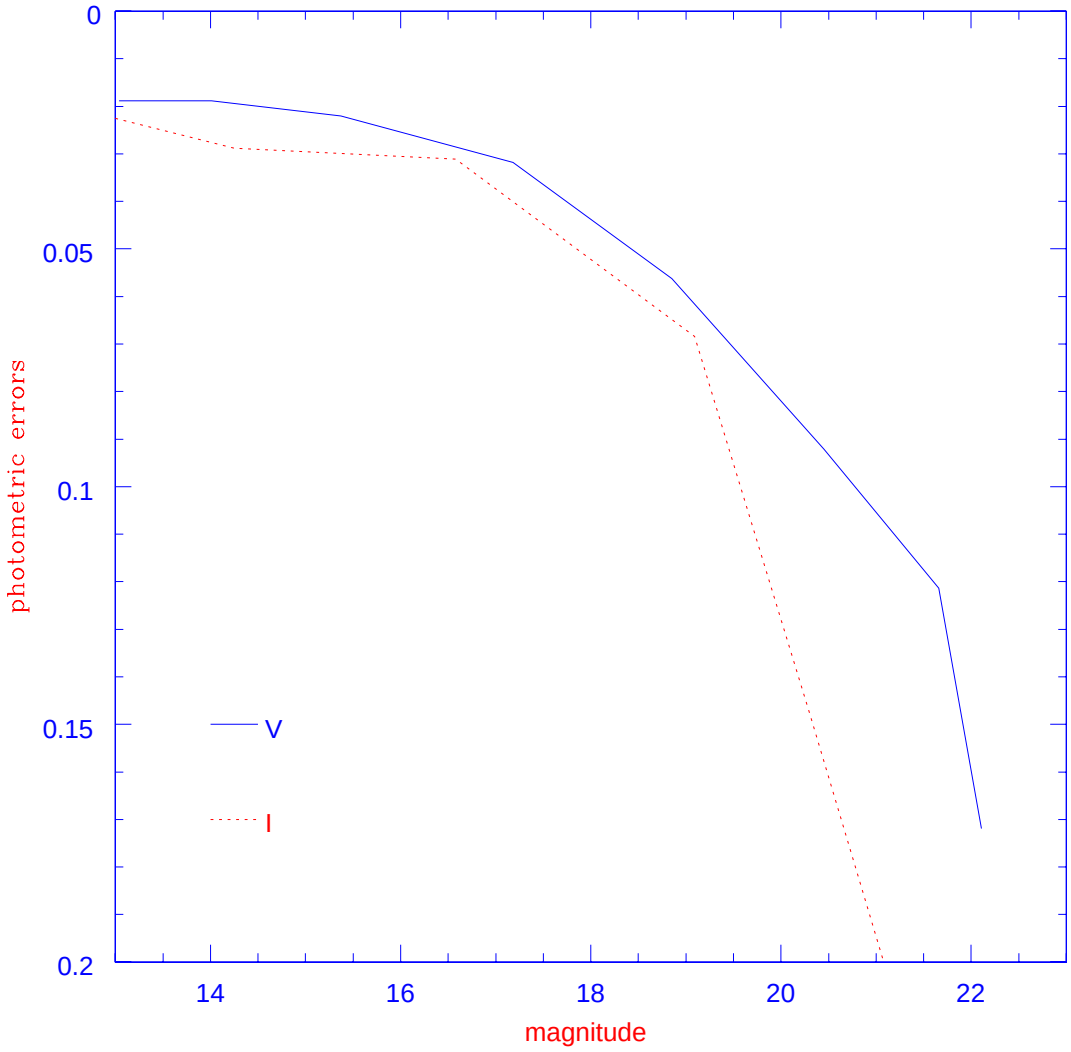

Figure 2.3: Photometric errors as functions of the V and I magnitude

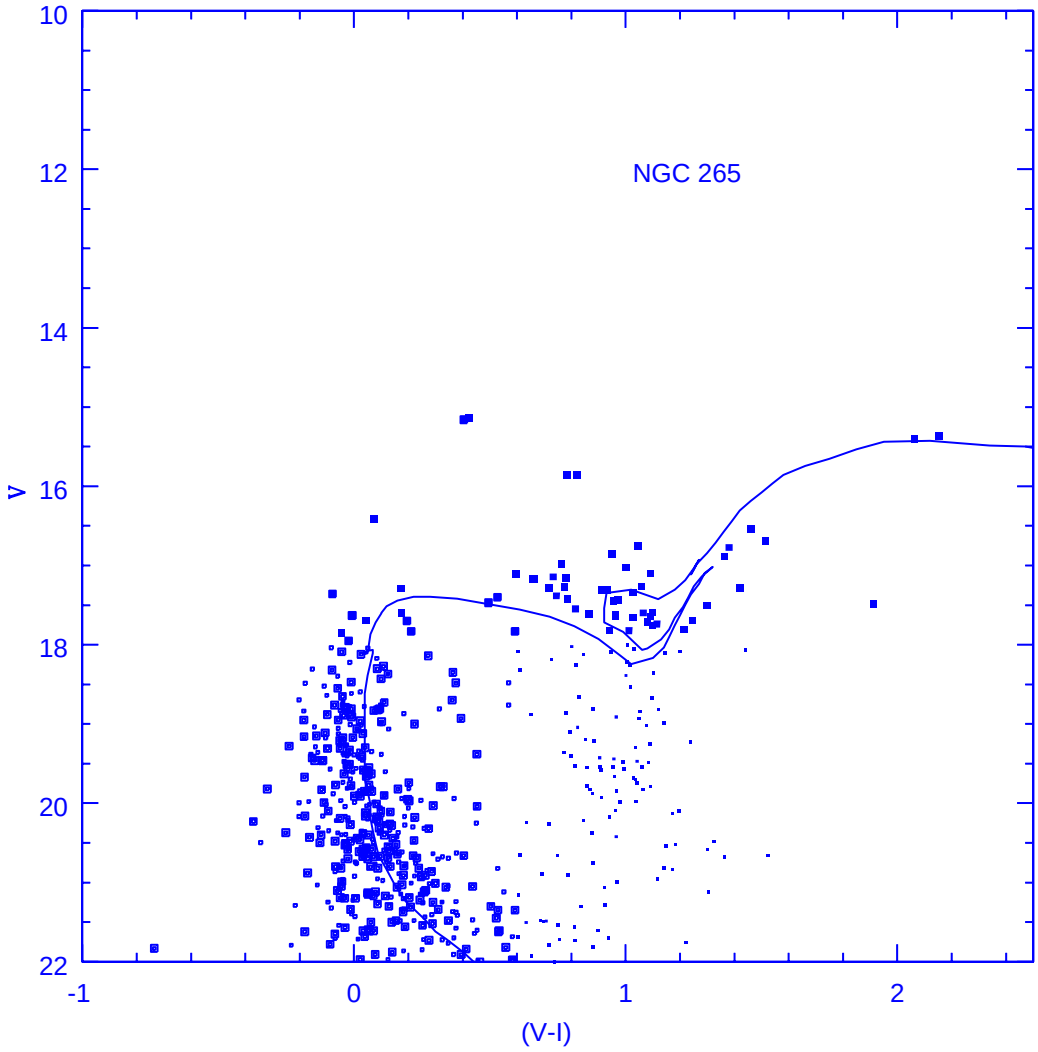

Figure 2.4: CM diagram of cluster NGC 265 showing field stars (light dots) and cluster stars (heavy dots). An isochrone having Z=0.008 and an age of 2.5 $\times 10^8$ is over-plotted on the data

to V=20.5 mag in the most and in the least crowded fields, respectively. For magnitudes brighter than V=20.5, the incompleteness correction is not very significant in the field population. The 50% level is reached at about V=21 mag in the most crowded fields. This means incompleteness correction is suitable not only for the field population, but as well for sparse clusters. Inside dense clusters the completeness might be very different. In order to estimate the incompleteness correction in these objects, we compare the region of NGC 269 we observe and of which we estimate the completeness, with OGLE data. We select the core of dense clusters. The incompleteness correction we derive for the field population is in agreement with the nominal values by Udalski et al. (1998). Inside the radius of the densest clusters given by Bica and Dutra (2000), the OGLE data are complete at 80%, 70% and 50% level at magnitudes V=19.0,19.5,20.3 respectively. This correction is then applied to derive the ages of dense clusters.

2.4 Cluster age distribution

In this Section we derive the age distribution of the SMC clusters located in the main body of the SMC using isochrone fitting. The catalog of the studied objects along with coordinates and radii is taken from Bica and Dutra (2000). 82 clusters and associations are identified in the region centered on NGC 269, while 229 clusters and about 164 associations are studied in the OGLE regions. The cluster list, their coordinates, and the derived ages are available from the authors upon request and are available on Vizier CDS Strasburg. In this Section, we first describe the method, and we compare the age determination with previous studies, then we present the spatial distribution of clusters of different ages.

2.4.1 The Method

The age and the reddening of each cluster are derived by means of isochrone fitting on the CMDs in two ways, by visual inspection and by χ^2 minimization. Isochrones are taken from the library of Girardi et al. (2002). The main body of the SMC is a highly crowded region. For this reason, field star contamination severely hampers the age determination. Field subtraction is a critical issue in order to derive the cluster ages. When ages are derived by visual inspection, then field stars are statistically subtracted from the CMDs of the clusters. First we consider an equivalent area of the field close to the area of the cluster, but outside the cluster radius given by Bica and Dutra (2000). Then, the CMDs of both cluster and field are divided in boxes of size $\Delta V = 0.5$ and $\Delta(V-I) = 0.2$. The incompleteness correction is taken into account by dividing the field and cluster CMDs in magnitude-color bins and then adding on each bin having N_{th} stars, $\Lambda \times N_{th}$ objects, where Λ is the smallest of the V and I completeness factors. Then, in each box of the cluster CMD, for every field

star, the closest cluster star is subtracted. Finally isochrones are superimposed on the CMDs in order to fit the location of the main sequence and of the evolved stars. When the ages are derived using a χ^2 minimization, first single stellar populations at changing ages are generated using a Monte Carlo method, taking into account the observational errors on the magnitudes. Then the simulations are corrected for incompleteness, subtracting on each bin $(1 - \Lambda \times N_{th})$ objects. The observational field population corrected for the ratio of the field and cluster incompleteness factors is derived as described in the previous paragraph and added to the simulated CMDs. Then the CMDs are divided into bins of 0.2 both in mag and in colour and the χ^2 function of the difference between the observational CMD and the theoretical ones at changing ages is minimized. A mean metallicity of Z=0.008 is assumed, in agreement with observational determination for young objects (Pagel and Tautvaišienė, 1999). However, when the isochrone fitting requires it, a different metal content is adopted. Clusters in which the age values derived in both methods are in reasonable agreement are included in Table 10.1 and a mean value of the age is given. Table 10.1, given in the appendix, contains the catalog of the clusters, their position, ages, and reddening. Due to the limiting magnitude of the photometry, clusters having turnoff magnitude fainter than V=21.5 mag in our NGC 269 region data, or V=20 in OGLE fields cannot reasonably be identified. This sets a limit of 3 or 1 Gyr, respectively (assuming Z=0.008), to the oldest age we can derive. For homogeneity, we restrict ourselves to study clusters younger than 1 Gyr. To minimize the effect on the age determination of the young clusters and associations due to the saturation limit of the OGLE photometry we make use of the bright star catalog and of the catalog of stars of known spectral type by Massey (2002). To test our method and derive the uncertainties on the age determination, we perform Monte Carlo simulations where synthetic clusters at different ages are generated, field contamination is included and ages are re-derived using χ^2 minimization. Ages derived from integrated colours suffer from several effects such as discreteness of isochrones, patchy distribution of the interstellar reddening producing artifacts and spurious peaks in the age distribution (de Grijs and Anders, 2006). Those effects are less relevant when ages are derived from CMD fitting. Interstellar extinction plays a minor role on the determination of the ages from the main sequence turnoff location. Uncertainties on the interstellar extinction are of the order of $\Delta(A_V) \sim 0.1$. In the age range under discussion, this results in an uncertainty of about 0.03 on log(age). The uncertainties on the age determinations are partly a function of the age itself, in the sense that older clusters are less easily identified, and partly a function of the cluster density. $\Delta(Log(age))$, the errors on log(age) are of the order of 0.22 taking into account the uncertainties on the metal content for relatively dense objects younger than about 2 $\times 10^8$ yr. A poor age resolution is expected for objects younger than 1 $\times 10^7$ yr due to the difficulty of distinguishing massive main sequence and evolved stars, in absence of spectroscopic information. Uncertain membership can further

complicate the age determination of those clusters/associations. In addition, the youngest age in the Padova isochrones is Log(age(yr))=6.6. Objects younger than this limit are therefore assigned to this minimum age. Clusters older than 2 $\times 10^8$ yr have a mean error $\Delta(Log(age)) \sim 0.3$. This uncertainty is mainly due to the fact that Padova isochrones have problems to reproduce both the turnoff and the luminosity of the clump of He-burning stars in the above age range. Very sparse clusters having less than 50 members might have highly uncertain determinations ($\Delta(Log(age) > 0.5$), especially at old ages.

In Fig. 2.4 we present as example the CMD of NGC 265, one of the bright clusters in the region surrounding NGC 269. The CMD is fitted with an isochrone having Z=0.008 and an age of 2.5 $\times 10^8$ yr. It is evident that it is difficult to reproduce the colour of the main sequence and the location of the red evolved stars at once. This is a well known problem. Differential reddening can mimic this effect. However it cannot be excluded that the uncertainties affecting the opacities, and/or the adopted value of the envelope mixing length are responsible of this discrepancy. In Table 10.1 an index gives the degree of reliability of the age measurement we estimate. Class 1 indicates objects having $\Delta(Log(Age(yr))) < 0.3$; class 2 indicates objects having $0.3 < \Delta(Log(Age(yr))) < 0.5$; class 3 indicates objects having $\Delta(Log(Age(yr))) > 0.5$.

In Fig.2.5 the cluster ages derived in this paper are compared for the common objects to those obtained via isochrone fitting by Pietrzynski & Udalski. Our ages are broadly correlated to those presented there. No systematic difference is present. The dispersion about the line 1:1 correlation for the whole sample is σlog(age) = 0.3. We compare our ages with the compilation by Rafelski and Zaritsky (2005) where 204 star clusters are identified and their ages are derived using integrated colours. In principle the color of a stellar population provides a reliable chronometer to date clusters. In practice however, as already pointed out by Rafelski and Zaritsky (2005) stochastic effects on the number of bright stars, uncertainties on the metallicity and on the adopted stellar models make it difficult to precisely infer the cluster formation. Fig. 2.6 shows the comparison between ages derived via isochrone fitting by us and via integrated colours by Rafelski and Zaritsky (2005) (for Z=0.004). Neglecting a few outliers, the dispersion around the 1:1 correlation line is σLog(age)/$Log(age)$ = 0.4. A reasonable agreement is found. The outliers having very large uncertainties are all inside large groups of clusters having small separation along the line of sight or they are very sparse objects. In these clusters to derive star memberships on the basis of photometric information is a cumbersome affair.

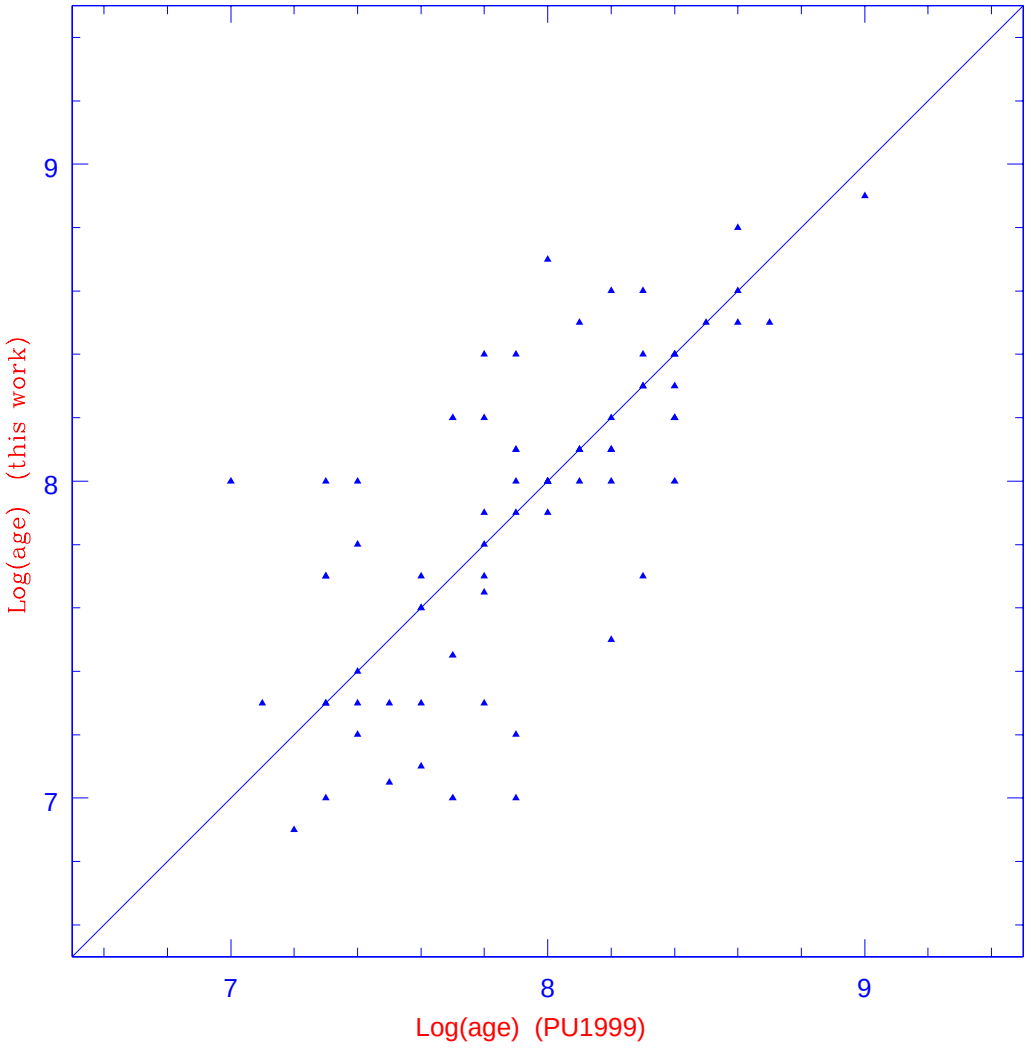

Figure 2.5: Cluster ages derived in this paper are compared with the ages by Pietrzynski & Udalski (1999) for the clusters in common. The solid line shows the loci of the 1:1 correlation

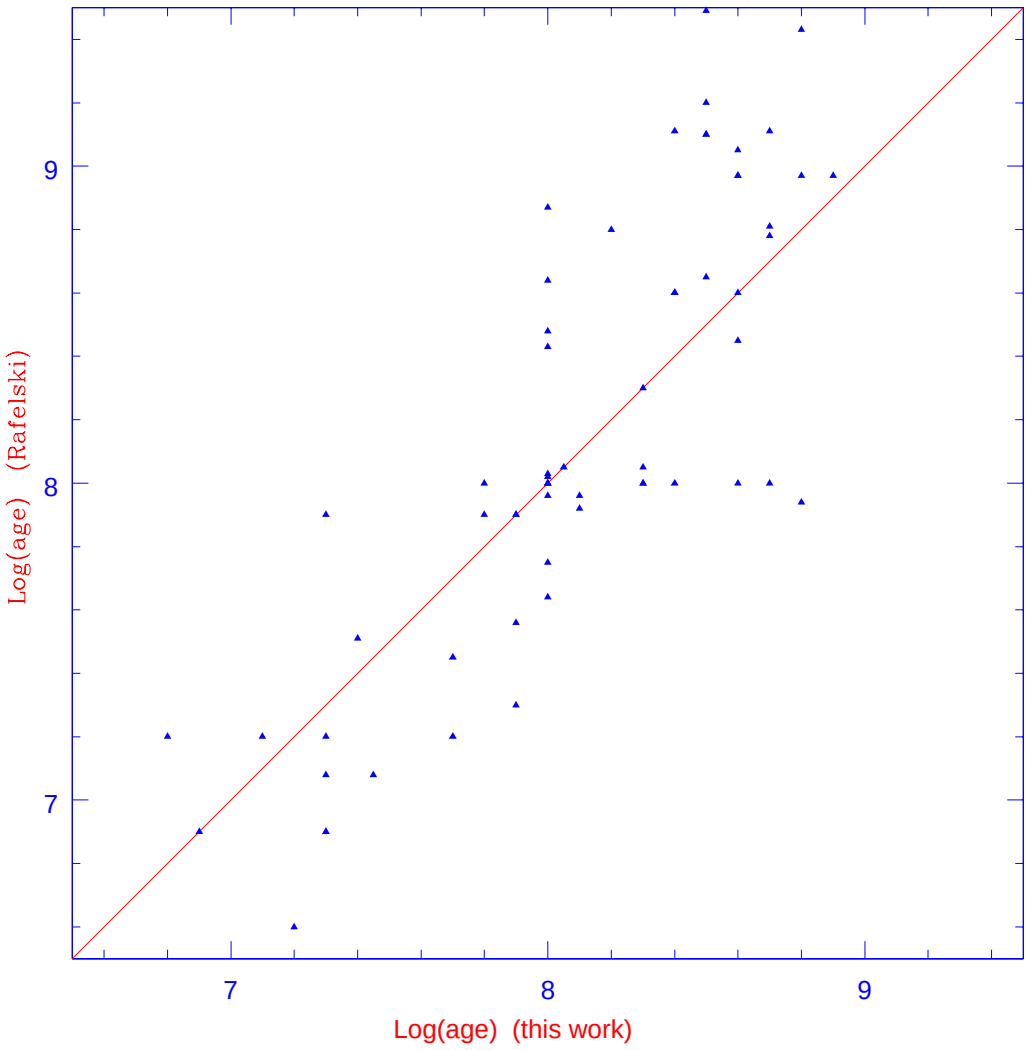

Figure 2.6: Cluster ages derived in this paper are compared with the ages by Rafelski and Zaritsky (2005) (indicated by the label Rafelski) for the clusters in common. The solid line shows the loci of the 1:1 correlation

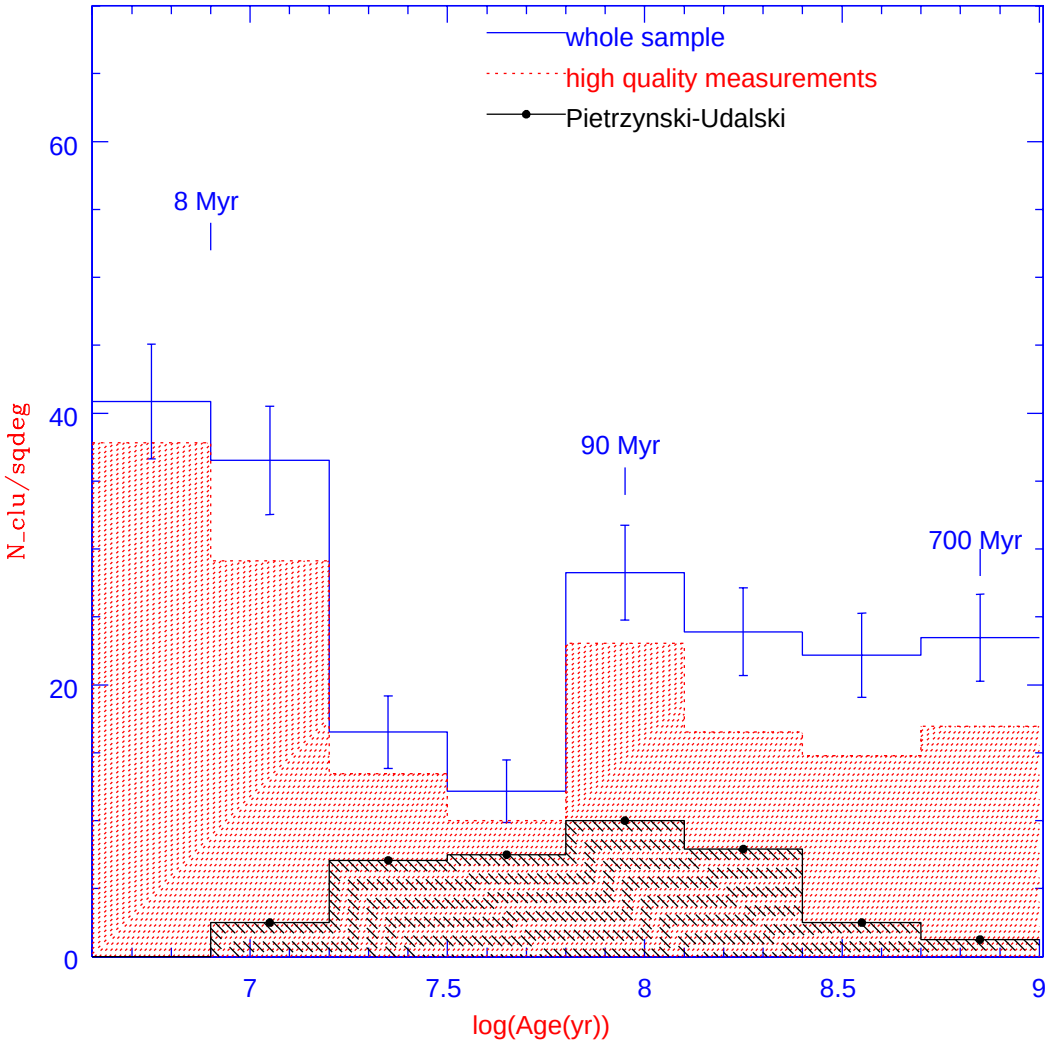

Figure 2.7: The cluster age distributions. The continuous line shows the whole sample discussed in this work. The dotted dashed histogram represents the high quality measurements of ages (classes 1 and 2 of Table 10.1). Squares indicate Pietrzynski and Udalski (1999) sample

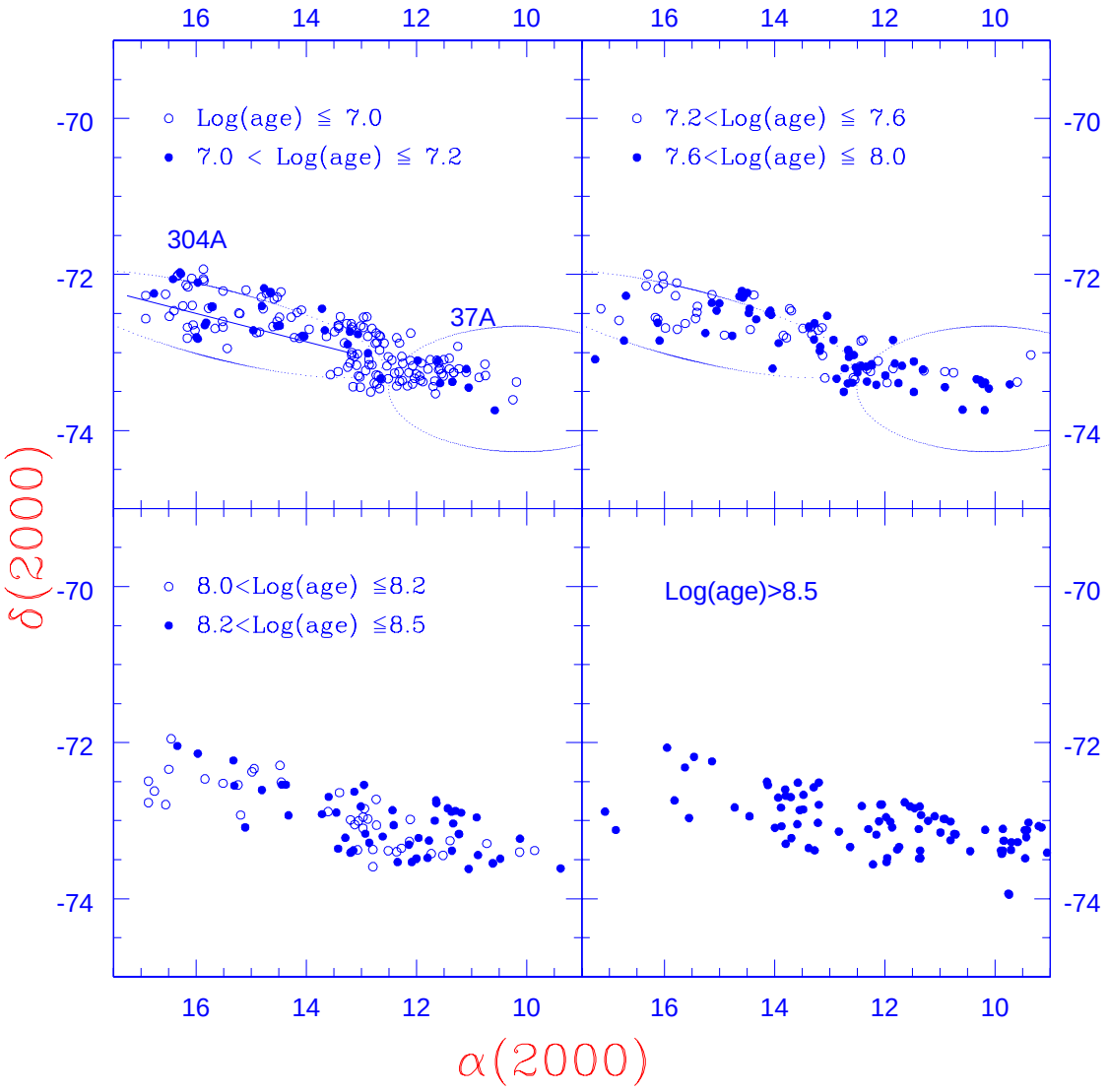

Figure 2.8: Spatial distribution of clusters of different ages in the SMC. The approximate locations of the super-shells 37A and 304A are shown

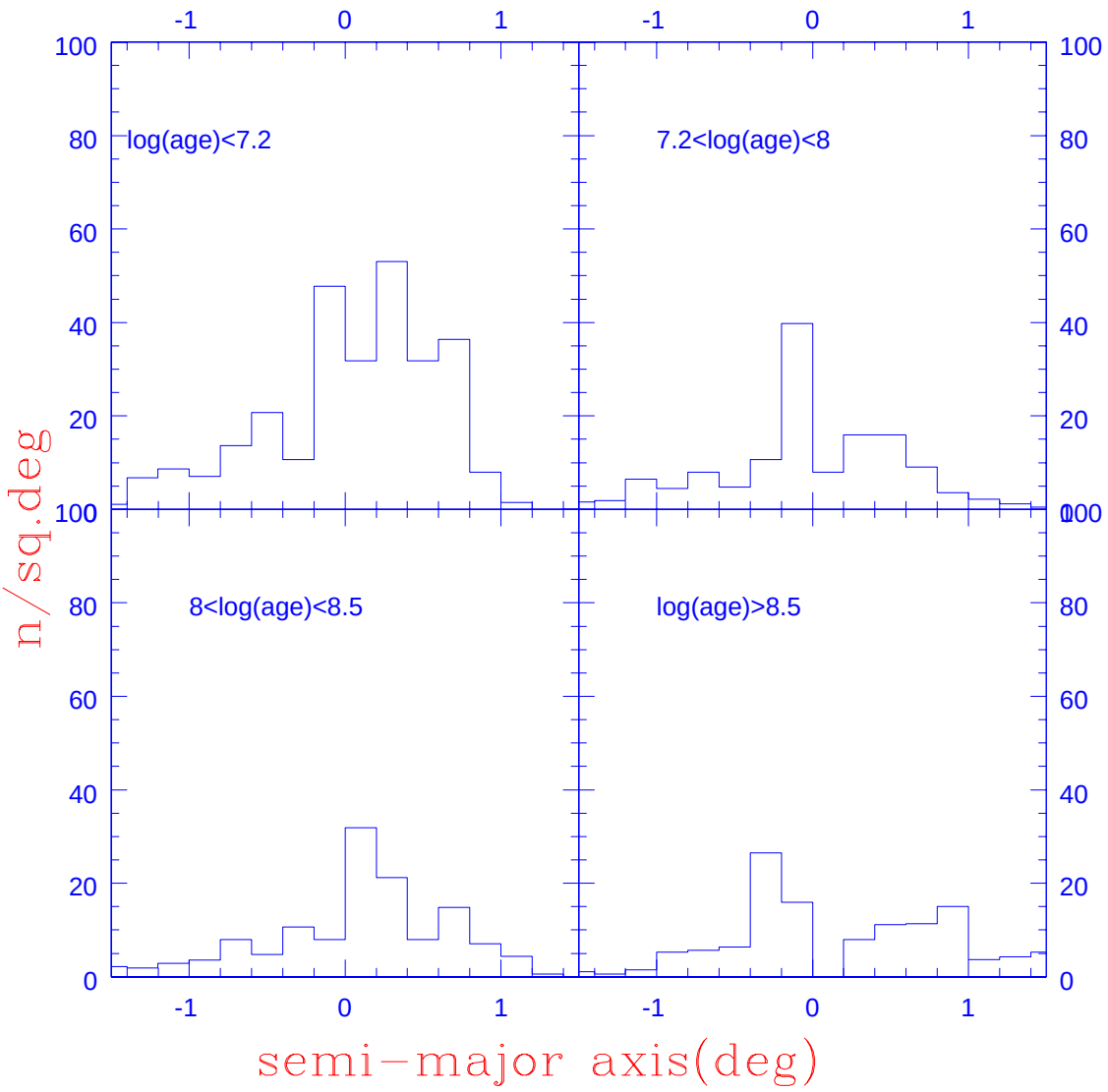

Figure 2.9: Cluster distribution as a function of distance from the SMC centre at changing ages. Negative axis values indicate the regions East of the centre, while positive axis points toward the West

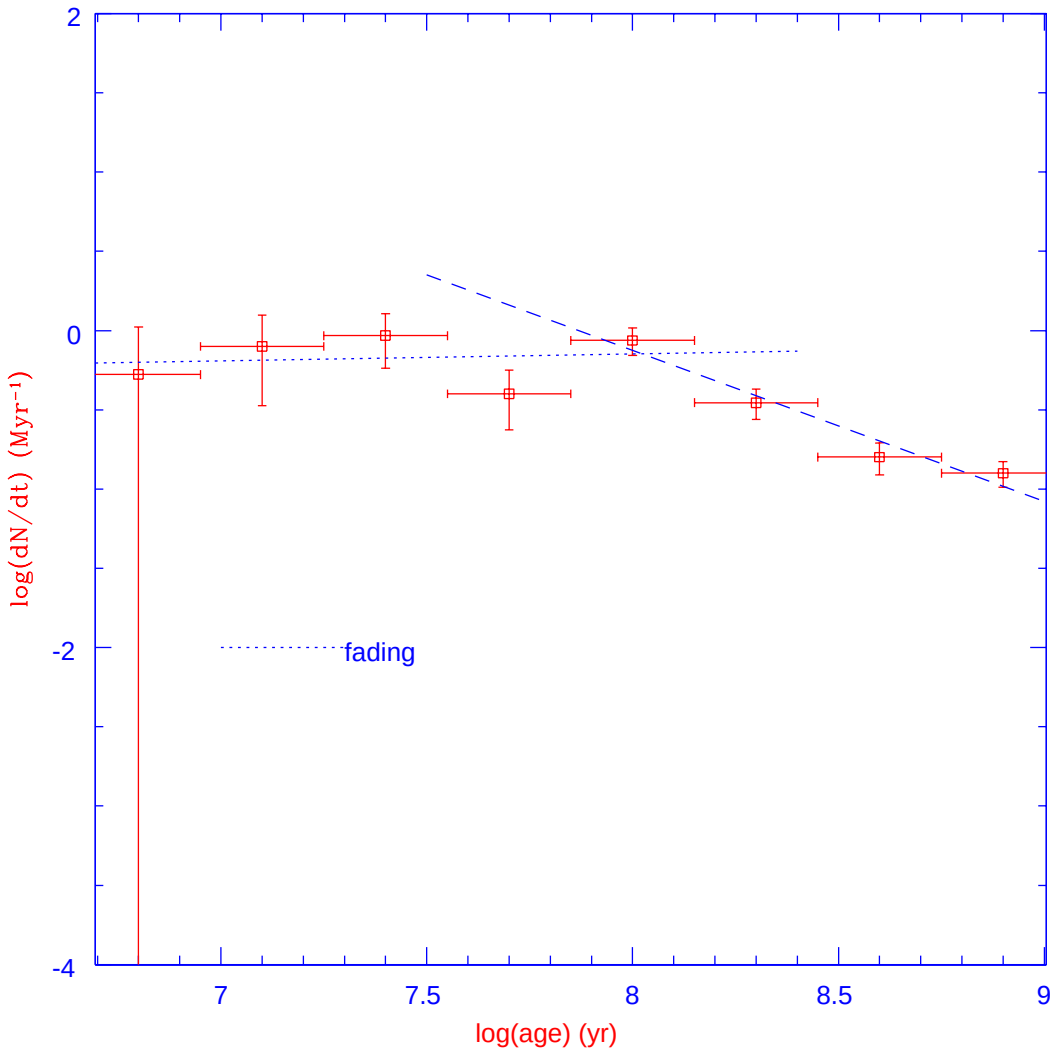

Figure 2.10: Cluster age distribution(squares). Only objects classified as C are included in the sample. The data are fitted by two lines. The dotted line represents the fading line, while the dashed line is the fit for ages where most likely the disruption and the sample incompleteness dominate fading

2.4.2 Cluster age distribution in the main body of the SMC

The age distribution of the clusters in the studied regions is shown in Fig. 2.7. Two main episodes are found, the first from 5 to 15 Myr, the second at 90 Myr about. This latter is followed by an almost constant rate till 1 Gyr. The uncertainties on the age determinations do not allow a finer age resolution. We point out that these peaks are present in the whole sample and in the clusters having the most reliable age measurements (classes 1 and 2 in Table 10.1). It is worth noting that our age distribution significantly differs from the one obtained by Pietrzynski and Udalski (1999) in particular in the range of young ages (about $log(age) < 7.5$ yr). To single out the reason of it is not easy. Different sampling of the objects over a region in which star formation was less efficient and in general somewhat older than in our sample? Different estimate of the age of younger clusters assigning them a slightly older age? The present data does not allow us to elucidate the point.

Looking at the spatial distribution of the clusters (see Fig. 2.8), it is evident that clusters in a given age range are not uniformly distributed across the SMC, but the bursts are associated with localized enhanced SFR. Since rotational mixing did not have enough time to smooth the cluster distribution, this points in favour of the fact that these SFR enhancements are not due to artifacts in the age determination procedure, but are likely real.

To describe the spatial distribution of the clusters, we model the SMC disk as an ellipse centered at $\alpha = 00^{\rm h}\ 52^{\rm m}\ 45^{\rm s}$, δ =-72 $^\circ$ 49 $'$ 43 $''$ (J2000) (Crowl et al. 2001) and having an axial ratio $b/a = 1/2$. Then we define the distance along the major axis as the major axis of the ellipse having the same centre and axial ratio and passing on the object. Fig.2.9 presents the distribution of the clusters per area unit at changing ages as a function of the distance from the SMC centre. A complex picture is emerging. Two main regions located East and West of the centre were active at very young ages (< 15 Myr), while the cluster formation process was less significant 100 Myr ago. These regions can be identified with the two HI super-shells 37A and 304A. More detail can be found in the following sections, where the two regions will be analyzed.

Finally, we address the question whether the age distribution we find is representative of the cluster formation rate or whether the tidal field of the SMC was effective in disrupting the less massive clusters. Following the discussion by Boutloukos and Lamers (2003), in a survey of clusters having a given magnitude limit, two effects contribute to the age distribution of clusters born at a time t_0. The first is the fading. Clusters get fainter with time as a result of the evolution of their stars. As a result, the number of observable clusters as a function of age for a given magnitude limit is decreasing. This effect is dominant for young objects. The second is the

cluster disruption due to the galactic tidal field and is relevant for old clusters. A steep slope of dN_{obs}/dt is expected. The mass of a cluster decreases almost linearly with time, until the cluster is finally disrupted. This defines the disruption time, t_{dis}. Ignoring burst, the mean cluster formation rate might be assumed as roughly constant. Under this hypothesis, a slope change in the distribution dN_{obs}/dt is expected at a time t_{cross} where the effects of the disruption begin to be significant. t_{cross} depends on the photometric evolution of the stellar populations, but is as well a function of the magnitude limit of the cluster sample. Fig.2.10 presents dN_{obs}/dt, the observed age distribution of the SMC clusters. Only objects classified as type C by Bica and Dutra (2000) are included in the sample. The age distribution of the SMC clusters is rather flat for objects with ages below log(t)=8.0 and decreases steeply at higher ages. This identifies t_{cross}. It cannot be excluded that the sample of clusters we discuss is biased toward dense and massive objects which are more easily recognized than less dense or lower mass objects. However the fact we find a flat distribution at young ages supports the idea that selection effects, fading and incompleteness play a minor role for clusters younger than this limit. In principle t_{dis} can be derived from t_{cross} and the slope of the disruption line. However in our case, the fact that the completeness correction of the cluster sample is substantially unknown prevents any determination. In fact the sample of ages we derive is probably not complete especially at old ages. We remind that the SMC cluster disruption time derived in literature is of the order of 8×10^9 yr (de La Fuente Marcos, 1997; Boutloukos and Lamers, 2003). There are opposite opinions about the distributions of clusters in the SMC, specifically in the interpretation of the dN/dT distribution. Gieles et al. (2007) support the idea that there is no relevant cluster dissolution in the SMC clusters explained with a weak tidal field internal to the SMC, on another direction goes the work of Chandar et al. (2006); de Grijs and Goodwin (2008), determining a significative infant mortality of SMC clusters.

2.5 Final remarks

We have derived the ages and age distribution function for a large sample of clusters in the main body of the SMC. The age of 311 clusters and 164 associations is determined through isochrone fitting method. For a selected number of clusters, the ages we have obtained are compared with those estimated by other authors. The corresponding age distribution function is also compared with others in literature. We have also looked at the spatial distribution of clusters of different age with respect to the distance from the SMC centre and two super-shell regions. The main results of this analysis are that

"the cluster age distribution supports the idea that clusters formed in the last 1 Gyr of the SMC history in a roughly continuous way with periods of enhancement. The

age distribution of the clusters in the whole disk presents enhancements, namely between a few Myr and 15 Myr and at 90 Myr. Old objects are mainly located close to the SMC centre and on the SW side. Models of the interactions between LMC-SMC and Milky Way predict a close encounter between the MCs roughly 100–200 Myr ago. At that time the star formation is expected to be enhanced not only in the tidal arms, but also in the main body of the SMC. In fact an episode at 90 Myr is found in the age distribution of the clusters that might be due to tidal trigger. However the age distribution presents younger episodes that might have different origin and are possibly due to local phenomena."

Chapter

3

Three clusters of the SMC: NGC265, K29, and NGC290

3.1 Introduction

The aim of this chapter is to derive better estimates of the age and metallicity of three clusters of the SMC, to check the ages derived in chapter 2, and to evaluate the slope of their initial mass function (IMF) down to $M \simeq 0.7 M_{\odot}$.

The clusters under investigations are: NGC265, K29, and NGC290. They are located at the border of an hydrogen shell in the north-western part of the SMC. The first object, NGC265 is an intermediate age object with age Log(Age)=8.5 while the other two are younger objects with an age respectively Log(Age)=8.0 and Log(Age)=7.8. A former determination of the age was already given in the previous chapter but in this case we make use of HST data. These data have a lower completeness limit in magnitude that allows us to fit the main sequence down to a mass limit of $0.7 M_{\odot}$. We will discuss later the technique of luminosity function fitting. We also give an estimate of metallicity, reddening and IMF of these three clusters. At the end we also discuss the presence of overshoot in the cluster population comparing different models of population synthesis.

In section §3.2 we present the data and describe the reduction procedure. In section §3.3 the techniques used to derive age, metal content and IMF are described. In section §3.4 the physical parameters of the clusters are derived and the problem of convective overshooting in the stellar models is investigated. In section §3.5 some

Table 3.1: Equatorial coordinates of three clusters of the SMC.

Cluster	RA (J2000)	DEC (J2000)
NGC 265	0:47:12	-73:28:38
K 29	0:51:53	-72:57:14
NGC 290	0:51:14	-73:09:41

preliminary conclusions are drawn.

3.2 Data presentation, reduction and calibration

Reduction. We make use of HST archive data taken in 2004 using the Advanced Camera Survey (ACS/WFI) in the filters F555W and F814W. Two exposure times per filter are available, namely 120s and 440s. We make use of pre-reduced data that are already corrected for the geometric distortion of the camera. The data reduction is made with the DAOPHOT II/ALLSTAR packages by Stetson(1994). In brief, the aperture photometry is calculated with an aperture of 3 pixels; the point spread function (PSF) is derived for each colour and each CCD, and the PSF photometry is performed. Data are finally corrected for the charge transfer efficiency (CTE) using the Dolphin (2000a) transformations. This correction goes from 0.01 mag for the brightest magnitudes to 0.1 mag for the faintest magnitudes.

Calibration. The transformation from the instrumental magnitudes to the ACS/WFI-Vega system, taken from Bedin et al. (2005), is given by

$$\begin{aligned} m_{filter} \equiv \quad & -2.5 log_{10} \tfrac{I_{e^-}}{exptime} + Z_p^{filter} \\ & -\Delta m_{PSF-AP(r)}^{filter} - \Delta m_{AP(r)-AP(\infty)}^{filter} \end{aligned} \tag{3.1}$$

with $Z_p^{F555} = 25.718$ and $Z_p^{F814} = 25.492$ (Bedin et al., 2005).

The aperture correction consists of two terms: the first compares the PSF magnitudes with the aperture magnitudes at a finite magnitude (3 pixels in our case) and the second is the difference between aperture magnitude at finite size and magnitude at infinite aperture. The first term tabulated in Table 3.2 is statistically calculated for the brightest magnitudes as the mean difference. We assume as aperture corrections from r=3 pixel to infinity the value given by Sirianni et al. (2005): $\Delta m_{AP(r)-AP(\infty)} = 0.243$ for F555W filter, $\Delta m_{AP(r)-AP(\infty)} = 0.291$ for F814W filter.

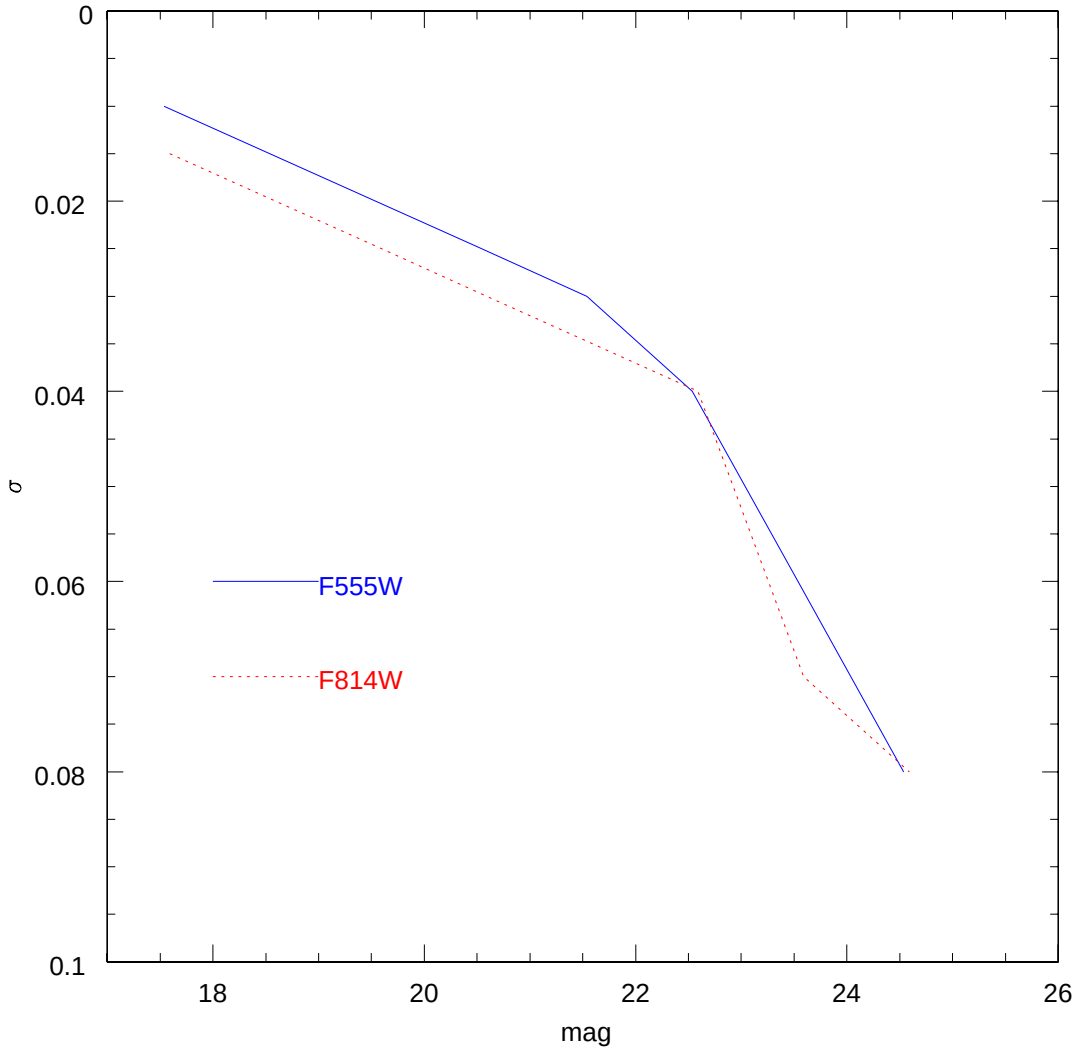

Figure 3.1: Mean photometric errors σ as function of the magnitude for the F555W and F814W pass-bands for the studied fields

Table 3.2: Aperture corrections for both filters F555W and F814W. CCDs are split in 2 parts: the upper row (1) refers to the cluster whereas the lower row (2) to the field.

Cluster		$\Delta m^{F555W}_{PSF-AP(3pix)}$	$\Delta m^{F814W}_{PSF-AP(3pix)}$
NGC 265	(1)	-0.14 ± 0.02	-0.18 ± 0.04
	(2)	-0.15 ± 0.02	-0.21 ± 0.03
K 29	(1)	-0.14 ± 0.02	-0.19 ± 0.02
	(2)	-0.15 ± 0.02	-0.19 ± 0.03
NGC 290	(1)	-0.14 ± 0.02	-0.18 ± 0.02
	(2)	-0.13 ± 0.02	-0.18 ± 0.03

ACS/WFI magnitudes are converted to the Johnson-Cousins V, I following Sirianni et al. (2005). The magnitudes are compared with V,I ground-based data from OGLE II (Udalski et al., 1998) survey for NGC 265, K 29 and NGC 290. We make use of the stars brighter than V=18 and fainter than V=17 to avoid deviation from linearity due to saturation on HST data. The mean magnitude differences are $\Delta_V = V(HST) - V(OGLEII) = 0.02 \pm 0.04$ and $\Delta_I = I(HST) - I(OGLEII) = 0.01 \pm 0.04$. These small differences allow us to take the magnitudes of the saturated stars in the ACS photometry from OGLE II catalog (see following Sections for more detail).

We estimate the photometric errors in the two pass-bands by means of the artificial stars experiments as the difference between the assigned and recovered magnitude for any simulated star. The results are shown in Fig. 3.1 as a mean of all the studied fields. This is justified by the fact that differences between the fields are not relevant.

The observational CMDs of the three clusters are presented in the top left panels of the Figs. 3.2, 3.3 and 3.4. They will be examined in detail below. They refer to a circular area of 22" radius inside which the vast majority of the cluster stars falls as shown by the surface brightness profiles in the top right panels of the Figs. 3.2, 3.3 and 3.4 (see the discussion in the following Sections).

Incompleteness. Correction for incompleteness is derived as usual by means of artificial star experiments where artificial stars of known magnitude are added to the original image and data are re-reduced. The number of injected stars is about 10% of the total number of stars in the CCD. The ratio between the number of recovered stars and the original number of added stars gives the completeness correction Λ.

The results are shown in the bottom right panels of the Figs. 3.2, 3.3, and 3.4 which present Λ as function of the magnitude for the inner radius of the clusters (22") and for the external regions. More details can be found in the sections below.

3.3 Method to derive ages, metallicities and IMFs

Age, metal content and IMF are estimated by comparing theoretical luminosity functions (that depend on the three parameters under examination) to the observational ones and by plotting the corresponding isochrones on the CMD to check the mutual consistency of the results. The determination is first made by visual inspection and is refined with the aid of χ^2 minimization. Theoretical luminosity functions and isochrones are taken from the library of Girardi et al. (2002).

Corrections for completeness and field subtraction are the preliminary step to be undertaken to derive good experimental luminosity functions. We proceed as follows:

1. Equal areas are considered for each cluster and companion field.

2. The luminosity interval spanned by the cluster and field stars in each pass-band is divided in number of intervals of 0.5 mag width. In each interval, and separately for the cluster and field, we count the stars and apply the correction for incompleteness (the cluster and field completeness factors are used as appropriate) and finally we calculate the ratio

$$N_{true} = \frac{1}{\Lambda} \times N_{obs} \tag{3.2}$$

where Λ is the completeness factor.
3. In each magnitude interval the field stars are statistically subtracted from the cluster stars.

4. The above procedure is applied to derive both the luminosity function and the CMD of the cluster. The corrected luminosity function for each cluster is presented in Figs. 3.7, 3.8 and 3.9 together with its theoretical counterparts, see below.

5. From the Girardi et al. (2002) isochrone library we select one of suitable age and metallicity that best matches the CMD paying particular care to the location of the main sequence and of the evolved stars. Once the above estimates of age and metal content are obtained we refine them by means of the χ^2 minimization of the luminosity functions. We start from the previous estimates, use the Padova

simulator of synthetic CMDs that can take the photometric errors on magnitudes into account, and apply the Monte Carlo technique to generate many simulations of the luminosity function and companion CMD at varying age, metallicity and slope of the IMF. Finally the χ^2 minimization technique is applied to pin down the best combination of the three parameters.

The IMF is derived in the mass range from the turnoff mass to the limit set by the completeness of the photometry, i.e. at about $0.7M_{\odot}$. We assume an IMF of the form:

$$dN \propto M^{-\alpha} dM \tag{3.3}$$

where the slope α is a free parameter and is derived in two mass ranges, namely $0.7M_{\odot} < M < 1M_{\odot}$ and $1M_{\odot} < M < 4M_{\odot}$. In the adopted notation, the Salpeter slope is $\alpha = 2.35$.

Binary stars. A large fraction of stars in clusters and fields are unresolved binaries, either physical binaries or chance superposition of stars along the line of sight. Their presence blurs the main sequence, the giant branch, the clump of red stars, and the loop, thus making it more difficult to derive precise estimates of age, metallicity and IMF slope. Particularly cumbersome is the use of the turn-off or termination magnitude of the main sequence to infer the age by fitting isochrones and luminosity functions when binaries are present. The effect of unresolved binary stars on the CMD and luminosity functions of stellar clusters has been investigated in many studies among which we recall Chiosi et al. (1989a) Vallenari et al. (1991) and Barmina et al. (2002). As long known, the presence of unresolved binaries would first brighten the turn-off and termination magnitude and broaden the main sequence. Second if the photometry is particularly good they would even split the main sequence into two parallel loci, the one of unresolved binaries being systematically cooler and brighter (about 0.7 mag for binary stars of equal mass) than that of single stars, thus facilitating the task of assigning the true age and metallicity. Our present data do not allow this. Therefore we are left with the brightening of the turn-off and termination magnitude which would mimic a younger age and also yield a different slope for the IMF in the upper mass range. For the three clusters under examination we do not have information on their percentage of binary stars nor on the distribution of the mass ratio and separation of the components. Despite this, we apply the synthetic CMD technique to include the effect of unresolved binaries. We assume that binary stars obey the same IMF of single stars and the mass ratio falls in the range 0.7 to 1. Systems with mass ratios different from these cannot be excluded. However they would be hardly distinguishable from single objects. Finally, we suppose that the percentage of unresolved binaries is the same as indicated by open clusters of the Milky Way that amounts to about 30 % – 50 %

of the cluster population (Mermilliod and Mayor, 1989; Carraro et al., 1994), and other well studied clusters of the LMC such as NGC1818 (Elson et al., 1998) and NGC1866 (Barmina et al., 2002). Here we adopt 30% for all the three clusters.

3.4 Physical parameters of the clusters

In this Section, we first discuss the field population, then we derive the brightness profile, and finally we determine the age, metallicity , IMF slope of each cluster.

3.4.1 Field population contamination

The sampling of the field population is a critical issue for surface profile determination and for the determination of the luminosity function. The field contaminations of the three clusters are marginally different, (see Fig 3.5) indicating an inhomogeneous distribution. For this reason and because of the relatively small size of the field of view of the ACS, we are forced to sample the field population close to the cluster centre. We sample the field population at about 1.6' from the cluster centres. To make it sure that the cluster population does not significantly affect the field sample, we compare the LFs of the field population taken in this way with the field population taken from OGLE II data at a distance of about 1 deg. from the cluster centres down to a magnitude of V=21, where the completeness of the OGLE II data becomes critical. Fig 3.5 shows that, once that the LFs are normalized to an equal area, the samples of field population close to the cluster are statistically comparable to the more distant ones. This suggests that the contamination by cluster stars inside the area selected to represent the field is probably not very relevant.

3.4.2 Surface brightness profiles

In this Section, we derive the surface brightness profiles of each cluster. The profiles will be then compared with King (1962) and Elson et al. (1987) to determine the parameters of the clusters. First, pixel coordinates of each star are converted into the absolute coordinates α and δ using the task IRAF STSDAS xy2rd. Then, the centre of the cluster is determined calculating the luminosity weighted centroid at increasing radii. The photometry of the stars saturated in the ACS/WFI observations are taken from OGLE data, then they are converted to the F555W pass-band and finally used to construct the surface brightness profile. We are confident that this does not introduce errors in the derived profiles since the consistency of the OGLE II photometry in the V magnitude with ACS/WFI HST V calibration was checked in the previous Sections. Many SMC clusters have elliptical isophotes. This

is not the case of the objects studied in this paper, having only moderate ellipticity $(1 - b/a) \sim 0.13 - -0.3$ (Hill and Zaritsky, 2006). For this reason, we make use of circular apertures in the profile calculation. Because of the high resolution of our images, the surface brightness given as $Log(f)$ inside the i-th circle having radius b_i is obtained simply by adding up the flux of the stars falling inside the circle itself:

$$log(f) = 1/(\pi b_i^2) \times \sum_j \Lambda_j F_j$$

Λ_j in the above formula is the completeness factor inside the ring and F_j the stellar flux. Crowding can cause significant number of stars to be missed by ALLSTAR. Their flux can affect the surface brightness profile and must be accounted for. This is the reason why the completeness correction is applied to the flux determination. We restrict the determination of the surface profile to the area completely falling inside the small field of view of the ACS/WFI camera. In all the cases, the profiles have maximum radii of log(r)$\sim$ 1.5 arcsec.

The sky background subtraction is a critical step in the determination of the surface profile especially in the outer regions of the cluster. The field population is sampled as discussed in the previous Section, the contamination is calculated as the mean flux in a field area of about $22''$ and is finally subtracted.

Two families of models are fitted on the brightness profiles. The first one is the tidally truncated King functions (King, 1962) having the form:

$$f(x) = \pi r_c^2 k \left[ln(1+x) - 4\frac{(1+x)^{1/2} - 1}{(1+x_t)^{1/2}} + \frac{x}{1+x_t} \right] \tag{3.4}$$

with $x = (r/r_c)^2$ and $x_t = (r_t/r_c)^2$ where k is a constant and r_t and r_c are the searched parameters, specifically r_t is the tidal radius and r_c is the core radius.

The second one is the Elson et al. (1987) family of functions having the form:

$$f(r) = \frac{2\pi\mu_0 a^2}{\gamma - 2} \left[1 - \left(1 + \frac{r^2}{a^2} \right)^{1-\gamma/2} \right] \tag{3.5}$$

where a is a scale length and γ is the power law index. These models are essentially the same as the King models, but they do not assume tidal truncation. The parameter a is related to the King core radius r_c by:

$$r_c = a(2^{2/\gamma} - 1)^{1/2}$$

The fitting of the profiles is achieved using χ^2 minimization. The uncertainties on the profiles are calculated as Poisson errors.

Results and comparison with previous work

Figs. 3.2, 3.3, 3.4 present the surface brightness profiles of each cluster and Table 3.3 gives the derived parameters. The core radii obtained using Elson et al. (1987) and King profiles are substantially in agreement, as expected since the main differences between the models arise at larger radii. The tidal radius is quite uncertain, first because it is strongly depending on the sky subtraction and second, because our photometry does not extend to large enough radii. Table 3.4 compares our results on cluster parameters with those by Hill and Zaritsky (2006). In comparison with our results, their values of r_c are in agreement for NGC 265, but they tend to be overestimated for the other two clusters, especially concerning the fit with Elson et al. (1987) profiles. The values of γ by Hill and Zaritsky (2006) are overestimated for all the clusters.

The question whether MC clusters are tidally limited or not is a long lasting one. King models are expected to describe bound systems that have isothermal and isotropic stellar distribution functions and are limited by a strong tidal field. Elson et al. (1987) models were empirically derived in order to reproduce the profiles of young MC clusters. The lack of tidal cut-off was originally explained with the dynamical youth of those clusters having extra-tidal stars. In this view, a cluster is supposed to evolve or not from an Elson et al. (1987) profile to a King one, depending on the environment and on its individual characteristics. However, on an observational ground, no clear correlation is found between the age of the clusters and the presence of tidal cut-off (Hill and Zaritsky, 2006). Hill and Zaritsky (2006) find that SMC clusters are fitted in a satisfactory way with both models, although King profiles provide a slightly superior fit in $\sim 90\%$ of the cases. McLaughlin and van der Marel (2005) compare King models, Elson et al. (1987) profiles and modified isothermal spheres based on Wilson (1975) models. These latter are spatially more extended than King functions, but still include a finite, tidal cut-off in the density. These authors come to the conclusion that un-truncated power-law distributions, Wilson models and King profiles give comparable fit to MC clusters. McLaughlin and van der Marel (2005) conclude that extended star envelopes around MC clusters may not be transient features due to the age, but more probably halos of self-gravitating objects. Elson et al. (1987) derive for LMC clusters a relation between the core radius and the age. The observed trend probably represents real evolution in the structure of the clusters that are expanding while growing old as a consequence of the significant and rapid mass loss from stellar evolution. This result is confirmed by other authors (we quote as the most recent Mackey and Gilmore, 2003). Noyola and Gebhardt (2007) find that clusters are probably born more concentrated and then evolve towards flatter central profiles. Finally Carvalho et al. (2008) give the idea that profiles deviating from ideal Elson profiles could be traces of possible cluster mergers.

Table 3.3: Core and tidal radius as determined by the fit with the King and Elson functions.

Cluster	King			Elson			
	r_c (pc)	$log(r_t/r_c)$	χ^2	r_c (pc)	a (pc)	γ	χ
NGC 265	2.61	0.75	1.06	1.98	2.85	2.63	1.06
K 29	2.40	2.50	1.27	2.35	2.35	2.01	1.16
NGC 290	0.87	1.50	1.55	0.76	0.76	2.01	1.53

Table 3.4: Structural parameters of the clusters as determined by Hill and Zaritsky (2006).

Cluster	Hill & Zaritsky			
	King		Elson et al	
	r_c (pc)	r_{90} (pc)	r_c (pc)	γ
NGC 265	2.75	11.37	3.51	3.20
K 29	1.22	14.58	5.63	6.00
NGC 290	1.22	14.78	1.83	3.25

The three clusters studied in this work follow the trend already found for the LMC clusters (see Fig.3.6). To verify whether this is a property of SMC clusters, we combine cluster age determinations derived from isochrone fitting by Chiosi et al. (2006) with the values of the King core r_c obtained by Hill and Zaritsky (2006). A large scatter is found, however a core-age relation for SMC clusters seems to be present. Young clusters have more compact core, and the spread in core size is increasing with age. It is less clear why a large scatter is present, suggesting a more rapid expansion for some objects, possibly due to the effect of the surrounding tidal field or to evolution influenced by some external processes (i.e. they are not isolated). A wider discussion of this problem is outside the scope of this thesis and can be found in Elson (1991); Mackey and Gilmore (2003). It cannot be excluded that such a large scatter is due to observational uncertainties on the derived core radius of the clusters. Better quality data are needed before reaching a firm conclusion.

3.4.3 Age, metallicity, IMF determinations

In this Section the age, metal content and IMF determination for each cluster are given.

NGC 265

The cluster population is sampled in a circular region of 22" radius centered on the cluster. This radius is bigger than the core radius of ~ 18" , what assures that the cluster population is well represented. We sample the field population at $1.6'$ apart from the cluster center (see previous sections for a wider discussion of the field population). For field star subtraction of the LF, we consider a field area of $22''$. The field population is statistically subtracted from the luminosity function. Inside the radius of $22''$ about 1000 cluster stars are detected down to F555W=25 where the incompleteness reaches the 50% level. Starting from an initial guess obtained from visual inspection of the CMD, and using the CMD and LF simulator, we derive by means of χ^2 minimization, an age of log(Age)=8.5±0.3 yr, an interstellar reddening of E(F555W-F814W)=0.08±0.06, corresponding to $A_{F555W} = 0.158$ following Bedin et al. (2005), and finally a metallicity of Z=0.004±0.003. All the errors on the determinations of the parameters are given at the 68% confidence level. The top left panel of Fig. 3.2 presents the CMD where the isochrone for the age we have determined is superposed. The turn-off mass is about $4M_{\odot}$. The IMF slope in the mass range $M > 1M_{\odot}$ turns out to be $\alpha_2 = 2.5 \pm 0.5$, while in the mass range $(0.7 < M < 1M_{\odot})$ is $\alpha_1 = 2.4 \pm 0.4$, substantially in agreement with the Kroupa (2000) IMF. We recall that the Kroupa (2000) IMF has $\alpha_1 = 2.2$ for $0.5M_{\odot} < M < 1M_{\odot}$ and $\alpha_2 = 2.7$ for $M > 1M_{\odot}$.

When binary stars are included a slightly older age is found. We add a percentage of binaries of about 30% of the stars. Instead of an age of log(Age(yr))=8.5 we find the best fit at an age of log(Age(yr))=8.7±0.2. As a consequence, the determination of the exponents of the IMF changes. For all the studied clusters, the summary of the IMF determination is presented in Table 3.5. The quality of the fit is shown in Fig.3.7 where the observational LF is compared with the best fit simulation.

K 29

We sample the cluster population inside a radius of 22" where about 700 stars are detected down to $F555W = 25$ mag. As for NGC 265, this radius is larger than the core radius. The field population of K 29 is located outside the core radius (see previous sections for a discussion of the field population).

Table 3.5: The best fit IMF coefficient in the range of low masses α_1 ($0.7M_\odot < M < 1M_\odot$) and in the range of higher masses α_2 ($M > 1M_\odot$) is given for the three different clusters. The 68% confidence interval is also given (σ_1 and σ_2).

No binaries				
Cluster	α_1	σ_1	α_2	σ_2
NGC 265	2.4	0.4	2.5	0.5
K 29	1.8	0.2	2.7	0.3
NGC 290	2.2	0.2	2.7	0.4
Binaries				
NGC 265	2.2	0.4	2.7	0.5
K 29	2.2	0.2	2.7	0.3
NGC 290	2.2	0.2	2.7	0.4

Fig.3.3 (top left panel) presents the CMD of the cluster (inside a radius of 22″), where bright stars saturated in the ACS/WFI photometry are taken from OGLE data, analogously to the procedure adopted in the determination of the brightness. The age derived by χ^2 minimization is Log(Age)=8.2 ± 0.2 yr, the metallicity $Z = 0.003 \pm 0.002$ and E(F555W-F814W) =0.14 ± 0.08. The turn-off mass is about $4.5M_\odot$. The slope of the IMF in the mass interval from $4M_\odot$ to $1M_\odot$ is $\alpha_2 = 2.5 \pm 0.5$, while in the mass range ($0.7 < M < 1M_\odot$) is $\alpha_1 = 1.8 \pm 0.2$ in marginal agreement with the Kroupa law. Observational data are compared with the best fit model in Fig.3.8. When binaries are included, the age of the cluster becomes Log(Age)=8.3 ± 0.2 yr.

NGC 290

Inside a radius of $\sim 25''$ about 660 stars are found. Once more this radius is larger than the cluster core. Evolved stars brighter than F555W=17 mag are beyond the saturation level of the photometry. To cope with this we integrate our data for the red giants with those by OGLE II, whose photometry is converted in the F555W and F814W pass-bands, as described in the previous Sections. Mounting the two sets of data has been made using equal areas in the two frames. No stars are missing in the HST photometry at the turnoff level F555W=18. This assures that no spurious effects due to the usage of ground-based and HST photometry influences the age determination. The top left panel of Fig.3.4 presents the composite CMD.

As for the other two clusters, the preliminary inspection of the CMD provides estimates of age and metallicity which are then refined by the Monte Carlo technique. The automatic fit gives Log(Age)=7.8 ± 0.5 yr with $\chi^2 = 1.5$, the metallicity is $Z = 0.003 \pm 0.002$ and E(F555W-F814W) =0.15 ± 0.05 . The IMF slope gives

$\alpha_1 = 2.2 \pm 0.2$ in the mass range $0.7 M_\odot \leq M \leq 1 M_\odot$, and $\alpha_2 = 2.7 \pm 0.4$ in the mass range $M \geq 1 M_\odot$. Fig. 3.4 presents the CMD of NGC 290 compared with our best fit isochrone. Fig 3.9 presents the observational LF compared with the best fit model. An older age is found when 30% of binary stars are included: Log(Age)=8.0 ± 0.3 yr.

3.4.4 Revisiting an old question: convective overshoot

Becker and Mathews (1983), comparing observational and synthetic CMD of NGC1866, first noticed that classical stellar models they used predicted a number of red giants larger than observed, and a smaller number of main sequence stars in turn as compared to the observations. The same authors suggested that a more careful treatment of core convection (i.e. larger convective cores) could remove the discrepancy. A number of subsequent studies confirmed this idea and demonstrated that the inclusion of overshooting in the description of convective motions could reproduce the correct ratio $N_{\rm PMS}/N_{\rm MS}$. Chiosi et al. (1989a), in particular, clearly showed that the overshooting scheme, by reducing the ratio $t_{\rm He}/t_{\rm H}$, offers a good and simple solution to the problem. This conclusion was also reinforced by Lattanzio et al. (1991), who analyzed the CMD of NGC1866 by means of overshooting and classical models.

The classical theory of stellar structure predicts that in a star whenever the condition

$$\nabla_r \leq \nabla_a \tag{3.6}$$

is violated the region becomes unstable to convective motions and fully mixed. This region is surrounded by stable radiative layers. This is only an approximation: what happens physically in the border region passing from unstable to stable conditions? If we define the Schwarzschild core as the region at whose border acceleration of convective bubbles vanishes there still will be a shell in which velocity is not zero. The thickness, the thermal properties, and mixing efficiency in the overshooting region are still a matter of discussion. In any case, it is worth recalling that first convective overshooting is a consequence of the inertia principle, so that neglecting its existence would not be physically sound, second it is quite common in Nature (Deardorff et al., 1969). As demonstrated in a number of studies, including numerical simulations (Freytag et al., 1996), the penetration depth of convective elements into a formally stable region represents a non-negligible fraction of the size of the unstable zone. In addition to this, there is a number of astrophysical situations in which the hypothesis of substantial convective overshooting has been found to offer better and more elegant solutions than other explanations (see Bertelli et al., 1986a; Chiosi et al., 1992). Among others, suffice it to recall here the so-called mass discrepancy of Cepheid stars (Bertelli et al., 1986b; Chiosi et al., 1992). The first

studies of this subject were by Shaviv and Salpeter (1973); Prather and Demarque (1974); Maeder (1975); Cloutman and Whitaker (1980b); Bressan et al. (1981); Stothers and Chin (1981), followed over the years by more sophisticated formulations standing on turbulence theories (Cloutman and Whitaker, 1980a; Xiong, 1980) and fluid hydro-dynamics (Canuto and Mazzitelli, 1991; Canuto et al., 1996; Unno and Kondo, 1989; Canuto, 2000). Particularly suited to the calculation of stellar models, is the ballistic approach to the problem proposed by Bressan et al. (1981) which has been proved to best reproduce the numerical results of laboratory fluid-dynamics simulations (Zahn, 1991). The Bressan et al. (1981) procedure will be shortly summarized below.

Despite all this, it has been often argued that unresolved binaries could mimic the effects of convective overshooting and easily account for the low ratio of red giant to main sequence stars observed in the young LMC clusters. This hypothesis has been investigated by many authors, both in open clusters of the Milky Way (see Carraro et al., 1994) and young clusters of the LMC (Chiosi et al., 1989a,b; Vallenari et al., 1992) with somewhat contrasting results. Worth of mention is the study by Testa et al. (1999) of NGC1866, who introducing about 30 % of binary using the classical models of Dominguez et al. (1999) came to the conclusion that convective overshooting is not required. The subsequent analysis of Barmina et al. (2002) of the same cluster carried out on the Testa et al. (1999) data, discovered that the correction for completeness applied by Testa et al. (1999) was wrong thus invalidating their conclusions. In addition to this Barmina et al. (2002) performed a systematic analysis of the effects of binary and stochastic fluctuations in the IMF and came to the opposite conclusion: convective overshoot in unavoidable.

Here we have three clusters whose turn-off mass is about 4 $M_{\odot}$ so it might be worth of interest to contribute further to this subject. In order to check which model better suits the data we need to have different sets of stellar populations. There are two sets with convective overshooting i.e. the models by Girardi et al. (2002) and those by Pietrinferni et al. (2004) with a different prescription so that comparison is possible, and the classical ones by Pietrinferni et al. (2004).

As already recalled, the ballistic description of convective overshoot by (Bressan et al., 1981) is particularly suited to stellar models. The algorithm adopts a non-local treatment of convection in the context of the mixing-length theory (MLT) by Böhm-Vitense (1958): it looks for the layers where the velocity of convective elements (accelerated by the buoyancy force in the formally unstable regions) gets zero into the surrounding stable regions, then adopts a suitable temperature stratification in the overshooting regions, and finally assumes straight mixing over-there. Since the Bressan et al. (1981) formalism makes use of the MLT, it expresses the

mean free path of the convective elements as $l = \Lambda_{\rm c} \times H_{\rm p}$ where $H_{\rm p}$ is the local pressure scale height. According to this definition adopted by Bressan et al. (1981) Λ_c represents the overshoot distance *across the Schwarzschild radius* in units of the pressure scale height. In Bressan et al. (1981) Λ_c was assumed to be the same for all stellar masses. Over the years, this was slightly modified to treat overshoot in that particular range of mass which sees the transition from radiative core H-burning to convective core H-burning and during this phase the convective core starts small, grows to a maximum and then decreases. In this mass interval Λ_c is not kept constant but let vary with mass according to the recipe in Girardi et al. (2000):

1) $\Lambda_c = 0$ for $M \leq 1.0 M_\odot$ (when the core is radiative)
2) $\Lambda_c = M/M_\odot - 1.0$ for $1 M_\odot < M \leq 1.5 M_\odot$
3) $\Lambda_c = 0.5$ for $M > 1.5 M_\odot$

The last value stands also for the whole He-burning phase.

Pietrinferni et al. (2004) adopt a similar prescription:

1) $\Lambda_c = 0$ for $M \leq 1.1 M_\odot$ (when the core is radiative)
2) $\Lambda_c = (M/M_\odot - 0.9)/4$ for $1 M_\odot < M \leq 1.5 M_\odot$
3) $\Lambda_c = 0.2$ for $M \geq 1.7 M_\odot$

where we have to keep in mind that Λ_c is "measured" from the Schwarzschild border. Therefore it corresponds to about half of the Girardi et al. (2000) definition. Considered these premises, the two sets of tracks are practically coincident. This finding also secures that using the classical models by Pietrinferni et al. (2004) is safe as the input physics adopted by the two groups is nearly the same.

The analysis is made comparing the integrated luminosity function of main sequence stars normalized to the number of red giants (thereinafter NILF) first introduced by Chiosi et al. (1989a), which has been proved to be the only way to effectively discriminate between the two different evolutionary schemes. It is worth reminding that the NILF is by definition proportional to the lifetime ratio $t_{\rm H}/t_{\rm He}$ (Chiosi et al., 1989a).

The NILF requires that the number of red giants truly belonging to the cluster is known. The task is not trivial because it requires an accurate decontamination by field stars. The procedure is as follows. First of all we apply to the CMD of the cluster and field the correction for completeness (less than a problem at the magnitude range of interest) and area coverage. Second in the area of the cluster and field CMD where the red giants are expected to occur we perform star counts. We

Table 3.6: Number of red giants in the cluster and field CMDs

ID	Radius(″)	Cluster	Field	Final	Uncertainty
NGC 265	30	51	17	34	±5
K 29	25	16	9	7	±3
NGC 290	25	7	0	7	±3

statistically subtract from the cluster counts a number of red giants as large as that in the field. What remains are the expected cluster red giants. Finally, we consider only NGC 265 because the small number of giant stars in NGC 290 and K 29 would introduce too large statistical uncertainties as it is evident from Table 3.6 where the number of giant stars is given.

We discuss the uncertainty due to the dependence on the adopted cluster area since mass segregation cannot be excluded inside the clusters. Recent estimate of the two-body relaxation time t_r inside MC clusters is given by Kerber and Santiago (2006). They find values of t_r of the order of $10^7 - -10^8$ yr inside the core radius, while for the whole clusters t_r is of a few Gyr. Although t_r does not exactly correspond to the time scale for stellar evaporation, this latter is expected to scale with it. The authors find a significant variation of the present day mass function exponent with the radius in the inner regions of the studied clusters as a result of the mass segregation in the core. If we assume that t_r inside the clusters studied in the present paper is of the same order and due to the fact that they have log(age)$\sim$ 8, we come to the conclusion they can suffer of mass segregation in their core. Fig. 3.11 shows the ratio of N_{MS}/N_R with the radius for the studied clusters for a limiting magnitude F555W=25. This ratio increases with the radius in the case of NGC 265, becoming constant at 30″. This is due to the fact that red giants are more centrally concentrated than main sequence stars. In order to discuss the amount of convective overshoot in the NGC 265 stars, the region inside a radius of 30″ should be considered, to minimize the effects of mass segregation.

The result of the fit of the integrated luminosity function for NGC 265, shown in Fig.3.10, seems to give an experimental function that is intermediate between the two theoretical ones. This would mean that a certain amount of overshoot is needed to explain the data.
To cast light on the reliability of this result, we perform an analysis of the uncertainties affecting the NILF. We first discuss the effects of the uncertainties due to photometric errors, mainly acting on the integrated luminosity function $\sum N_{MS}$. An estimate of the errors affecting the integrated luminosity functions is derived considering the photometric errors. From crowding tests we draw the law that relates

Table 3.7: Comparison of the ages of the three clusters derived here (labelled 1) with those presented in chapter 2 (labelled 2). Ages are years and in logarithmic form.

Name	Ages (1)	Metallicity (1)	Age (2)	Metallicity (2)
NGC 265	8.5±0.3	0.004	8.4	0.008
K 29	8.2±0.3	0.003	8.0	0.008
NGC 290	7.8±0.5	0.003	7.8	0.008

photometric errors and magnitudes. Then we compute how many stars fall in each bin of the histogram with a Monte Carlo simulation, giving to each star an equal probability to fall in the interval $v \pm \Delta v$ where Δv is the relative photometric error. We repeat the test 100 times in order to build a sufficient statistical sample. Then we calculate for each of the bins the mean value and the mean square root that we consider as our uncertainty. The final error is calculated as the partial sum of single bin errors in the same way as we build the integrated luminosity function in Fig.3.10.

Second, we evaluate the effect of the statistical uncertainties on the normalization factor N_{RG}. As expected the steepness of the NILF is very sensitive to it. The experiment is made for NGC 265 data looking how the LF varies at changing the number of red giants from 30 to 40. The results are shown in Fig. 3.12. We notice first that the photometric errors do not significantly affect the NILF, second that neither in those limits for the number of red giants the NILF superposes with the models lying right in the middle Fig. 3.12.

3.5 Concluding remarks

The primary conclusion of this chapter is that the ages obtained for the three clusters fairly agree with those derived in chapter 2 using data of lower quality and a much less accurate procedure. The ages are compared in Table 3.7. The two determinations agree within an acceptable uncertainty. This implies that the age distribution function derived in chapter 2 is reliable at least in statistical sense thanks to the large number of cases considered.

Additional conclusion concerning the three clusters are related to the slope of the IMF and the efficiency of convective overshoot from the central core:
We estimated the slope of the IMF, especially at low masses, between $0.7M_{\odot}$ and $1M_{\odot}$ to check whether the Kroupa exponent, $\alpha_1 = 2.2$, is recovered in this range. We see that all the clusters have the minimum of χ^2 function for α_1 close but not identi-

cal to the Kroupa value. The values are $\alpha_1 = 2.4 \pm 0.4$ for NGC 265, $\alpha_1 = 1.8 \pm 0.2$ for K 29, $\alpha_1 = 2.2 \pm 0.2$ for NGC 290. The differences are not significant at the 68% confidence level.

For NGC 265 we also tested the theory of convective overshoot: we fitted the experimental NILF with two theoretical models, one including overshoot and the other without it (classical case). All the models in use here are from the BaSTI library for the sake of internal consistency in the input physics. They are fully compatible with the correspondent ones of the Padova library. We can say that a certain amount of overshoot is needed in order to fit the experimental data.

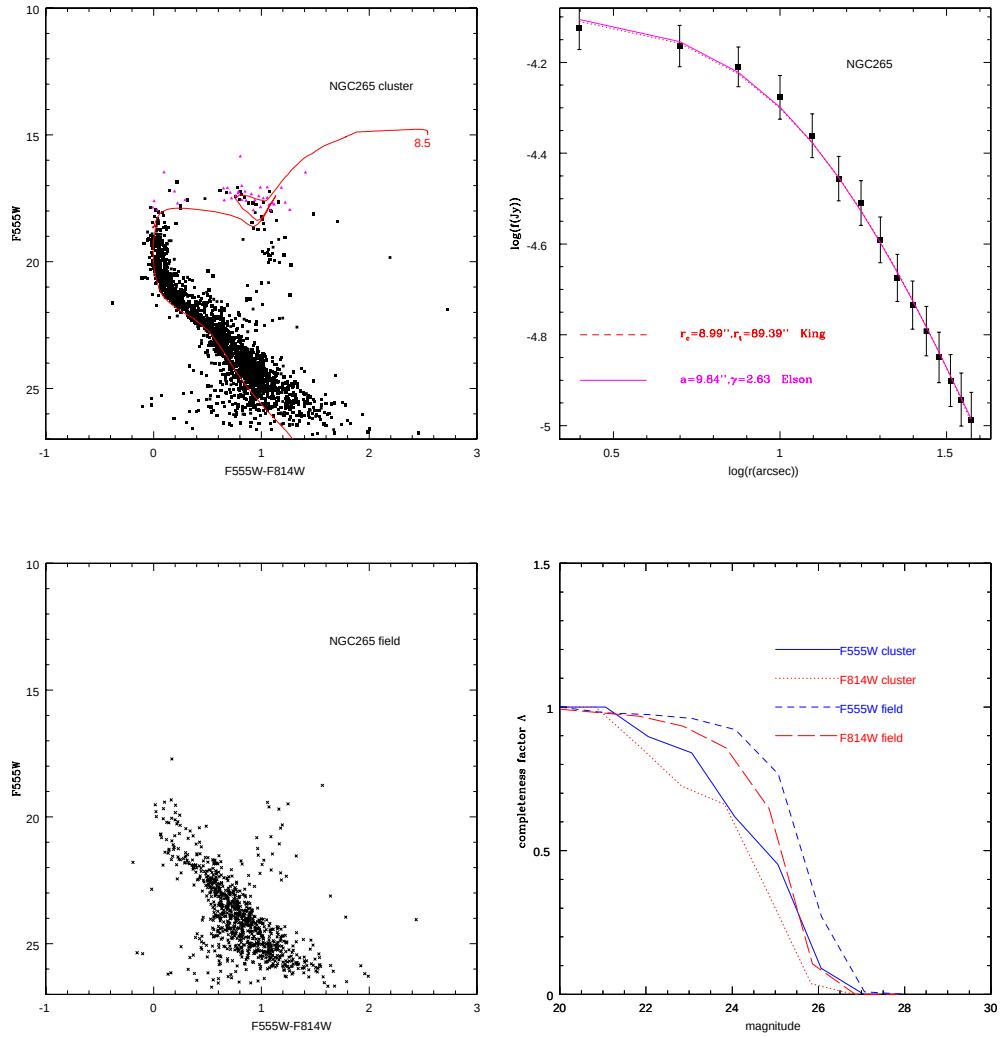

Figure 3.2: Summary panels for NGC 265. In the top left panel is the CM diagram (inner 22") with a superposed isochrone of log(age)=8.5, Z=0.004 and E(F555W-F814W)=0.08. The brightest stars settle at F555W=16. In the top right panel the surface brightness profile (in arbitrary units) is fitted by one of the King functions(dashed line) and by Elson profile (solid line). From this distribution we can determine core and tidal radius. Vast majority of the stars sets within a radius of 22" corresponding to log(r)=1.3. In the bottom left panel the CMD of field stars is shown. The field population is taken at about 1.6' from the cluster centre and the area is comparable to the area of the cluster (see text for details). The bottom right panel shows the completeness factors for the cluster and field regions as indicated

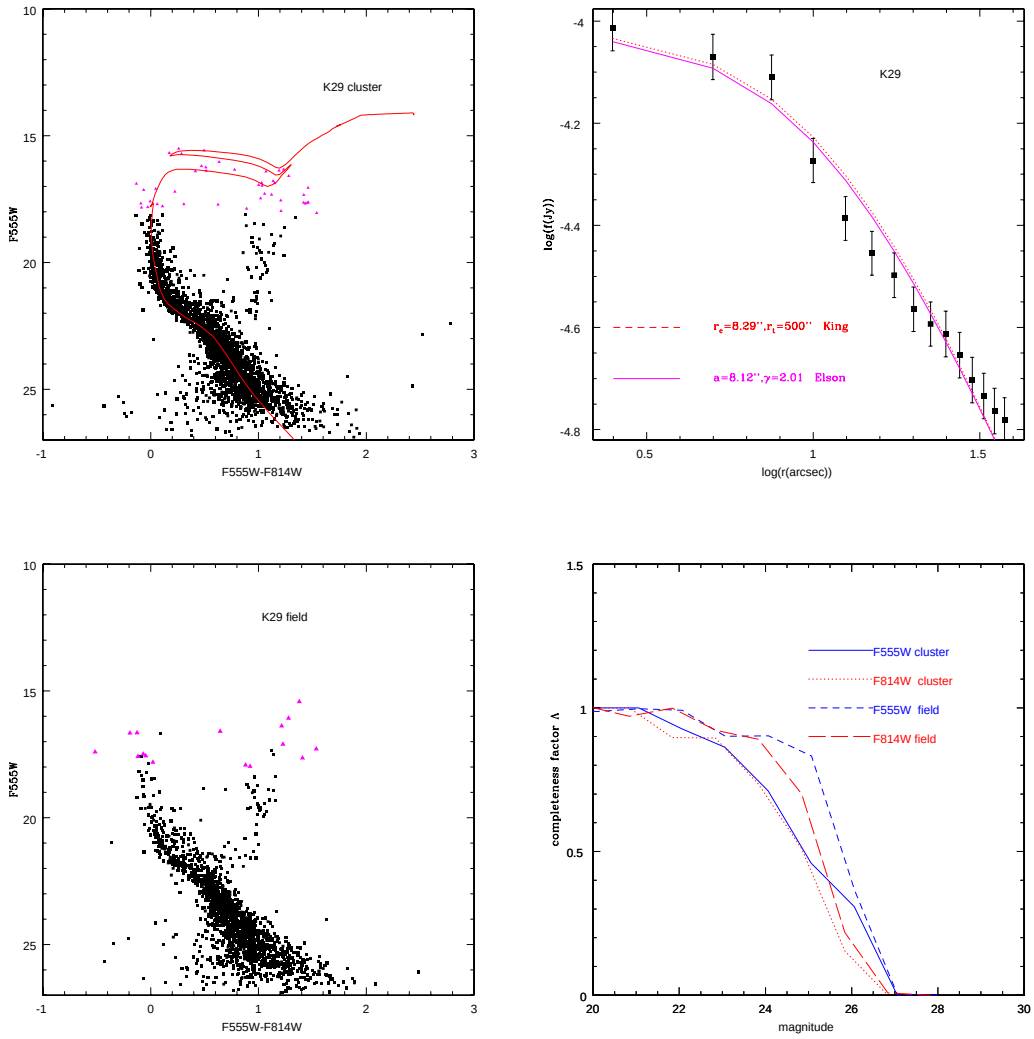

Figure 3.3: Summary panels for K 29. In the top left panel is the CM diagram (inner 22") with a superposed isochrone of Log(age)=8.2, Z=0.003 and E(F555W-F814W)=0.14. The OGLE bright stars are indicated by the triangles. The brightest stars settle at F555W=15. In top right is the brightness profile (in arbitrary units) fitted with one of the King (dashed line) and with the Elson functions (solid line). From this distribution we can determine core and tidal radius. Vast majority of the stars sets within a radius of 22" (or log(r)=1.3). In the bottom left panel the CMD of field stars is shown. The field population is taken at about 1.6' from the cluster centre and the area is comparable to the area of the cluster (22"). The bottom panels shows the completeness factors for the cluster and field (right) and the CMD of the field region (left)

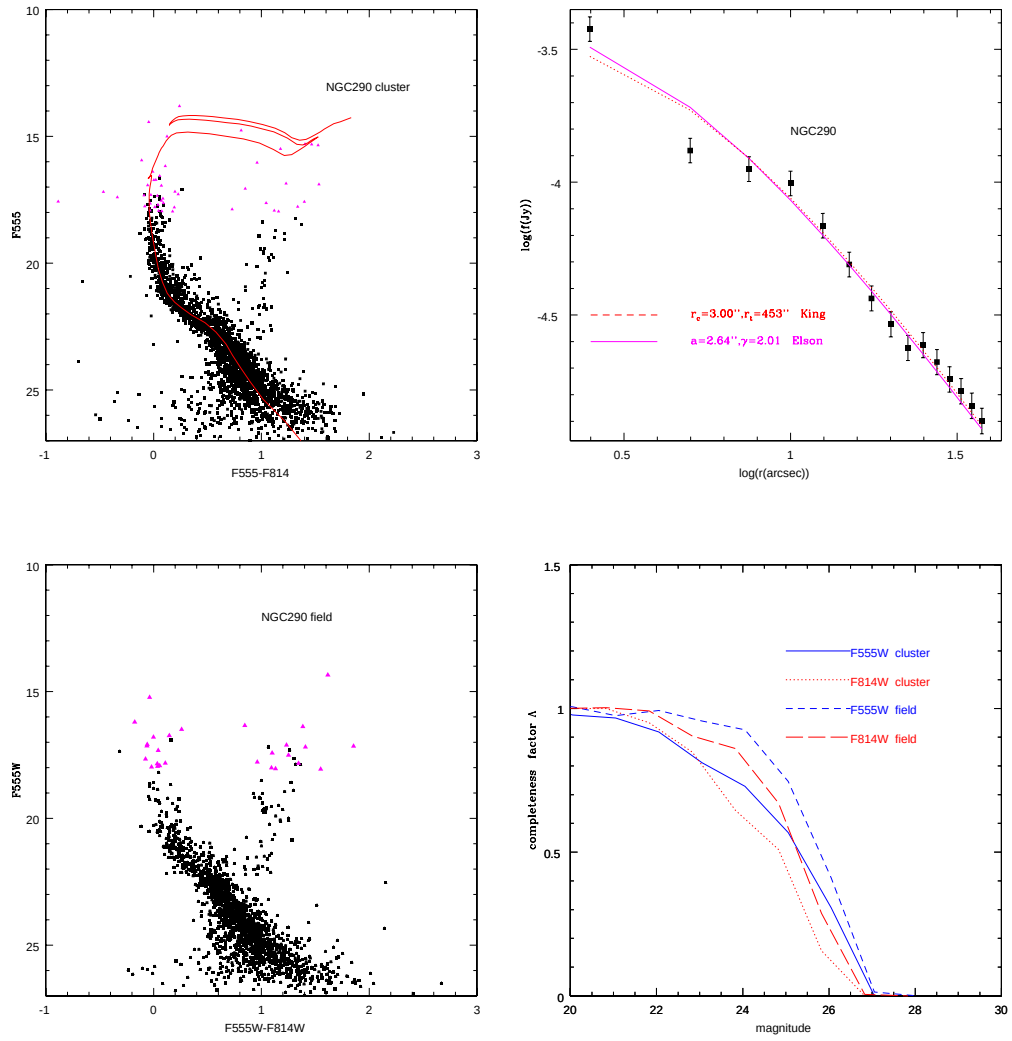

Figure 3.4: Summary panels for NGC 290. In the top left panel is the CM diagram (inner radius of 25") with a superposed isochrone of Log(age)=7.8, Z=0.003, E(F555W-F814W)=0.15. The OGLE bright stars are indicated by the triangles. The brightest stars settle at F555W=14. In top right is surface brightness profile (in arbitrary units) fitted with the King profile (dashed line) and with the Elson function(solid line). From this distribution we can determine the core and tidal radius. Vast majority of the stars sets within a radius of 25". In the bottom left panel the CMD of field stars is shown (see text for details). The field population is taken at about 1.6' from the cluster centre and the area is comparable to the area of the cluster (25"). The bottom right panel shows the completeness factors for the cluster and field regions as indicated

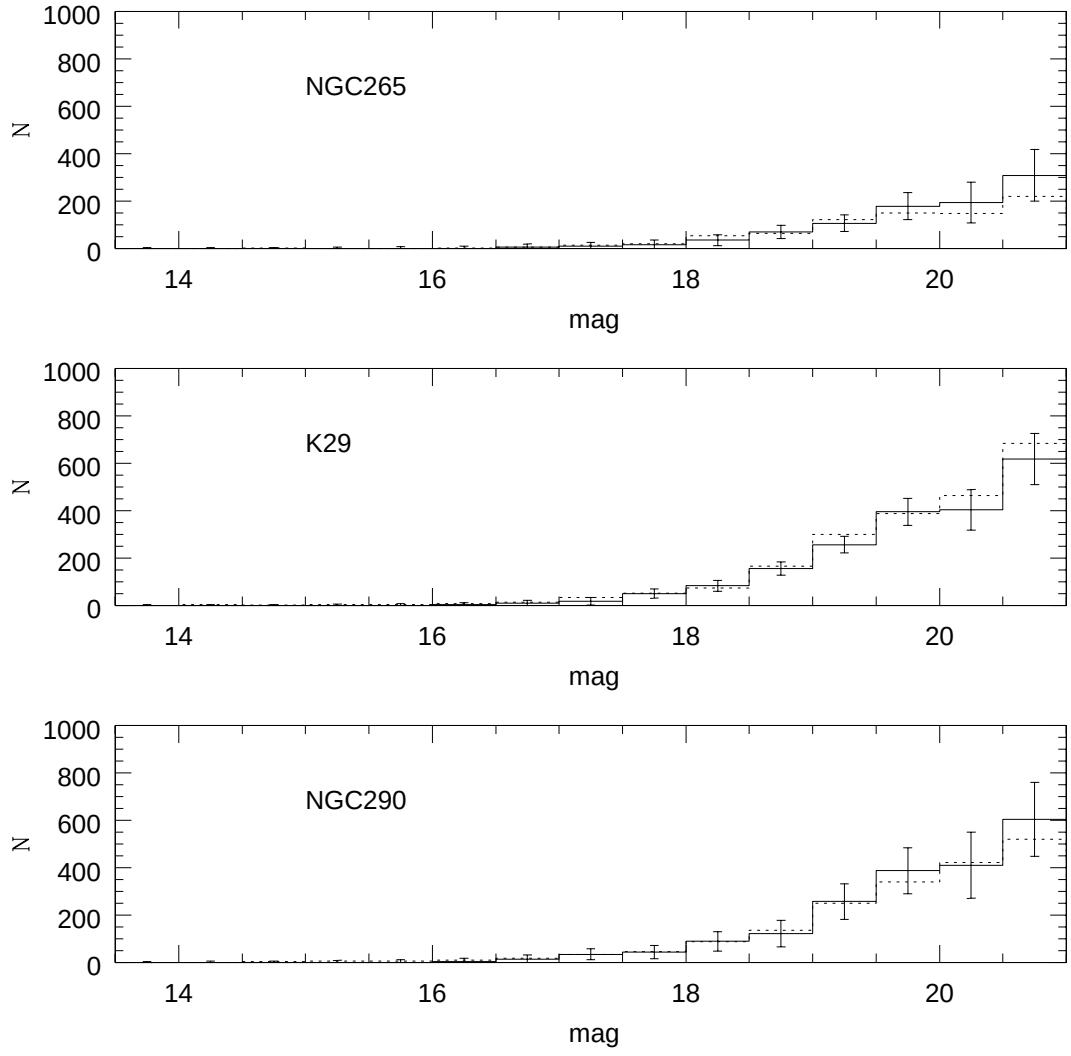

Figure 3.5: The luminosity functions of HST(continuous line) data and OGLE II(dashed line) data for the field area are compared. OGLE II field areas are taken at a distance of 1 deg from the clusters. The number of objects is normalized to an area of $22''$

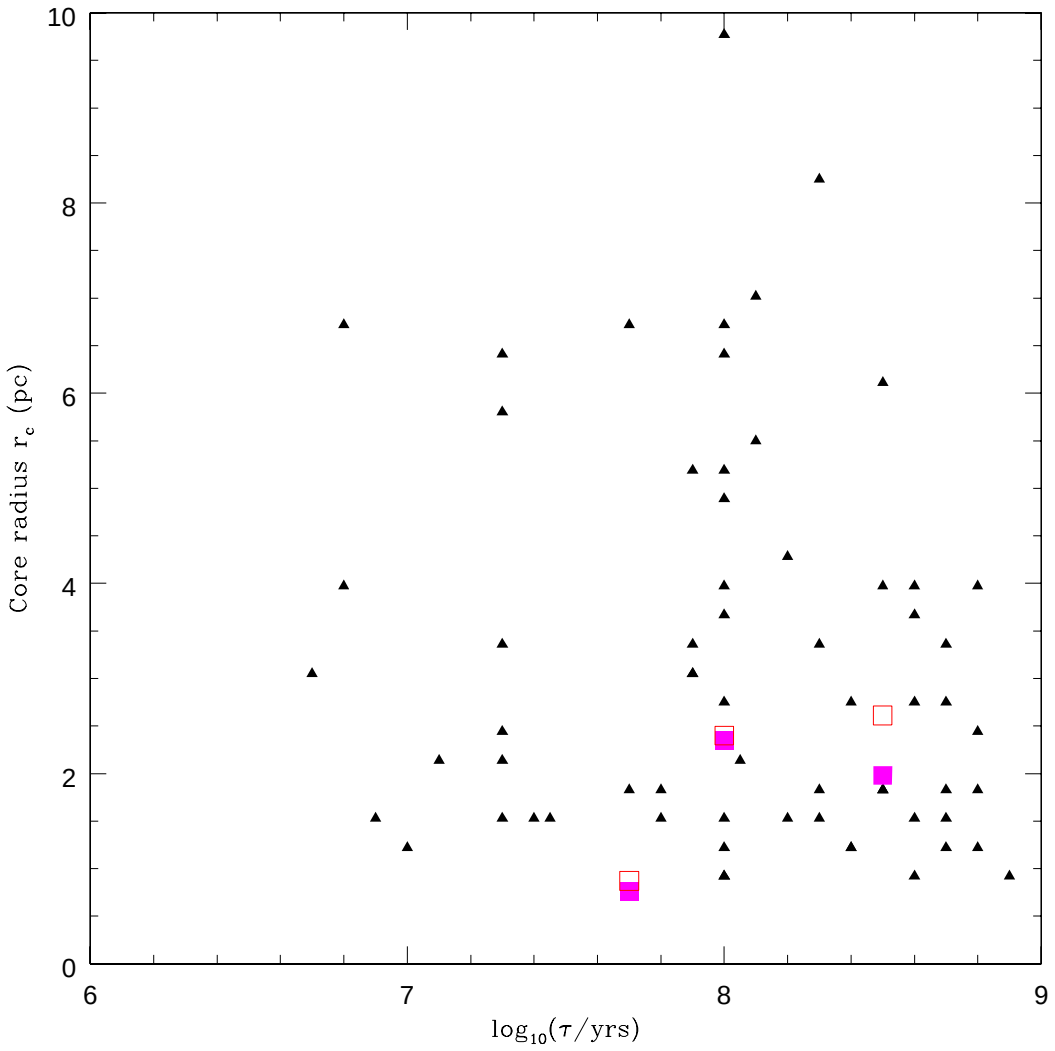

Figure 3.6: The core radius versus age relationship for SMC clusters from the sample derived as described in the text. The clusters discussed in this paper are plotted as filled squares (Elson et al. (1987) models) or empty squares (King models)

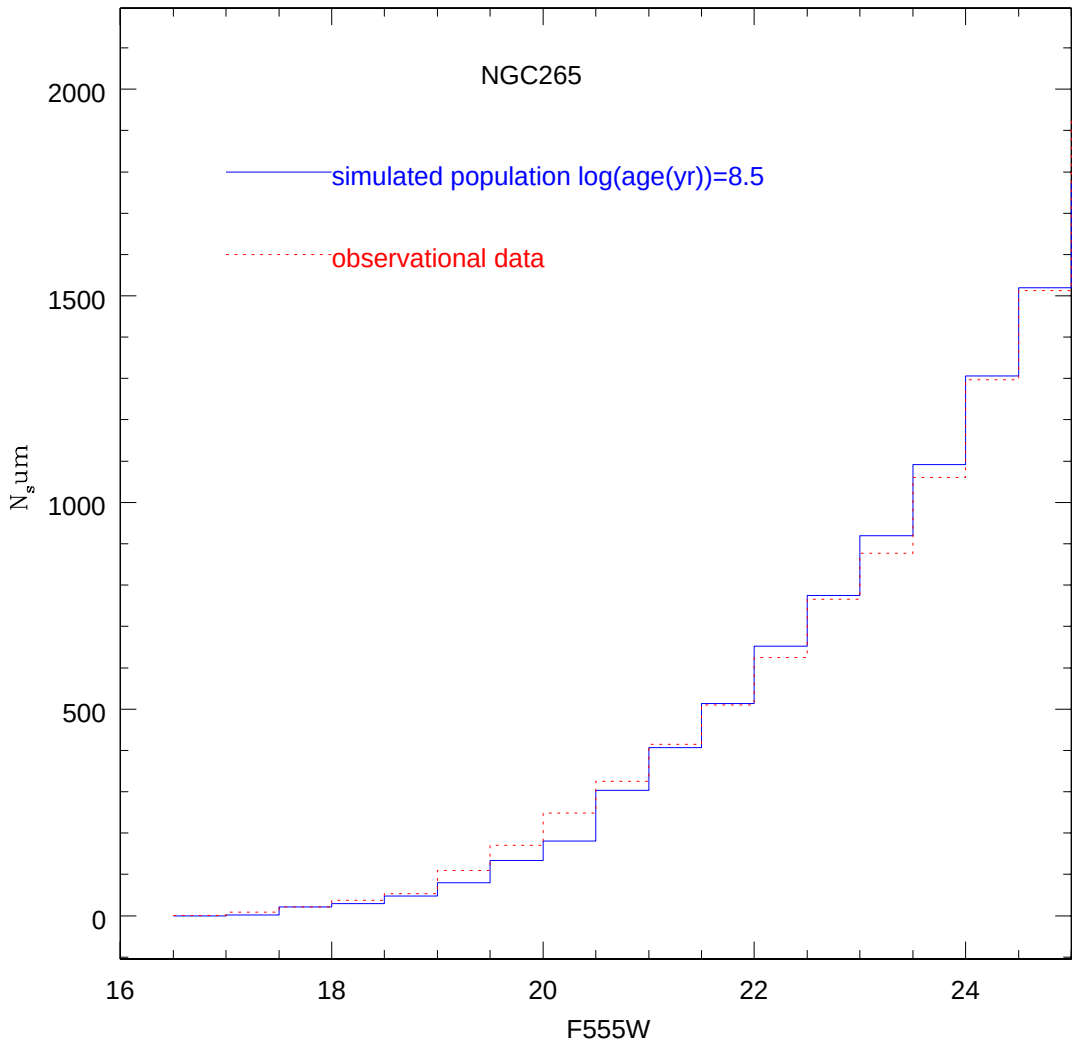

Figure 3.7: LF of the cluster NGC 265. The best fit is done with a population of Log(Age)=8.5 yr

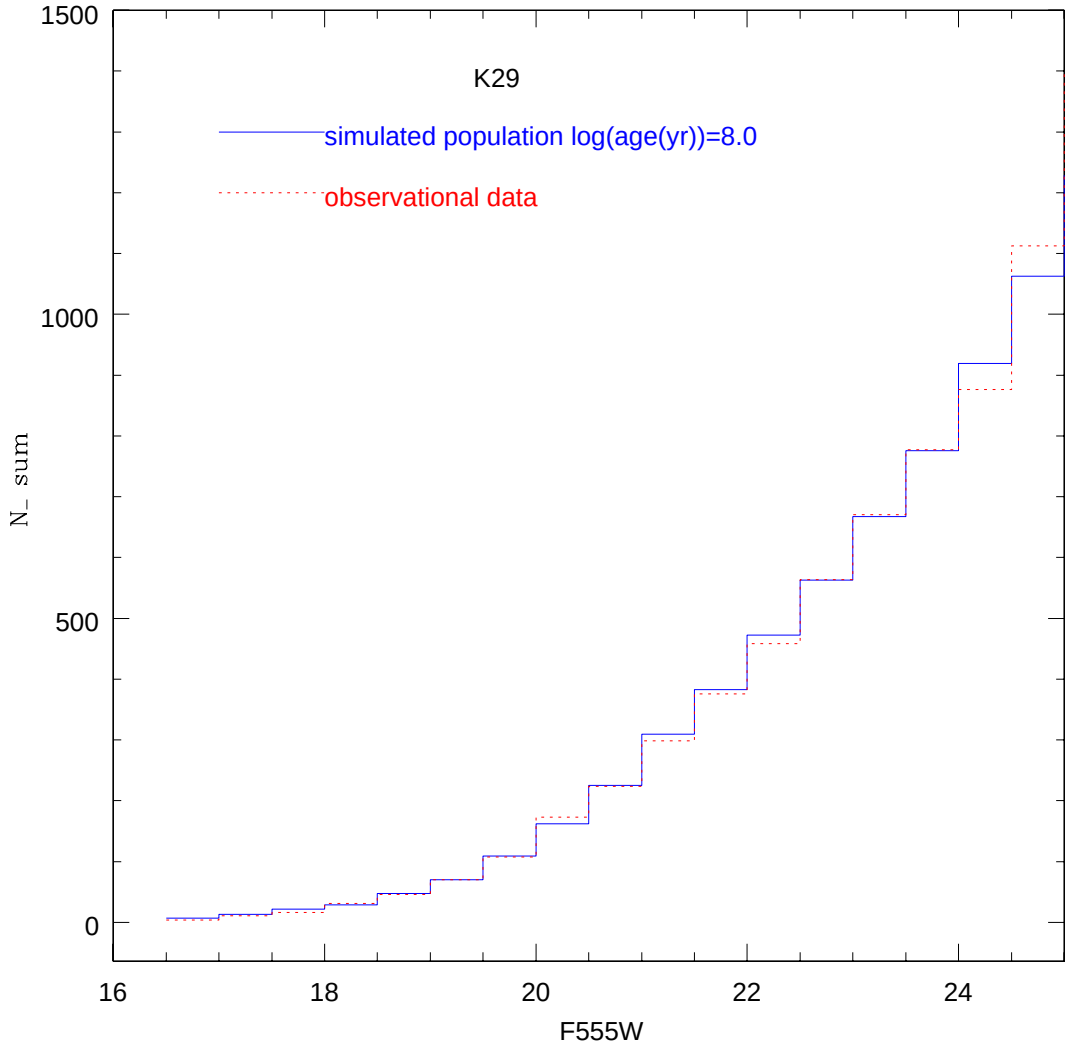

Figure 3.8: LF of K 29 fitted with a population of Log(Age)=8.0 yr

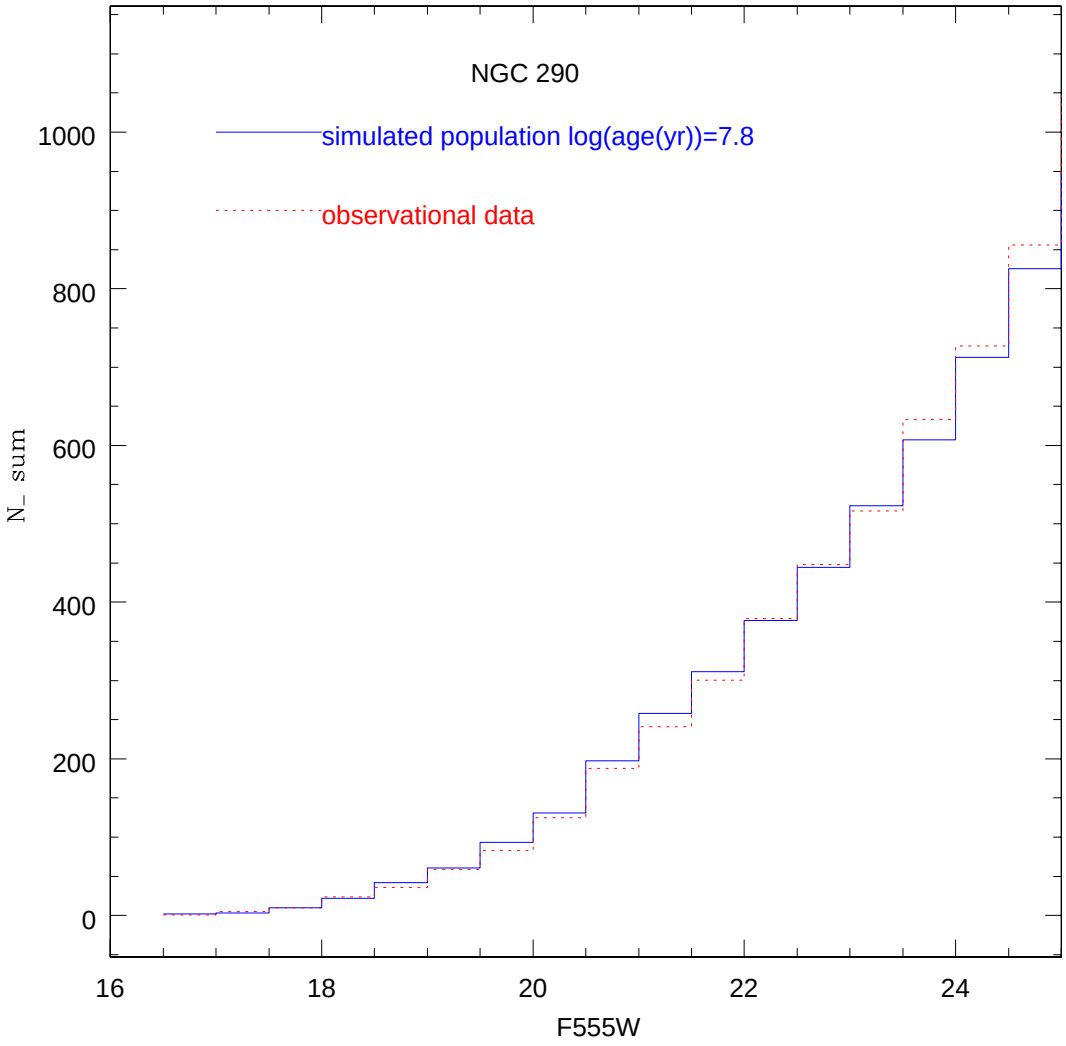

Figure 3.9: LF of the cluster NGC 290 fitted with a simulated population having Log(Age)=7.8 yr

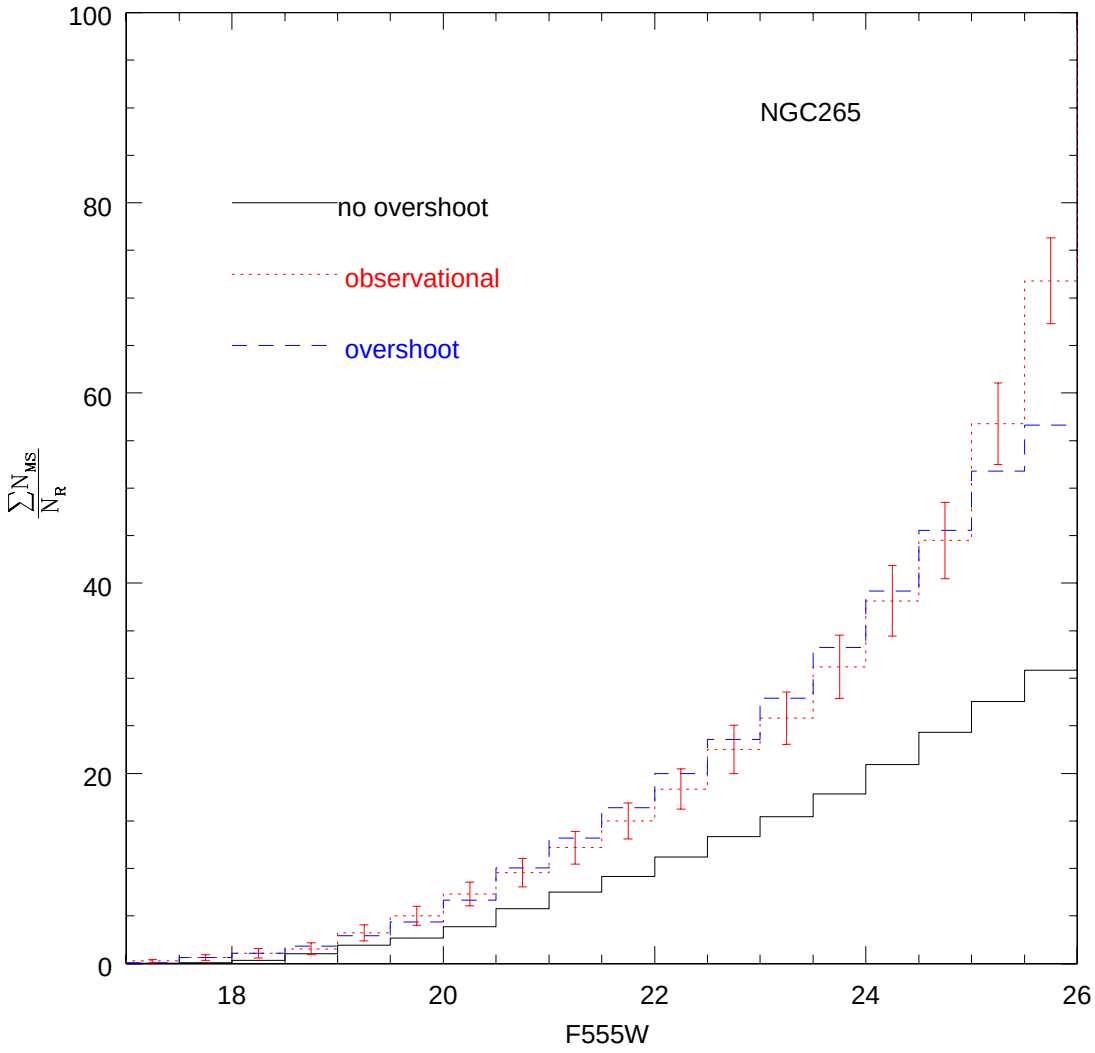

Figure 3.10: Cluster NGC 265. We fit the NILF with canonical models taken from the BaSTI library and overshooting models from the Padova Library. Error bars are calculated taking into account photometric errors on the magnitudes (see text for details)

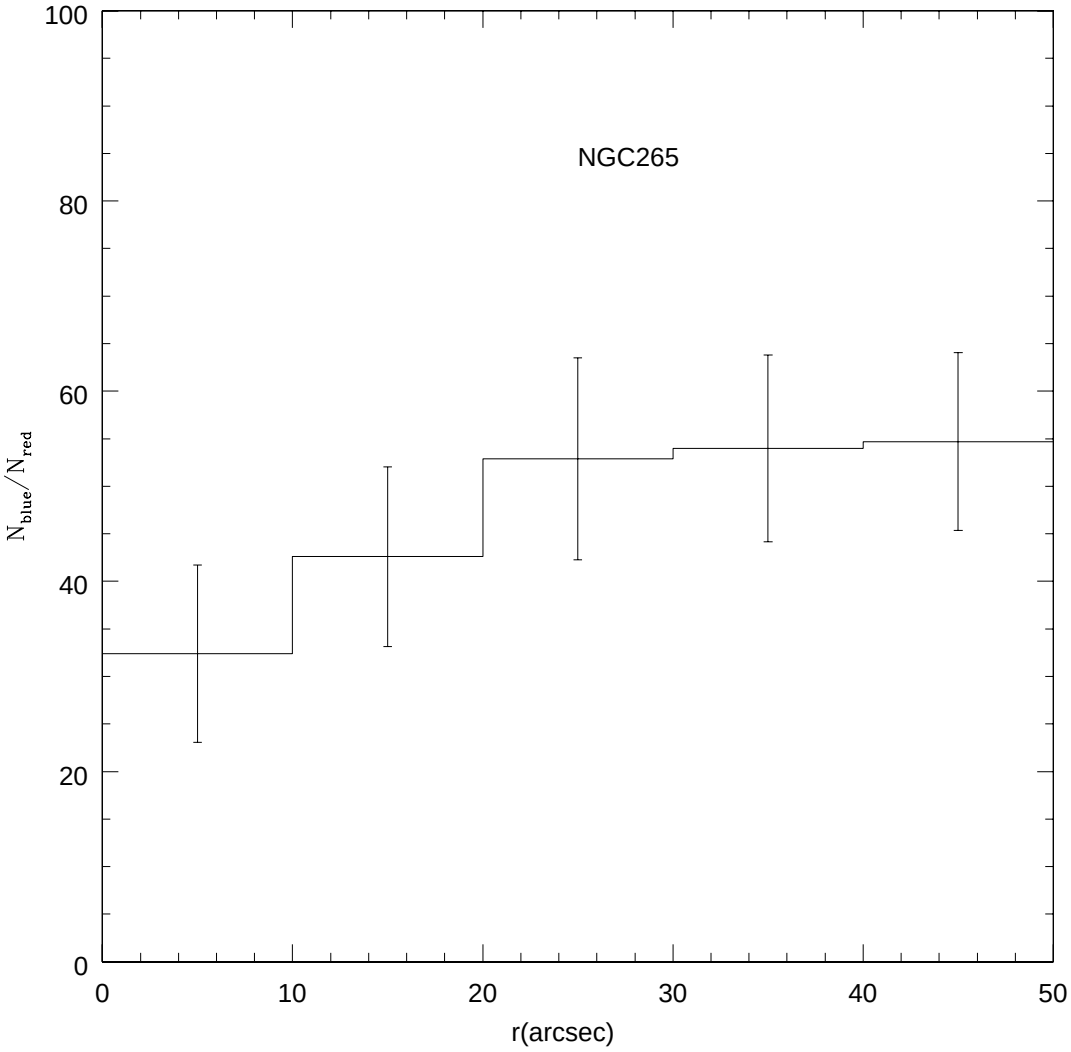

Figure 3.11: The variation of the ratio N_{MS}/N_R with the radius for NGC 265 for a limiting magnitude F555W=25. The numbers take into account field subtraction and completeness correction. The error bars are calculated using a Poisson statistics

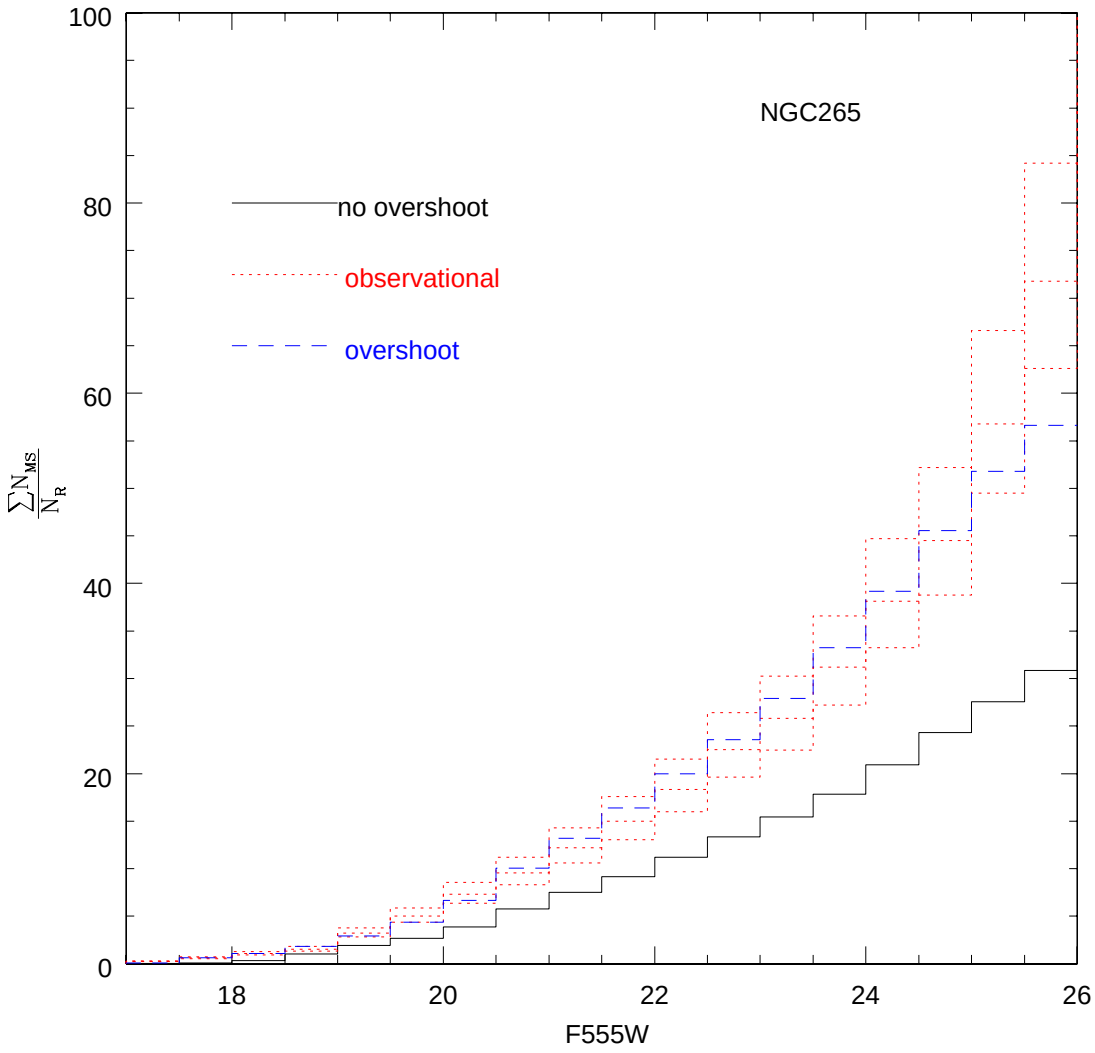

Figure 3.12: The variation of NILF steepness at changing the number of red giants. Observational NILF (dashed line) is compared with theoretical models with overshoot (dotted line) and classical models (solid line). Upper lines are normalized to 30 giants, intermediate to 34, lower lines to 40. We made these estimates on the consideration that the number of red giants is known within a certain uncertainty. The subtraction of field red giants gives a number of 34 ± 5 stars

Chapter 4

Cluster formation and environment

4.1 Introduction

In this chapter we address the question whether the cluster formation process and efficiency is somehow related to the physical conditions of the environment in which clusters are formed. The obvious sites to look at are the HI and CO clouds in which undergoing star formation is observed.

In section §4.2 we present the distribution of HI clouds. In section §4.3 the two supershells, 37A and 304A are discussed. In section §4.4 we discuss the correlation with the CO clouds. In section §4.5 the spatial distribution of the clusters is compared with the environment properties. Finally, concluding remarks are given in section §4.6.

4.2 Neutral hydrogen

Neutral hydrogen is an important tracer of the SMC. It has a complicated morphology. It surrounds the SMC and the LMC, then extends through the Magellanic Bridge, in six HI separated regions MSI-VI. Many authors have contributed in the past to the definition of the intensity and velocity fields of HI in the SMC (Kerr et al., 1954; Hindman et al., 1963; Hindman and Balnaves, 1967). A great advantage from the observational point of view came with the survey made by Staveley-Smith et al. (1997) using the Australia Telescope Compact Array (ATCA). This survey

revealed the true structure of the gas showing that it is composed of huge number of expanding shells (more than 500). ATCA survey has an angular resolution of 1.6 arcmin (28 pc). The total area covered is $4°.5 \times 4°.5$. The structure of the shells is circular or elliptical, shape that is explained if we think at them as expanding shells of gas. Physical models claim at stellar winds from supernovae and massive stars that sweep up surrounding interstellar gas. The largest shells are explained with collisions between high velocity clouds and galaxy discs. Dynamical ages are also calculated for the shells according to the following

$$T_s = \frac{3}{5}(r_s/v_s) \tag{4.1}$$

(Weaver et al., 1977), where r_s and v_s are the shell radius and velocity, respectively.

Large scale HI morphology of SMC is irregular and does not show symmetries. It shows a main body that lies in the direction NE to SW, and an arm extending on the East side. These are usually referred to as the "bar" and the "eastern wing". On small scales the gas shows to have a conspicuous number of substructures like shells, filaments and arcs. Also an estimate of the total mass of the gas is given by Stanimirovic et al. (1999): it is about $4.2 \times 10^8 M_\odot$. If we superpose photometric plates and HI column density image we can make a first rough guess of how gas and stars do correlate: correlation is quite good along the bar but HI extends much further toward SW, SE and NW directions.

A second impression on the structure of the HI of the SMC is given from the maps of the velocities. We have two maps available, that of the first moments that is the intensity-weighted mean velocity along the line of sight, and the second moment velocity map, or the intensity-weighted velocity dispersion. The velocity dispersion varies from $\sim$ 5 to 40 km s^{-1} across the SMC. We will try to correlate this second map with the stellar populations present in the galaxy. It is well known how young and old stellar populations behave differently in the SMC. A stellar survey made by Zaritsky et al. (2000) shows how young stars (age $\leq 200 Myr$) have an irregular distribution similar to that of HI while old stars (age $\geq$ 1Gyr) show a uniform spheroidal distribution.

Besides the great number of shells of dimension from a few pc to several hundreds pc, three super-shells were found, whose dimensions are of the order of one kpc. The positions for the two of them we are going to study are given in Tab.4.1. We will later see how these super-shells are favoured loci of star formation.

HI gas is detected through emission in 21 cm line. We can see its puzzling distribution and we could ask ourselves which is the origin of these peculiar structures (Dib and Burkert, 2005). Not all the shell structures are the result of supernovae

Table 4.1: Coordinates of the super-shells in HI regions of SMC. a is the major axis, a/b is the axis ratio, θ is the position angle. Data from Stanimirovic et al. (1999).

Name	α	δ	a (pc)	a(deg)	a/b	θ
37A	$00^h40^m26^s$	$-73°28'06''$	840	0.84	0.89	160°
304A	$01^h02^m16^s$	$-72°38'12''$	910	0.80	0.45	80°

explosions. This is shown by Kim et al. (1999) for the LMC on the basis of the weak correlation between HI shells and HII regions. Moreover a study by Rhode et al. (1999) shows no signs of the presence of stellar remnant clusters inside 86% of HI holes. We do not want to deny the hypothesis of supernovae origin but to demonstrate that it can't be the only process of shell formation. Models that claim at this process as the only way of HI hole formation have to suppose a number of supernovae that goes over the detected one. In order to justify this, they invoke a nonstandard IMF in the sense that it should be top heavy. We have already said that HI holes can also be created by the impact of high-velocity clouds but this also does not seem to be the dominant process in the hole formation. There is also the possibility that the morphology could emerge from the combined action of turbulence, thermal instabilities and gravitational instabilities. This is the way run by Dib and Burkert (2005).

4.3 Triggering mechanism of cluster formation

In this section, we would like to address the complex relation between the clusters and their environment, in order to cast light on the cluster formation process. Several mechanisms of cluster formation have been proposed in literature. Here we quote a few. SMC is believed to have been involved in several peri-galactic encounters with the Milky Way and with the LMC, over the past 12 Gyr. The epoch of the most recent peri-galactic encounter with the LMC is found to range from 500 Myr ago (Oh et al., 1995) to 200 (Gardiner et al., 1994; Yoshizawa and Noguchi, 2003) even if some authors suggest that the Magellanic Clouds could be at their first encounter with the Milky Way (Besla et al., 2007). At that time the star formation is expected to be enhanced not only in the tidal arms, but also in the main body of the SMC. Clusters are expected to form as a result of relatively high velocity cloud-cloud collisions (Zhang et al., 2001; Bekki et al., 2004). This mechanism is particularly efficient during galaxy interactions and mergers. The value of the turbulent velocity between clouds that can give rise to cluster formation is a highly uncertain parameter, going from 50-100 Km/s (Zhang et al., 2001) to 20-30 Km/s

(Bekki et al., 2004). Alternatively, high speed motions may produce a high-pressure environment that in turn, can trigger turbulence or shocks (Elmegreen, 1997). Finally, star formation might be triggered by stellar winds and supernovae explosions through compression by turbulent motions (Larson, 1993).

The correlation, if any, between young star clusters and their environment can cast light on the cluster formation process. In the following, we first discuss the age distribution in the regions of the two super-shells. Then we discuss the degree of clustering of the clusters and young field stars. Finally, we compare the spatial distribution with the column density of the gas observed in the HI and with the dispersion velocity field.

4.3.1 Super-shells and cluster formation

The interstellar medium of the SMC shows a fractal structure, consisting of a hierarchy of HI clouds and shells. Kinematic studies of the HI data have revealed the presence of two super-shells in the SMC disk, namely 37A and 304A (Stanimirovic et al., 1999) which may consist of smaller superimposed shells. The true origin of the holes and small shells in the interstellar medium is still under discussion. There is evidence that at least 10% of the small shells found in the SMC are not associated with recent star formation. For this reason, it is unlikely that those few shells are the result of supernova explosions (Hatzidimitriou et al., 2005) but they might be due to turbulence and gravitational instabilities (Dib and Burkert, 2005). However the vast majority of the shells and super-shells is associated with young objects and it is probably formed in the standard way, because of the combined effects of supernovae and stellar winds (McCray and Kafatos, 1987). Inside the shells, sequential or secondary star formation is expected to be triggered by supernova explosions. In the following we will discuss the spatial distribution of the clusters/associations of different ages inside 37A and 304A to clarify the relation between cluster formation and super-shells.

Cluster age distribution in the region of the super-shell 37A

In order to bring into evidence the spatial distribution of the clusters of different ages, we plot the age distribution of the clusters against the distance from the centre. As we did in the previous Section, we approximate the shell with an ellipse whose centre and axial ratio are given by Stanimirovic et al. (1999). For sake of clarity we remind that the super-shell is centered at $\alpha = 00^h40^m26^s$ and $\delta = -73^0 28' 06''$ and has a major axis a=840 pc (or 0.8 deg), axial ratio of 0.89 and a position angle of 160^0 (Stanimirovic et al., 1999). Because of its position angle, the minor axis of the ellipse is roughly aligned in the direction E-W. Fig. 4.1 presents the cluster age distribution as a function of the semi-minor axis. Our data do not completely

cover the super-shell at the Western side, but the vast majority of it is included in the data. While objects older than about 15 Myr are found East and West of the centre, a discontinuity in the spatial distribution of younger clusters is present. They are almost all located toward the Eastern rim of the super-shell 37A where gas and dust are located (Staveley-Smith et al., 1997; Stanimirovic et al., 1999). Only two clusters as old as 15 Myr are found West of the centre. This discontinuity clearly indicates the epoch of the shell formation which was preceded by a period of relative quiescence. This determination of the super-shell age is in agreement with the dynamical age of 17 Myr (Stanimirovic et al., 1999).

It is quite difficult to ascertain the presence of secondary or propagating star formation events as it is expected in the standard model by McCray and Kafatos (1987) if stellar winds and supernovae explosions were responsible for the formation of the super-shell. Standard model of shell formation predicts that young objects are located at the edges, while older stars are more centrally concentrated. The fact that objects younger than the dynamical estimate of the super-shell age are located toward the Eastern rim of the super-shell, while older clusters are widely distributed might be interpreted as a mild age gradient. However, we remind that the whole analysis is complicated by the extension of the SMC along the line of sight. The apparent distance of the clusters from the centre might be due to projection effects.

A quantitative description of the cluster age distribution is shown in Fig. 4.2. We subdivide the super-shell region in two parts, one West, from $\alpha = 00^h44^m00^s$ (or 11 degrees) to $\alpha = 00^h36^m00^s$ (or 9 deg.) and one East of $\alpha = 00^h44^m00^s$. The age distribution presents two episodes that might have different origin. Looking at the cluster age distribution, (see Fig. 4.2) it is evident that the epoch of the shell formation is coincident with an enhancement in the cluster formation rate in the Eastern part. In addition to this young episode, the cluster age distribution at the Eastern part shows an enhancements between 80 and 400 Myr. On the Western side the cluster formation was less efficient at ages younger than 15 Myr, while it was comparable at older ages.

Cluster age distribution in the region of the super-shell 304A

Analogously to what we did in the previous Section, we approximate the super-shell region with an ellipse and discuss the distribution of the clusters inside homologous ellipses having the same centre and axial ratio of the shell. We remind that the super-shell is centered at $\alpha = 01^h02^m16^s$ and $\delta = -72^0 38' 12''$ and has a major axis a=910 pc (or 0.87 ^{0}), axial ratio of 0.45 and a position angle of 80^0 (Stanimirovic et al., 1999). Fig. 4.3 shows the cluster age distribution as a function of the distance from the centre calculated along the major axis of the ellipse representing the super-shell (see previous section). The distribution of the clusters along the

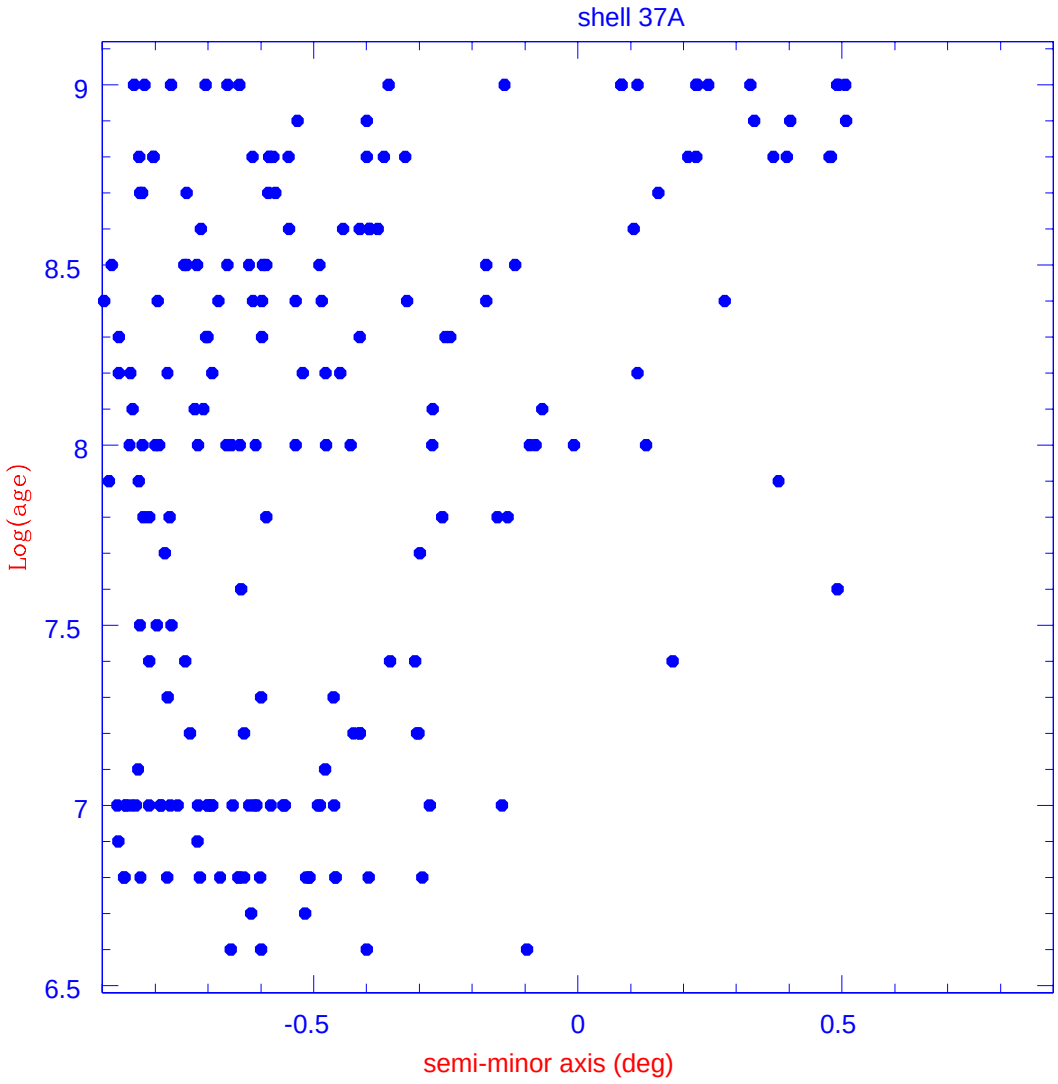

Figure 4.1: Age distribution inside the super-shell 37A plotted against the semi-minor axis (see text for details). Negative axis refers to the Eastern part of the shell

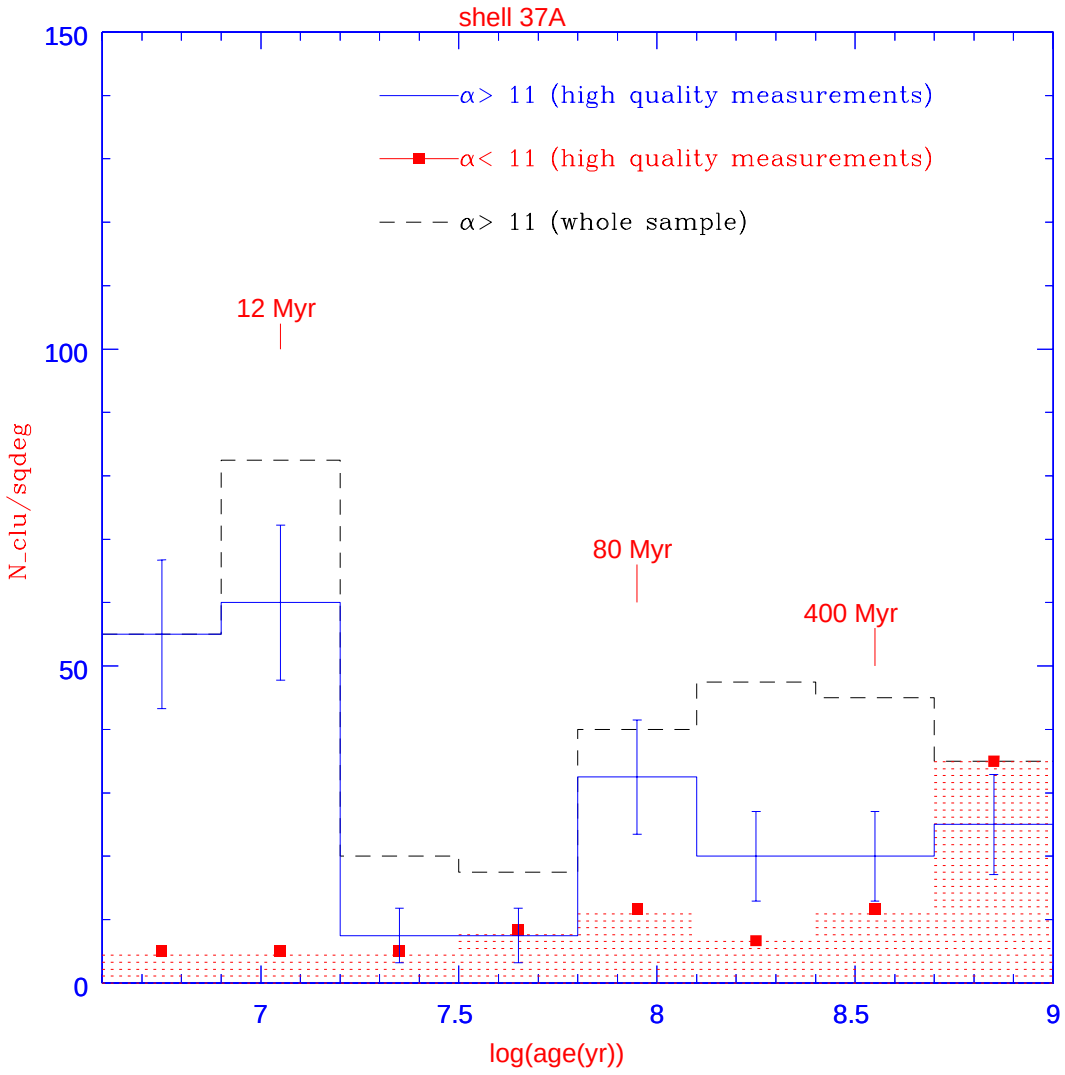

Figure 4.2: Dashed line is the age distribution of the whole cluster sample on the Eastern side of the shell 37A ($\alpha > 11$ deg or $\alpha > 00^h44^m00^s$). Continuous line is the analogous for high quality measurements (see text for details). Squares show the cluster age distribution on the Western side of the shell 37A ($\alpha < 11$ deg) for clusters having high quality measurements of the age. Error bars indicate the Poissonian uncertainties on the counts

major axis (approximately oriented in the direction W-E) clearly shows that at any ages the star formation took place preferentially in the Western part of the shell, in the direction of the shell 37A. An almost symmetric distribution is visible for ages younger than 20 Myr, while older objects are mainly located West of the centre. This epoch roughly indicates the time of the formation of the shell and is in agreement with the dynamical age of the super-shell of 14 Myr (Stanimirovic et al., 1999).

A quantitative description of the age distribution is derived subdividing the region in two parts defined by the line drawn in Fig.2.8, roughly separating the Northern region from the Southern. Fig. 4.4 presents the age distribution of the clusters. The star formation was more active in the Northern region, where the majority of the H_α emission is located. The cluster distribution in the super-shell 304A region shows a continuous formation from a few Myr to 1 Gyr with enhancements from a few Myr to 15 Myr, and at 90. The youngest episode is in coincidence with the epoch of the formation of the super-shell.

Summarizing this section, the two super-shells are clearly visible in the age distribution of the clusters. From the epochs of their formation up to now, an enhancement in the cluster formation took place. It is evident that the same mechanism (SN explosions, stellar winds, turbulence) producing the shells in the gas distribution is responsible of the formation of the objects younger than 15-20 Myr. The super-shells probably formed in a more complex way than what is described by the simple model by McCray and Kafatos (1987): even if young objects are more numerous at the edges of the shells, a clear age gradient from the centres to the rims is not evident. The inter-shell region was specially active, possibly due to compression phenomena related to the expansion of the shells. Finally, an episode at about 90 Myr is found in both shells, even if it is more relevant in the shell 304A. This latter is possibly related to the most recent epoch of close interaction between SMC and LMC.

4.4 CO clouds

There are essentially two surveys of CO emissions in the Magellanic Clouds. One was established in 1988 by a joint ESO-Swedish Key Programme on the SEST. The Programme had two main goals. The first was to find the relation between CO emissions and the molecular hydrogen. The second was to map the CO itself in order to derive the relation to star formation processes. Magellanic Clouds permit the analysis of CO complexes under conditions of low metallicity and high radiation densities compared to the Solar neighbourhood. The observational programme was completed in 1995. Many of the detected molecular clouds are relatively isolated and quite small with dimensions of typically 20pc. The observations with a linear resolution of 12pc allowed the determination of a set of about 15 molecular clouds.

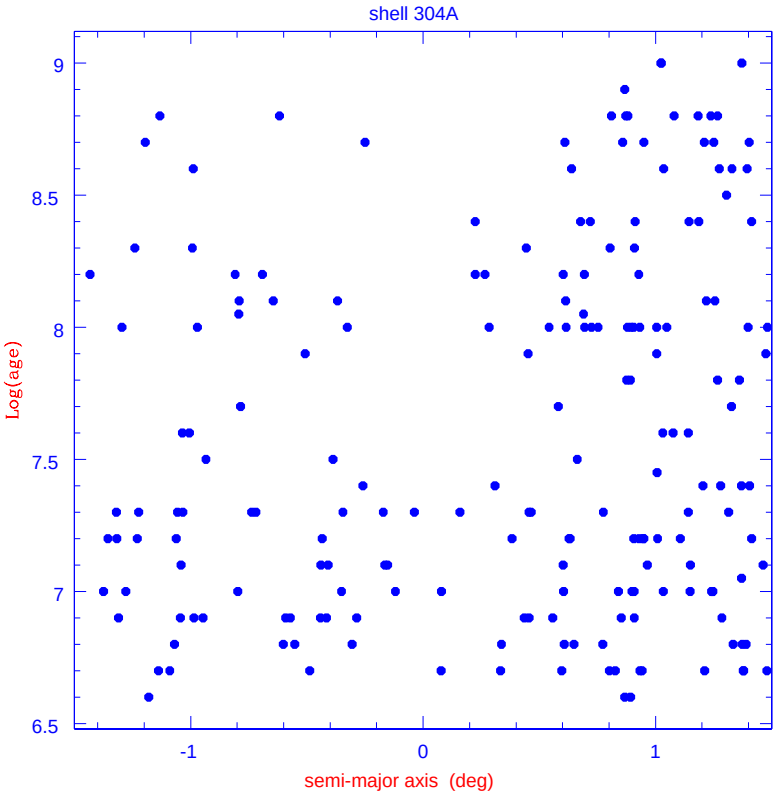

Figure 4.3: Age distribution inside the super-shell 304A plotted against the semi-major axis (see the text for details). Negative values of the semi-major-axis indicate objects located East of the centre, while positive values refer to clusters West of the centre.

The second survey is the CO Survey of the SMC with NANTEN millimeter-wave telescope. The area covered by the SEST survey was only 2% of the area covered by NANTEN survey. The results of this survey are presented by Mizuno et al. (2001). They performed new observations of the SMC in the J=1-0 rotational transition of the interstellar carbon monoxide (CO) molecule at 2.6mm wavelength. The NANTEN telescope, with an angular resolution of 2'.6, is the ideal instrument to determine the properties of giant molecular clouds (GMCs) at a linear resolution of ∼50pc. Mizuno et al. (2001) analyzed carefully the correlations between cluster, association and emission nebulae and the CO clouds. Young emission objects like HII regions are well correlated to CO clouds. They analyzed two regions in the NE and SW of the SMC, and gave a quantitative estimate of the correlation saying that ∼31% in the NE and ∼39% of the objects in the SW are correlated to CO

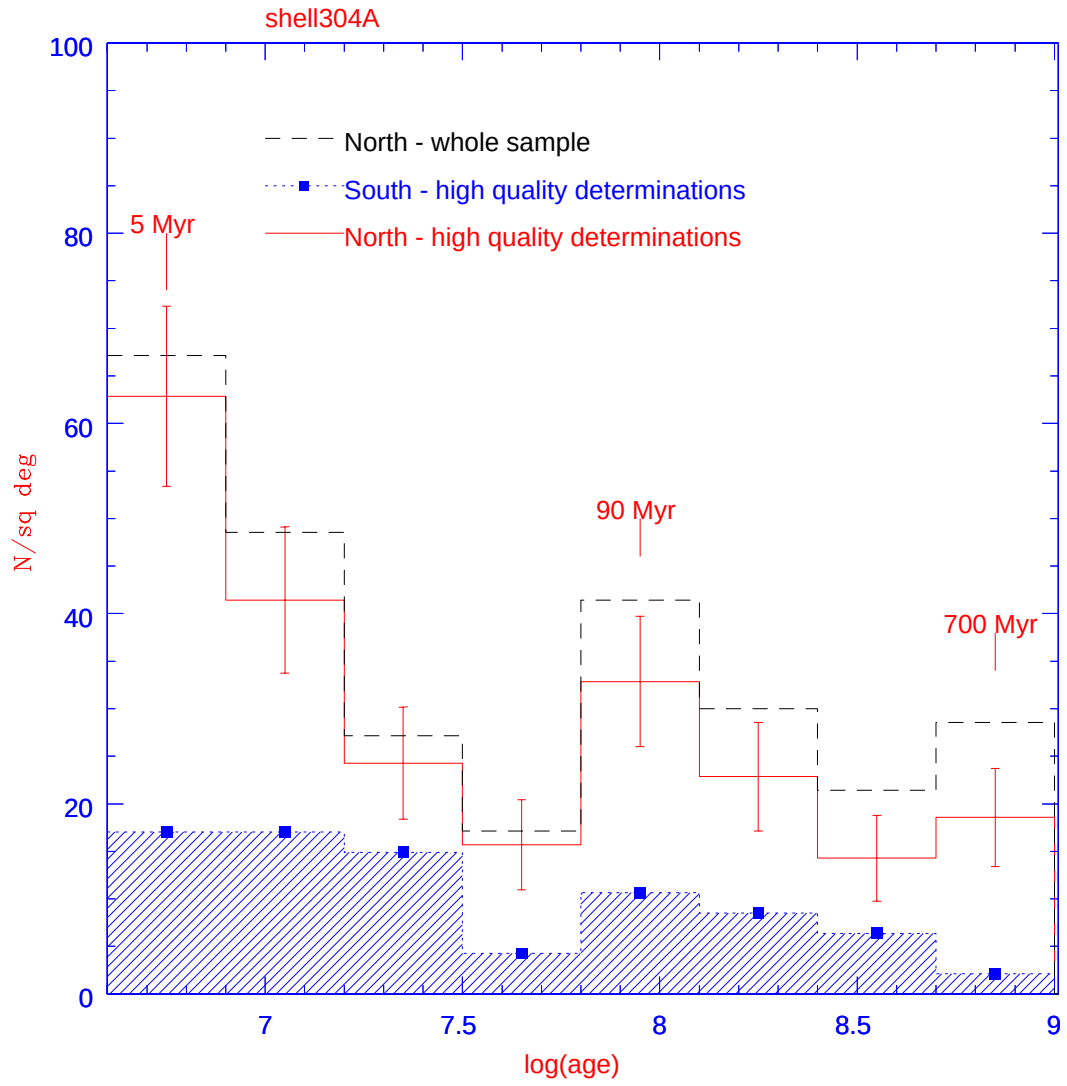

Figure 4.4: Dashed line shows the cluster age distribution for the whole sample of objects inside the shell 304A North of the line drawn in Fig. 2.8 where the large regions of H_α emission are located. Continuous line is the analogous for clusters having high quality determinations of the age, while dashed histogram is the analogous at the Southern side. Error bars indicate the Poissonian uncertainties on the counts.

clouds. These fraction are higher than the probability of a chance coincidence. The probability of a chance coincidence is calculated as

$$P_c = \frac{Area_{CO}}{Area_{TOT}} \tag{4.2}$$

where P_c is the probability of a chance coincidence, $Area_{CO}$ is the area covered by CO clouds and $Area_{TOT}$ is the total surface. The probability of a chance coincidence is $\sim$5% in the NE area and $\sim$11% in the SW. For older objects the probability of a chance coincidence is of the same order as the probability of being associated.

The estimate for the molecular mass present in the SMC derived from the luminosity is about $4.2 \times 10^6 M_\odot$ that corresponds to 0.6% of the total atomic mass (Hindman and Balnaves, 1967).

4.5 Correlation of the clusters with their environment

In this section we first make use of the correlation function to discuss the degree of clustering of the objects and derive the spatial scale of the formation. Then we explore the correlation between the clusters and their environment, in particular the HI flux and velocity dispersion, and the location of the CO clouds.
We adopt the two-point correlation function as a description of the distribution of clusters and associations with the HI flux map by Stanimirovic et al. (1999). This allows a quantitative measurement of the clustering to complement the visual exploration of the maps (see following). $\xi(r)$, the autocorrelation function, is defined using the probability $1 + \xi(r)$ of finding a neighbour in a shell element of volume d^3r at a distance r from an object of the sample as:

$$1 + \xi(r) = 1/(Nn) \sum_{i=1}^{N} n_i(r)$$

where $n_i(r)$ is the number density of objects found in an annulus centered on the i-th object and having radius between r and r+dr, N is the total number of objects, and finally, n is the average number (Peebles, 1980). A Monte Carlo algorithm is used to derive the area included in the data when the annulus extends outside the studied region.

When the clusters are associated with a continuous map, then the cross correlation function is defined as:

$$1 + \xi(r) = 1/(Nf) \sum_{i=1}^{N} f_i(r)$$

where $f_i(r)$ is the average flux in an annulus with radius r centered on the object, and f is the average flux over the whole region. Using the above definitions, a random distribution of clusters will produce a flat correlation, with $\xi(r) \sim 0$. A peaked $\xi(r)$ at small radii indicates a positive correlation, and the full width half maximum of the peak itself represents the spatial scale of the association between the cluster distribution and the flux. The absolute value of $\xi(r)$ is a measure of the concentration of the flux at a given distance r from the cluster centre, relative to the average flux. Since only clusters in the disk of the SMC are under discussion, the regions of the HI map outside the OGLE fields are masked out.

4.5.1 Clustering of star clusters and field stars

Fig. 4.5 presents the autocorrelation function of the clusters. Objects younger than 10 Myr show a peaked distribution with half maximum full width of the order of 500pc. This distribution might reflect the structure of the interstellar medium from which they formed. The scale of the clustering is larger than the typical size of molecular clouds in the SMC and LMC which is going from about 10 to 100 pc (Israel et al., 2003b) but is comparable to the size of the complexes and groups of molecular clouds found in the LMC and SMC (Mizuno et al., 2001; Israel et al., 2003b). The autocorrelation function of the clusters is getting flatter with age, implying a weaker correlation. In fact, because of cinematic effects, older clusters are more spread out than young objects. In order to verify whether clusters and field stars show evidence of different formation mode, we compare the distribution of the young clusters and young field stars in the SMC disk using the bright star survey by Massey (2002). We select only field stars younger than 10 Myr having $V < 14$. Fig. 4.5 presents the autocorrelation function of the bright field stars showing the same spatial scale as the clusters, but a higher degree of correlation.

4.5.2 Cross-correlation of the cluster distribution with HI map

The HI 21-cm emission line provides a measurement of the content and kinematics of the atomic hydrogen. Fig.4.6 compares the HI map by Stanimirovic et al. (1999) with the location of the young clusters. The region of the maximum HI intensity is located at $\alpha = 00^h47^m33^s$ and $\delta = -73^0 05' 26''$ and shows cluster formation at the edges, where the rim of the super-shell 37A is located. A quantitative measurement of the degree of correlation between clusters and HI is presented in Fig.4.7 showing the correlation function at different ages. Clusters younger than 10 Myr show a

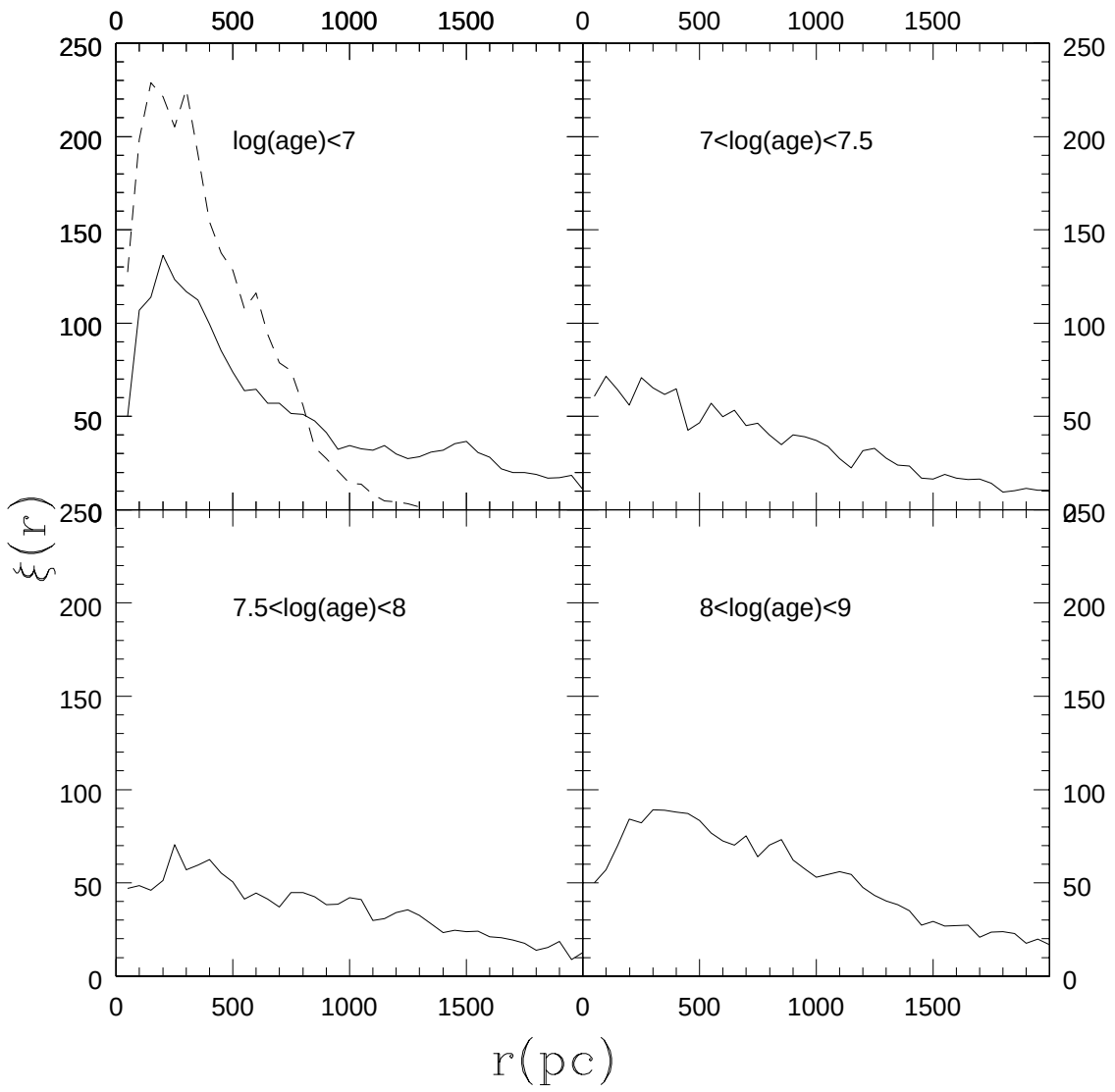

Figure 4.5: Autocorrelation function of clusters (solid line) and field stars younger than 10 Myr (dotted line)

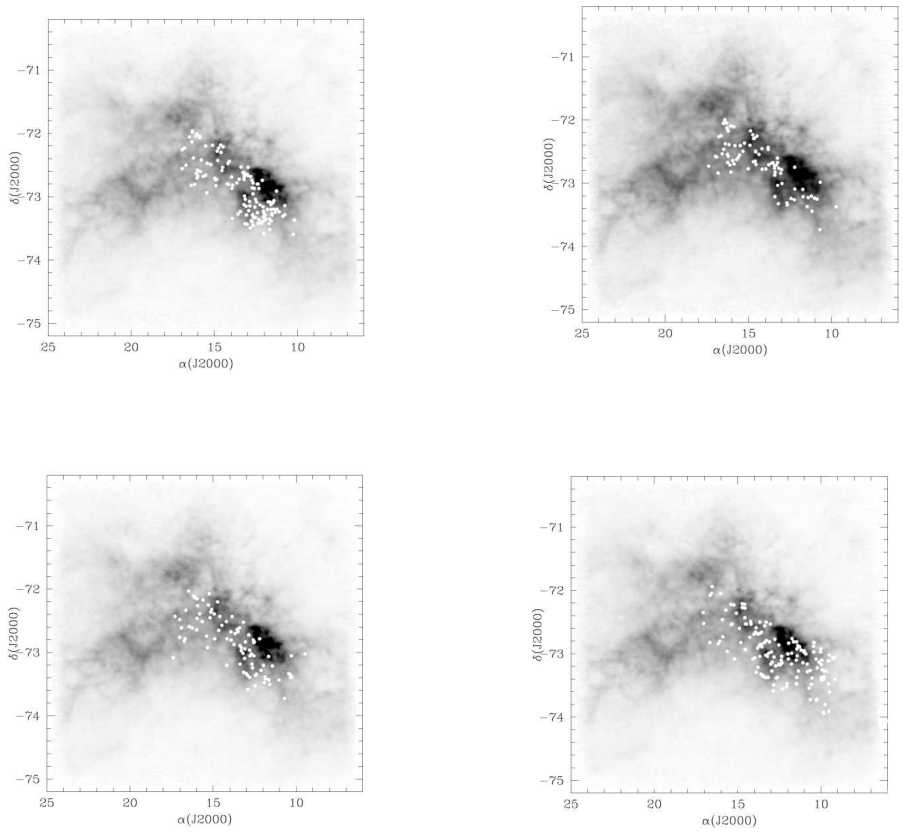

Figure 4.6: The HI column intensity map in SMC is compared with the location of clusters of different ages. Top left panel refers to object younger than 10 Myr; top right panel presents clusters in the age range 10-30 Myr; bottom left panel shows the objects having ages going from 30 to 100 Myr; bottom right presents clusters from 100 to 1000 Myr old

positive correlation with the HI map. The degree of correlation is decreasing with age. The correlation is the weakest for clusters in the age range 300-1000 Myr, with a plateau in $\xi(r)$ in the inner 250 pc, implying that the clusters are located away from the peaks of the HI. This positive correlation confirms that the formation of clusters is related to the presence of atomic gas.

4.5.3 Comparing cluster distribution and HI velocity dispersion

A comparison between the cluster distribution and the velocity field provides additional information about the formation and evolution of young clusters. Tidal

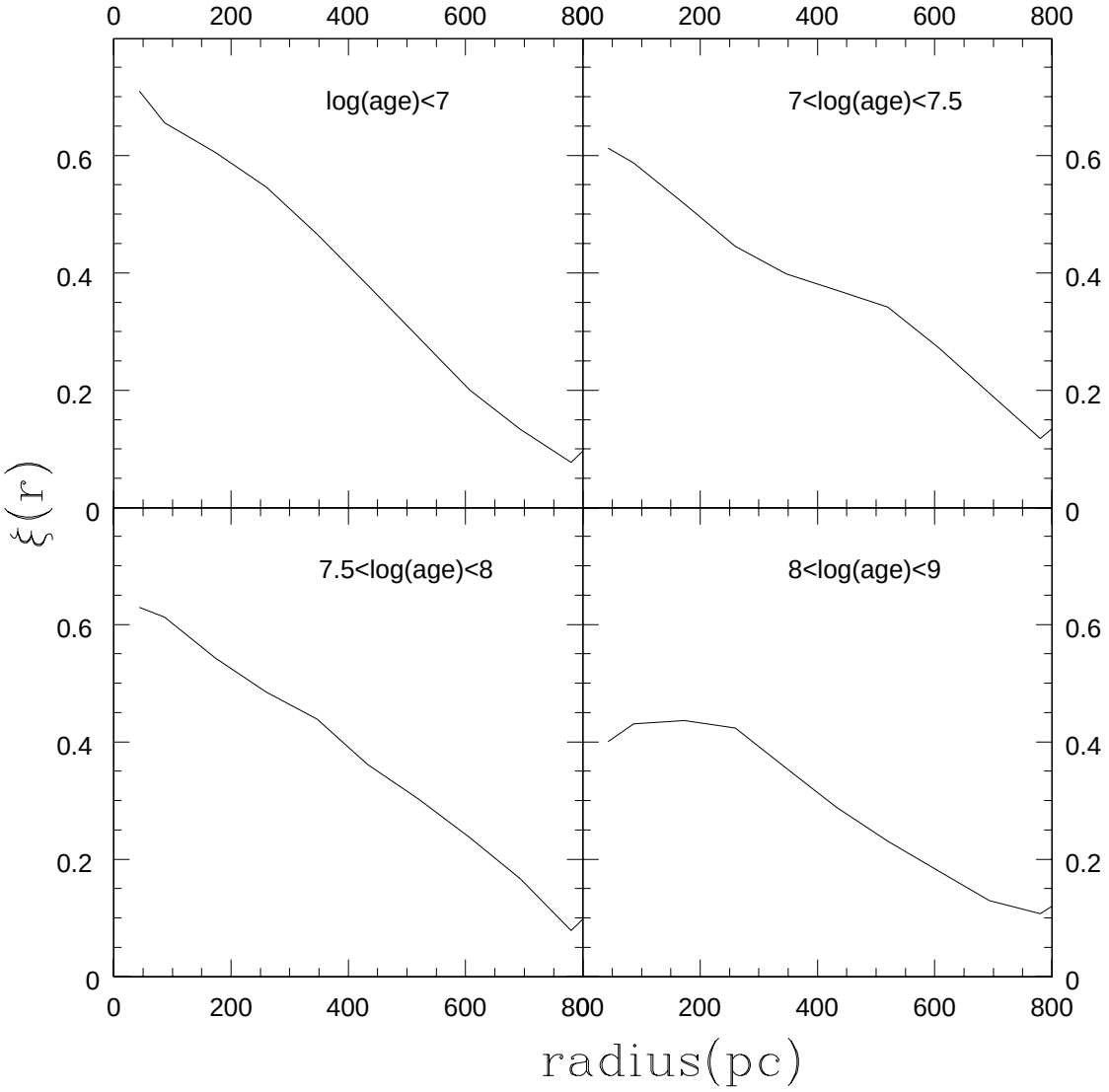

Figure 4.7: Correlation function between clusters and HI flux map

interaction between the SMC and LMC/MW involves a motion of the gas, which in turn might cause shocks and trigger star and cluster formation. The quasi periodic approaches of the SMC to the LMC sustain tidally and hydrodynamically the large scale turbulent motions in the gas (Kumai et al., 1993). In fact the SMC gas is found to present large scale motion elongated on the line of sight (Mathewson et al., 1986; Stanimirovic et al., 1999). On the other hand, supernovae explosion and stellar winds from young clusters can put energy into the interstellar medium influencing the motion of the gas. So a correlation between clusters and high velocity dispersion of HI can cast light on both the cause and the effects of the cluster formation. We compare in Fig.4.8 the velocity dispersion field of the HI in SMC (Stanimirović et al., 2004) with the location of the clusters of different ages. If clusters are formed in high velocity gas motion, then we expect a correlation between the position of young objects and the velocity dispersion of HI. The super-shells 37A and 304A are clearly visible as disturbances on the velocity field. In the shell 304A about 48% of the clusters younger than 10 Myr are apparently located in the high dispersion regions ($\sigma_v > 25$ Km/s). The percentage of objects related to high velocity motion is still 45% in the age range 20-100 Myr, and is about 35% at ages of 1 Gyr. In the shell 37A clusters and associations younger than 10 Myr are found in regions of intermediate velocity ($\sigma_v \sim 15 - 25$ Km/s). Only the 8% of young clusters is apparently located in the high velocity regions. Surprisingly, about 30% of clusters in the age range 100-1000 Myr seems to be correlated with high velocity motions, which might be due to chance superposition along the line of sight. If we assume that the distribution of the clusters is uniform, then the probability of a chance superposition is given by the ratio of the area of the high velocity regions over the total disk area. Under this assumption, the probability of a chance superposition is of the order of 32%.
Summarizing this section, cloud collisions might have triggered cluster formation in the region of 304A. However this mechanism does not seem to account for the formation of clusters in 37A.

4.5.4 CO clouds

Finally, to derive more information about the recent star formation process, we compare the distribution of the clusters and of the CO clouds. CO emission provides a probe of molecular gas inside the galaxies, since it is related to H_2 column density. Rubio et al. (1993), Mizuno et al. (2001) reveal the presence of two main complexes of CO molecular clouds located in the South West $\alpha = 0^h45^m$ and $\delta = -73^0 35'$ and North East at $\alpha = 1^h00^m$ and $\delta = -72^0 20'$. They find that the location of Giant Molecular Clouds (GMCs) shows a good spatial correlation with the HII regions and young emission clusters indicating that cluster formation is ongoing.

We compare the age distribution with the CO cloud catalog by Mizuno et al. (2001)

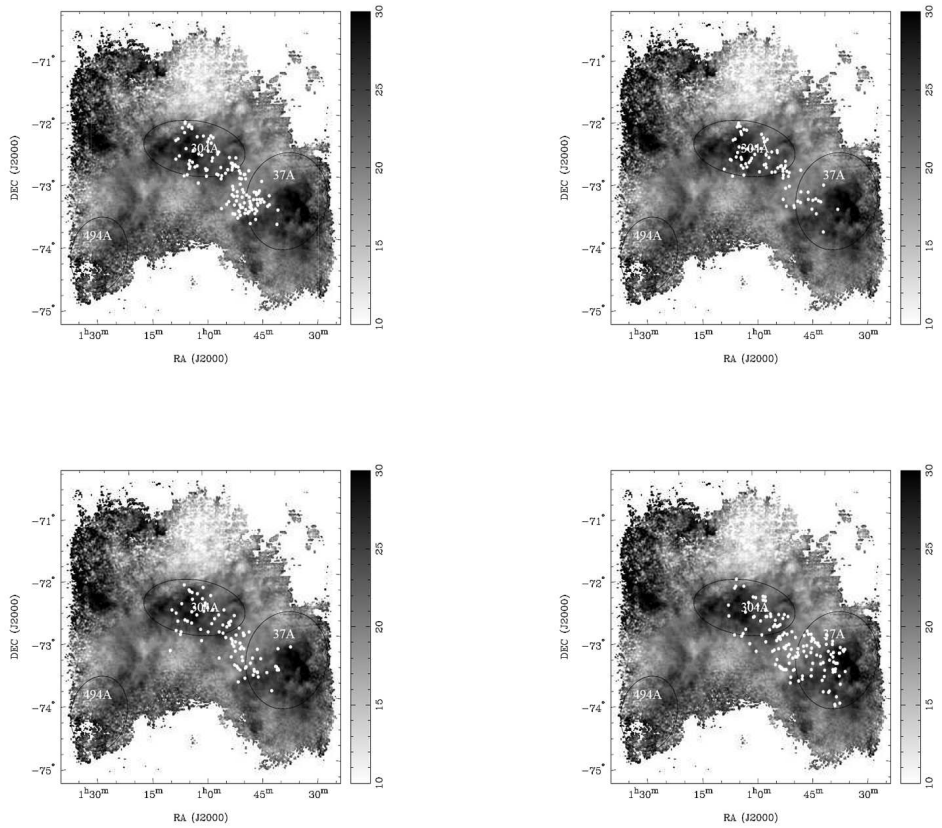

Figure 4.8: The velocity dispersion field of the HI in SMC taken by Stanimirovic et al (2004) is compared with the location of clusters of different ages. Top left panel refers to object younger than 10 Myr; top right panel presents clusters in the age range 10-30 Myr; bottom left panel shows the objects having ages going from 30 to 100 Myr; bottom right panel presents clusters from 100 to 1000 Myr old

in the SW region of the disk. This region is located at the Eastern rim of the supershell 37A. We find that about 20% of the clusters older than 10 Myr are located close to the CO emission (Fig.4.9). The percentage of associated clusters becomes 35% when younger objects are considered. Assuming a uniform cluster distribution, the probability of a chance superposition is of the order of 11% (Mizuno et al., 2001). A significant fraction of the objects younger than 10 Myr are probably physically associated with the clouds. Our result implies a rapid dissipation of the CO clouds. This is in agreement with the evolutionary time scale of the giant molecular clouds derived in the LMC by Fukui (2005). Fig. 4.10 compares the location of the clouds with field stars younger than 10 Myr (or brighter than V=14) taken from the catalog by Massey (2002). The 38% of the stars younger than 6 Myr (or brighter than V=13)

are associated with the clouds, while only 25% of the stars in the age range 6-10 Myr are located in the proximity of the CO emission. This gives further support to the idea that the formation of young clusters and field stars is closely related to the CO clouds. In addition, about 70% of the stars younger than 10 Myr and associated with the clouds are located close to the Eastern side of the clouds themselves. We point out that the SW CO clouds are located toward the interface between the two super-shells, 37A and 304 A: dynamical effects due to the expansion of the super-giant shells may be important in triggering the compression of the molecular clouds and the formation of new stars. Fig. 4.10 might indicate that young stars are more easily found at the compression edge of the clouds. This effect is more relevant for field stars, while is not obvious for the cluster distribution. The Northern region studied by Mizuno et al. (2001) where CO clouds are found is not included in OGLE data. Fig.4.11 shows the location of field stars brighter than V=14 and of the CO clouds in this region. The data are from Massey (2002). Only a negligible percentage of stars is apparently associated to the CO clouds. This is in agreement with Mizuno et al. (2001) who find a substantial difference between the CO cloud complexes in the SW and in the North of the disk. In the Northern region, the clouds are smaller in size than those of SW region. No particular correlation is found with the distribution of young associations and clusters except for the objects associated with N66. In our Galaxy massive stars are formed in clusters in giant molecular cloud (GMC) complexes and almost no GMCs are found in the solar vicinity lacking of massive young stars (Fukui, 2005). Discussing the distribution of CO clouds in the LMC, Fukui et al. (1999) and Fukui (2005) find a different behaviour, classifying the giant molecular clouds in three groups: 1) without massive OB stars (which does not exclude that low mass stars are formed); 2) associated with small HII regions; 3) associated with clusters and large HII regions. About 38% of the molecular clouds in the LMC are not related to recent massive star formation. If CO emission surveys over larger areas confirm this finding, then the properties of massive star formation regions are probably different in the Milky Way from those in the MCs.

4.6 Final remarks

1) The two shells 37A and 304A are clearly visible in the spatial age distribution of the clusters younger than about 15 Myr: the mechanism responsible of the shell formation (SN, stellar winds, and/or turbulence) is closely related to the cluster formation. The regions have been very active especially at the edges of the shells and in the inter-shell region since 1 Gyr ago. In the super-shell 37A clusters younger than a few 10^7yr are located at the Eastern rim of the super-shell 37A where gas and dust are located, while older episodes are widely distributed. The cluster age distribution at the Eastern part shows a young episode at a few Myr, and several enhancements, namely between a few Myr and 15 Myr, and at 80 Myr. On the

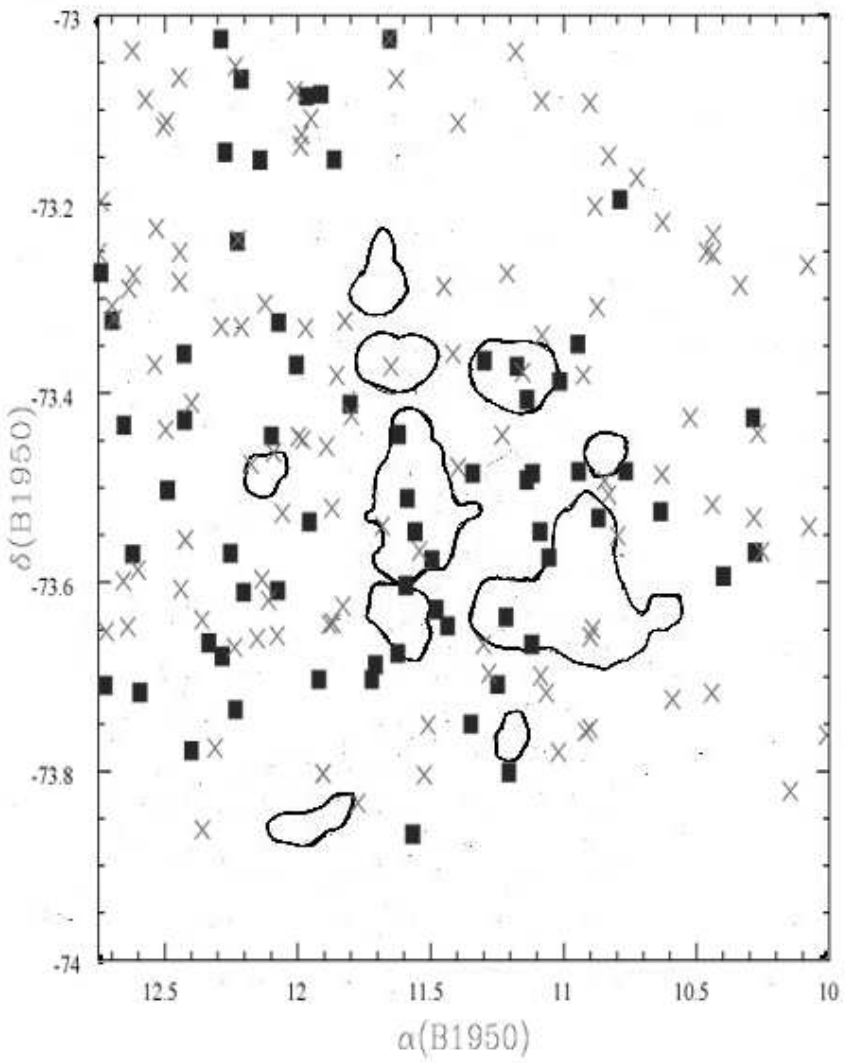

Figure 4.9: The distribution of clusters and associations younger than 10 Myr (squares), and clusters older than 10 Myr (crosses) is compared with the approximate location and size of the CO clouds (heavy solid line) in the region of the shell 37A

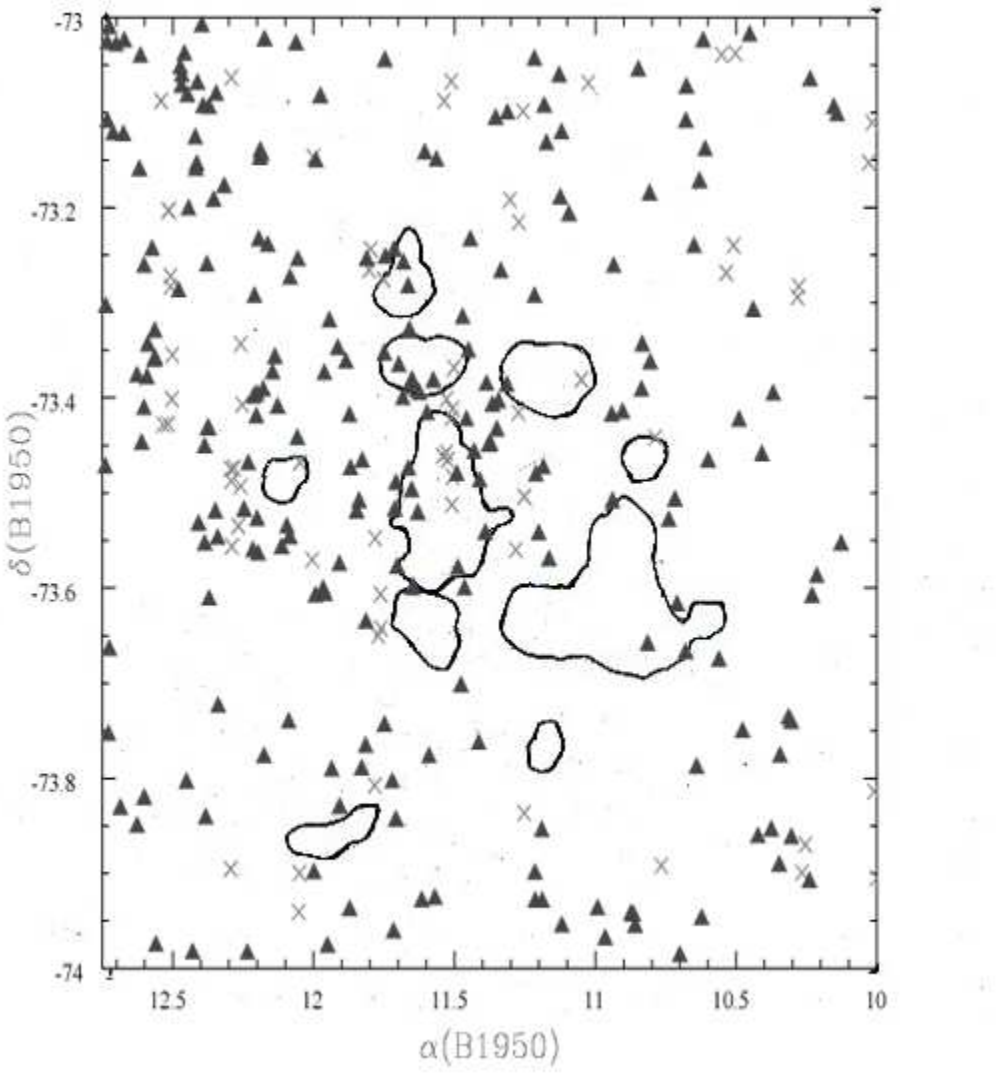

Figure 4.10: The distribution of field stars younger than 6 Myr (crosses), and stars in the age range 6-10 Myr (triangles) is compared with the approximate location and size of the CO clouds (heavy solid line) in the region of the shell 37A

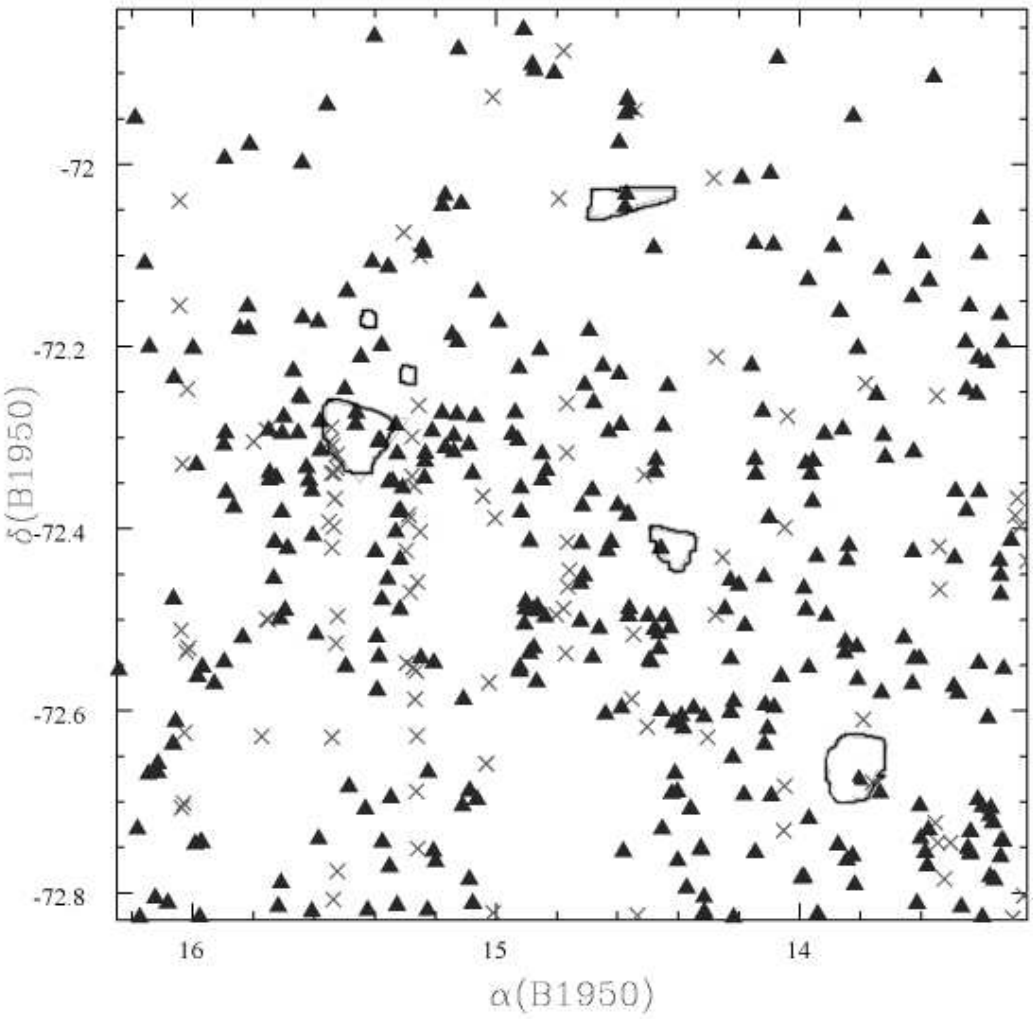

Figure 4.11: The distribution of field stars younger than 6 Myr (crosses), and stars in the age range 6-10 Myr (triangles) is compared with the approximate location and size of the CO clouds (heavy solid line) in the Northern region of the disk

Western side, the star formation was less efficient at ages younger than 15 Myr, while it was comparable at older ages. The cluster distribution in the super-shell 304A shows a continuous formation from a few Myr to 1 Gyr. The dominant episode was between a few Myr and 20 Myr. An enhancement is found at 90 Myr.

2) We find that star clusters and associations form in clustered distribution. The typical correlation scale of the clusters is of the order of 500pc, comparable with the dimensions of the large molecular cloud complexes found in the LMC and in the SMC. The two point autocorrelation function of the young massive field stars shows a stronger correlation, but on a comparable scale.

3) A tight cross-correlation between young clusters and the HI intensity is found. The degree of correlation is decreasing with the age of the clusters. Finally clusters older than 300 Myr are located away from the HI peaks. Clusters and associations younger than 10 Myr are related to the CO clouds in the SW region of the disk, but not in the NE where smaller clouds are found. Older generation is more evenly distributed. This is in agreement with the evolutionary time scale of the giant molecular clouds that is found to be of the order of 10 Myr. This correlation indicates that the molecular gas content is associated to the field and cluster formation, but that its presence does not necessarily imply star formation.

4) A weak relation between the location of the young clusters and the velocity dispersion field of the atomic gas is derived. The shell 304A (where a positive correlation is found) is coincident with a high velocity dispersion region where shocks among clouds might have triggered cluster formation. However this mechanism cannot account for the majority of young objects in the southern shell 37A where young clusters are located in a region of intermediate velocity dispersion.

Chapter 5

Field star formation in the HI super-shell region

5.1 Introduction

We now consider the star formation in field areas, i.e. regions that don't contain any star overdensity recognizable as a cluster. It is not clear if the same mechanism is subtended under both processes: star formation in clusters and star formation in the field. We can analyse and compare the rates of star formation of clusters and of the corresponding fields and draw some conclusions.

Concerning the SFR of the field stars in the SMC, no real consensus is reached whether the star formation has proceeded with several periods of enhancements, namely at 400 Myr, 3 Gyr, 9 Gyr as found by Harris and Zaritsky (2004) in the SMC disk, or in a more continuous way, with a main episode between 5 and 8 Gyr as derived by Dolphin et al. (2001) in the halo.

In the study of the field population, assumptions should be made about the line of sight SMC depth, interstellar extinction and age-metallicity relation. We adopt a SMC line of sight depth of 4 Kpc implying a difference in the distance modulus of about 0.14mag (Welch et al., 1987; Zaritsky et al., 2002).

The present-day knowledge of the age-metallicity relation in the SMC is mainly based on clusters. The interpretation of the existing SMC age-metallicity relation widely varies from author to author and is going from continuous enrichment from

the oldest to the youngest objects as found by Da Costa and Hatzidimitriou (1998) and by Dolphin (2000b) to a burst-mode of star formation and enrichment as derived by Olszewski et al. (1996), Pagel and Tautvaišienė (1999), Piatti et al. (2001) Harris and Zaritsky (2004). In the study of the star formation from field stars, we assume the enrichment history by Pagel and Tautvaišienė (1999), while the cluster metallicity is derived from isochrone fitting.

5.2 Field star formation

In this Section we derive the star formation rate of the field stars in order to compare it with the cluster formation epochs. The goal is to verify whether field objects and clusters follow similar modes of formation. We make use of our data inside the super-shell 37A and of OGLE data in the rest of the disk. The CMD of the field stars in this region is shown in Fig.5.1. In the following, we first present the method, then we discuss the star formation history of the field population in the two super-shells, comparing the periods of enhancements with what we derive for the clusters.

5.2.1 The Method

To infer the SFR of this galaxy, theoretical CMDs in different age ranges are simulated. Simulations include the spread due to observational photometric errors and reddening as described in the previous Sections. For each age bin, from 10000 to 15000 stars were generated down to the photometric completeness limit. The generation of the synthetic populations makes use of the set of stellar tracks by Girardi et al. (1996, 2000). The constancy of the initial mass function (IMF) slope in different environments is still a matter of discussion, although a number of recent papers proposed the idea of a universal IMF (Kroupa and Boily, 2002; Wyse et al., 2002; Chabrier, 2003; Weidner and Kroupa, 2004). The determination of the IMF is beyond the scope of this paper. Here the IMF of Kroupa (2001, 2002) is assumed. This IMF is a power-law function with a slope $x = 2.3$ for stellar masses m > 0.5 $M_\odot$, while $x = 1.3$ in the mass range 0.08-0.5 $M_\odot$ (when the standard Salpeter value is 2.35).

The completeness of the data is taken into account by dividing the simulated CMD in magnitude-color bins and then subtracting from each bin having N_{th} stars, (1-Λ)N_{th}, where Λ is the smallest of the V and I completeness factors as given in Fig.2.2.

Finally, the SFR is derived by means of a downhill simplex method (Harris and Zaritsky, 2004), minimizing the χ^2 function in a parameter-space having N dimensions. At each step the local χ^2 gradient is derived and a step in the direction of the gradient is taken, till a minimum is found. In the following, the observational

Table 5.1: Ages and metallicities of the synthetic populations in use.

Age(Gyr)	Z
0.005:0.015	0.006
0.015:0.025	0.006
0.025:0.040	0.006
0.040:0.063	0.006
0.063:0.100	0.006
0.100:0.160	0.006
0.160:0.250	0.006
0.250:0.400	0.006
0.400:0.630	0.006
0.630:1.000	0.006
1.000:1.600	0.001:0.006
1.600:2.500	0.001:0.003
2.500:4.000	0.001:0.003
4.000:6.000	0.001:0.003
6.000:10.0	0.001:0.001
10.0:12.0	0.001:0.001

CMD is divided into bins. Recent work concerning the determination of the SFR from the CMDs has pointed out the importance of using a binning, that takes into account the various stellar evolutionary phases, as well as the uncertainties on the stellar models (Rizzi et al., 2002). In section §3.3 we show that problems arise when isochrones are used to fit the main sequence and the He-burning stars. For this reason, while a coarser magnitude bin distribution is used on the main sequence, only a few bins are considered for the red evolved stars. This avoids that the uncertainties on both the observational errors and the theoretical models (i.e. on bolometric corrections, RGB and AGB location, extension of the core He-burning loop) result in spurious solutions. For this reason, we are not very sensitive to the SFR at ages older than 1 Gyr. This is illustrated in Fig. 6.1. To prevent settling on local rather than global minima, the simplex is first started from a random position, then when a possible solution is obtained, it is re-started from a position very close to it. Finally, when a minimum is found 30000 random directions are searched for a new minimum.

The first guess solution is obtained by comparing the observational CMD with isochrones of different ages and metallicities. We use N=16 stellar populations, whose ages, metal content are listed in Table 7.5.

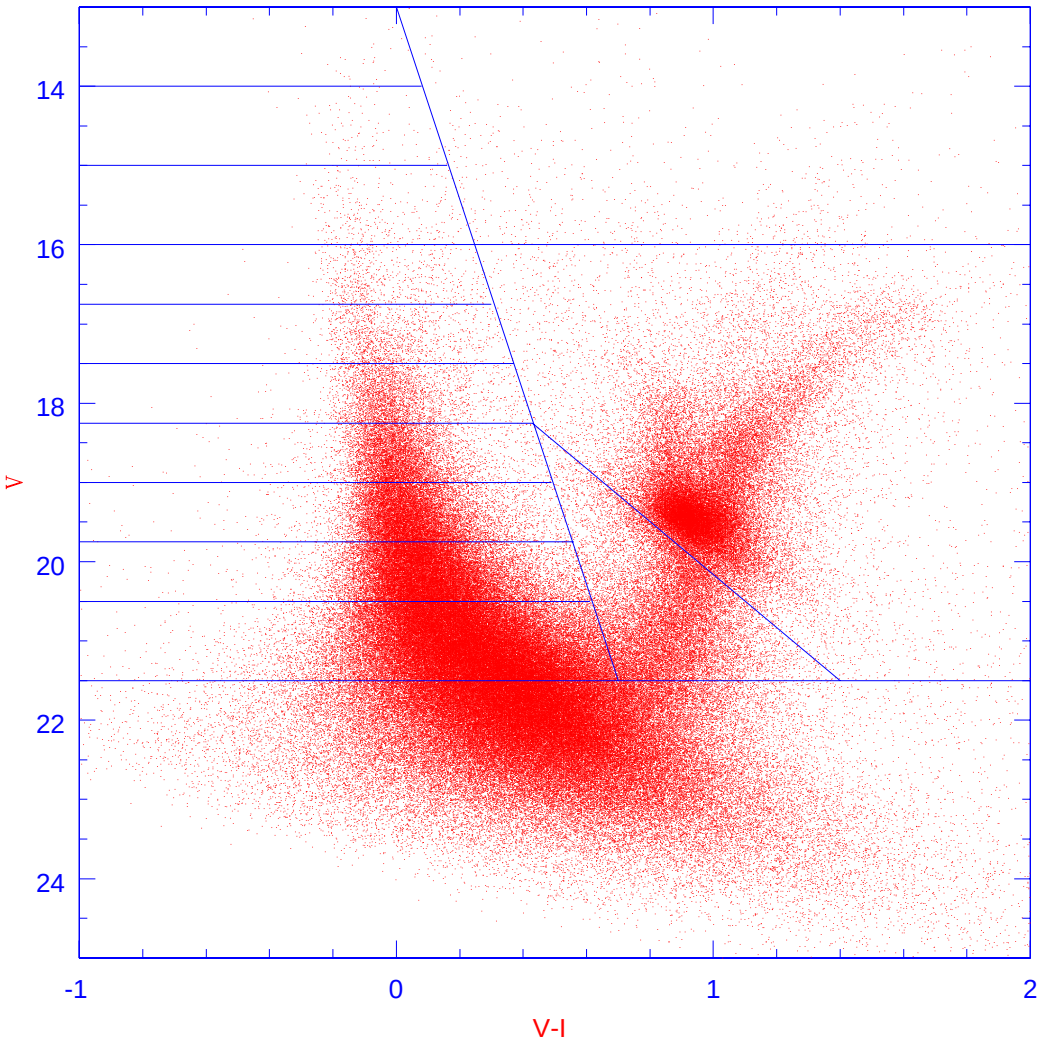

Figure 5.1: The CMD of the field stars in the super-shell 37A together with the adopted bin division

5.2.2 Testing the downhill simplex

Before proceeding with the star formation rate determination we really need to test our method. Uncertainties may come both from downhill simplex precision limit and from stochastic variables in the generation of stellar populations. Other sources of uncertainties may come from reddening parameter or other parameters intervening in the determination of the histograms.

First we want to cast light on the limits of the method. On this purpose we generate a mixture of synthetic population from a first set of populations. Then we try to recover the rate of star formation of this known mixture with another set of populations. This second set of populations is generated with another seed for random variables. Solutions are in good agreement up to the age of 1Gyr as you can see in Fig. 5.2. Then at that point it results an uncertainty of 1Gyr in the position of the peaks of the two distributions.

The same test was repeated changing the reddening, in order to see the response of the solution to little variation of the parameters. First we set E(B-V)=0.13, then we changed to E(B-V)=0.08 and see how the histogram varies. We can notice that it has approximately the same behaviour as in the first case, with an uncertainty of about 1Gyr for the older ages.

5.2.3 Field star formation history in the HI-shells

Analogously to section 4.3.1 we subdivide the shells in two regions. Fig. 5.4 shows the SFR in the shell 37A. As noticed in the cluster age distribution (see Section 3.3) the star formation process has been much more active on the East side of 37A, in the region between the two shells. Concerning the young population, enhancements of the SFR are found at 5, 50, 130 Myr both on the East and on the West side.

Fig. 5.5 presents the SFR in the shell 304A. In the Northern side of the super-shell the SF was more active at young ages. The SF was continuous from a few Myr to about 160 Myr with period of enhancements from 5 to 40 Myr and between 100-160 Myr. The SFR in both shells is consistent, even if the intensity of the younger episodes was higher in the shell 304A.

Summarizing, in both shells the field star formation was continuous in the past 160 Myr. A global burst of SF is found at ages of a few Myr, which might be responsible of the fractal structure of HI interstellar medium (Stanimirovic et al., 1999; Hatzidimitriou et al., 2005). The SF rate at older ages was less active. Enhancements are found between 100-150 Myr and between 1 and 1.6 Gyr, corresponding to

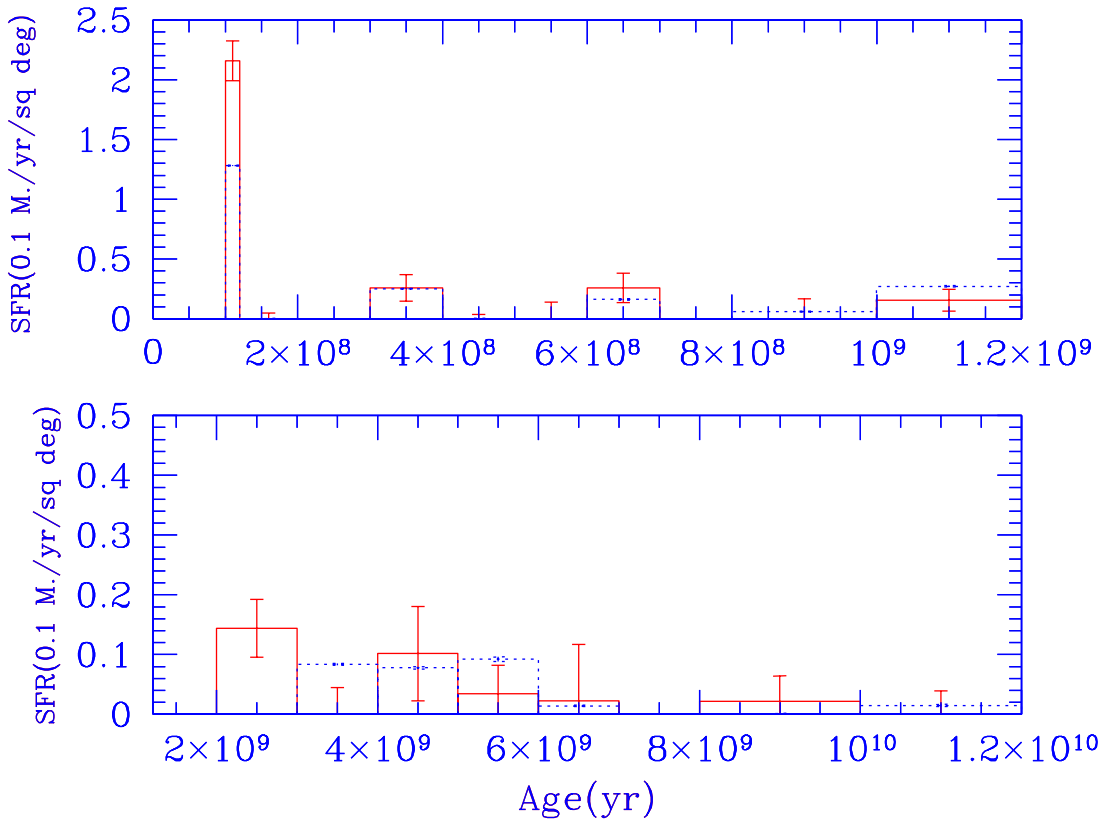

Figure 5.2: The original rate from the synthetic population mixture (solid line) is compared to the recovered one (dotted line).

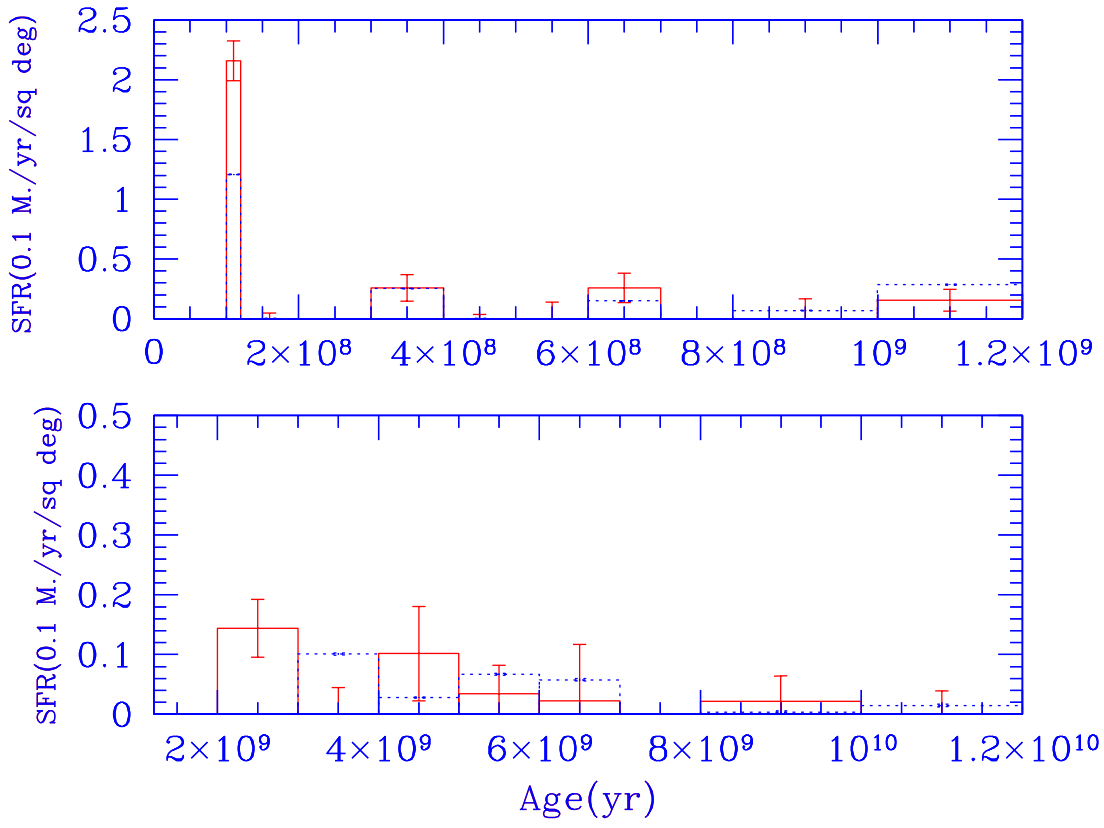

Figure 5.3: The original rate from the synthetic population mixture (solid line) with E(B-V)=0.13 is compared to the recovered one (dotted line) with E(B-V)=0.08.

a close interaction between SMC and LMC. We remind that the data do not allow precise determination of the SF at older ages.

Comparing with the cluster age distribution (see previous Sections), we find that there is not a complete coincidence between cluster and field star formation, suggesting a different mode of formation. However, formation episodes involving both happened at 5, 20, and finally at 100-150 Myr, in coincidence with SMC perigalactic passage as it will be discussed in Chapter 8.

At present, no detailed studies of the cluster and field star formation due to tidal interaction in the SMC are available. However the evolution and star formation history of LMC has been derived in great detail by Bekki and Chiba (2005). They pointed out that gravitational interactions do not necessarily influence in the same way cluster and field star formation. In fact, cluster formation is expected to take place only if the perturbation due to tidal effects is strong enough to trigger high velocity cloud-cloud collision. Field star formation is more sensitive to tidal triggers and it is expected to take place under less restrictive conditions. The model by Bekki and Chiba (2005) predicts no cluster formation in the LMC at the time of the first perigalactic passage, 6.8 Gyr ago, when field star formation was enhanced, while a strong enhancement of the cluster and field star formation rate in the LMC is expected as a consequence of the strong Galaxy-LMC-SMC interaction between 2-3.5 Gyr ago. At that time, the peak of the cluster formation is almost coincident with the peak of the field star formation, although slightly delayed, taking place 2.5 Gyr ago. Cluster and field star formation is expected in the LMC 100-200 Myr ago, at the time of the most recent interaction with the SMC.

Our results point out that the last interaction between SMC and LMC has triggered cluster and field star formation in the SMC, in agreement with what is found in the LMC and is predicted by the models.

5.3 Final remarks

The field star formation was continuous in the past 160 Myr. Then periods of quiescence were followed by enhanced activity. A global burst of SF is found at ages of a few Myr, which might be responsible of the fractal structure of HI interstellar medium. Enhancements are found between 100-150 Myr and between 1 and 1.6 Gyr, perhaps corresponding to a close interaction between SMC and LMC. If so, the last tidal interaction between the MCs (100-200 Myr ago) has triggered the formation of both clusters and field stars. However, clusters and field formation rates are not completely coincident, suggesting a different mode of formation.

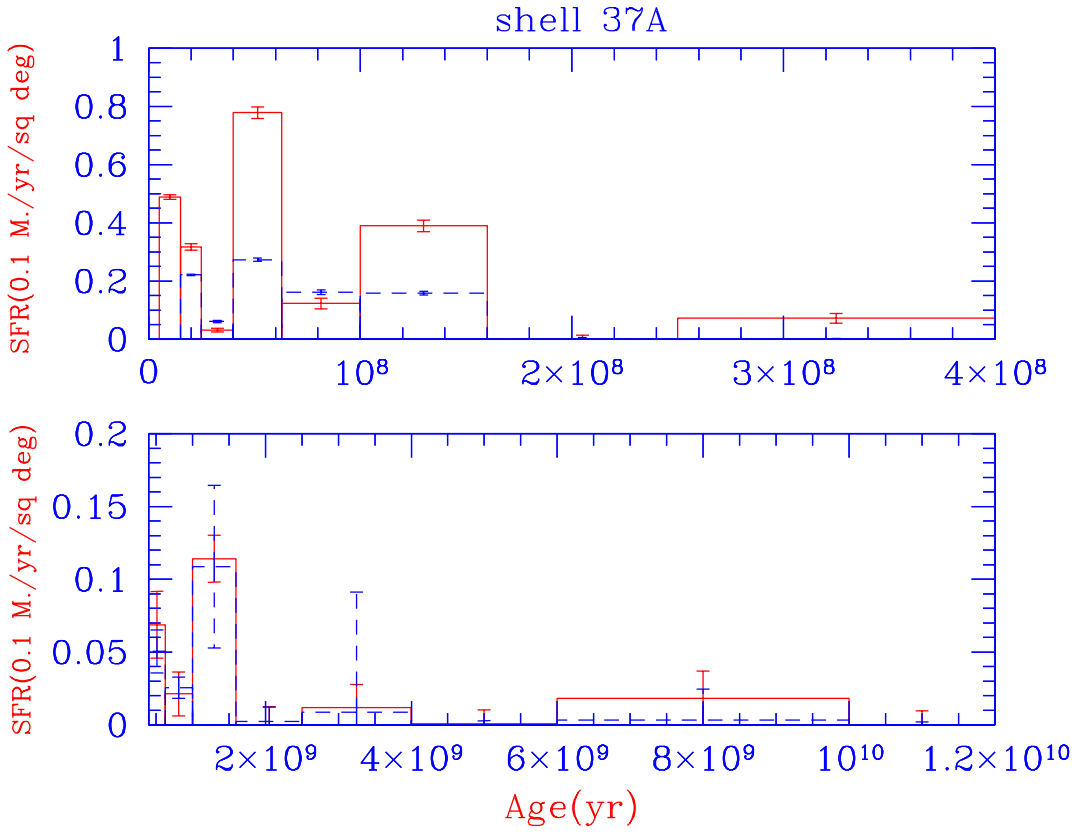

Figure 5.4: SFR on the East side of the super-shell 37A (solid line) and on the West side (dashed line).

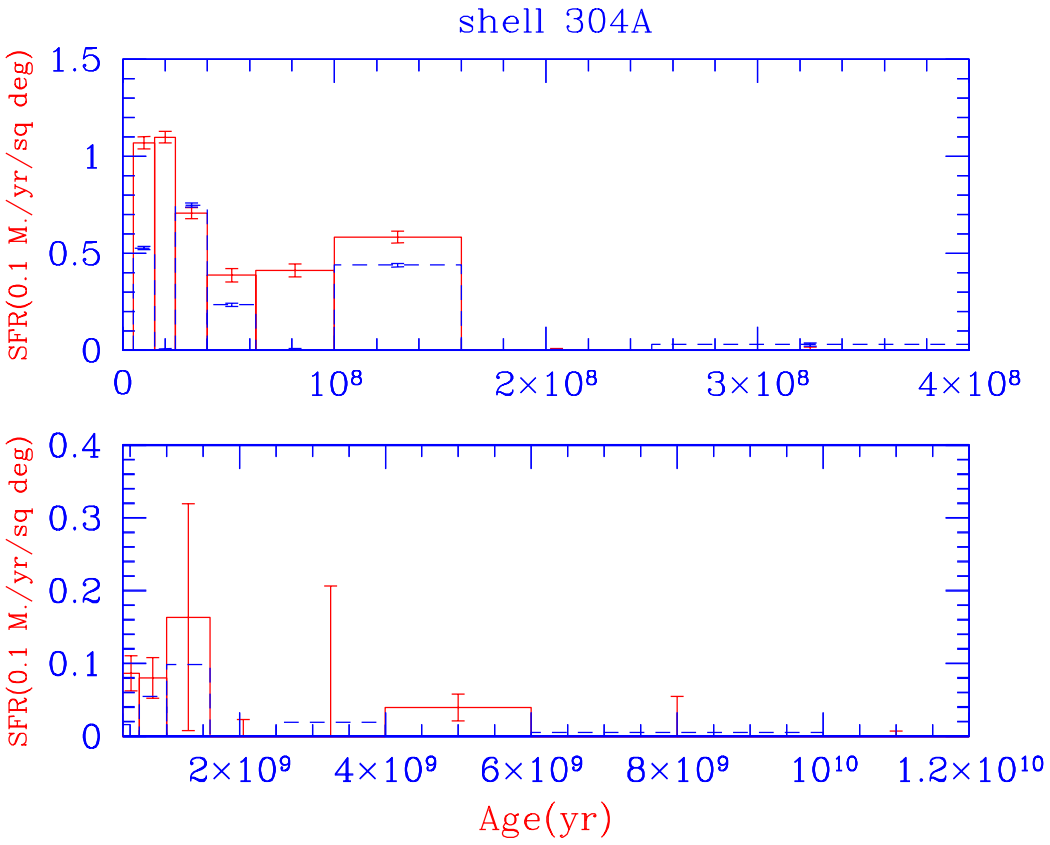

Figure 5.5: SFR on the Northern side of the super-shell 304A (solid line) and on the southern side (dashed line).

Chapter 6

SFH in the fields of NGC265, K29, and NGC290

6.1 Introduction

In this Section we derive the SFH of field stars using the companion fields of the clusters NGC265, K29 and NGC290 for which high quality HST photometric data are available. This is an important step of the analysis as the dynamical interaction of the SMC with nearby galaxies, i.e. the LMC and the MW is still a matter of debate with a high degree of uncertainty. Therefore, accurate determinations of the age at which intense star formation activity took place would help us to constrain the dynamical problem (Yoshizawa and Noguchi, 2003).

In Chiosi et al. (2006) we made use of the OGLE II data to derive the SFH in the SMC disk. We found evidence of several bursts of star formation younger than 2 Gyr together with episodes due to local phenomena. A burst is found at 200 Myr which can be ascribed to the dynamical interaction between the MW and the MCs. The limiting magnitude of the ground-based photometry did not allow any firm conclusion concerning older episodes. The much deeper limiting magnitude of the present HST-data allows the study of the star formation rate at significantly older ages.

6.2 SFH of the cluster fields

In the following, first we present the method, then we discuss the star formation history of the field population in the studied regions. To derive the field star formation rate, we make use of the whole area of the ACS/WFI CCD#2 covering 202×101 arcsec, where the cluster centre is not located. This would allow a good statistics. Although in each cluster we are well outside the core radius, some residual cluster contamination might still be present, but this would result in a spurious peak at younger ages. Since we are most interested in the determination of SFR at old ages, this would not be a problem.

6.2.1 The Method

Detailed description of the adopted method can be found in Chiosi et al. (2006). Here we recall a few points. To infer the SFR of a galaxy, theoretical CMDs in different age ranges are simulated. The simulations include the spread due to observational photometric errors, reddening, and the effect of photometric incompleteness. For each age bin, from 10000 to 15000 stars were generated down to the photometric completeness limit. The synthetic populations stand on the sets of stellar tracks by Girardi et al. (2002). The relative contribution of different populations to the total CMD and luminosity/colour functions to be compared with the observational ones, in other words the past history of the SFR, is derived from a minimization algorithm that stands on the downhill simplex method (Harris and Zaritsky, 2004). It minimizes the χ^2 function in a parameter-space having N+1 dimensions (the component stellar populations, here discretized to a finite number N). At each step of the simplex method, the local χ^2 gradient is derived and a step in the direction of the gradient is taken, till a minimum is found.

In the following, the observational CMD is divided into suitable magnitude-colour bins. Due to the very small field of view of ACS/WFI data, red evolved stars are statistically not very significant. Since the fit is mainly based on the main sequence, 28 bins of variable width, going from 0.5 mag from 14 to 19 mag, to 0.25 mag from 19 to 25 mag are used to describe the main sequence, while only two bins of suitable mag width describe the red giant region, i.e. one in the subgiant region and one in the core He-burning clump. This is illustrated in Fig. 6.1.

Care is paid to prevent settling of the simplex on local rather than global minima. Simplex is first started from a random position, then when a possible solution is obtained, it is re-started from a position very close to it. Finally, when a minimum is found, 30000 random directions are searched for a new minimum.

We use N=15 stellar populations, whose ages and metal content are listed in Table

Table 6.1: Ages and metallicities of the synthetic populations in use.

Age (Gyr)	Z
0.08:0.12	0.006
0.1:0.3	0.006
0.3:0.4	0.006
0.4:0.5	0.006
0.5:0.6	0.006
0.6:0.8	0.006
0.9:1.0	0.006
1.0:2.0	0.001:0.006
2.0:3.0	0.001:0.003
3.0:4.0	0.001:0.003
4.0:5.0	0.001:0.003
5.0:6.0	0.001:0.003
6.0:8.0	0.001:0.001
8.0:10.0	0.001:0.001
10.0:12.0	0.001:0.001

7.5. Populations younger than 100 Myr are under-sampled and will not be considered in the discussion. The entries of Table 7.5 also show that the component stellar populations are chosen in such a way that a suitable chemical enrichment history is assumed. The one at work here is the chemical history found by Pagel and Tautvaišienė (1999).

6.3 Discussion

Star formation in the three fields shows several common features (see figures 6.2, 6.3, 6.4). In all the fields, the star formation was not continuous but proceeded in a number of bursts taking place at 0.3-0.4 Gyr, 3 Gyr and 6 Gyr ago.

The bursts at 3 and 0.4 Gyr are temporally coincident with past peri-galactic passages of the SMC about the Milky Way. It is well known that the young field population presents an asymmetric structure biased toward the eastern LMC -facing side of the SMC . Crowl et al. (2001) find the same trend among the SMC populous clusters: those toward the eastern side tend to be younger and more metal rich than those on the western side. This is interpreted as the effect of the perturbations developed by the interaction of LMC-SMC-MW (see Chiosi et al. (2006) for a wider

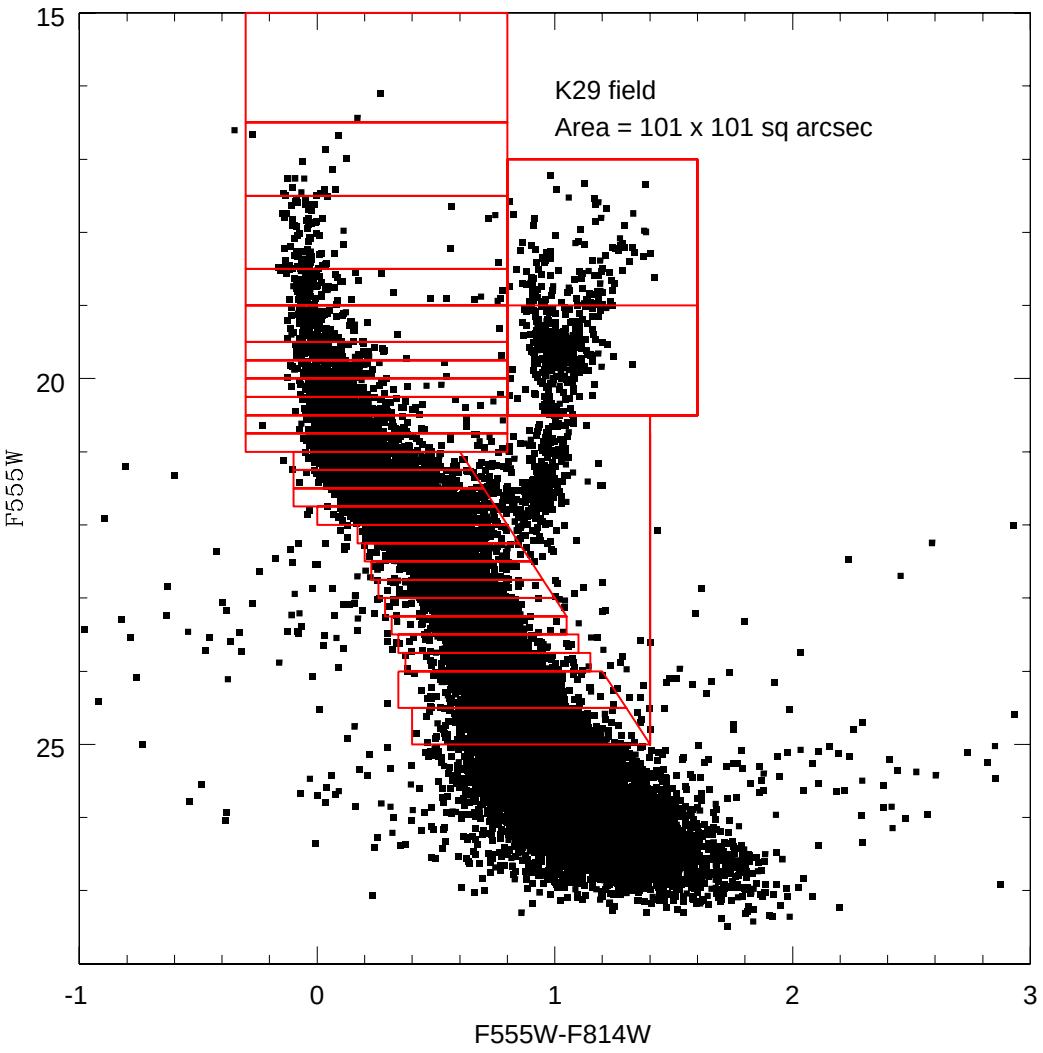

Figure 6.1: The CM diagram of the field of K 29 with superimposed the grid adopted to derive the star formation. The same grid is used for the theoretical simulations. We count all the stars inside each box both in the synthetic and observational diagrams to construct the final SF history. The solution of the downhill simplex is the combination of coefficients (i.e.the mix of synthetic diagrams) that better fit the observational diagram.

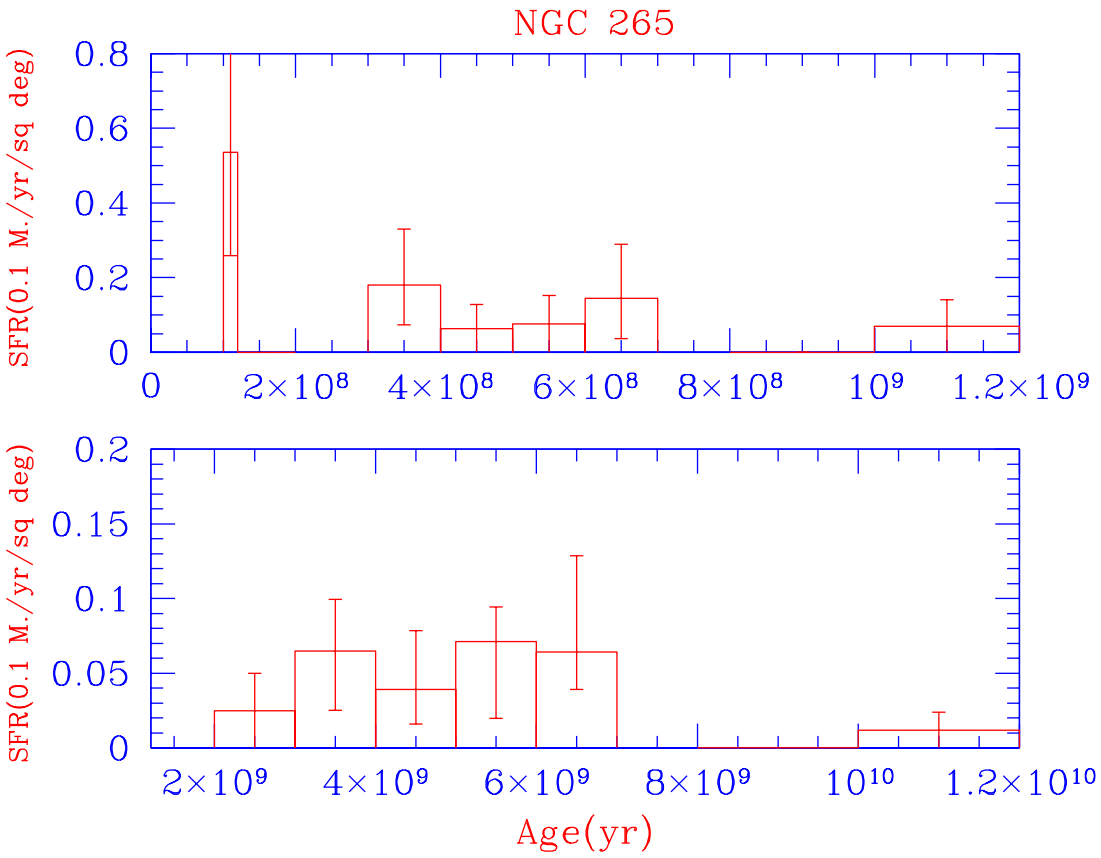

Figure 6.2: Star formation history for the field of NGC 265. The age of the associated cluster corresponds to the burst of star formation at 300 Myr. The SFR is normalized to the area

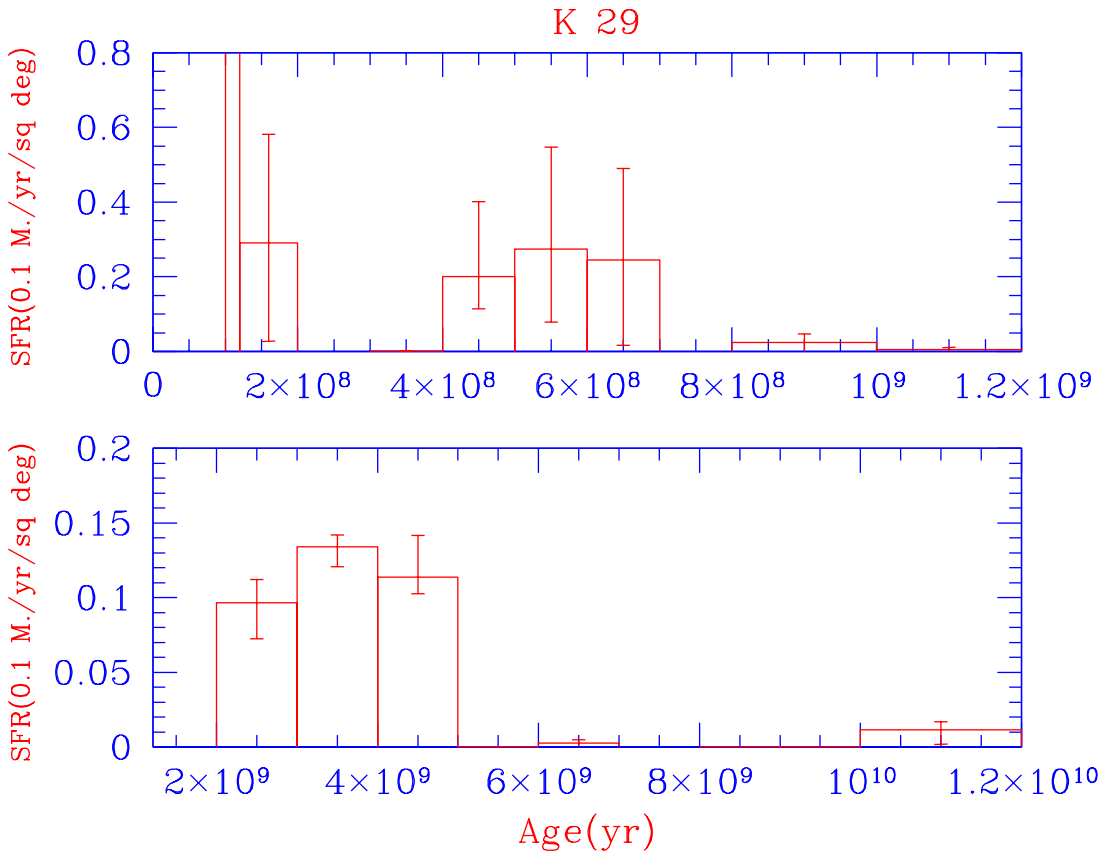

Figure 6.3: Star formation history for the field of K 29. We can see bursts of star formation at ages 200-400 Myr, 3 Gyr and 4 Gyr. The age of the associated cluster corresponds to the first peak. The SFR is normalized to the area

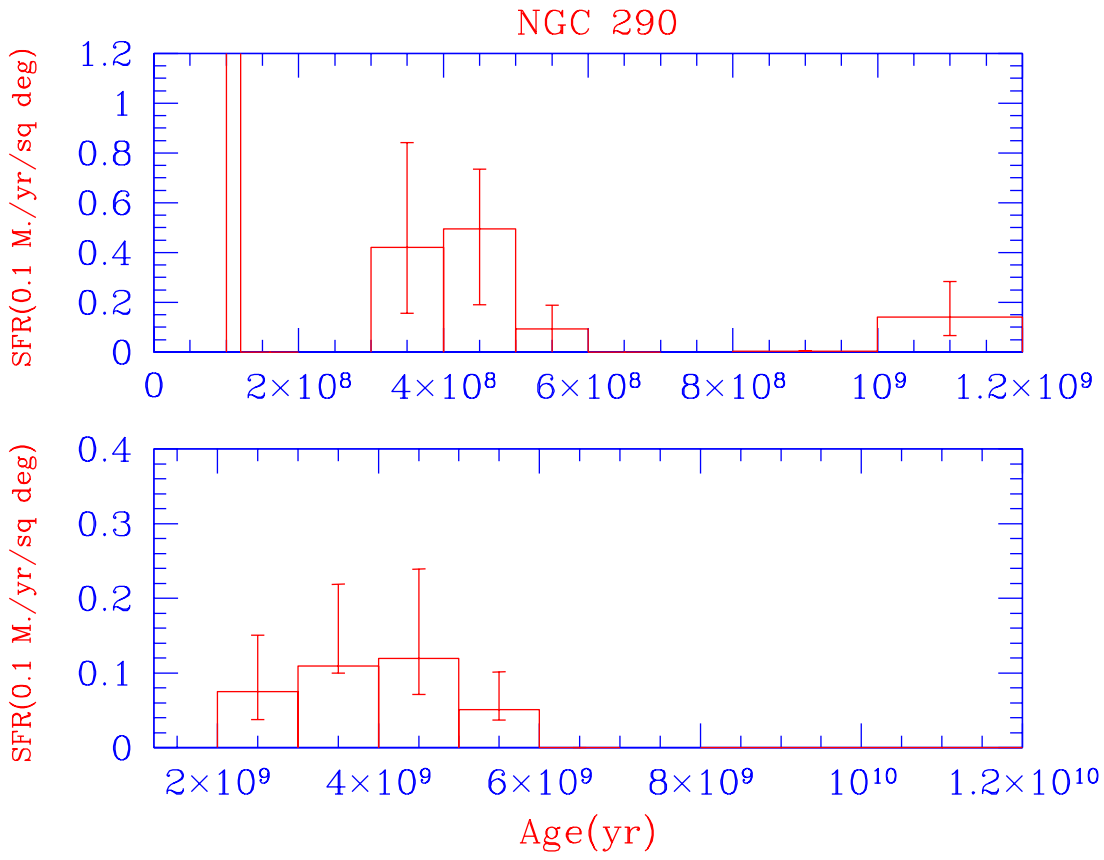

Figure 6.4: Star formation history for the field of NGC 290. Main star formation episodes are at 300-400 Myr, 3 Gyr and 4 Gyr. Those episodes are common to the three areas suggesting a global triggering mechanism. The rate is normalized to the area.

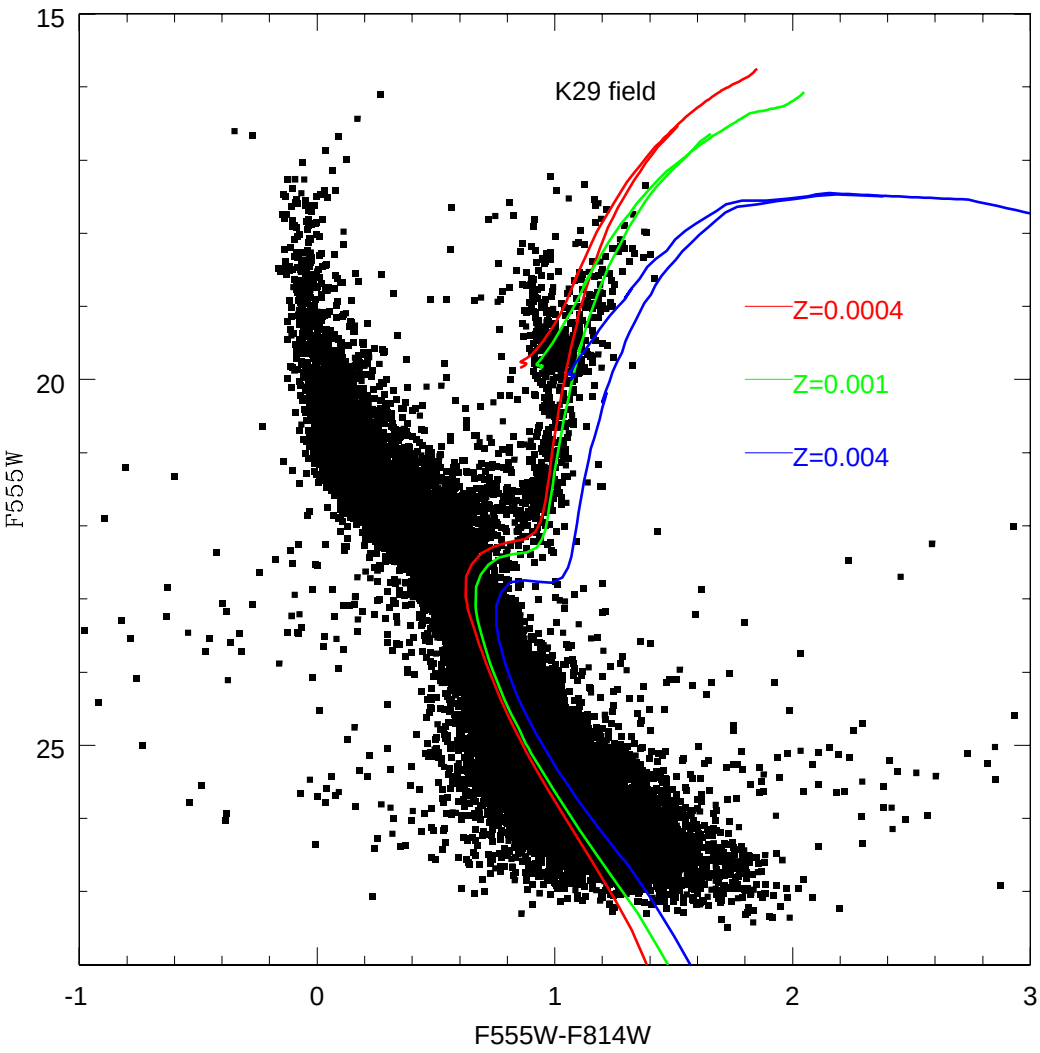

Figure 6.5: The CMD of the field K 29 with superimposed three isochrones of the same age (10 Gyr) and different metallicity. Other combinations of these parameter would not fit the narrow distribution of stars in the sub-giant region

discussion). This is the kind of reshaping that a low mass disc galaxy ought to undergo after a few passages around a more massive galaxy (Pasetto et al 2003).

While a larger consensus is reached in literature concerning the SFR at young ages and the influence of the interaction between the MC and the Milky Way, still controversial results are obtained concerning the old population. In a pioneering work based on photographic plates, Gardiner and Hatzidimitriou (1992) found that the bulk of the stellar population in the SMC is about 10 Gyr old. Harris and Zaritsky (2004) find that 50% of the stars ever born in the SMC formed prior to 8.4 Gyr ago. More precisely, the SMC formed relatively few stars between 8.4 and 3 Gyr ago, but there was a rise in the mean SFR during the most recent 3 Gyr with bursts at ages of 2.5, 0.4, and 0.06 Gyr. Dolphin et al. (2001) find that the star formation has proceeded in a more continuous way, with a main episode between 5 and 8 Gyr. Noel et al. (2006) find a strong gradient with the galacto-centric distance and no significant star formation activity in the SMC at ages older than 6-9 Gyr.

The present result is pointing in favour of a low efficiency of the star formation at old epochs. Using Monte Carlo simulations, we derive the uncertainty on this result. Small changes in the assumed line-of-sight SMC depth, extinction, age-metallicity relation result in an uncertainty of at least ± 2 Gyr on the age of the components older than 3 Gyr. We remind that for a population older than 10 Gyr, 1 Gyr of age difference corresponds to about 0.07 mag difference in the turnoff magnitude, while a 0.25 mag uncertainty on the turnoff magnitude results in 2 Gyr age difference for a component of 5 Gyr, and Z=0.004. When the metallicity changes from 0.004 to 0.001, the age-metallicity degeneracy is responsible of an additional uncertainty of about 0.5 Gyr for a population of 4 Gyr.

To assess whether a significant component as old as 10 Gyr is present in our fields, we compare the isochrones at changing metallicity with the CMD. The result is plotted in Fig. 6.5. The sub-giant branch width is not compatible with the presence of a significant component as old as 10 Gyr.

This is in agreement with the age distribution of the clusters. In fact the SMC is known to have at least six populous clusters of intermediate age, namely in the range 5-9 Gyr, but only one true old object (NGC 121) having an age > 10 Gyr is known in this galaxy (Stryker et al 1985, Dolphin et al 2001). The SFR of the field population in the LMC at older ages is not inconsistent with these results. In fact the majority of the authors find a strong population at intermediate ages (between 2-6 Gyr) (we quote among others Elson et al., 1997; Geha et al., 1998; Harris and Zaritsky, 1999, 2004; Olsen, 1999; Dolphin, 2000a; Javiel et al., 2005), but only in a few cases enhancements at older ages are found. Vallenari et al. (1996) find that in the regions

East and South-East of the Bar the star formation had a sort of enhancement about 6-8 Gyr ago. Harris and Zaritsky (2004) derive two main episodes of star formation at epochs younger than 2 Gyr and older than 7 Gyr respectively, with a quiescent period in between. Smecker-Hane et al. (2002) find that the Disk SFR has been relatively smooth and continuous over the last 13 Gyr, while the Bar was dominated by SF episodes at intermediate ages, more precisely from 4 to 6 Gyr and 1 to 2 Gyr ago.

How can this be related to the interaction between the MCs and our Galaxy? Over the years our understanding of the problem has been much improving thanks to studies aimed at reproducing the properties of LMC and SMC by shaping their SFH by means of the mutual dynamical interactions in the triplet LMC+SMC+MW. However, it is still not clear whether the MCs have existed in a binary state for most of their history (Fujimoto and Murai, 1984; Gardiner et al., 1994) or if their strong interaction happened just recently (Mathewson et al., 1986; Byrd et al., 1994; Bekki and Chiba, 2005; Yoshizawa and Noguchi, 2003). The solution is not unique owing to uncertainty in the initial conditions, and furthermore in many cases the MCs cannot keep their binary status for more than about 5-6 Gyr (Bekki and Chiba, 2005; Yoshizawa and Noguchi, 2003). The present results suggest that at old ages, the tidal interaction between the MCs, if any, was not strong enough to trigger star formation episodes in both galaxies.

CHAPTER

7

Star formation in LMC: N11

7.1 Introduction

In this chapter we present some preliminary results of a study on the SFH for a selected area of the LMC, i.e. the region N11 that is described below. It is consolidated that most stars form in groups or clusters even if some authors propose possible models of isolated massive star formation (Bonnell et al., 2004; McKee and Tan, 2003) but we are still far from defining the processes that bring from the initial molecular cloud to stars. If we concentrate on the triggering we see that many aspects are still obscure. One of the sources of triggering is considered to be the explosion of massive stars which inject energy and matter in the surroundings. Some models comprehend turbulence phenomena that can explain the balance with gravitational forces on large scale while provoking collapse on small scales (Klessen, 2003; Larson, 2003). Star formation can be subsequent in adjacent regions without a causal relation: a sign of triggering instead is interpreted to be the presence of more than one stellar population (Oey et al., 2005).

N11 is a very interesting region for all the arguments we proposed before. This nebula is believed to be one of the best candidates for triggering phenomena: LH9 region induced star formation in other two adjacent regions, LH10 and LH13 (Hatano et al., 2006; Mokiem et al., 2007; Barbá et al., 2003; Elmegreen and Lada, 1977). In this Chapter, we analyze the CMDs of clusters and associations in this region. Statistical methods are used to discuss the presence of clustering. In section 7.2 we

present the region; in section 7.3 we discuss the distance modulus and the metallicity; in section 7.4 we present the data, HST/ACS data and Spitzer data; in section 7.5 we discuss the methods we used in the data analysis; in section 7.6 we present the results, concerning CMD analysis and star clustering. Finally we present the concluding remarks.

7.2 N11

N11 is the second largest nebula of the LMC after the 30 Doradus Nebula. It is located in the north-western corner of the LMC. The whole complex has a diameter of 45', corresponding to a linear extent of 705 pc, assuming a distance for the LMC of 54 kpc . It is formed by a large bubble surrounded by 9 bright nebulae and filaments. These bubbles are observed for example with the interferometer at Hα and [OIII] 5007 Å wavelengths, see Rosado et al. (1996).
The different emission areas are cataloged according to the emission brightness starting from N11 A to B,C,D,E,F and I. The OB association LH9 is located at the centre of a cavity of about $80pc \times 60pc$ (Hodge and Lucke, 1970; Lucke and Hodge, 1970; Parker et al., 1992).

Which is the origin of those bubbles and super-bubbles? According to the standard theory bubbles are supposed to take origin from massive star winds. Intermediate and large diameter bubbles origin is less understood. Preliminary condition for the formation of bubbles is the presence of a stellar cluster whose degree of evolution severely affects the formation itself. According to the theory of Tenorio-Tagle and Bodenheimer (1988) two fundamental factors account for the formation of super-bubbles, that are both stellar winds and SN explosions. On the other side a different scenario opens when we consider the so-called sequential star formation. This mechanism essentially claims for an expansion of the front of star formation from the inside of the bubble triggered by an original population of stars at the centre.
Another origin of the bubbles stands on the observation that many bubbles don't have a star in the middle of the expanding shell (Hatzidimitriou et al., 2005). This is true especially for small and intermediate-size bubbles. In this case turbulent mechanisms are expected to be responsible of the formation of the bubbles (Dib and Burkert, 2005).

Several surveys of this region were taken at different wavelengths, as this region is visible not only at optical wavelengths but also in the infrared and radio continua and in particular with the ESO-SEST Key Programme CO transitions were detected (Israel et al., 2003b). The Southern part of N11 appears to be a filamentary shell of diameter 200 pc.

Table 7.1: Clusters and associations of particular interest in the region under investigation.

Id	r	Ra	Deg	Class	D	D	Name	Loc
					Min	Max		
1	2.235	04 56 38	-66 30 26	NA	7.30	5.90	LH9	LMC-N11
2	2.241	04 56 43	-66 31 28	NA	5.10	2.10	NGC1760, LMC-N11F, ESO85EN19	LH9
3	2.321	04 56 39	-66 29 00	A	4.20	3.00	NGC1761, SL122, ESO85SC18	LH9
4	3.038	04 56 34	-66 28 25	C	1.00	0.90	HD32228, KMHK307	NGC1761
5	4.198	04 56 23	-66 28 00	NA	0.95	0.75	BSDL270	NGC1761
6	4.480	04 56 30	-66 26 40	NA	26.00	23.00	LMC-N11, LMC-DEM34	LMC-N10
7	4.638	04 57 44	-66 28 30	NC	0.30	0.25	HNT1	NGC1769
8	4.892	04 56 19	-66 27 19	A	1.30	0.90	BCDSP1	LH9
9	4.970	04 57 45	-66 27 52	NA	4.10	2.60	NGC1769,LH13, LMC-N11C ESO85SC23	LMC-N11
10	5.275	04 56 09	-66 31 25	NA	1.50	0.90	BSDL264	LH9
11	5.343	04 57 17	-66 24 56	NA	0.80	0.70	HT3	LMC-N11
12	5.647	04 57 44	-66 26 27	NA	0.65	0.55	BSDL324	NGC1769
13	5.723	04 56 49	-66 24 23	NA	5.20	3.60	NGC1763, IC2115, LMC-N11B, SL125, LH10	LMC-N11
14	5.985	04 57 22	-66 24 26	NA	0.60	0.45	HT2	LMC-N11
15	6.566	04 55 55	-66 28 57	NA	0.70	0.55	LMC-N11H	LMC-N11
16	6.648	04 57 08	-66 23 24	NC	0.45	0.45	HDE268726, Sk-66o36,HT1	NGC1763
17	6.836	04 57 02	-66 23 10	NC	0.65	0.55	HT4	NGC1763
18	6.839	04 57 16	-66 23 21	NC	0.60	0.60	IC2116, LMC-N11A	LMC-N11
19	6.978	04 57 43	-66 24 30	C	0.50	0.50	BSDL322	LMC-N11
20	8.250	04 55 50	-66 34 25	NA	2.00	1.10	LMC-N11I	LMC-N11
21	8.637	04 55 49	-66 25 04	NA	1.50	1.20	BSDL244	LMC-N11
22	8.879	04 58 00	-66 23 27	C	0.35	0.35	BSDL333	LMC-N11
23	9.589	04 57 24	-66 20 43	NA	2.80	1.70	BSDL308	LMC-N11
24	9.867	04 57 00	-66 20 08	NC	0.60	0.55	H88-47	BSDL287

Our fields are optical fields located in this region, being interesting for detecting the regions of more active star formation and the possible differences between the area where the nebulae are located and pure field zones.

In Fig.7.1 we sketch the position of our fields in the N11 complex in which many peculiar clusters and associations are found. The most interesting objects, their coordinates, and radii are listed in Table 7.1. The data are from Bica et al. (2000) catalog.

7.3 Distance modulus and metallicity

In order to know the absolute magnitudes of our sources we need to know the distance modulus of the LMC. In the following we assume the intrinsic distance modulus $(m - M)_o = 18.5$ in agreement with the recent determination of Szewczyk et al. (2008); Keller and Wood (2006) and Salaris et al. (2003). Other determinations

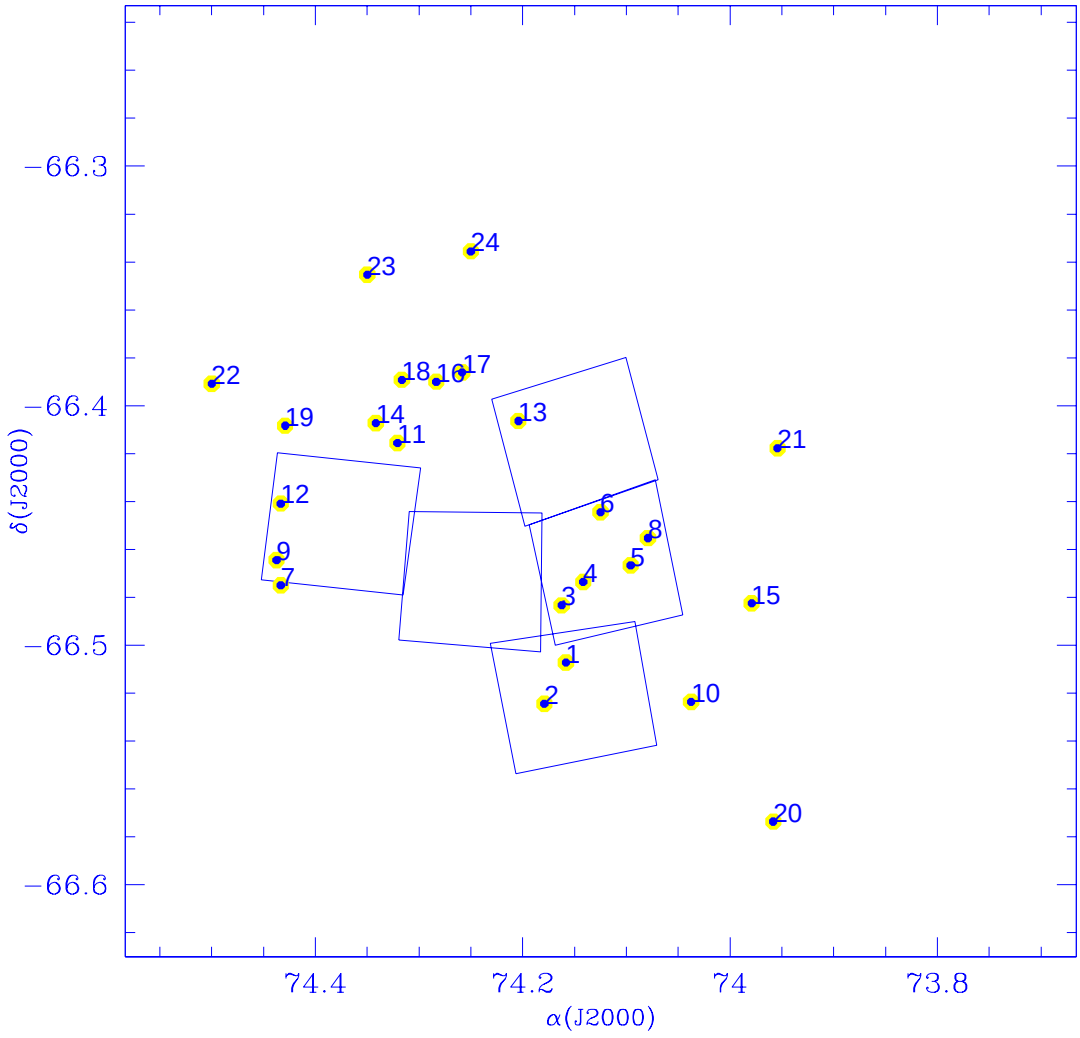

Figure 7.1: The region containing HST/ACS observed fields is schematically represented. Circles represent objects of particular interest, like clusters and associations as listed below in Table 7.1.

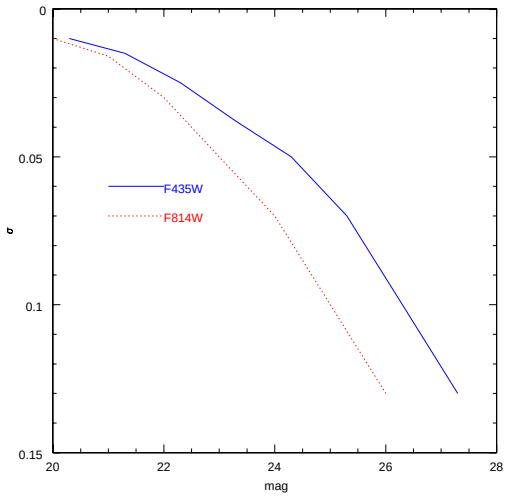

Figure 7.2: Photometric errors in the two pass-bands as a function of the magnitude, as recovered from artificial star experiments

give $(m - M)_o = 18.4$ (Catelan and Cortés, 2008; Groenewegen and Salaris, 2001). We assume also an age-metallicity relation for our populations. In particular we refer to the work by Salaris et al. (2003, and references therein), Pagel and Tautvaisiene (1998); Dopita et al. (1997); Dirsch et al. (2000). The determination of the extinction is made in section 7.6.2.

7.4 The data

In this section first we present the HST-ACS/WFI archive data in the F814W and F435W passbands, then we discuss the HST-ACS/HRC data in the F250W and F330W for the region of the cluster HD32228. Finally infrared Spitzer data are presented.

7.4.1 ACS/WFI data: F814W and F435W passbands

In the following we analyze 6 selected fields in the region of N11. Data are taken from ACS/WFI HST archive. Observations were made in the year 2002 and data released in the year 2003. Observations were made in two different filters F435W and F814W with a long exposure of 496 s and a short exposure of 1-2 s. We made use of drizzled files which already account for image distortion. We do not correct for cosmic rays, since cosmic rays can be removed in the match between the two filters. The data were then reduced by means of the packages DAOPHOT/ALLSTAR by Stetson(1994).

Table 7.2: Aperture corrections for both filters F435W and F814W. CCDs are split in 2 parts: the row (1) contains the upper part whereas the row (2) the lower part.

Cluster		$\Delta m^{F435W}_{PSF-AP(3pix)}$	$\Delta m^{F814W}_{PSF-AP(3pix)}$
CCD 2	(1)	-0.13 ± 0.04	-0.14 ± 0.04
long	(2)	-0.12 ± 0.04	-0.17 ± 0.05
CCD 2	(1)	-0.12 ± 0.08	-0.18 ± 0.06
short	(2)	-0.20 ± 0.08	-0.14 ± 0.07
CCD 3	(1)	-0.05 ± 0.02	-0.17 ± 0.04
long	(2)	-0.12 ± 0.03	-0.19 ± 0.04
CCD 3	(1)	-0.19 ± 0.08	-0.13 ± 0.06
short	(2)	-0.14 ± 0.09	-0.08 ± 0.04
CCD 4	(1)	-0.12 ± 0.04	-0.17 ± 0.04
long	(2)	-0.13 ± 0.04	-0.0 ± 0.1
CCD 4	(1)	-0.09 ± 0.08	-0.16 ± 0.06
short	(2)	-0.0 ± 0.1	-0.15 ± 0.05
CCD 5	(1)	-0.13 ± 0.04	-0.14 ± 0.04
long	(2)	-0.13 ± 0.03	-0.15 ± 0.08
CCD 5	(1)	-0.16 ± 0.04	-0.15 ± 0.04
short	(2)	-0.17 ± 0.08	-0.16 ± 0.04
CCD 6	(1)	-0.25 ± 0.02	-0.11 ± 0.04
long	(2)	-0.14 ± 0.04	-0.17 ± 0.06
CCD 6	(1)	-0.15 ± 0.07	-0.20 ± 0.06
short	(2)	-0.15 ± 0.07	-0.15 ± 0.06
CCD FIELD	(1)	-0.11 ± 0.04	-0.17 ± 0.04
long	(2)	-0.13 ± 0.03	-0.16 ± 0.06
CCD FIELD	(1)	-0.16 ± 0.02	-0.15 ± 0.09
short	(2)	-0.18 ± 0.09	-0.15 ± 0.06

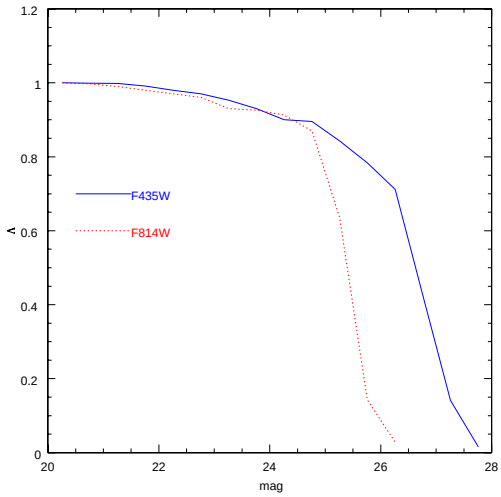

Figure 7.3: Completeness factor Λ in the two pass-bands

The charge transfer efficiency (CTE) correction was applied.

The calibration of the data is performed following Bedin et al. (2005) and Sirianni et al. (2005) as already explained in section 3.2. The instrumental magnitudes are transformed to the ACS-Vega system. Aperture corrections from r=3 pixels to infinity are assumed from the tabulated values of Sirianni et al. (2005) where $\Delta m^{F814W}_{AP(3pix)-AP(\infty)} = 0.291$ and $\Delta m^{F435W}_{AP(3pix)-AP(\infty)} = 0.284$.

Photometric errors. In this case as for the clusters in the SMC, the photometric errors are estimated from artificial stars experiments, consisting in the injection of a certain number of artificial stars of known magnitude in the original image: stars are then recovered through the whole reduction pipeline and recovered magnitudes are compared to the original ones. The mean magnitude difference between injected and recovered stars, which is taken as an estimate of the mean photometric error, is plotted in Fig. 7.2 as a function of the magnitude.

Completeness factor. We remind that completeness factor Λ is calculated from crowding tests as the ratio between the recovered stars at a certain magnitude interval and the number of original stars at the same interval. In Fig. 7.3 we show as an example the trend of the completeness factors in the two filters F435W and F814W for the upper part of CCD 2. We can notice how the drop of the completeness factor down to the limit of 50% is deeper for the F435W filter by about one magnitude.

7.4.2 ACS/HRC UV data

The UV filter data were taken from the HST archive. Observations were made in years 2002-2003 by Maiz-Apellaniz with the HST ACS/HRC camera. The High Resolution Camera (HRC) has a very small field of view (26"x29"). Exposures of 359s were taken in the F250W and F330W filters. Reduction was performed with the usual packages DAOPHOT/ALLSTAR provided by Stetson. The magnitudes were calibrated following Bedin et al. (2005) and Sirianni et al. (2005). CTE correction was applied.

7.4.3 Infrared Spitzer Data

The region was observed by the infrared survey SAGE (Surveying the agents of a Galaxy's evolution) using the Infrared Array Camera IRAC (3.6,4.5,5.8,8 μm) and MIPS(24μm) instruments on board of the Spitzer Space Telescope (Meixner et al., 2006, 2007). The Spitzer data are somehow complementary to the HST data. In fact while HST data can reveal faint pre-main sequence stars, Spitzer data are sensitive to young stellar objects.

7.5 Methods

In this Section the methods used to study the stellar population in N11 will be presented. First we discuss the method for deriving the field star formation using the down-hill simplex method. Then we describe how to subtract the field star contamination in the cluster CMDs. Then we analyze the clustering of the young populations. This is made in two ways: first by the two-point correlation function and second by the introduction of a parameter Q that can discriminate between clusters with a smooth radial density gradient and objects presenting sub-clustering (Cartwright and Whitworth, 2004a).

7.5.1 The Down-hill simplex

The procedure is analogous to that described in Chapter 5 for the SMC fields. We just would like to remind the parameters in use in this case. Synthetic populations of 10000 or 15000 stars are produced down to the completeness limit. These populations refer to the library of Girardi et al. (2002) and the adopted age-metallicity relation is taken from Pagel and Tautvaišienė (1999) in agreement with the recent work of Carrera et al. (2008).
We would like to point out once more how important is the choice of an opportune grid in the CMD in order to get reliable results, as discussed in previous Chapters.

Here the main sequence plays a master role. We adopted a binning of 0.5 mag from 16 to 19 mag and of 0.25 mag from 19 to 25 mag. Then we have a box for the sub-giant region and a box for the He-burning clump.

7.5.2 Field star subtraction

Field star subtraction is critical to discuss the stellar population. The adopted procedure is already discussed in Chapter 5. Here we recall for clarity a few points. The CMDs of both association and field population are divided in boxes of size $\Delta F435W = 0.2$ and $\Delta(F435W - F814W) = 0.3mag$. Then, first the data are corrected for photometric incompleteness. The correction is taken into account by dividing the field and association CMDs in magnitude-color bins and then adding on each bin having N_{th} stars, $\Lambda \times N_{th}$ objects, where Λ is the smallest of the $F345W$ and $F814W$ completeness factors. Then, in each box of the N11 CMD, for every field star, the closest cluster star is subtracted.

7.5.3 Two-point correlation function

The definition of the correlation function is given in Chapter 5, section 4.5.
Here we remind that a flat correlation function is the sign of a random distribution of objects without correlation, while a peaked correlation function means that a correlation within the objects is present. The correlation length is taken to be the full width half maximum of the distribution.
The correlation function is shown in picture 7.12 and the results are discussed in section 7.6.5.

7.5.4 The minimal spanning tree

The Minimal Spanning Tree (MST) is a powerful method used in literature for a statistical analysis of the spatial distribution of the stars in a cluster (see Cartwright and Whitworth, 2004b; Schmeja and Klessen, 2006, for a detailed discussion). Here we briefly summarize the method. The MST is the unique network of straight lines joining a set of points (vertexes), such that it minimizes the total length of all the lines (called edges) without creating closed loops. In this paper, we make use of Prim's algorithm (Prim, 1957) to construct the MST. Starting from an arbitrarily chosen first point an edge is created joining that point to its nearest neighbor. The tree is then calculated constructing the shortest link between one of its nodes and the unconnected points, until all the points are connected. Once that a MST is calculated, its mean edge length $\bar{m}$ is straightforwardly defined. The $\bar{m}$ is dependent on the total number N of stars in the cluster, in the sense that as N decreases, more short edges are created and $\bar{m}$ decreases. For this reason, $\bar{m}$ should be normalized to $(NA^{1/2})/(N-1)$ when comparing clusters having different areas A and/or N

(Cartwright and Whitworth, 2004b). The structure of a cluster can be derived comparing the $\bar{m}$ of the MST describing it, to the normalized correlation length $\bar{s}$ of the cluster defined as the mean separation between the stars of the cluster normalized to the radius of the cluster.
This defines the parameter Q as

$$Q = \frac{\bar{m}}{\bar{s}} \tag{7.1}$$

Cartwright and Whitworth (2004b); Schmeja and Klessen (2006) show that Q is a good indicator of the structure of a cluster. In fact $\bar{s}$ decreases more quickly than $\bar{m}$ as the degree of central concentration becomes more severe (indicating the presence of a radial gradient), while $\bar{m}$ decreases more quickly than $\bar{s}$ as the degree of sub-clustering becomes more severe. Q can be used to distinguish between sub-clustering ($Q < 0.8$),and the presence of a large scale radial density gradient ($Q > 0.8$). It should be reminded that Q cannot give any information about the presence of fractal structures, i.e. cannot say whether the sub-clustering is hierarchically self-similar.
In the following, we will derive this parameter for the cluster and associations in the observed fields, in particular we would like to discriminate between clustered young star forming regions and slightly older regions.

7.6 Results

In this section we discuss the results.
First the CMDs of the most important clusters/associations are presented and their properties are discussed. Then the interstellar extinction in the direction of N11 is derived. Finally, the clustering of the young stars, and their relation with the environment are studied.

7.6.1 CMD discussion: PMS in N11

The field population shows a turnoff at about F435W $\sim 17 - -19$ and the stars burning He in the core are located at F435W ~ 20 (see Fig.7.7). This red clump is also visible in the association CMDs, due to the contamination of the underlying field stars. In the CMDs of N 11 a well defined upper main sequence (MS) of young blue stars is present. Below the turnoff, moving to fainter magnitudes, the main sequence in the CMDs of the associations and of the field population is increasingly densely populated. A striking difference at faint magnitudes between field and association CMDs is evident in the region redder than the MS, where a well populated sequence running almost parallel to the MS itself is found in the associations, but is completely absent in the field region. The location of these stars fits very well the PMSs previously discovered in other MC associations (Gouliermis et al., 2007, 2006). After

field star subtraction, the clean diagrams are compared with pre-main sequence isochrones by Siess et al. (2000) having ages from 3 to 10 Myr at different values of the extinction, once that PMS isochrones are converted from the Johnson-Cousins pass-bands to the HST/ACS pass-bands using the transformations by Sirianni et al. (2005). PMS stars are widely distributed in almost all the clusters/associations in the studied region (see Figures 7.4,7.5,7.6). A conspicuous group is located in HD32228, inside LH 9. The data are in agreement with PMS having ages from 3 to 10 Myr. The comparison with PMS isochrones suggests that these PMS stars have masses from 1.3 to 3 $M_{\odot}$. This age determination is in agreement with the age derived in literature from spectroscopy of bright blue stars. Mokiem et al. (2007) derived the ages of LH9 and LH10, giving respectively an age of 7.0 ± 1.0 Myr and 3.0 ± 1.0 Myr. HD32228 presents W-R star of type WC5-6, and evolved O stars (Nazé et al., 2004; Parker et al., 1996). Its age has been estimated from spectroscopy by Walborn and Parker (1992) and is of about 3-4 Myr.

7.6.2 The discussion of the reddening in the whole area

The reddening across the region is highly variable, since N11 is a region full of dust and gas. The determination of the reddening is a critical point in the discussion of the stellar populations. Suspicion might arise that the stars we identify as PMS are instead highly reddened MS objects. For this reason, we first derive the extinction in the whole area as E(F814W-F435W), then we made use of the photometry in the filters F250W and F330W in the area surrounding HD32228.
The extinction in the area covered by the six CCDs in the F435W and F814W filters is derived comparing the color of MS stars brighter than 19 mag ($F435W < 19 \quad mag$) with the corresponding points on the theoretical isochrone (Girardi et al., 2004), once that the extinction law A_{F435W}/A_{F814W} by Sirianni et al (2500) is assumed. The total number of stars used for this determination is 1200. Then a map is derived interpolating between the derived values, using an appropriate smoothing parameter R=0.0005 in the interpolating function $B(h) = 1/\sqrt{h^2 + R^2}$ where h is the anisotropically scaled distance from the interpolant to the node. The resulting map is shown in Fig. 7.8 where the values of E(F435W-F814W) as function of the coordinates are given. This map will be used to derive the values of the reddening of all the other stars in the field. The reddening varies in the range E(F435W-F814W)=0.01:0.50. These values are in agreement with the determination of the extinction from the spectroscopy of bright stars (Nazé et al., 2004; Parker et al., 1996).

7.6.3 Reddening in HD32228 from UV data

In this Section we derive the extinction in the region of HD32228 using UV and optical HST photometry already discussed in previous Sections for the area in com-

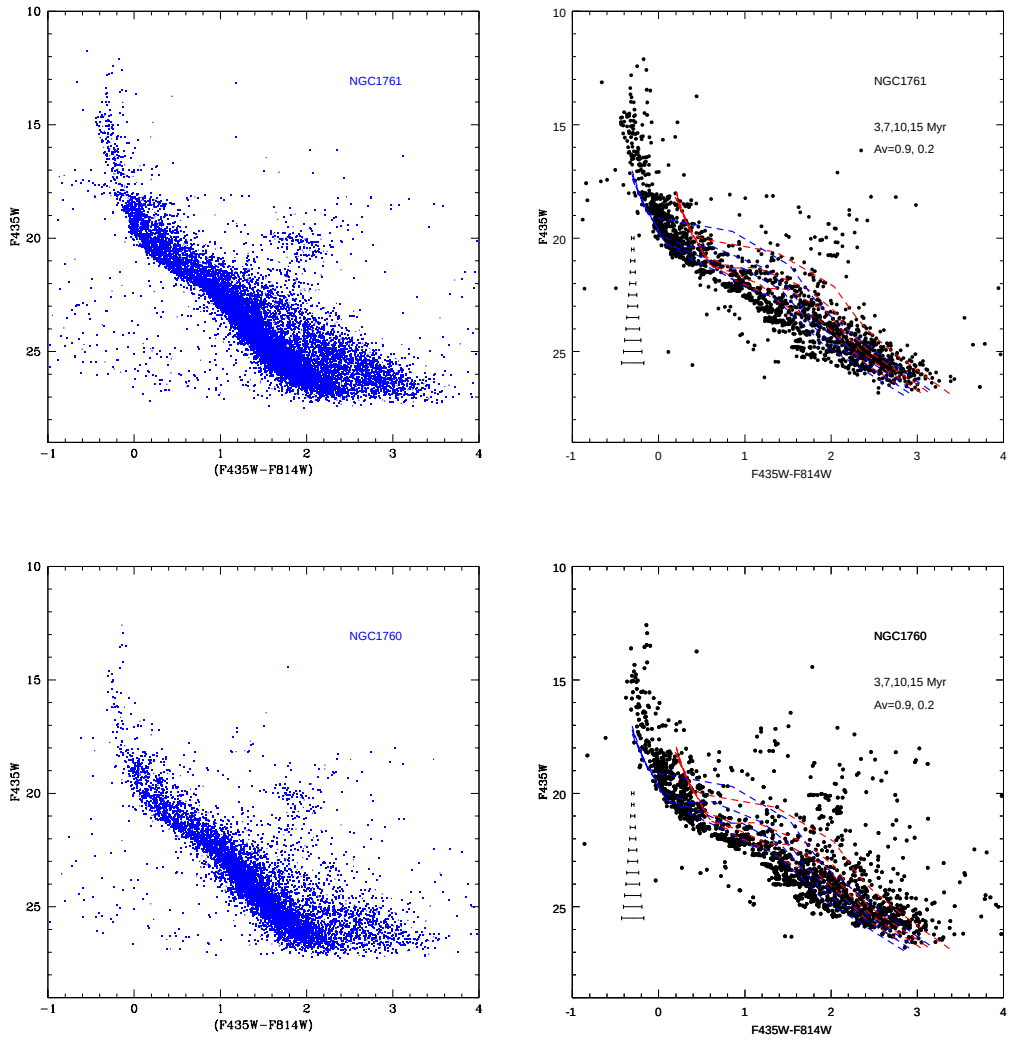

Figure 7.4: CMDs of NGC 1760, NGC 1761 in LH 9 (left panels). CMDs of the same objects when the field population is subtracted. The bars show the photometric errors on the color. PMS isochrones by Siess et al are superimposed on the data at different values of the extinction A_V.

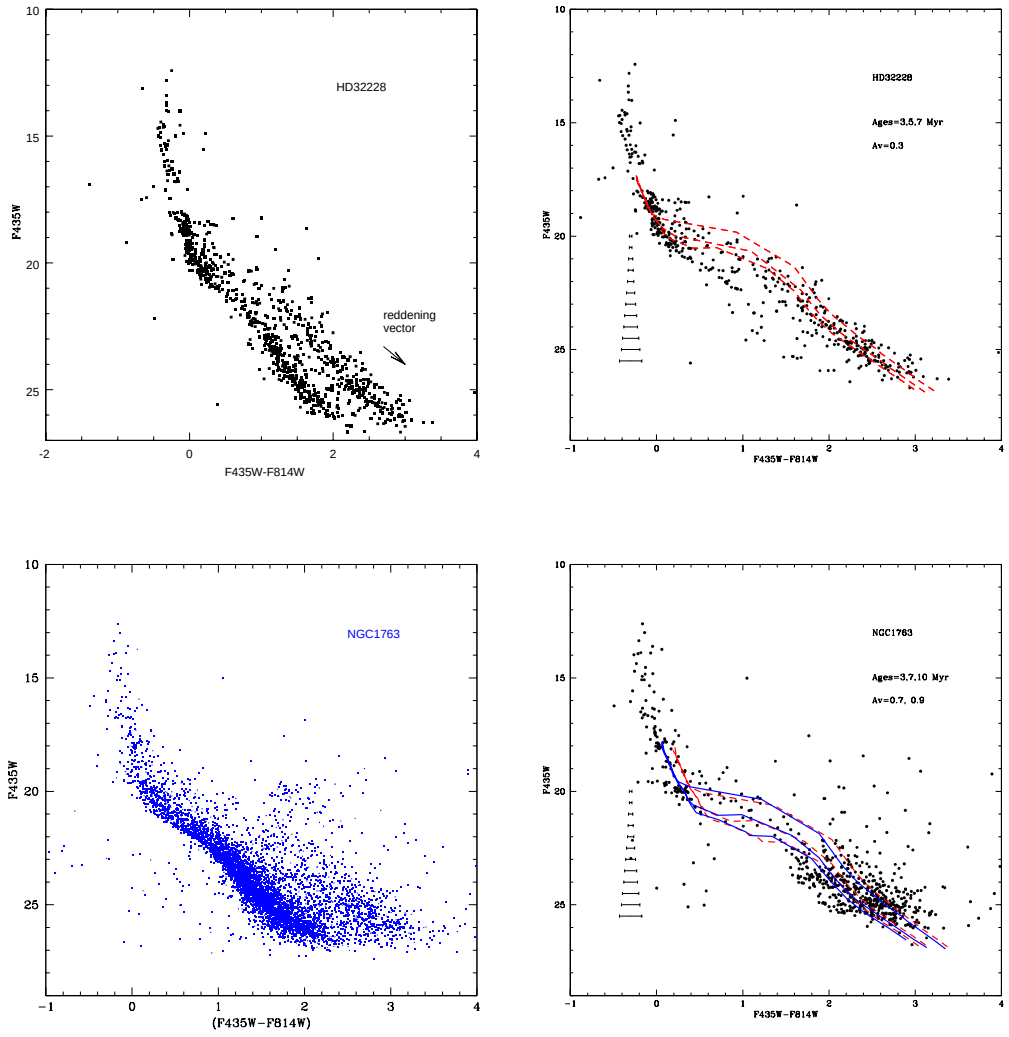

Figure 7.5: CMD of HD 32228 in LH 9 and NGC 1763 in LH 10 (left panels). CMDs of the same objects when the field population is subtracted. The bars show the photometric errors on the color. PMS isochrones by Siess et al are superimposed on the data at different values of the extinction A_V.

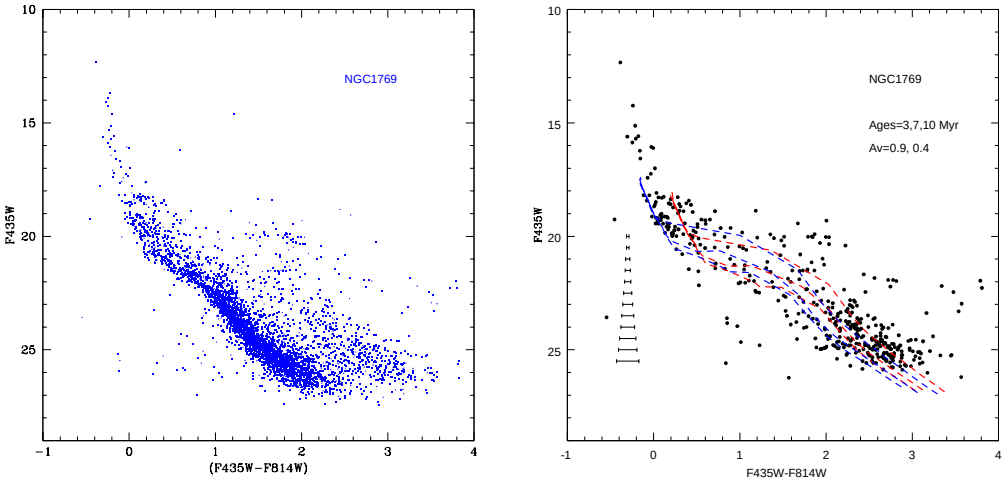

Figure 7.6: CMDs of NGC 1769 (LH 13) (left panels). CMDs of the same objects when the field population is subtracted. The bars show the photometric errors on the color. PMS isochrones by Siess et al are superimposed on the data at different values of the extinction A_V.

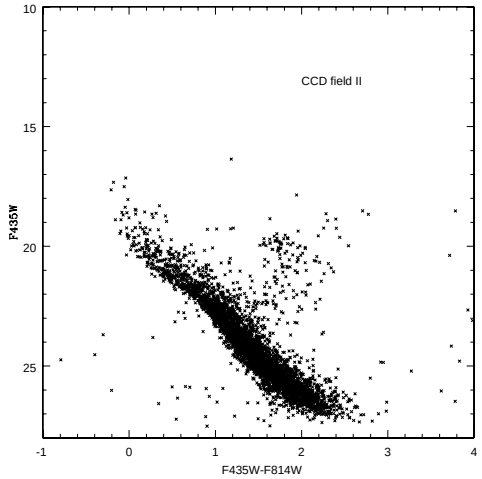

Figure 7.7: CMD of the field.

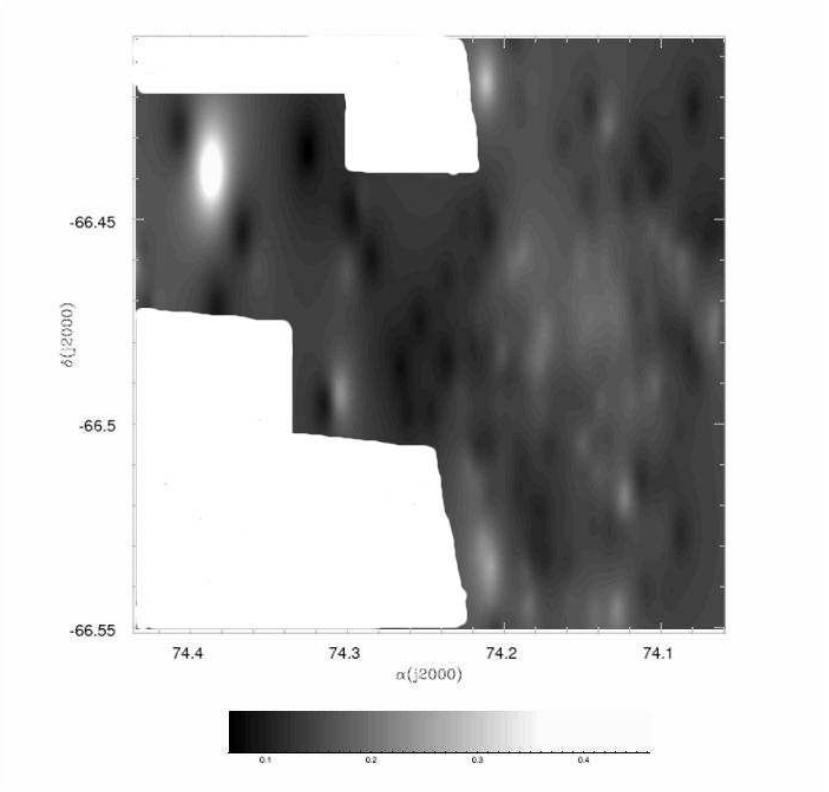

Figure 7.8: Reddening map of the central area of N11 as $E_{F435W-F814W}$.

Table 7.3: In this table we present the mean values of the extinction in the different colors derived from isochrone fitting and from color-color diagrams for HD32228.

Color	Reddening
E(F250W-F814W)	0.62
E(F435W-F814W)	0.35
E(F330W-F435W)	0.20
E(F250W-F330W)	0.19

mon, i. e. the field of view of the instrument (HRC), 26"x29".

The main sequence of HD32228 in the UV filters is used for the determination of the reddening in the filters F250W and F330W analogously to what was done in the previous Section. First we select the main sequence stars having $F250W < 19$ in the CMDs, then we fit each star color and magnitude with the theoretical isochrone of age Log(age)=6.6 and Z=0.008. Assuming the relation A_{F250W}/A_{F330W} from Sirianni et al. (2005) the extinction is derived. The resulting extinction map is shown in Fig 7.9 where the values of E(F250W-F330W) are presented as function of the spatial coordinates α, δ. The mean values are given in Table 7.3. In figures 7.10 the CMDs of the stars in common in the four studied filters are presented and the MS location is fitted with an isochrone. The mean value of the extinction is applied. Figure 7.11 is the analogous in the color-color plots in the filters F814W, F435W, F330W, F250W. Using Sirianni et al relation, we find E(F250W-F330W)/E(F814W-F435W) ~ 0.53. Comparing the extinction maps in the area in common, we derive from our data E(F250W-F330W)/E(F814W-F435W) $\sim 0.5 \pm 0.3$, in agreement with expected results. The extinction law in this region is found to be the standard one, having Rv=3.1

7.6.4 The effect of the interstellar extinction on the PMS candidates

As we can see from the extinction map the extinction of the pre-main sequence stars is in the range E(F435W-F814W)=0.06:0.4. The interstellar extinction vector in the passbands F814W-F435W is running almost parallel to the PMS sequence (see Fig.7.5). This states in favor of the hypothesis that these stars are true PMSs.

7.6.5 Clustering of the stars

In this section we discuss the degree of clustering of the stars first using the two-point correlation function and then using the Q parameter.

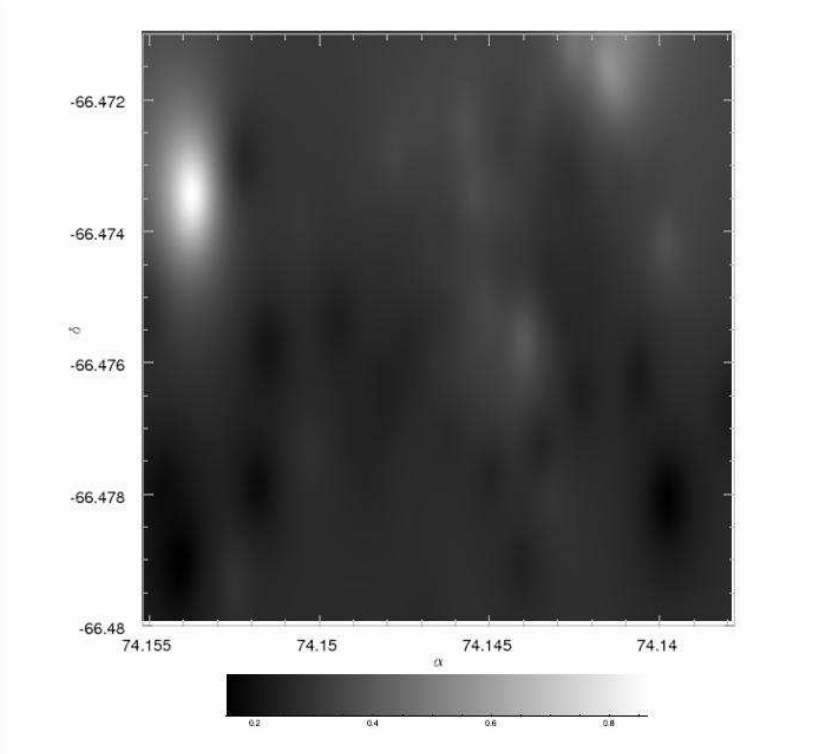

Figure 7.9: Reddening map of the area of the cluster HD32228 in the UV filters, as E(F250W-F330W).

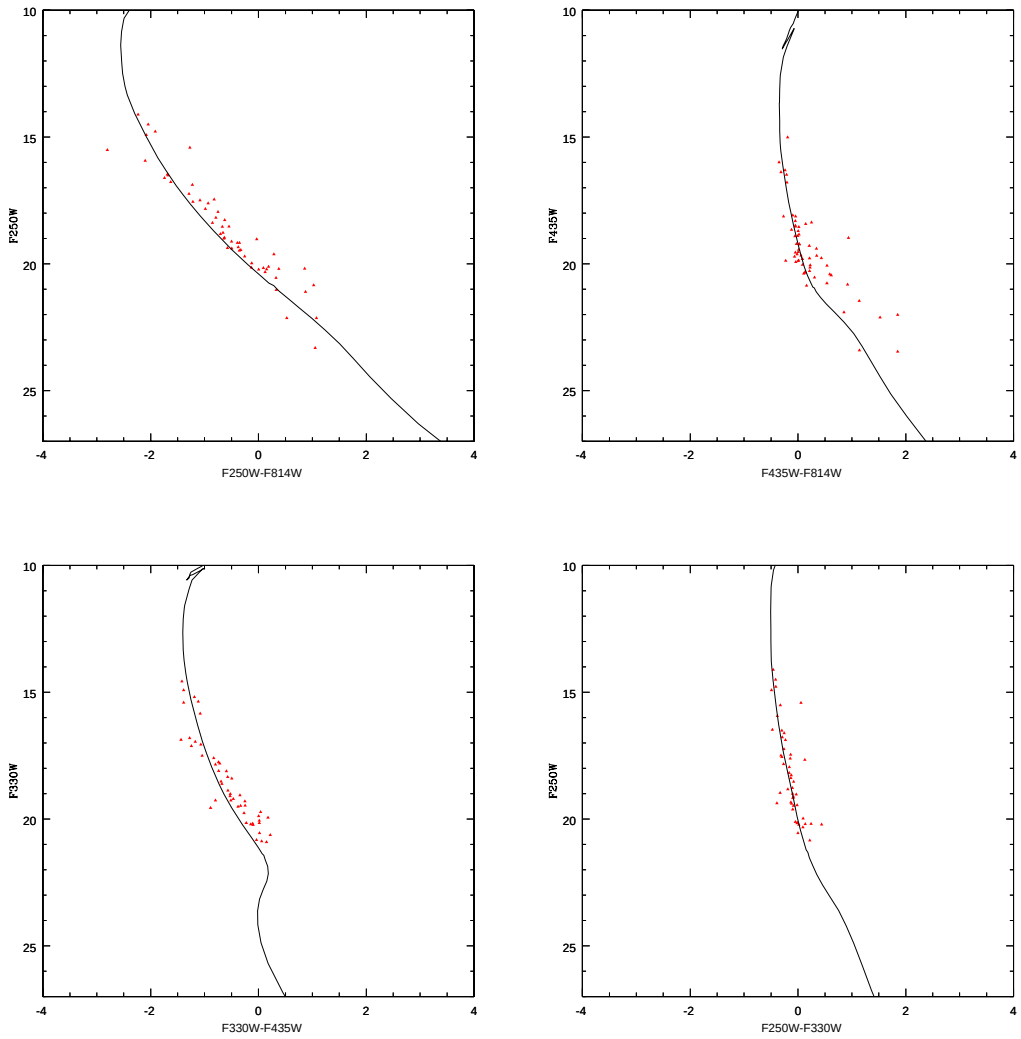

Figure 7.10: Upper left panel:CM diagram in the F250W and F814W filters. The applied reddening was E(F250W-F814W)=0.62.Upper right panel:CM diagram in the F435W and F814W filters. The applied reddening was E(F435W-F814W)=0.35.Lower left panel:CM diagram in the F330W and F435W filters. The applied reddening was E(F330W-F435W)=0.20.Lower right panel:CM diagram in the F250W and F330W filters. The applied reddening was E(F250W-F330W)=0.19.

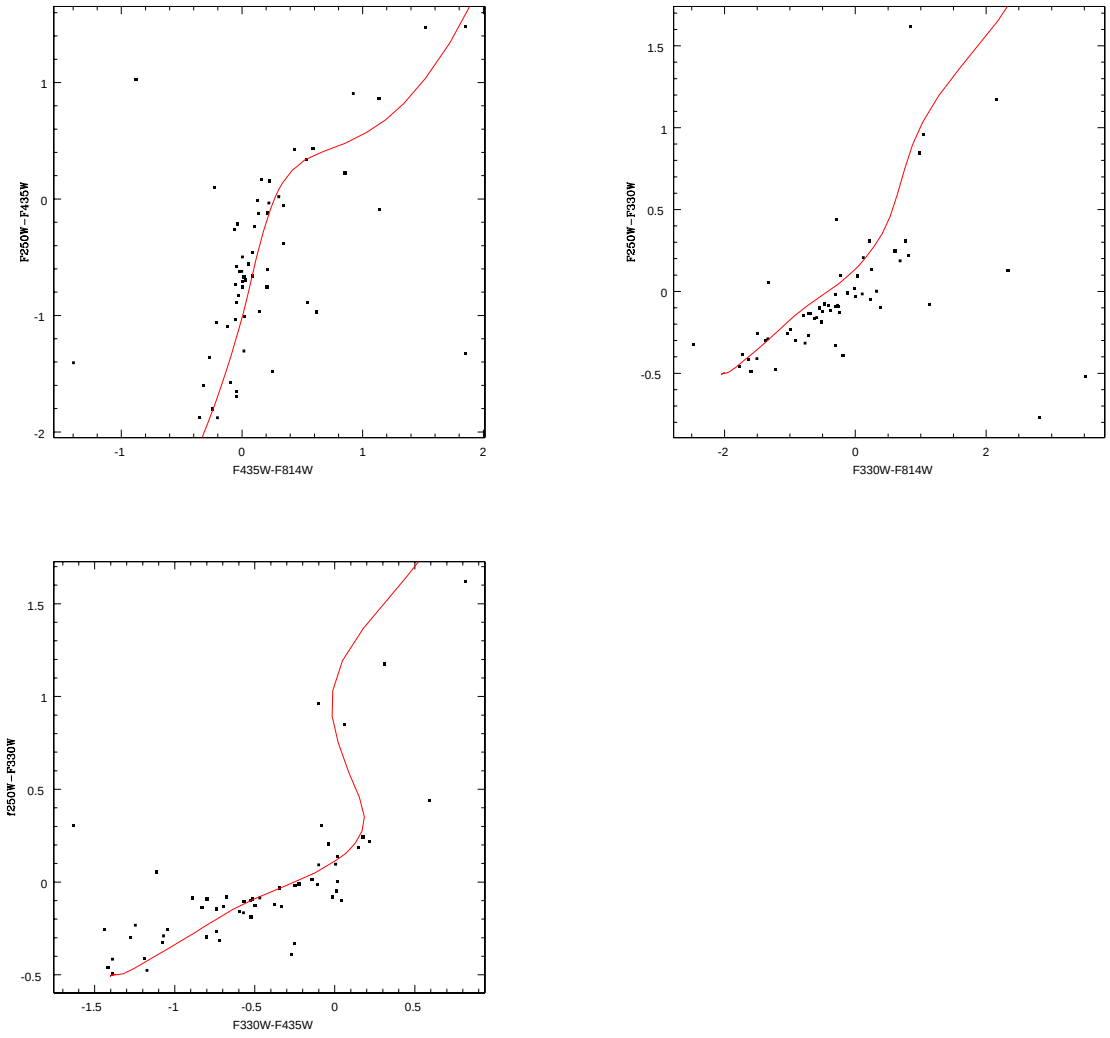

Figure 7.11: Upper left panel:Color-color diagram in the colors F435W-F814W and F250W-F435W. Upper right panel: Color-color diagram in the colors F330W-F814W and F250W-F330W. Bottom panel:Color-color diagram in the colors F330W-F435W and F250W-F330W.

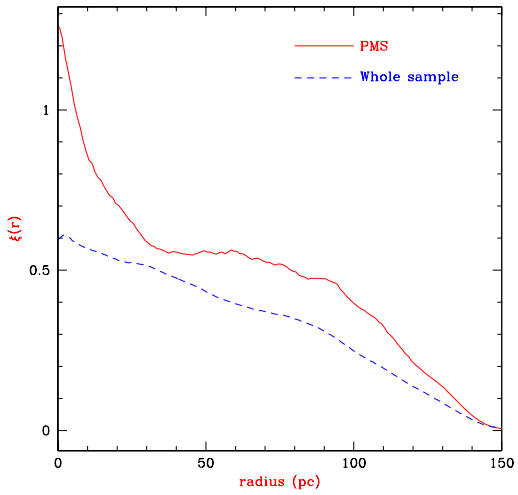

Figure 7.12: Two point-correlation function of the PMSs (solid line) and the whole sample of stars (dashed line).

Fig. 7.12 presents the correlation function of the PMSs and of all the stars in the studied region. The correlation function for the PMSs shows a well defined peak, while in the case of the whole star sample it is considerably flatter, implying a weaker correlation. The maximum value of the correlation function of the PMSs is comparable to the peak values of 0.5,1.5,6 found in Galactic star forming regions such as Rosetta Molecular cloud (Li and Smith, 2005) or M16 (Indebetouw et al., 2007) and reflects the strong degree of clustering of the population.

The full width half maximum of the peak for PMSs is of $\sim$ 10 pc, of the order of the typical size of molecular clouds in the SMC and LMC which is going from about 10 to 100 pc (Israel et al., 2003a)

In Figs.7.14 and 7.13 we present the MST graphs of some of the clusters and associations in the region. In 7.6.5 we present the values of the Q parameter. All of them present the signs of clustered substructures, having a $Q < 0.8$.

We finally discuss the relation of the PMS stars with their environment. In order to define the correlation of the PMS stars with the environment we overplot the PMS stars to the map of OB stars and Herbig Ae/Be stars from Hatano et al. (2006), as you can see from Fig. 7.18. The most conspicuous concentrations of PMS stars are seen in N11B (in LH10) and at the periphery of LH9, in HD32228. These concentrations correspond to the location of OB stars. Concerning Herbig Ae/Be stars (having ages in the range 1-3 Myr), they are found in all these locations, but inside LH9.

In Fig.7.19 the PMS stars positions are superimposed on the Hα emission map (Mac

Table 7.4: Values of the Q parameter for the considered cluster and association.

Cluster	$\bar{m}$	$\bar{s}$	Q
NGC1769	0.865	1.33	0.65
NGC1763	0.733	0.98	0.75
NGC1761	0.775	1.18	0.66
NGC1760	0.735	1.20	0.56
HD32228	0.735	0.93	0.79
BSDL324	0.808	1.11	0.73
BSDL270	2.452	3.64	0.67
BCDSP1	0.787	1.19	0.66

Low et al., 1998) and CO emissions (Israel et al., 2003b). PMS stars are found near the maxima of Hα emission and at the border of the CO clouds in N11B and N11C.

7.6.6 YSOs from near-IR archive data

In this section we proceed with the identification of young stellar objects (YSO) from the Spitzer archive data in the region of N11. For the classification of the objects we substantially refer to the work of Robitaille et al. (2006).
The old classification by Lada (1987) was based on the energy distribution of the object. Three distinct classes could be identified: I) sources with broader than blackbody energy distribution which were rising at wavelength longer than 2 microns, II) sources with broader than blackbody energy distribution but flat or decreasing energy distributions, III) sources whose energy distributions could be modeled with reddened blackbodies with no or little excess near infrared emission, and slight mid infrared excess emission most likely caused by the relatively cool and distant grains responsible for the observed extinction to the objects. This classification can be made more quantitative through the spectral index

$$a = \frac{dlog(\lambda F_\lambda)}{dlog(\lambda)} \tag{7.2}$$

For class I sources $0 < a < 3$; for class II sources $-2 < a < 0$ and for class III sources $-3 < a < -2$.

Robitaille et al. (2006)use another classification of the young stellar objects similar to the old one but referring more on the evolutionary stages of the objects and on their physical properties rather than on the pure energy distribution.
There are indeed three categories of YSO:
1) Stage 0-I, that present infalling envelope and have age of less than 0.1 Myr

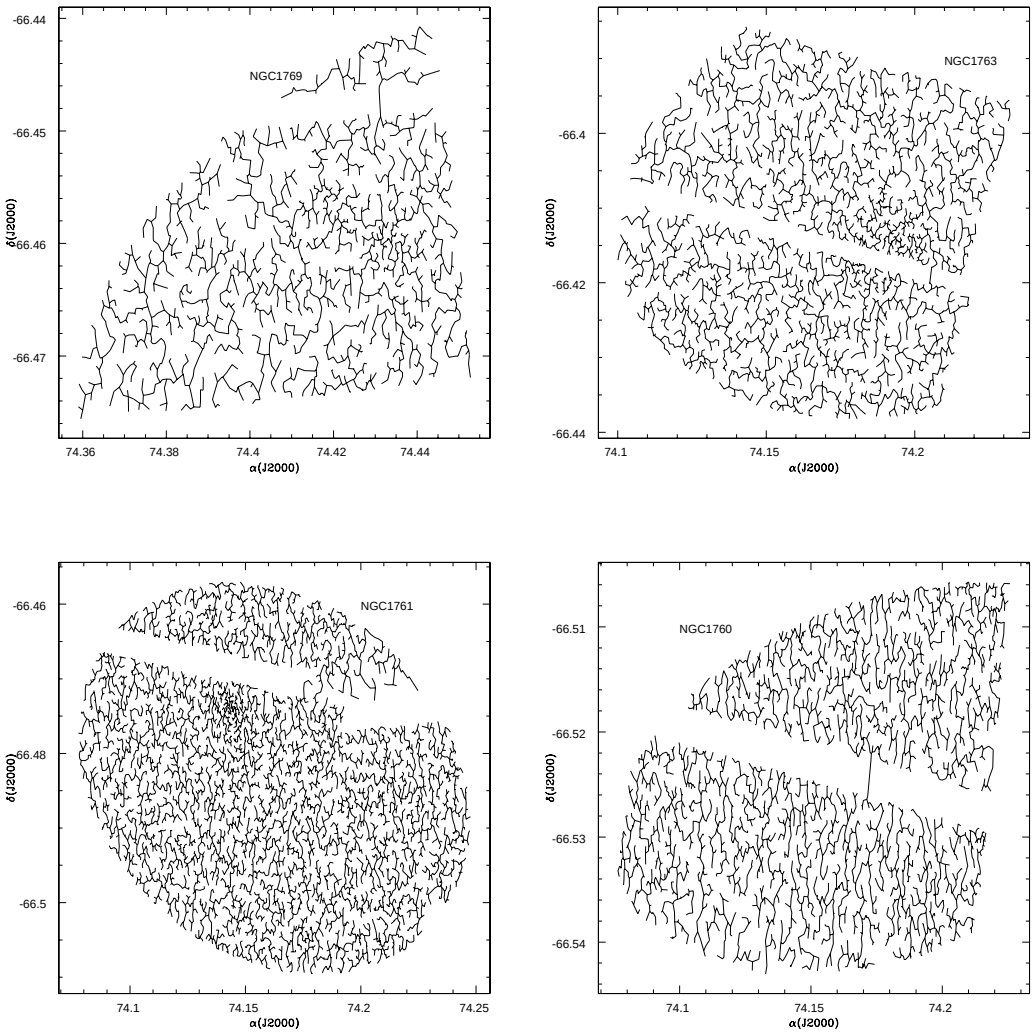

Figure 7.13: The MST of the regions of NGC1769,NGC1763,NGC1761 and NGC1760. All the associations have clustered substructures.

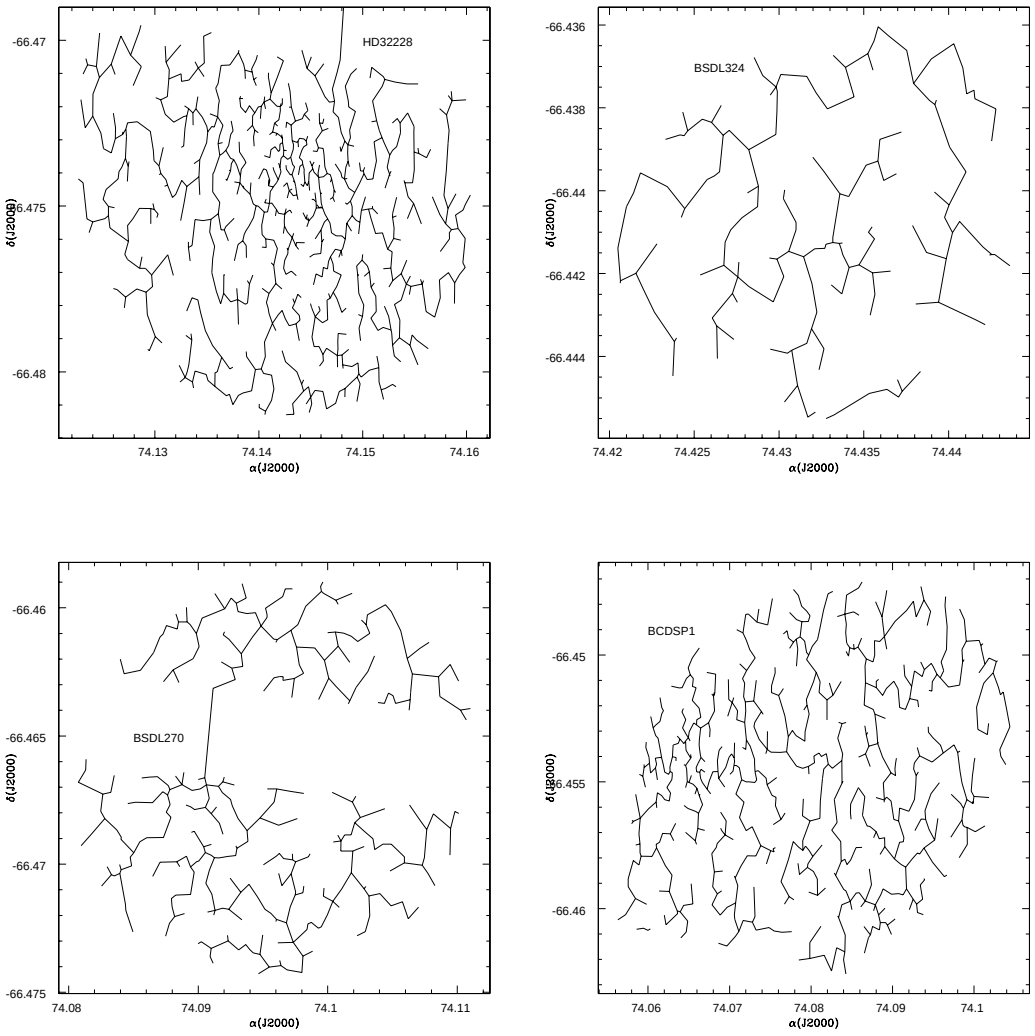

Figure 7.14: The MST of the regions of HD32228, BSDL324, BSDL270 and BCDSP1. All clusters and associations show to have clustered substructures.

2) Stage II, that have a disk source and an age of a few Myr
3) Stage III, that have an optically thin disk or no disk at all
Concerning our work we would limit to the first two categories.
Robitaille et al. (2006) computed more than 200,000 models at 10 viewing angles. In this work we will make use of IRAC color-color plots ([5.8][8.0])-([3.6][4.5]): in these plots we highlight regions where the fraction (Stage 0-I/All YSOs) is close to 100% (see Fig. 7.15). Then there is an intermediate region where the fraction (StageII/All sources) is higher than 80 %, including however a small fraction of Stage 0-I stars. IRAC-MIPS ([5.8][8.0])-([3.6][4.5]) are effective in separating stars with no circumstellar material from Stage 0-I and Stage II objects (Fig.7.15). Finally YSOs candidates selected on the basis of magnitude diagrams are examined in the [8.0]-([3.6]-[8.0]) color-magnitude diagram and compared with Whitney et al. (2004) models (see Fig. 7.15).About 30 objects are identified as YSO candidates.
To derive the background contamination we select an area equivalent to that of the entire N11 region but located outside the observed fields, namely at α(J2000)=4h 58m 40s, δ(J2000)=-66^{0}34$'$47"`. We find 6 objects redder than ([3.6]-[8.0]) 1 in the [8.0]-([3.6]-[8.0]) color-magnitude diagram (Fig.7.16) and only 3 in the region occupied by YSO candidates in the ([5.8][8.0])-([3.6][4.5]) color-color plot (Fig.7.15). Only 10% of the YSO candidates having [8.0] < 14 are expected to be background objects.The percentage of background galaxies is in agreement with the statistic by Meixner et al. (2006).
We notice that YSO type I (showing large infalling envelopes) and II (characterized by the presence of an optically thick disk) having ages from 0.1 to 1 Myr are located at the same positions of the candidates PMS stars. The presence of YSOs and PMSs seems to suggest that the star formation in the region is a long lasting process where stars from 0.1 to 7 Myr are widely distributed.

7.7 Field SFR

In this section we derive the field star formation rate in N11. Populations are generated with the corresponding metallicity as described in 7.5. The method was already described in section 7.5.1. The results are the following. As described in figure 7.17 the SFR presents several bursts at ages 0.4, 0.6, 1.2, 4, 12 Gyr. This result is in agreement with the previous determination of Javiel et al. (2005).

7.8 Final remarks

In this Chapter, using archive HST/ACS photometry and infrared Spitzer photometry we study the stellar content of the region associated with N11 in the LMC.
Young stars are well known to trigger star formation on local scale by injecting

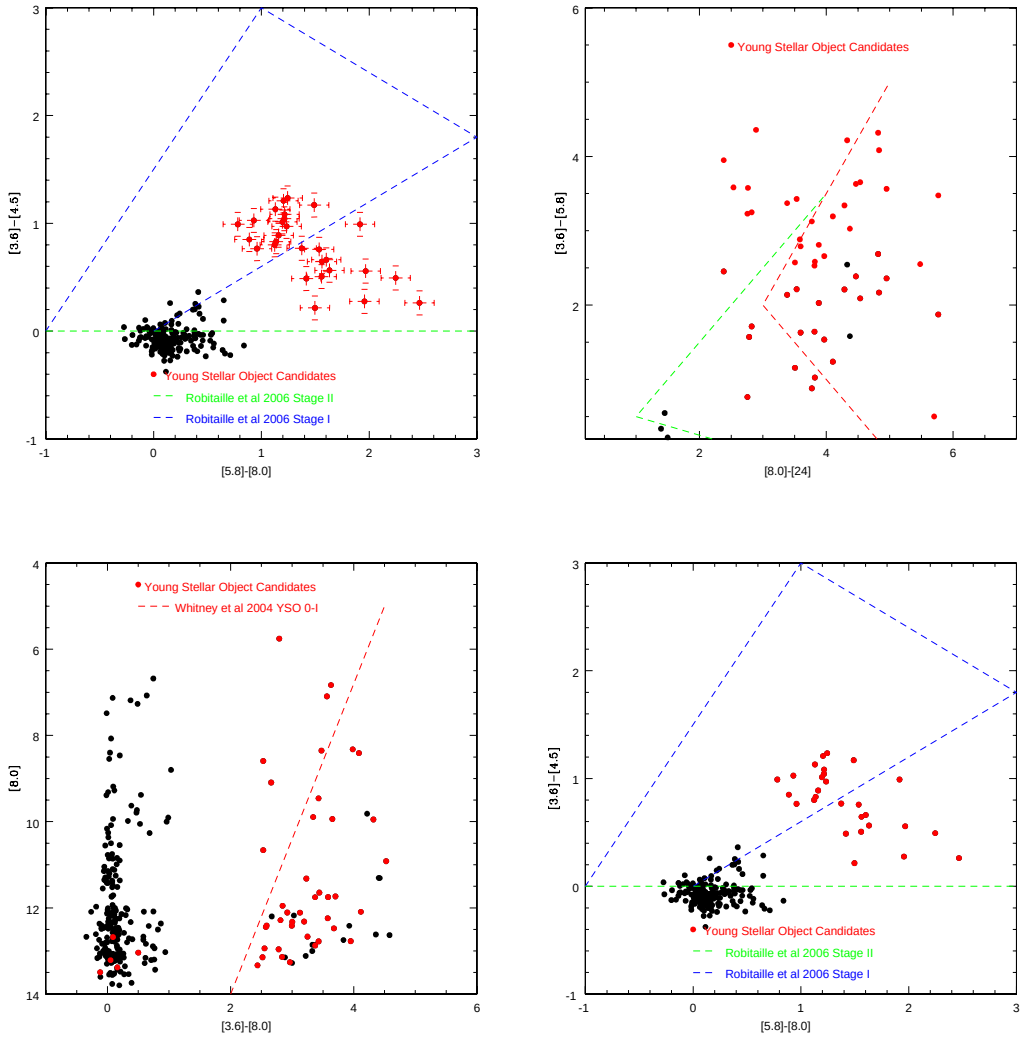

Figure 7.15: Upper left panel:([5.8]-[8.0])-([3.6][4.5]))color-color plot of the N11 field. Red identifies YSO candidates. Error bars show the nominal errors on the photometry as given by the SAGE catalog. The blue line outlines the region where Stage 0-I objects are found, on the basis of Robitaille et al. (2006) photometric models. In the region redder than [5.8][8.0]$\tilde{0}$ between the green and the blue line Stage II/Stage III objects can be detected. Upper right panel:IRAC-MIPS color-color plot in the pass bands ([8.0][2.4])-([3.6][5.8]). The short dashed red line separates the region where Stage 0-I objects are found, on the basis of Robitaille et al. (2006) photometric models. The long-dashed green line shows the region where Stage II objects can be detected. Lower left panel:[8.0]-([3.6]-[8.0]) color-magnitude diagram compared with Whitney et al. (2004) models. The objects redder than the line are likely to be YSOs of Stage 0-I. Lower right panel:([5.8]-[8.0])-([3.6][4.5]))color-color plot of the control field. The blue line separates the region where Stage 0-I objects are found on the basis of Robitaille et al. (2006) photometric models. The green line shows the region where Stage II objects can be detected. Red squares indicate the field objects falling inside the YSO candidate region.

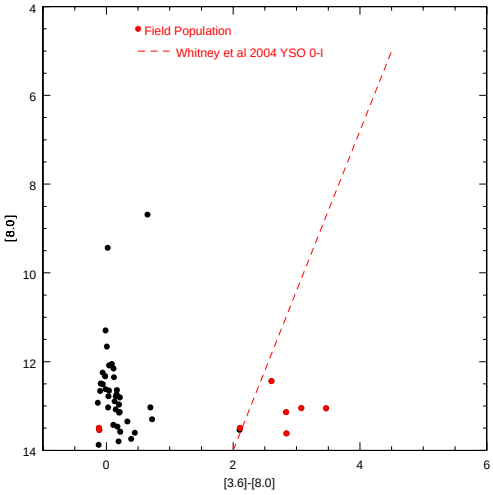

Figure 7.16: [8.0]-([3.6]-[8.0]) CMD of the field population is presented to show the contamination by the Milky Way stars and background galaxies. Only a few field objects are inside the region redder than the line where the YSO candidates are expected to be found following the models by Whitney et al. (2004) .

Table 7.5: Ages and metallicities of the synthetic populations in use.

Age (Gyr)			Z
0.08	–	0.12	0.006 – 0.010
0.12	–	0.30	0.006 – 0.010
0.30	–	0.40	0.006 – 0.010
0.40	–	0.50	0.006 – 0.010
0.50	–	0.60	0.006 – 0.010
0.60	–	0.80	0.006 – 0.010
0.80	–	1.00	0.006 – 0.010
1.00	–	2.00	0.006 – 0.010
2.00	–	3.00	0.005 – 0.010
3.00	–	4.00	0.003 – 0.005
4.00	–	5.00	0.003 – 0.005
5.00	–	6.00	0.003 – 0.005
6.00	–	8.00	0.0017 – 0.003
8.00	–	10.00	0.0017 – 0.0017
10.00	–	12.00	0.0017 – 0.0017

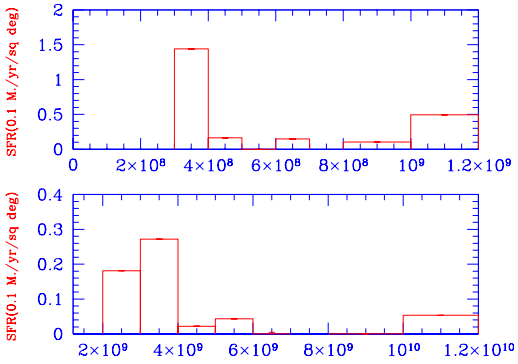

Figure 7.17: SFR of the field population is presented.

energy in the surrounding interstellar medium. N 11 region in the LMC is often presented as one of the most promising candidate of triggered star formation. In this Chapter we discuss the star formation process in this region. We report on the discovery of a PMS candidates associated with N 11 from HST ACS/WFC photometry. The main conclusions are as follows:

- The PMSs are consistent with ages going from 1 to 10 Myr. The comparison with the isochrones shows that PMSs have masses from 1.3 $M_{\odot}$ to 2.0 $M_{\odot}$.

- PMSs present a higher degree of clustering in comparison with the whole star sample. The maximum value of the correlation function is comparable to peak values of 0.5,1.5,6 found in Galactic star forming regions such as Rosetta Molecular cloud or M16.

  The distribution of the nearest neighbor distance might reflect the structure of the interstellar medium. The full width half maximum of the peak of the correlation function for PMSs is $\sim$ 10 pc, of the order of the typical size of molecular clouds in the SMC and LMC which is going from about 10 to 100 pc.

- The MST method shows high degree of subclustering in all the clusters and associations.

- Spitzer IRAC and MIPS observations of the region, made by the SAGE project reveal the presence of YSO candidates. YSOs type I and II having ages $<$ 1 Myr are found at the same location as the PMSs. The data seem to suggest

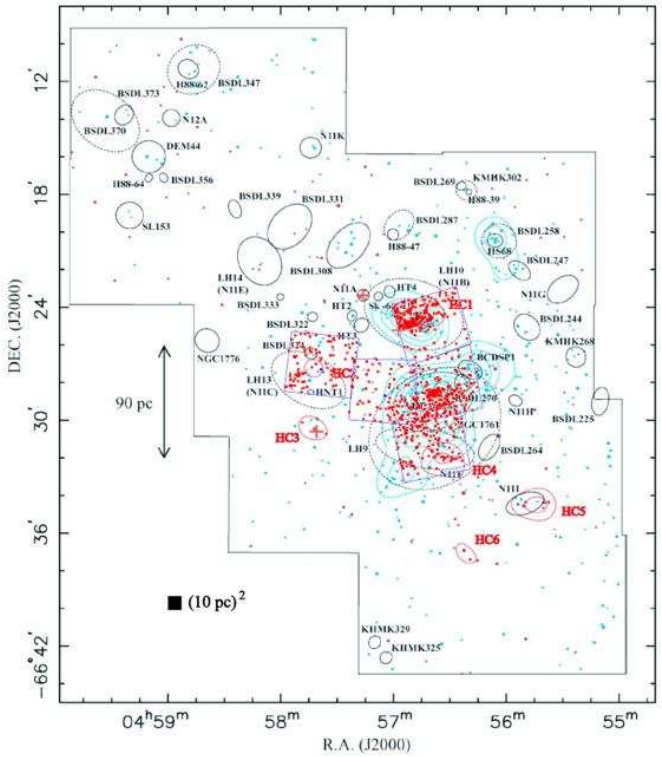

Figure 7.18: Bica clusters and associations are overplotted on the distribution of PMS(red dots) , the concentration of OB stars (blue lines, labeled OC1-4) and Herbig Ae/Be stars (red lines, labeled HC1-6) (from Hatano et al. (2006)). Ellipses represent Bica et al object dimensions. The contours show the observed area.

that the star formation in the region is a long lasting process where stars from 0.1 to 7 Myr are widely distributed.

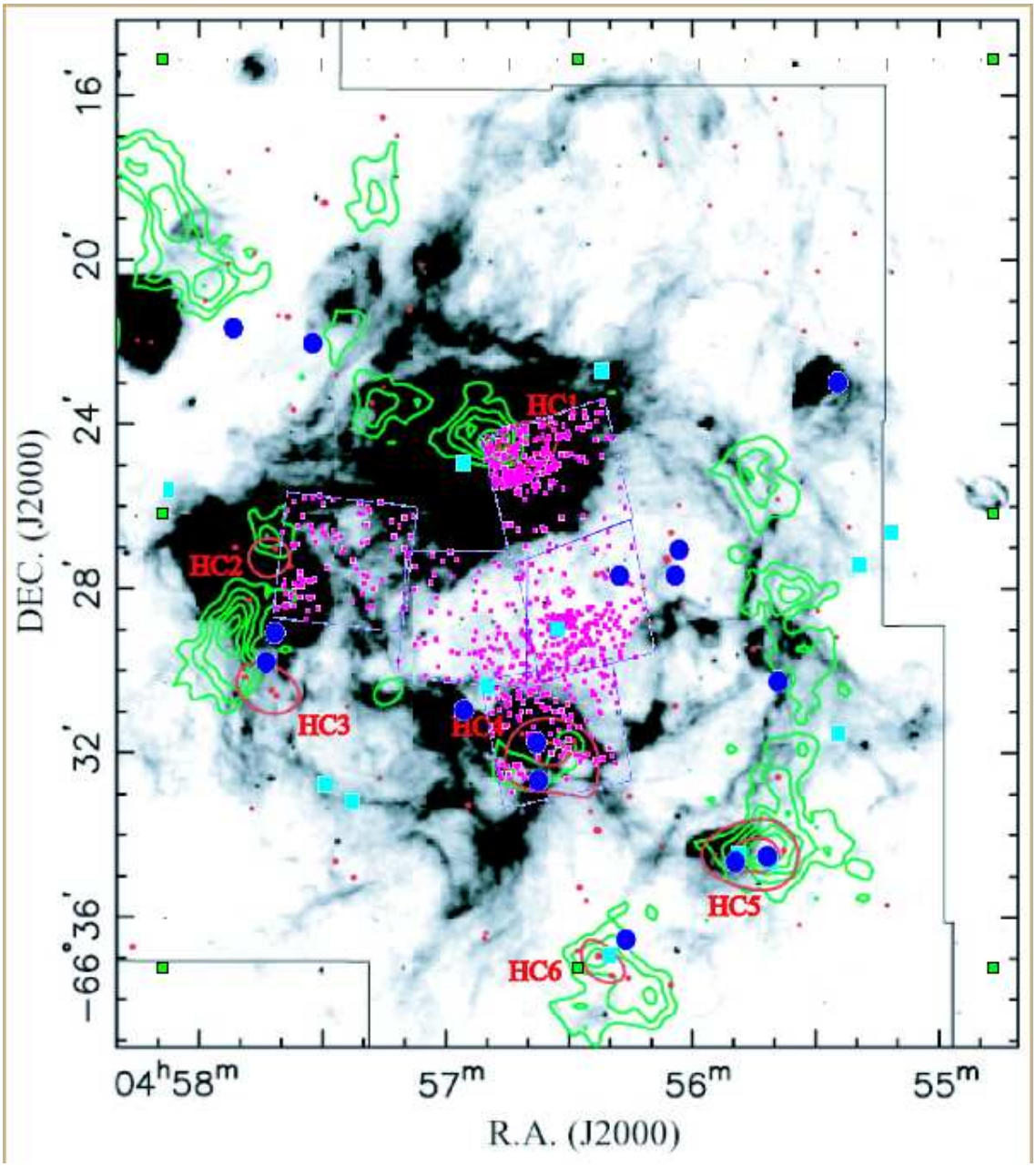

Figure 7.19: Hα emission map (inverted intensity scale) by Mac Low et al. (1998). Large boxes show the ACS/WFC fields. Green contours indicate the CO clouds (Israel et al., 2003b) , small red dots show the PMS candidates selected on the basis of ACS photometry, large green squares show the location of YSOs type II selected using IR Spitzer photometry, large blue dots represent the location of YSOs type I. Finally red circles (marked by HC1 to HC6) show the Herbig Ae/Be candidates by Hatano et al. (2006).

CHAPTER

8 Stellar SFHs and dynamics of LMC+SMC+MW

8.1 Introduction

In this chapter first we compare the various SFHs we have obtained, i.e. from the young clusters, the fields immersed in the HI regions, the fields around the clusters NGC265, K29 and NGC290 and the N11 field. In Table 8.1 we list the age intervals in which the SFR is significant. Then we compare the age intervals of maximum activity with the age of the close encounters between SMC-LMC, SMC-MW and LMC-MW predicted by the dynamical models for the triplet by Murai and Fujimoto (1980), Bekki et al. (2004), and Yoshizawa and Noguchi (2003), looking for coincidences between periods of enhanced stellar activity and close encounters.

8.2 Comparison with other SFHs

Prior to any other consideration, it is worth noting that the three SFHs do not have the same resolving power nor evenly extend over the whole age interval from very old (10-12 Gyr) to very young (a few Myr). The SFH from clusters is clearly skewed toward young objects simply by the way these have been selected. The SFHs from stellar fields selected in the HI regions extend to slightly older ages up to say 3 Gyr. The widest age coverage is by the SFHs derived from the companion fields of NGC265, K29, and NGC290.

Despite the uncertainties, there are a number of interesting coincidences:

Table 8.1: Age and/or intervals of significant star formation. Ages are in Gyr.

SFH	Region		
Cluster Fields SMC	NGC265	K29	NGC290
	0.1 0.3–0.7 1.0–1.3 2.0–7.0 10–12	0.1–0.2 0.4–0.7 2.0–5.0 10–12	0.1 0.3–0.6 1.0 3.0–6.0
HI Regions SMC	Shell 37A	Shell 304A	
	<0.1 0.1–0.2	<0.1 0.15 1.2 2.0–3.0	
Clusters SMC	<0.02 0.06–1		
N11 LMC	0.4 1.0 2.0–4.00 10–12		

1) the activity centered at about 1 Gyr is common to all the SFHs.

2) The same can be said for the activity in the age interval 2-3 Gyr.

3) Traces of older activity are revealed only by the three companion fields. Something happened in the range 2 to 6 Gyr that at the present resolution seems to have occurred at nearly constant efficiency.

4) There is some hint of a very early activity in the age range 10-12 Gyr.

5) Finally, at the very young epochs, two dominant periods of activity have likely occurred, i.e. at ages shorter than 0.02 Gyr and from 0.06 to 1 Gyr.

Previous studies of the subject did not lead to firm indications. As already reported several episodes of enhanced SF (at 400 Myr, 3 Gyr and 9 Gyr) were suggested by Harris and Zaritsky (2004) whereas nearly continuous SF, with a main episode between 5 and 8 Gyr was indicated by Dolphin et al. (2001). Both alternatives find partial confirmation in the present analysis. The problem is far from being settled down.

8.3 Comparison with dynamical models of LMC+SMC+MW

The interactions inside the triple system have been studied at different levels of complexity and detail, as far as the global gravitational potential, the various kinds of gravitational effects that are taken into account, the detail with which the three galaxies are modelled taking into account their own SFH under the effect of internal processes (spontaneous star formation) and external triggers (star formation induced, enhanced by the mutual interactions).

The pioneer study by Murai and Fujimoto (1980) best illustrates the technique in use to address this problem. The three galaxies are first considered as mass points for each of which a suitable gravitational potential field around is adopted and the mutual interactions and gravitational friction are taken into account. Usually the centre of mass of the triple system is located at the centre of the MW. Suitable initial conditions, present day position and velocity vectors for LMC and SMC are adopted however constrained to match the present observational data. Furthermore the orbital plane of the LMC (characterized by the inclination angle with respect to a reference plane) is adopted however constrained on the Magellanic Stream that

approximately lies on a great circle passing by the northern and southern galactic poles and crossing the galactic equator at $l \simeq 90°$ and 270°. This means that the inclination angle is $i \simeq 0° \pm 10°$. The orbits of the LMC and SMC are calculated back in time under the condition of energy and angular momentum conservation and their distances with respect to MW and to one another are derived. The epochs and relatives distances of close encounters are finally obtained. Then the satellite galaxies are thought of to be made by a number of particles to study the effect of tidal interaction and stripping. The emphasis was made on the LMC. Subsequent studies more or less followed the Murai and Fujimoto (1980) scheme, however with important changes in the kind of gravitational interactions, assumptions for gravitational potentials, and the modelling of the satellite galaxies till full exploitations of NB-TSPH simulations. They are briefly summarized below.

Murai and Fujimoto (1980). The study presents the detailed orbital evolution of the LMC+SMC system with respect to the MW. Depending on the initial conditions (present position and velocity of LMC and SMC, the inclination angle of the orbital plane, and the sense of revolution of the LMC as seen from the present position of the Sun, either counter- or clockwise) solutions in which LMC+SMC is a binary system for about 10 Gyr are possible. The results indicate that this occurs only for suitable choices of the velocity components of the SMC velocity and that the binary state can be easily destroyed choosing slightly different values. It would not last longer than about 3 Gyr going back in time. The distances LMC-MW and SMC-MW at the peri-galactic decrease with time because of dynamical friction. The periodicity of close encounters is about 1.5 Gyr increasing toward the past to about 2 Gyr. The separation between LMC and SMC is particularly interesting because the two galaxies may come very close to each other (from 20 to about 3 kpc) with a period of about 2 Gyr. For the sake of comparison we consider their best model for the binary state but also make use of their solution in which the LMC-SMC pair becomes unbound some time back in the past. The results are shown in Table 8.2 which displays the age and the distance of pair of galaxies at the closest encounters as indicated.

Bekki et al. (2004). We consider their best model A characterized by the parameters (U_L, V_L, W_L) = (-5, -225, 194 km/s) and (U_S, V_S, W_S) = (40, -185, 171 km/s) with dynamical friction. The evolution of the MCs during the past 9 Gyr reveals that the present orbital period of the MCs about the MW is $\simeq$1.5 Gyr (for the adopted gravitational potential and the masses of the MCs and MW). Although the distance LMC-SMC remains very small (<40 kpc) over the past 4 Gyr, they cannot keep their binary status for more than about 5 Gyr. Disintegration of the binary orbit is inevitable with this model. The data of the epochs of the closest encounters are reported in Table 8.2. The main results of this study relevant here are:

(i) The SFR in the LMC disc is moderately and repeatedly enhanced owing to the repetitive interaction between the MCs and the MW. The SFR increases from $\simeq 0.1 M_{\odot}$ yr^{-1} to $\simeq 0.4 M_{\odot}$ yr^{-1} at the first peri-centre passage of the LMC with respect to the MW about 7 Gyr ago. The SFR also becomes moderately high when the LMC begins to interact violently (with the LMC-SMC peri-centre of less than 10 kpc) about $\simeq$3.5 and 2 Gyr ago. Most of the new stars ($\simeq$90 per cent) are formed within the central 3 kpc, in particular, within the bar for the last 9 Gyr. Consequently, the half-mass radius is different by a factor of 2.3 between old field stars and newly formed ones. These structural differences between field stars with different ages are characteristic of the LMC disc under tidal interaction with the MW and the SMC. Furthermore the LMC and the SMC should have sinchronized star formations only at young ages.

(ii) Efficient formation of globular clusters does not occur until the LMC starts to interact violently and closely with the SMC (about 4 Gyr ago). This is due to the fact that cloud-cloud collisions with moderately high relative speed ($30 \simeq V_{rel} \simeq 100$ km s^{-1}) and with the small impact parameter (b < 0.25) required for globular cluster formation occurs most frequently when both the SMC and the MW dynamically influence the LMC disc strongly. The newly formed GC system has a disc-like distribution with rotational kinematics, and its mean metallicity is $\simeq 1.2$ higher than that of new field stars because of the pre-enrichment by the formation of field stars prior to cluster formation.

(iii) About 15 (20) per cent of the field stars (gas) initially within the LMC disc is tidally stripped to form a great stellar (gaseous) circle of a relic stream around the Galaxy during the last 9 Gyr evolution of the LMC. The great stellar circle shows inhomogeneity in some parts and is composed only of metal-poor old stars. The unique distributions of distance and radial velocity in the tidal stream may well enable us to pick out the stream among the Galactic halo stars. The stellar total mass of the tidal stream depends on the initial mass of the LMC (i.e. smaller for the larger LMC mass), so that the stellar number density along the stream provides valuable information on the LMC mass.

(iv) The LMC evolution depends on its initial mass and orbit with respect to the Galaxy and the SMC. In particular, the epoch of the bar and thick disc formation is determined by the LMC mass in such a way that the stellar bar and the thick disc are formed later in the model with a larger LMC mass. The mass fraction of the stellar halo is smaller for the model with a larger LMC mass. These are essentially because the LMC with a larger mass is more strongly bounded by its self-gravity so that the tidal perturbation from the Galaxy and the SMC does not influence the

Table 8.2: Ages (Gyr) and distances (kpc) at close encounters. The age is counted going back in time from the present. The sources of data are: (1) Murai and Fujimoto (1980), (2)Bekki et al. (2004), and (3)Yoshizawa and Noguchi (2003).

	Binary State						Unbound State	
Source	SMC-LMC		SMC-MW		LMC-MW		SMC-LMC	
	Age	D	Age	D	Age	D	Age	D
(1)	0.2	3	0.2	60	0.2	50	0.2	3
	3.2	10	1.5	45	1.5	58	1.8	4
	5.0	20	3.2	55	3.0	60	3.5	4
	7.0	10	4.8	62	5.0	63		
	9.5	20	6.8	53	6.8	70		
			9.0	75	9.0	80		
(2)							0.2	7
							1.5	10
							2.8	10
							3.6	5
							5.3	20
							7.2	110
(3)	0.2	6	0.25	55	0.1	45		
	1.4	15	1.6	55	1.7	55		

dynamical evolution of the LMC so significantly.

Yoshizawa and Noguchi (2003). This is the only study entirely dedicated to the SMC. The tidal response of the SMC to the LMC and MW has been investigated using numerical simulations including interstellar gas dynamics and star formation processes. The best model produces a gas stream with almost no stars, the morphology and velocity field of which agree with the observational data. The result depends on the initial SMC model supposed to be made by a compact stellar disc surrounded by an extended gas disc. The simulations also reproduce the observed distribution of young stars in the SMC. The central and wing regions of the SMC contain an excess of young stars as observed. The simulations show that this is due to the last interaction of the SMC with the LMC about 0.2 Gyr ago. The models also reproduce the large depth of the SMC indicated by the spatial distribution of the Cepheid stars. All this suggests that the observational structure, kinematics and stellar properties of the SMC are primarily of tidal origin. The data on the epochs of the closest encounters are reported in Table 8.2.

Comparison. Looking at the data of Table 8.2, the recent close encounter at about

0.2 Gyr ago is common to all models. It could find its counterpart in the very recent enhancement shown by the SFHs from the clusters and fields stars.

There is a close encounter at about 1.4 Gyr which is in common to Bekki et al. (2004) and Yoshizawa and Noguchi (2003) and missing or poorly evident in Murai and Fujimoto (1980). Hints of significant stellar activity at about this age can be found in Table 8.2 for the stellar fields NGC265 and NGC290 and the super-shell 304A.

The close encounter at about 3 Gyr is in common to Murai and Fujimoto (1980) and Bekki et al. (2004). It is not shown by Yoshizawa and Noguchi (2003) simply because they do not go that far back in time. The counterpart in the SFH of the stellar populations is common to all the three fields and super-shell 304A (see Tab.8.1).

Older close encounters are difficult to identify in our fields. The only comment we can make is that traces of star formation up to the age of about 6-7 Gyr can be found in the three fields, and in NGC265 and K29 also some evidence of an even older population (10-12 Gyr).

CHAPTER

9

Summary and Conclusions

General aims. The thesis touches upon several aspects of the cluster and field star formation in the MCs.

Cluster formation history. We revise the history of cluster formation in the main body of the Small Magellanic Cloud. The age of 311 clusters and 164 associations is determined through isochrone fitting method using CMDs derived from the OGLE data. Our main results are as follows:

1) The cluster age distribution supports the idea that clusters formed in the last 1 Gyr of the SMC history in a roughly continuous way with periods of enhancement. The age distribution of the clusters in the whole disk presents enhancements, namely between a few Myr and 15 Myr and at 90 Myr. Older objects are mainly located close to the SMC centre and on the SW side. Models of the interactions between LMC-SMC and Milky Way predict a close encounter between the MCs roughly 100–200 Myr ago. At that time the star formation is expected to be enhanced not only in the tidal arms, but also in the main body of the SMC. In fact an episode at 90 Myr is found in the age distribution of the clusters that might be due to tidal trigger. However the age distribution presents younger episodes that might have different origin and are possibly due to local phenomena.

Three clusters in particular. As the data used to estimate the age for the large sample of clusters and associations are not very deep, we check the quality of the

age assignment by performing an accurate study of three clusters in the appropriate age range using HST data. The clusters (and companion fields) are observed by Olszewski (2004) as part of the ACS/WFI program. The three clusters are located at the east side of HI super-shell 37A whose borders overlap a region of active star formation, most likely caused by the propagation of the gas pressure wave (Staveley-Smith et al., 1997; Stanimirovic et al., 1999).

In the ACS/WFI field containing the cluster we select a circular region inside which most of the cluster stars are located and derive the CMD and integrated luminosity function. The luminosity function and CMD are then compared to a library of synthetic luminosity functions and isochrones covering a large range of ages and metallicities. This yields a provisional value of the age and metal content best reproducing these two constraints. The results are then refined with the aid of population synthesis technique and the χ^2-minimization algorithm. We find the following ages and metallicities: for the cluster NGC 265 the age is Log(Age)=8.5 ± 0.3 yr and the metallicity is 0.004 ± 0.003; for the cluster K 29 the age is Log(Age)=8.2 ± 0.2 yr and the metallicity is 0.003 ± 0.002; for the cluster NGC 290 the age is Log(Age)=7.8 ± 0.5 yr and the metallicity is 0.003 ± 0.002. The ages assigned to the clusters on the basis of their CMD and luminosity function seem to be too old to be related to the dynamical age of the shell (Stanimirovic et al., 1999).

We also estimate the slope of the IMF, especially at low masses, between $0.7 M_{\odot}$ and $1 M_{\odot}$. We check whether the Kroupa exponent, $\alpha_1 = 2.2$, is recovered in this range. We see that all the clusters have the minimum of χ^2 function for α_1 close but not identical to the Kroupa value at the 68% confidence level.. The values are $\alpha_1 = 2.4 \pm 0.4$ for NGC 265, $\alpha_1 = 1.8 \pm 0.2$ for K 29, $\alpha_1 = 2.2 \pm 0.2$ for NGC 290.

For NGC 265 we also test the theory of convective overshoot: we fit the experimental NILF with two theoretical models, one including overshoot and the other without it (classical case). All the models in usage are from the BaSTI library. They are fully compatible with the correspondent ones of the Padova library. We can say that a certain amount of overshoot is needed in order to fit the experimental data.

Cluster formation and environment. The main goal here is to perform a study of the correlation between young objects and their interstellar environment to check whether there is any correlation between their SFH and the ambient medium in which they formed.

The spatial distribution of the clusters is compared with the HI maps in which two super-shells are identified, with the HI velocity dispersion field, with the location of the CO clouds and with the distribution of young field stars. The conclusions are:

1) The two super-shells 37A and 304A are clearly visible in the spatial age distribution of the clusters younger than about 15 Myr: the mechanism responsible of the shell formation (SN, stellar winds, and/or turbulence) is closely related to the cluster formation. The regions have been very active especially at the edges of the shells and in the inter-shell region since 1 Gyr ago. In the super-shell 37A clusters younger than a few 10^7yr are located at the Eastern rim of the super-shell 37A where gas and dust are located, while older episodes are widely distributed. The cluster age distribution at the Eastern part shows a young episode at a few Myr, and several enhancements, namely between a few Myr and 15 Myr, and at 80 Myr. On the Western side, the star formation was less efficient at ages younger than 15 Myr, while it was comparable at older ages.

2) The cluster distribution in the super-shell 304A shows a continuous formation from a few Myr to 1 Gyr. The dominant episode was between a few Myr and 20 Myr. An enhancement is found at 90 Myr.

3) We find that star clusters and associations form in clustered distribution. The typical correlation scale of the clusters is of the order of 500pc, comparable with the dimensions of the large molecular cloud complexes found in the LMC and in the SMC. The two point autocorrelation function of the young massive field stars shows a stronger correlation, but on a comparable scale.

4) A tight cross-correlation between young clusters and the HI intensity is found. The degree of correlation is decreasing with the age of the clusters. Finally clusters older than 300 Myr are located away from the HI peaks. Clusters and associations younger than 10 Myr are related to the CO clouds in the SW region of the disk, but not in the NE where smaller clouds are found. Older generation is more evenly distributed. This is in agreement with the evolutionary time scale of the giant molecular clouds that is found to be of the order of 10 Myr. This correlation indicates that the molecular gas content is associated to the field and cluster formation, but that its presence does not necessarily imply star formation.

5) A weak relation between the location of the young clusters and the velocity dispersion field of the atomic gas is derived. The shell 304A (where a positive correlation is found) is coincident with a high velocity dispersion region where shocks among clouds might have triggered cluster formation. However this mechanism cannot account for the majority of young objects in the southern shell, 37A where young clusters are located in regions of intermediate velocity dispersion.

6) The field star formation is continuous in the past 160 Myr. Then periods of quiescence are followed by enhanced activity. A global burst of SF is found at ages

of a few Myr, which might be responsible of the fractal structure of HI interstellar medium. Enhancements are found between 100-150 Myr and between 1 and 1.6 Gyr, corresponding to a close interaction between SMC and LMC. The last tidal interaction between the MCs (100-200 Myr ago) has triggered the formation of both clusters and field stars. However, clusters and field formation rates are not completely coincident, suggesting a different mode of formation.

Star formation in the companion fields of the clusters. Taking advantage of the deeper photometry of the HST data we have determined the past SFH in the companion fields of the three clusters. This SFH shows several common features suggesting a common triggering mechanism over the scale length of interest here ($\sim 700pc$). Main episodes are at 300-400 Myr, 3 Gyr and 4 Gyr in common for all the fields. However the SFR is not very efficient at older ages. This result is in agreement with the SFR at old ages in the LMC. This suggests that at old ages, the tidal interaction between the MCs, if any, is not strong enough to trigger star formation episodes in the SMC.

Star formation in the N11 region of the LMC. We analyze the data of 6 fields in the N11 region of the LMC. The data are taken from the ESO archive and the instrument in use is the ACS/WFC of the HST. We build CMDs of the 6 fields and notice the presence of a double low main sequence. We interpret the second redder sequence as the presence of pre-main sequence stars in the considered fields. We also discussed the possibility of a differential reddening.
We derive the rate of star formation in the field area, giving enhancements at 0.1,0.6,2 and 10 Gyr.
We discuss the clustering of the pre-main sequence stars inside the observed area, both through the correlation function and other statistical methods like the minimal spanning tree. We find that the stars are correlated with a correlation length of $\sim$ 10 pc , the same order of a typical molecular cloud in the MC. We finally look for the presence of YSOs in the area using archive Spitzer data, suggesting a long lasting star formation process from 0.1 to 7 Myr.

Comparing SFH from photometry to predictions from theoretical dynamical models. We compare the SFH obtained for the large sample of clusters and associations, selected fields inside the HI regions, and the companion fields of the three clusters, looking for common periods of activity. Although due to the different kind of data the age overlap is marginal, periods of common activity can be identified and periods of star formation activity above the average value can be singled out.

These are then compared with the theoretical prediction from studies of the dynamical interaction inside the triple system MW+LMC+SMC for the two possi-

ble alternatives: LMC+SMC were in the binary status from very early epochs, or LMC+SMC got bound in the recent past. In general several intriguing coincidences are found.

Appendix Finally, the thesis contains an appendix. Appendix A is the catalog of clusters and associations where an estimate of the age has been derived.

CHAPTER

10 Appendix A: The SMC Cluster Catalog

Table 9.1
Catalog of SMC clusters for which we have obtained a provisional estimate of the age using the mean metallicity Z=0.008. For each cluster we adopt the appropriate reddening E(V-I) as indicated. Column 1: Identification number in the Bica and Dutra (2000) list; Columns 2 and 3: Coordinates; Column 4: Name; Column 5: Radius: Column 6: Age in years; Column 7: Reddening E(V-I); Column 8: Cluster Type from Bica and Dutra (2000); Column 9: Class. It gives an estimate of the uncertainties on the age determination. Class 1 indicates objects having $\Delta(Log(Age(yr))) < 0.3$; class 2 indicates objects having $0.3 < \Delta(Log(Age(yr))) < 0.5$; class 3 indicates objects having $\Delta(Log(Age(yr))) > 0.5$. The catalog contains 462 clusters.

ID	α(2000) (deg)	δ(2000) (deg)	Name	Radius (deg)	Log(Age) (yr)	E(V-I)	Type	Class
60	9.0583	-73.4117	H86-30	0.003	8.9	0.04	C	1
65	9.1583	-73.0858	H86-35,SMC-OGLE1	0.003	8.8	0.04	C	1
66	9.2083	-73.0711	H86-36	0.007	8.8	0.10	AC	1
70	9.3500	-73.0306	H86-38	0.010	7.6	0.04	A	1
72	9.3875	-73.6119	HW11,SMC-OGLE2	0.010	8.4	0.04	C	1
73	9.3917	-73.0250	BS10	0.005	9.0	0.04	C	1
74	9.4208	-73.1211	H86-42	0.004	8.9	0.00	C	1
75	9.4250	-73.9083	L19,SMC-OGLE3	0.014	8.9	0.04	C	1
76	9.4333	-73.2111	B10,SMC-OGLE4	0.007	9.0	0.04	C	3
77	9.4542	-73.4839	H86-40	0.004	8.8	0.04	C	1
78	9.4625	-73.1211	H86-43	0.005	8.8	0.04	C	1
79	9.5917	-73.2750	B12	0.004	9.0	0.04	C	1
80	9.6000	-73.3783	BS11	0.010	7.4	0.04	A	1
81	9.6542	-73.8058	B14,SMC-OGLE162	0.005	7.9	0.04	C	2
82	9.7042	-73.2756	H86-47	0.002	9.0	0.04	C	1
83	9.7125	-73.3742	HW12,SMC-OGLE163	0.007	8.7	0.30	C	2
84	9.7333	-73.4089	H86-48,SMC-OGLE164	0.004	8.0	0.08	C	2
86	9.7458	-73.9469	B16	0.002	9.0	0.04	C	1
87	9.7583	-73.9347	BS12	0.003	9.0	0.04	C	1
90	9.8417	-73.2578	SMC-OGLE5	0.007	9.0	0.01	CA	1
91	9.8583	-73.3831	HW12A	0.005	9.0	0.04	C	3
92	9.8583	-73.1064	H86-55,SMC-OGLE167	0.004	8.8	0.20	C	1
93	9.8792	-73.4239	HW13,SMC-OGLE168	0.006	9.0	0.04	C	1

94	9.8958	-73.3828	H86-54	0.004	8.6	0.00	C	1
104	10.1125	-73.4611	H86-59	0.004	8.0	0.08	C	3
105	10.1250	-73.2306	SMC-OGLE7	0.008	8.3	0.15	CA	1
106	10.1292	-73.4028	NGC220,K18,L22,ESO29SC3	0.010	8.1	0.08	C	2
109	10.1792	-73.1181	H86-60	0.003	9.0	0.10	C	3
111	10.1875	-73.7406	B26,SMC-OGLE169	0.007	8.0	0.08	C	2
113	10.1833	-73.3833	NGC222,K19,L24,ESO29SC4	0.010	8.0	0.10	C	1
114	10.1875	-73.3783	H-A3	0.065	6.6	0.04	A	1
118	10.2292	-73.4019	B23,SMC-OGLE170	0.005	8.0	0.08	C	1
120	10.2500	-73.6061	SMC-DEM5	0.024	7.0	0.04	NA	1
122	10.2750	-73.3519	NGC231,K20,L25,ESO29SC5	0.015	7.8	0.10	C	1
126	10.3375	-73.3419	BS15	0.020	7.8	0.10	A	1
128	10.4500	-73.3908	SMC-OGLE172	0.002	9.0	0.08	C	1
129	10.4833	-73.4878	SMC-OGLE166	0.005	8.5	0.10	C	1
134	10.5792	-73.7419	SMC-DEM7	0.008	7.2	0.08	NA	1
135	10.5917	-73.7342	HW16,SMC-OGLE13	0.005	7.7	0.00	CN	2
136	10.6167	-73.5472	SMC-OGLE14	0.007	8.5	0.20	AC	1
138	10.7125	-73.1756	BS249	0.004	8.8	0.20	CA	1
139	10.7250	-73.2936	SMC-OGLE15	0.008	8.1	0.08	CA	3
140	10.7500	-73.2944	H-A4	0.020	7.0	0.20	A	1
143	10.7417	-73.1686	BS16,SMC-OGLE16	0.005	8.6	0.20	C	1
144	10.7583	-73.1519	H-A5	0.030	6.8	0.20	A	1
145	10.7542	-73.2578	BS18	0.010	7.4	0.20	A	1
147	10.8083	-73.0119	BS17,SMC-OGLE174	0.007	8.9	0.08	CA	1
148	10.8125	-73.2514	BS250	0.005	8.8	0.08	AC	1
149	10.8667	-73.3197	BS19	0.033	6.8	0.20	A	3
150	10.8875	-73.4403	NGC241,K22w,L29W	0.008	8.3	0.10	C	1
152	10.9083	-73.4436	NGC242,K22e,L29e	0.006	7.8	0.08	C	3
153	10.9083	-72.9586	B31,SMC-OGLE19,SMC-OGLE175	0.004	8.5	0.10	C	1
155	10.9083	-72.9800	BS20,SMC-OGLE20	0.004	8.8	0.10	C	1
156	10.9083	-73.2442	H-A6	0.033	7.4	0.08	A	1
157	10.9333	-72.9767	H86-70,SMC-OGLE21	0.005	8.8	0.00	C	1
160	10.9917	-73.1522	SMC-OGLE22	0.006	8.6	0.20	CA	1
161	11.0542	-73.4506	SMC-DEM10	0.040	7.2	0.20	NA	1
162	11.0542	-73.6189	B33,SMC-OGLE23	0.004	8.4	0.08	C	1
163	11.0958	-72.9456	B34A	0.006	9.0	0.08	CA	3
164	11.0958	-73.2125	BS23	0.020	7.2	0.10	A	1
165	11.1000	-73.2517	BS24	0.020	6.6	0.20	A	1
166	11.1917	-72.8981	BS25	0.008	8.3	0.20	CA	1
168	11.2167	-73.0019	B34,SMC-OGLE176	0.005	8.8	0.10	C	1
170	11.2292	-73.1742	BS27,SMC-OGLE177	0.003	8.4	0.08	C	3
173	11.2292	-73.2092	SMC-DEM13nw	0.016	7.0	0.10	NA	3
174	11.2333	-73.1697	SMC-N10,L61-60,SMC-DEM11	0.003	8.5	0.20	NC	1
175	11.2542	-72.9214	SMC-OGLE24	0.016	7.0	0.08	A	3
178	11.2917	-73.2342	SMC-DEM13se,H-A7	0.024	7.3	0.20	NA	1
179	11.2958	-72.8753	BS28,SMC-OGLE178	0.006	8.5	0.12	CA	1
180	11.3083	-73.2192	H86-74,SMC-OGLE25	0.006	8.0	0.08	C	1
182	11.3292	-73.2589	SMC-DEM14,H-A8	0.016	6.8	0.08	NA	1
182	11.3292	-73.2589	SMC-DEM14,H-A8	0.016	6.8	0.20	NA	1
183	11.3375	-73.0356	SMC-OGLE179	0.004	8.4	0.20	CA	1
184	11.3500	-73.3761	NGC248n,SMC-N13B,L61-67n	0.006	7.2	0.20	NA	1
186	11.3458	-72.9286	SMC-OGLE180	0.002	9.0	0.08	C	1
187	11.3583	-73.3844	NGC248s,SMC-N13A,L61-67s	0.006	8.6	0.08	NC	2
189	11.3583	-73.4814	B39,SMC-OGLE27	0.005	8.6	0.08	C	1
191	11.3667	-72.8194	SMC-OGLE28	0.003	8.8	0.08	C	2
192	11.3667	-72.8858	SMC-OGLE181	0.006	8.5	0.08	CA	3
194	11.3750	-73.4850	BS30	0.003	8.9	0.08	C	2
197	11.3875	-73.1075	SMC-OGLE30	0.006	8.7	0.25	CA	1
198	11.3917	-73.2572	B-OB1	0.030	8.2	0.08	AN	3
200	11.4042	-73.2094	SMC-DEM17	0.015	6.8	0.08	NA	1
201	11.4083	-73.0747	BS37	0.005	6.8	0.08	NA	1
203	11.4333	-72.8431	B36	0.006	8.4	0.08	C	3
204	11.4625	-72.8403	SMC-OGLE31	0.005	8.8	0.08	CA	3
206	11.4750	-73.1142	SMC-DEM20	0.020	7.8	0.12	NA	3
207	11.4750	-73.5067	NGC256,K23,L30,ESO29SC11	0.007	8.0	0.20	C	1
210	11.5083	-73.0936	SMC-N12,B-OB3	0.060	7.0	0.12	NA	3
211	11.5125	-73.3006	SMC-DEM19	0.050	7.0	0.20	NA	1
212	11.5208	-73.4439	BS31	0.023	8.2	0.08	AN	1
213	11.5458	-72.8175	H86-80,SMC-OGLE184	0.003	9.0	0.08	C	1
219	11.5458	-73.2733	BS32	0.016	6.8	0.08	NA	1
223	11.5750	-73.2117	SMC-DEM22	0.015	7.0	0.08	NA	1
224	11.5750	-73.3925	SMC-N16,MA130	0.010	7.1	0.24	NA	1
225	11.5958	-73.1333	BS33	0.015	7.0	0.08	NA	1
226	11.5958	-73.2186	H-A10	0.030	7.0	0.15	AN	1
227	11.6125	-73.1047	SMC-N12A,SMC-DEM23,MA133	0.015	7.2	0.08	NA	1
228	11.6333	-73.0986	NGC261,B42,ESO29EN12	0.010	6.8	0.08	NA	1
229	11.6458	-72.7422	L31,SMC-OGLE36	0.009	8.5	0.08	C	3
230	11.6417	-72.7739	H86-83,SMC-OGLE35	0.006	8.4	0.08	C	3
231	11.6417	-72.7656	H86-84,SMC-OGLE185	0.003	8.7	0.20	C	1
232	11.6583	-73.5283	SMC-N17,SMC-DEM25,MA140	0.020	7.0	0.08	NA	1
234	11.6708	-73.0000	SMC-OGLE37	0.007	8.5	0.08	C	2
235	11.6708	-73.3639	SMC-DEM24,MA142	0.015	6.7	0.20	NA	1
238	11.6875	-73.1714	MA143	0.003	8.0	0.20	NC	1
239	11.7000	-73.4353	SMC-DEM29	0.070	6.8	0.08	NA	1
240	11.7333	-73.4236	H86-85,SMC-OGLE186	0.005	8.2	0.08	C	1

242	11.7417	-73.3358	H86-88	0.007	8.8	0.08	CA	3
243	11.7542	-73.0928	SMC-DEM27	0.020	6.8	0.20	NA	1
245	11.7542	-73.3931	H86-86,SMC-OGLE40	0.007	8.0	0.08	C	1
246	11.7750	-73.2567	H86-89,SMC-OGLE38	0.007	8.5	0.08	C	3
247	11.7750	-73.3714	H86-87,SMC-OGLE187	0.007	8.6	0.08	C	3
248	11.7958	-73.2119	H-A11	0.030	6.7	0.14	A	1
249	11.8000	-73.4772	NGC265,K24,L34,ESO29SC14	0.010	8.4	0.08	C	3
251	11.8208	-73.1414	SNR0045-73.4,MA165	0.014	8.0	0.15	N	3
252	11.8542	-72.8408	L33,SMC-OGLE41	0.008	7.9	0.08	C	2
253	11.8500	-73.2056	H86-93,MA172,SMC-OGLE188	0.003	7.6	0.08	CN	2
256	11.8708	-73.0856	SMC-DEM31	0.013	8.6	0.15	N	1
258	11.8875	-73.3736	SMC-DEM30,MA184	0.014	7.0	0.20	NA	1
260	11.9042	-73.0142	H86-95	0.003	9.0	0.08	CA	1
261	11.9125	-73.1375	SMC-N19,SMC-DEM32,H-A12	0.060	7.0	0.12	NA	3
264	11.9292	-73.3561	H-A13	0.024	6.6	0.08	A	1
265	11.9458	-73.3031	SMC-DEM34,MA187	0.005	7.0	0.08	NA	1
268	11.9583	-73.4783	BS35,SMC-OGLE42	0.006	8.8	0.08	C	1
269	11.9583	-73.3883	H-A14	0.024	7.3	0.10	AN	3
270	11.9667	-73.2222	H86-97,SMC-OGLE43	0.006	8.5	0.08	C	3
272	11.9708	-73.5314	H86-94	0.005	8.7	0.08	C	2
273	11.9792	-72.9556	H86-98,SMC-OGLE44	0.007	8.8	0.08	CA	3
274	11.9833	-73.1025	MA199	0.002	7.2	0.08	NC	3
275	11.9917	-73.2944	SMC-N23,SMC-DEM36,MA202	0.007	8.0	0.08	NA	1
276	12.0042	-73.4861	K25,L35,SMC-OGLE45	0.010	8.4	0.08	C	3
277	12.0083	-73.2739	NGC267,SMC-N22,SMC-DEM37	0.017	7.0	0.15	NA	1
283	12.0417	-73.3308	SMC-N24,SMC-DEM42w,MA210	0.010	6.8	0.08	NA	1
284	12.0542	-72.7931	H86-99,SMC-OGLE190	0.005	8.9	0.08	CA	3
286	12.0708	-73.1708	SMC-DEM39,MA216	0.005	6.9	0.08	NA	1
287	12.0708	-73.4025	B-OB2	0.058	6.8	0.08	A	1
289	12.0833	-72.7950	H86-100,SMC-OGLE191	0.006	8.6	0.15	CA	3
290	12.0875	-73.5303	NGC269,K26,L37,ESO29SC16	0.010	8.5	0.10	C	3
294	12.1083	-72.7525	SMC-DEM46w	0.033	6.7	0.08	NA	1
296	12.1083	-73.0072	SMC-OGLE192	0.003	8.7	0.08	C	3
297	12.1125	-73.1003	MA228	0.003	7.0	0.20	NC	3
298	12.1167	-72.9833	SMC-OGLE47	0.010	8.2	0.08	AC	3
299	12.1208	-73.1081	MA231	0.004	7.5	0.08	NC	3
301	12.1292	-73.2681	SMC-N28A,MA234	0.007	8.2	0.08	NA	3
302	12.1375	-73.3069	B47,SMC-OGLE48	0.008	8.4	0.08	C	3
303	12.1417	-73.2586	SMC-N28,SMC-DEM43,MA244	0.015	7.0	0.20	NA	3
304	12.1542	-73.4147	B48,SMC-OGLE49	0.010	8.0	0.08	CA	3
305	12.1542	-73.1792	SMC-OGLE193	0.004	8.7	0.08	CA	3
307	12.1667	-73.4303	H-A16	0.020	6.6	0.08	A	1
310	12.2167	-73.5614	B49	0.004	9.0	0.08	C	1
311	12.2375	-73.1644	SMC-N30A,L61-126,MA267	0.003	7.8	0.15	NC	3
312	12.2458	-73.1511	SMC-OGLE50	0.006	7.7	0.08	NC	3
313	12.2500	-73.1389	SMC-N30,SMC-DEM45	0.023	7.0	0.15	NA	1
314	12.2625	-73.2436	SNR0047-73.5	0.024	7.4	0.04	N	3
315	12.2583	-73.3622	B50	0.005	7.0	0.08	C	3
316	12.2708	-73.0511	H86-103,SMC-OGLE51	0.005	7.0	0.08	C	3
317	12.2750	-73.3528	BS41,SMC-OGLE194	0.005	8.1	0.08	C	1
318	12.3000	-73.1086	H86-104,SMC-OGLE52	0.003	9.0	0.08	C	1
319	12.3125	-72.8800	SMC-DEM47,B-OB6w	0.035	6.9	0.15	NA	1
320	12.3167	-73.2492	BS42,SMC-OGLE195	0.008	7.0	0.20	CA	1
321	12.3125	-73.3708	BS43	0.009	6.8	0.08	A	2
322	12.3250	-73.3722	L39,SMC-OGLE54	0.006	8.0	0.08	C	2
323	12.3250	-73.2117	SMC-OGLE53	0.008	7.3	0.15	C	3
324	12.3375	-73.1839	SMC-OGLE55	0.005	8.0	0.20	C	2
325	12.3458	-73.5303	H86-102	0.005	8.3	0.10	C	2
326	12.3625	-73.3986	SMC-OGLE196	0.003	8.1	0.08	C	3
327	12.3625	-72.8114	SMC-DEM46e	0.032	6.8	0.20	NA	1
328	12.3625	-73.4306	SMC-DEM44	0.056	7.0	0.08	NA	1
331	12.4000	-73.2639	SMC-DEM49	0.035	6.8	0.20	NA	1
332	12.4000	-72.8369	SMC-OGLE56	0.007	7.6	0.14	CA	1
334	12.4167	-73.0589	B52,SMC-OGLE57	0.009	8.5	0.08	C	3
336	12.4208	-72.8119	SMC-N32,L61-137,H86-111	0.003	8.7	0.20	NC	3
337	12.4250	-73.1769	MA317	0.002	7.8	0.08	NC	2
338	12.4333	-72.8539	H86-110	0.006	7.3	0.18	CA	2
339	12.4375	-72.8661	H86-109,SMC-OGLE58	0.004	8.4	0.15	C	1
340	12.4417	-73.1736	SMC-N34,L61-142,SMC-DEM50	0.005	7.5	0.08	NC	3
341	12.4500	-73.0978	BS44	0.024	6.9	0.20	A	1
344	12.5000	-73.2550	H86-107,SMC-OGLE61	0.010	7.8	0.15	CA	1
346	12.5167	-73.0528	SMC-DEM51	0.038	6.8	0.60	NA	1
347	12.5167	-73.3367	H-A17	0.025	7.0	0.20	A	1
348	12.5167	-73.3844	B53,SMC-OGLE197	0.008	8.2	0.08	C	1
349	12.5417	-73.1731	H-A18	0.023	6.8	0.20	A	1
350	12.5333	-73.1906	H86-112,SMC-OGLE198	0.005	8.0	0.20	C	2
352	12.5500	-73.3472	BS39	0.004	7.5	0.08	C	1
354	12.5667	-73.0333	BS45,SMC-OGLE59	0.008	7.7	0.18	CA	1
355	12.5750	-73.3247	MA351	0.004	7.4	0.15	NC	1
356	12.5875	-72.8811	SMC-N36w,SMC-DEM54w,H-A19	0.032	6.9	0.15	NA	1
358	12.5917	-73.3878	B55,SMC-OGLE60	0.006	8.0	0.08	C	2
359	12.6167	-73.2033	B54,SMC-OGLE62	0.005	8.3	0.08	C	3
361	12.6292	-73.3364	H86-106w	0.004	8.7	0.15	C	3
362	12.6417	-73.3386	SMC-DEM52,MA370	0.010	6.8	0.15	NA	1
363	12.6542	-73.0578	H86-115,SMC-OGLE63	0.013	8.0	0.08	AC	1

364	12.6583	-72.7956	SMC-N37,SMC-DEM55,H-A23	0.050	6.8	0.15	NA	1
365	12.6542	-73.3364	H86-106e	0.005	7.1	0.15	C	3
367	12.6625	-72.9789	BS46,SMC-OGLE200	0.004	8.0	0.15	C	3
368	12.6667	-72.9653	H86-116,SMC-OGLE64	0.004	8.0	0.15	C	1
369	12.6708	-72.9672	L40,H-A22	0.015	6.6	0.60	A	1
370	12.6792	-72.7819	MA384	0.003	6.8	0.15	NC	3
371	12.6708	-73.4628	H-A21	0.029	7.0	0.08	A	1
373	12.6917	-73.2972	H-A24	0.020	7.0	0.15	A	1
374	12.6750	-73.3969	BS48,SMC-OGLE201	0.007	8.0	0.08	AC	1
376	12.7167	-72.8728	SMC-N36e,SMC-DEM54e,B-OB6e	0.035	6.8	0.15	NA	1
377	12.7333	-72.7278	L41,SMC-OGLE67	0.005	8.1	0.15	C	1
378	12.7208	-73.4061	H86-108,MA401	0.008	7.0	0.20	NA	1
379	12.7292	-73.0575	SMC-OGLE65	0.005	8.2	0.12	C	1
380	12.7333	-72.7531	BS49	0.013	6.8	0.25	NA	1
381	12.7292	-73.2031	B56,SMC-OGLE66	0.004	7.7	0.10	C	3
382	12.7333	-73.2892	BS40,SMC-OGLE68	0.007	7.0	0.16	CA	3
383	12.7500	-72.8844	SMC-N41,L61-166,MA424	0.003	6.7	0.30	NC	3
384	12.7458	-73.5036	H86-105,SMC-OGLE202	0.004	7.9	0.08	C	2
385	12.7708	-73.3922	SMC-DEM53	0.029	7.0	0.08	NA	1
387	12.7958	-73.3681	SNR0049-73.6	0.016	8.2	0.08	N	1
388	12.8083	-72.6928	H-A25	0.050	7.0	0.15	NA	1
389	12.8083	-73.1614	NGC290,L42,ESO29SC19	0.009	7.0	0.20	C	3
390	12.7917	-73.5900	H86-113,SMC-OGLE203	0.003	8.1	0.15	C	1
391	12.8375	-73.1386	H86-121,SMC-OGLE204	0.005	8.8	0.08	C	3
392	12.8333	-73.5064	SMC-DEM59	0.012	6.8	0.08	NA	1
393	12.8583	-73.2833	BS251,SMC-OGLE70	0.003	8.4	0.08	CA	2
394	12.8667	-73.0867	H-A27A	0.026	6.8	0.15	A	1
395	12.8625	-73.1567	BS51	0.027	7.0	0.20	A	1
396	12.8750	-73.3356	BS252	0.005	7.9	0.20	AC	1
398	12.8875	-72.7942	B-OB7	0.033	6.8	0.15	AN	2
399	12.8833	-72.9792	H86-124,SMC-OGLE205	0.007	8.1	0.08	C	1
400	12.9042	-72.5419	H86-119	0.005	7.0	0.15	C	3
401	12.8833	-73.0106	B57,SMC-OGLE71	0.010	7.1	0.20	C	2
403	12.9250	-73.2297	SMC-N45,L61-189,B60	0.006	6.6	0.20	NC	3
404	12.9333	-72.8403	B59,L61-183,MA488	0.007	8.0	0.14	CN	1
408	12.9333	-73.1669	H86-123,SMC-OGLE206	0.005	8.3	0.08	C	1
409	12.9458	-72.8464	SMC-N46,L61-184,SMC-DEM62	0.005	8.1	0.10	NC	3
411	12.9542	-72.5411	H86-127,SMC-OGLE207	0.005	8.4	0.08	C	2
412	12.9625	-72.5478	B-OB9	0.023	6.9	0.20	A	1
413	12.9667	-72.6786	SMC-DEM63,B-OB8	0.092	6.8	0.30	NA	1
415	12.9708	-72.9539	K29,L44,SMC-OGLE74	0.008	8.1	0.08	C	1
416	12.9750	-73.0981	H86-126,SMC-OGLE75	0.004	8.2	0.10	C	1
422	13.0125	-72.8178	H86-128,H86-131,SMC-OGLE208	0.004	8.3	0.08	C	1
423	13.0125	-72.6589	MA524	0.025	6.7	0.15	NA	1
426	13.0250	-73.4450	SMC-DEM70s	0.050	6.8	0.20	NA	1
427	13.0333	-73.3153	BS54	0.005	6.7	0.18	AC	3
430	13.0500	-72.5308	H86-129,SMC-OGLE76	0.005	8.0	0.08	C	1
431	13.0542	-73.0033	BS56,SMC-OGLE77	0.006	8.1	0.08	C	1
432	13.0625	-72.7661	BS253,SMC-OGLE209	0.005	7.1	0.18	AC	1
433	13.0542	-73.2986	SMC-DEM70n	0.083	7.0	0.30	NA	1
434	13.0708	-73.3756	H86-125,SMC-OGLE79	0.006	8.2	0.08	CA	1
436	13.0708	-73.0178	H86-130,SMC-OGLE78	0.006	7.0	0.08	C	3
438	13.0875	-73.1622	B-OB5ne	0.027	6.8	0.18	A	1
439	13.0875	-73.3272	H-A28	0.023	7.3	0.25	AN	1
440	13.1250	-73.0497	B64,SMC-OGLE210	0.006	8.1	0.08	C	1
441	13.1333	-73.0361	BS57,SMC-OGLE211	0.005	7.6	0.17	C	1
442	13.1417	-72.6817	H86-133,H86-137,SMC-OGLE81	0.006	7.4	0.20	C	1
444	13.1292	-72.6294	H86-132,SMC-OGLE80	0.004	8.4	0.08	C	3
445	13.1333	-73.0514	H-A29	0.022	6.7	0.28	A	1
448	13.1500	-73.3808	BS58	0.005	8.5	0.08	C	1
449	13.1667	-72.6744	BS59	0.023	6.8	0.25	NA	1
450	13.1542	-73.4378	SMC-N51,L61-219,SMC-DEM72	0.008	6.9	0.20	NA	1
451	13.1750	-72.9256	BS60,SMC-OGLE82	0.007	7.9	0.15	C	1
453	13.1833	-72.9800	B65,SMC-OGLE83	0.006	7.8	0.08	C	1
454	13.1750	-73.0008	H-A30	0.017	6.9	0.50	A	1
455	13.1792	-73.0292	BS61	0.005	6.8	0.08	CA	3
456	13.1875	-72.6325	SMC-N50,SMC-DEM68se	0.018	6.7	0.10	NA	1
457	13.1917	-72.7011	H-A31	0.025	6.7	0.14	A	1
458	13.2000	-72.7961	B66,SMC-OGLE85	0.005	8.6	0.08	C	1
459	13.2000	-72.9894	H86-134e,SMC-OGLE213	0.004	8.1	0.08	C	3
461	13.1958	-73.4069	BS63,SMC-OGLE84	0.004	8.5	0.08	C	3
462	13.2083	-72.7169	BS64	0.008	7.4	0.13	AC	1
463	13.2042	-73.4119	B67,SMC-OGLE87	0.005	8.5	0.20	C	3
464	13.2125	-72.7353	BS254	0.004	7.1	0.08	C	1
466	13.2000	-72.5106	H86-135,SMC-OGLE86	0.005	8.7	0.08	C	1
467	13.2167	-73.0292	BS255	0.003	8.9	0.08	C	1
468	13.2125	-73.1344	H-A32	0.033	6.9	0.10	A	1
470	13.2542	-72.8969	K31,L46,SMC-OGLE88	0.023	7.2	0.20	C	1
471	13.2542	-73.1872	BS66	0.010	7.0	0.15	AN	3
472	13.2667	-72.6308	H-A33	0.025	6.8	0.20	A	1
473	13.2792	-72.6244	B69,SMC-OGLE89	0.005	7.7	0.08	C	2
475	13.2750	-73.3803	NGC294,L47,ESO29SC22	0.014	8.6	0.13	C	1
476	13.2875	-72.8328	H86-140,SMC-OGLE214	0.004	7.8	0.08	C	2
477	13.2917	-72.5736	H86-138,SMC-OGLE91	0.004	8.6	0.08	C	1
479	13.2958	-73.2203	B-OB5se	0.046	8.3	0.15	AN	3

480	13.3083	-72.8772	SMC-DEM69	0.040	6.8	0.25	NA	2
482	13.3250	-72.7667	B71,SMC-OGLE92	0.007	7.3	0.15	C	1
486	13.3583	-72.6825	B72	0.010	7.4	0.08	C	1
487	13.3792	-72.6678	H86-143,SMC-OGLE93	0.007	7.8	0.08	C	3
488	13.3833	-72.5411	H-A36	0.052	6.9	0.20	A	1
489	13.3833	-73.3508	BS67	0.005	8.7	0.08	AC	1
491	13.4000	-72.6417	BS257	0.007	8.1	0.08	AC	1
493	13.4167	-72.6597	SMC-N52A,L61-243	0.004	7.0	0.20	NC	3
494	13.4167	-72.6831	H-A35	0.028	7.0	0.15	AN	2
496	13.4250	-72.6542	SMC-N52B,L61-244,B73	0.004	7.0	0.30	NC	3
497	13.4250	-73.2442	SMC-DEM74	0.075	6.8	0.15	NA	1
498	13.4250	-73.3589	BS68,SMC-OGLE95	0.007	8.3	0.15	CA	2
499	13.4583	-72.8964	H86-147,SMC-OGLE216	0.010	8.5	0.08	C	2
501	13.4792	-72.6689	H86-148	0.004	8.7	0.14	C	1
503	13.4833	-72.8567	BS69,SMC-OGLE217	0.005	8.8	0.08	CA	3
505	13.4917	-72.6933	B75	0.010	7.4	0.12	CA	1
506	13.4917	-72.7344	BS71	0.016	6.7	0.20	NA	1
510	13.5458	-72.8650	BS72,SMC-OGLE97	0.006	8.8	0.08	CA	1
512	13.5625	-73.2853	SMC-DEM78	0.011	6.8	0.20	NA	1
513	13.5792	-72.5147	H86-149	0.005	8.8	0.08	C	1
515	13.5958	-72.6947	H86-152,SMC-OGLE218	0.007	8.4	0.22	C	1
516	13.5917	-73.0456	H86-151	0.004	9.0	0.08	C	1
517	13.6083	-72.8847	BS258	0.005	8.1	0.15	A	1
520	13.6375	-72.7933	BS73	0.035	7.0	0.26	NA	1
522	13.6667	-72.7153	SMC-DEM80	0.090	7.2	0.27	NA	1
525	13.6958	-73.2236	B80,SMC-OGLE98	0.009	8.7	0.08	C	1
526	13.7000	-72.4661	B79,SMC-OGLE99	0.007	7.3	0.08	C	1
527	13.7083	-72.6989	H86-156	0.004	8.8	0.08	C	1
528	13.7167	-72.4386	H-A38	0.047	7.1	0.10	A	1
529	13.7167	-72.9164	B76,SMC-OGLE219	0.003	8.4	0.08	C	1
531	13.7292	-72.4419	BS259	0.005	7.6	0.08	C	1
533	13.8000	-72.6833	H86-159,SMC-OGLE102	0.004	9.0	0.08	C	1
534	13.7875	-72.8111	H86-158,H86-161,SMC-OGLE100	0.005	7.6	0.08	C	1
535	13.8000	-73.2967	H86-155,SMC-OGLE101	0.004	8.7	0.08	C	1
537	13.8083	-72.6011	SMC-OGLE220	0.003	9.0	0.08	CA	1
541	13.8417	-72.7825	B-OB12	0.038	7.6	0.15	AN	2
542	13.8750	-73.0714	B83,SMC-OGLE103	0.005	8.6	0.08	C	1
544	13.8875	-72.8328	K34,L53,SMC-OGLE104	0.005	8.6	0.08	C	3
550	13.9292	-72.8800	H86-165,H86-168,SMC-OGLE105	0.009	8.0	0.30	A	3
552	13.9375	-72.7050	H86-164,SMC-OGLE221	0.004	8.7	0.08	C	1
554	13.9500	-72.7019	BS262	0.010	6.7	0.25	A	1
557	13.9958	-73.0914	H86-167	0.006	8.7	0.08	C	1
564	14.0375	-72.7939	H86-169	0.003	7.2	0.08	C	3
566	14.0375	-73.2061	SMC-OGLE106	0.007	8.0	0.08	CA	1
568	14.0792	-72.4639	NGC330,K35,L54,ESO29SC24	0.023	8.0	0.08	C	3
569	14.0708	-72.7856	SMC-DEM88	0.013	7.2	0.11	NA	1
570	14.0667	-72.5164	B86,SMC-OGLE222	0.005	8.0	0.08	C	1
573	14.0917	-72.4547	H-A40	0.059	6.7	0.20	A	2
574	14.1083	-72.4958	BS81,SMC-OGLE223	0.005	8.0	0.08	C	3
575	14.1250	-72.5436	BS82	0.005	8.7	0.20	C	1
576	14.1250	-72.8181	BS264	0.014	7.0	0.20	NA	1
577	14.1417	-72.5022	H86-172,SMC-OGLE108	0.005	8.8	0.08	C	1
579	14.1667	-72.4875	SMC-DEM87	0.067	6.6	0.20	NA	1
583	14.2208	-72.8069	SMC-DEM89	0.027	7.0	0.20	NA	1
585	14.2750	-72.5456	BS83	0.007	6.8	0.18	AC	2
589	14.3250	-72.9336	H86-174,SMC-OGLE225	0.004	8.4	0.08	C	3
591	14.3375	-72.5753	H86-173	0.005	8.0	0.08	C	1
593	14.3792	-72.2644	L56,SMC-S26,SMC-OGLE109	0.008	7.4	0.15	C	1
594	14.3750	-72.5400	SMC-N61,L61-321,MA1011	0.002	8.4	0.08	NC	2
597	14.4417	-72.7058	H86-178,SMC-OGLE110	0.005	7.5	0.08	C	1
598	14.4500	-72.5394	BS87	0.007	8.4	0.08	AC	1
600	14.4625	-72.2239	BS266	0.020	7.0	0.10	A	1
601	14.4583	-72.9436	BS88,SMC-OGLE111	0.005	8.9	0.08	C	1
603	14.4583	-72.4400	H86-175,SMC-OGLE227	0.003	8.0	0.08	C	1
604	14.4583	-72.5081	H86-177,SMC-OGLE226	0.006	8.2	0.08	C	3
605	14.4708	-72.4967	H86-176	0.005	8.0	0.08	C	3
607	14.4792	-72.2911	B90	0.004	8.2	0.08	C	2
609	14.4833	-72.6572	SMC-N62,SMC-DEM93	0.010	7.2	0.20	NA	1
610	14.4958	-72.2344	BS267	0.005	7.9	0.08	AC	1
612	14.4917	-72.5483	B-OB13	0.075	6.8	0.14	A	1
614	14.5292	-72.2906	H-A43	0.028	6.9	0.15	AN	2
615	14.5292	-72.6606	H-A42	0.032	7.1	0.15	AN	2
616	14.5333	-72.5983	H-A41	0.004	7.0	0.08	A	1
624	14.5792	-72.2992	H86-181,SMC-OGLE228	0.005	7.8	0.08	C	2
625	14.5875	-72.3128	BS268	0.047	6.9	0.18	NA	1
626	14.5958	-72.2119	BS270	0.005	8.0	0.08	CA	1
630	14.6083	-72.6658	SMC-N64A,L61-335	0.006	6.9	0.12	NC	3
632	14.6417	-72.2367	SMC-DEM98	0.016	7.2	0.13	NA	1
633	14.6417	-72.2811	H86-183,SMC-OGLE115	0.005	8.0	0.08	C	2
634	14.6542	-72.2242	BS271	0.005	7.1	0.20	NC	3
635	14.6583	-72.2344	BS272,SMC-OGLE229	0.005	7.2	0.17	NC	1
638	14.7292	-72.2444	SMC-DEM99	0.010	7.0	0.10	NA	1
639	14.7292	-72.8303	H86-185	0.003	8.7	0.08	C	3
640	14.7708	-72.1769	NGC346,SMC-N66,K39,L60	0.070	7.2	0.14	NA	1
641	14.7708	-72.7867	SMC-OGLE116	0.008	8.0	0.08	AC	1

644	14.7875	-72.4389	SMC-DEM101	0.010	6.7	0.15	NA	1
650	14.8083	-72.4050	SMC-DEM100,MA1128	0.010	7.2	0.20	NA	1
651	14.8167	-72.2919	SMC-DEM102,H-A44,B-OB15	0.033	6.7	0.13	NA	1
652	14.8083	-72.6081	B96,SMC-OGLE117	0.008	8.3	0.08	C	1
655	14.8542	-72.7386	BS92	0.016	6.9	0.08	A	1
665	14.9083	-72.7472	B-OB14	0.058	6.9	0.08	A	1
666	14.9125	-72.7772	H-A46	0.037	7.3	0.08	A	1
667	14.9500	-72.3339	IC1611,K40,L61,ESO29SC27	0.013	8.1	0.08	C	1
668	14.9875	-72.3733	H86-186,SMC-OGLE119	0.005	8.1	0.08	C	1
669	14.9625	-72.7175	BS95	0.011	7.2	0.08	A	1
671	15.0042	-72.3689	IC1612,K41,L62,ESO29SC28	0.010	8.0	0.08	C	1
675	15.0542	-72.4622	H86-188,SMC-OGLE121	0.010	7.9	0.08	AC	1
681	15.0958	-72.1994	BS100	0.027	6.6	0.15	NA	1
684	15.1125	-73.0867	B99,SMC-OGLE122	0.006	8.3	0.08	C	1
685	15.1375	-72.2397	H86-189,SMC-OGLE123	0.003	8.8	0.08	C	3
686	15.1375	-72.2586	H86-190,SMC-OGLE230	0.002	7.3	0.08	C	1
688	15.1417	-72.3656	K42,L63,SMC-OGLE124	0.004	7.7	0.08	C	1
691	15.1958	-72.9281	SMC-OGLE125	0.003	8.2	0.10	CA	1
694	15.2083	-72.5031	SMC-DEM114	0.167	6.7	0.15	NA	1
697	15.2292	-72.4956	B-OB18	0.042	6.8	0.14	AN	2
700	15.2417	-72.5403	H86-191,SMC-OGLE231	0.007	8.2	0.08	C	1
701	15.2583	-72.7514	L65,H86-192,SMC-OGLE126	0.009	8.0	0.08	C	1
705	15.3083	-72.5508	H86-194,SMC-OGLE232	0.004	8.4	0.08	C	1
707	15.3250	-72.2283	H86-193,SMC-OGLE127	0.005	8.3	0.08	C	1
714	15.4042	-72.4069	B105,SMC-OGLE128	0.003	7.3	0.08	C	1
715	15.4125	-72.4842	H86-195	0.012	7.4	0.14	A	3
717	15.4375	-72.5644	L66,SMC-OGLE129	0.009	7.3	0.12	C	1
718	15.4375	-72.9478	B-OB20	0.033	6.8	0.20	A	1
719	15.4667	-72.1828	B108,SMC-OGLE130	0.003	8.8	0.08	C	3
722	15.5125	-72.2106	B-OB19	0.100	6.7	0.12	A	1
723	15.5125	-72.6739	B-OB21	0.033	7.0	0.14	A	1
724	15.5208	-72.5992	H-A48	0.023	6.7	0.18	A	3
727	15.5125	-72.5219	SMC-OGLE131	0.006	8.2	0.08	CA	1
729	15.5542	-72.9664	SMC-OGLE132	0.003	8.6	0.30	C	1
735	15.6250	-72.6281	BS105	0.009	7.3	0.08	CA	1
736	15.6292	-72.3183	SMC-OGLE133	0.003	8.8	0.08	C	1
739	15.6583	-72.6917	BS274	0.016	7.0	0.10	A	1
743	15.7125	-72.4131	SMC-DEM118,H-A50	0.025	6.9	0.14	NA	2
745	15.7208	-72.4147	B114,SMC-OGLE234	0.007	7.1	0.12	NC	2
750	15.7792	-72.1072	SMC-N76B,SMC-DEM120,MA1361	0.005	7.3	0.08	NC	1
751	15.7750	-72.4317	B-OB23	0.040	6.9	0.14	AN	1
752	15.7708	-72.7008	H-A51	0.017	7.3	0.08	A	1
753	15.8000	-72.2725	K47,L70,SMC-OGLE134	0.006	7.3	0.08	C	1
754	15.8208	-72.7408	SMC-OGLE135	0.006	8.7	0.08	AC	1
756	15.8208	-72.6158	H-A52	0.047	7.1	0.15	A	2
757	15.8417	-72.4658	SMC-OGLE136	0.007	8.1	0.08	CA	1
758	15.8458	-72.6517	B115,SMC-OGLE137	0.007	7.1	0.13	C	1
759	15.8625	-72.0817	H-A53	0.075	6.7	0.10	AN	2
761	15.8708	-71.9333	B-OB24	0.070	7.0	0.08	NA	2
762	15.8708	-72.0567	NGC371,SMC-N76,K48,L71	0.035	6.7	0.10	NA	1
767	15.9542	-72.0647	SMC-N76A,L61-420,MA1411	0.003	8.8	0.08	NC	3
769	15.9708	-72.1031	SMC-OGLE138	0.005	7.2	0.04	CA	2
770	15.9708	-72.1397	SMC-N76C,L61-422,MA1423	0.003	8.3	0.08	NC	2
771	15.9708	-72.8261	NGC376,K49,L72,ESO29SC29	0.015	7.2	0.08	C	1
772	15.9833	-72.6858	SMC-DEM122	0.012	7.4	0.08	NA	3
773	15.9958	-72.8050	BS114,SMC-OGLE235	0.058	7.1	0.08	AC	3
776	16.0208	-72.1208	SMC-OGLE144,SMC-OGLE236	0.005	7.6	0.10	CA 1	
779	16.0292	-72.0217	BS117	0.014	7.3	0.08	NA	3
780	16.0583	-72.6469	BS118,SMC-OGLE140	0.010	6.9	0.08	A	1
781	16.0208	-72.7181	H-A55	0.043	6.8	0.13	A	2
786	16.0708	-72.3958	SMC-DEM125	0.092	6.8	0.14	NA	2
789	16.0833	-72.0489	SMC-DEM124	0.158	6.6	0.12	NA	2
790	16.0917	-72.8478	BS121,SMC-OGLE237	0.013	7.9	0.04	C	3
794	16.1167	-72.1850	BS123	0.009	7.5	0.08	CA	1
795	16.1250	-72.6192	B121,SMC-OGLE141	0.005	8.0	0.08	C	1
797	16.1250	-72.5767	BS124	0.013	7.3	0.08	A	1
799	16.1500	-72.1606	K50,L74,ESO51SC15	0.008	6.9	0.14	C	2
800	16.1667	-72.5500	BS125,SMC-OGLE143	0.013	7.5	0.20	A	1
801	16.1583	-72.6767	B-OB25	0.033	7.0	0.14	A	2
802	16.1625	-72.8161	H-A56,B-OB27	0.068	6.7	0.14	A	1
803	16.1875	-72.1328	H-A54	0.050	6.9	0.13	A	1
807	16.2417	-72.4031	B-OB28nw	0.050	6.8	0.12	AN	1
813	16.2792	-71.9936	NGC395,K51,L75,ESO51SC16	0.013	7.2	0.08	NA	1
816	16.2958	-71.9744	SMC-N78D,SMC-DEM127	0.007	7.2	0.08	NA	1
818	16.3042	-71.9950	SMC-OGLE146	0.004	7.3	0.08	NA	2
819	16.3292	-72.0033	SMC-DEM126	0.032	6.9	0.14	NA	2
820	16.3417	-72.0431	IC1624,K52,L76,ESO51SC17	0.007	8.3	0.08	C	2
821	16.3375	-72.1456	SMC-DEM128	0.013	7.3	0.08	NA	2
822	16.3458	-72.0222	SMC-N78,H-A57,B-OB26	0.050	7.0	0.12	NA	1
825	16.4042	-72.4658	B-OB28se	0.028	6.9	0.10	AN	3
827	16.4208	-72.0594	SMC-N78C,SMC-DEM130,MA1543	0.006	7.2	0.20	NA	1
828	16.4583	-71.9511	B128	0.006	8.2	0.08	C	1
830	16.5000	-72.3414	BS131,SMC-OGLE150	0.005	8.1	0.08	C	1
831	16.4875	-72.5364	BS129	0.015	6.9	0.14	AN	2
835	16.5542	-72.7942	SMC-OGLE151	0.010	8.1	0.10	AC	1

837	16.5583	-72.2536	B-OB29	0.083	6.9	0.10	A	2
847	16.7000	-72.2736	K54,L79,ESO29SC31	0.007	8.0	0.04	C	3
850	16.7375	-72.8472	SMC-DEM133	0.010	7.7	0.15	NA	3
853	16.7667	-72.2436	BS137	0.012	7.1	0.12	A	1
854	16.7583	-72.6217	B129,SMC-OGLE154	0.009	8.2	0.14	CA	1
858	16.8250	-72.5892	B130	0.010	7.3	0.08	A	1
860	16.8667	-72.4933	K56,SMC-OGLE155	0.009	8.2	0.14	C	2
861	16.8667	-72.7694	L80,SMC-OGLE156	0.010	8.1	0.08	C	1
864	16.8833	-73.1197	K55,L81,SMC-OGLE157	0.008	8.7	0.15	C	1
865	16.9167	-72.2694	B-OB30	0.033	6.8	0.10	A	1
866	16.9167	-72.5667	H-A58	0.042	7.0	0.10	A	1
876	17.0792	-72.8842	NGC419,K58,L85,ESO29SC33	0.023	8.6	0.08	C	3
881	17.1542	-72.4392	SMC-OGLE160	0.005	7.6	0.08	CA	2
888	17.2625	-73.0867	K61,SMC-OGLE161	0.008	8.0	0.08	C	1

Bibliography

Barbá, R. H., Rubio, M., Roth, M. R., and García, J.: 2003, *AJ* **125**, 1940

Barmina, R., Girardi, L., and Chiosi, C.: 2002, *A&A* **385**, 847

Barry, D. C.: 1988, *ApJ* **334**, 436

Becker, S. and Mathews, J.: 1983, *AJ* **270**, 155

Bedin, L. R., Cassisi, S., Castelli, F., Piotto, G., Anderson, J., Salaris, M., Momany, Y., and Pietrinferni, A.: 2005, *MNRAS* **357**, 1038

Bekki, K. and Chiba, M.: 2005, *MNRAS* **356**, 680

Bekki, K., Couch, W. J., Beasley, M. A., Forbes, D. A., Chiba, M., and Da Costa, G. S.: 2004, *ApJL* **610**, L93

Bertelli, G., Bressan, A., Chiosi, C., and Angerer, K.: 1986a, *A&AS* **66**, 191

Bertelli, G., Bressan, A., Chiosi, C., Mateo, M., and Wood, P.: 1986b, *ApJ* **412**, 160

Bertelli, G., Mateo, M., Chiosi, C., and Bressan, A.: 1992, *ApJ* **388**, 400

Bertelli, G. and Nasi, E.: 2001, *AJ* **121**, 1013

Besla, G., Kallivayalil, N., Hernquist, L., Robertson, B., Cox, T. J., van der Marel, R. P., and Alcock, C.: 2007, *ApJ* **668**, 949

Bica, E. and Dutra, C. M.: 2000, *AJ* **119**, 1214

Bica, E. L. D. and Schmitt, H. R.: 1995, *ApJS* **101**, 41

Böhm-Vitense, E.: 1958, *Z. Astroph.* **46**, 108

Bonnell, I. A., Vine, S. G., and Bate, M. R.: 2004, *MNRAS* **349**, 735

Boutloukos, S. G. and Lamers, H. J. G. L. M.: 2003, *MNRAS* **338**, 717

Bressan, A. G., Chiosi, C., and Bertelli, G.: 1981, *A&A* **102**, 25

Brocato, E., Castellani, V., Ferraro, F. R., Piersimoni, A. M., and Testa, V.: 1996, *MNRAS* **282**, 614

Butcher, H.: 1977, *ApJ* **216**, 372

Byrd, G., Valtonen, M., McCall, M., and Innanen, K.: 1994, *AJ* **107**, 2055

Canuto, S. and Mazzitelli, I.: 1991, *ApJ* **370**, 295

Canuto, V. M.: 2000, *ApJL* **534**, L113

Canuto, V. M., Goldman, I., and Mazzitelli, I.: 1996, *ApJ* **473**, 550

Caputo, F., Marconi, M., and Ripepi, V.: 1999, *ApJ* **525**, 784

Carraro, G., Chiosi, C., Bressan, A., and Bertelli, G.: 1994, *A&AS* **103**, 375

Carrera, R., Gallart, C., Hardy, E., Aparicio, A., and Zinn, R.: 2008, *AJ* **135**, 836

Cartwright, A. and Whitworth, A. P.: 2004a, *MNRAS* **348**, 589

Cartwright, A. and Whitworth, A. P.: 2004b, *MNRAS* **348**, 589

Carvalho, L., Saurin, T. A., Bica, E., Bonatto, C., and Schmidt, A. A.: 2008, *A&A* **485**, 71

Catelan, M. and Cortés, C.: 2008, *ApJ* **676**, L135

Chabrier, G.: 2003, *PASP* **115**, 763

Chandar, R., Fall, S. M., and Whitmore, B. C.: 2006, *ApJ* **650**, L111

Chiosi, C., Bertelli, G., and Bressan, A.: 1992, *ARA&A* **30**, 235

Chiosi, C., Bertelli, G., Meylan, G., and Ortolani, S.: 1989a, *A&A* **219**, 167

Chiosi, C., Bertelli, G., Meylan, G., and Ortolani, S.: 1989b, *A&AS* **78**, 89

Chiosi, E., Vallenari, A., Bertelli, G., Held, E. V., Rizzi, L., and Moretti, A.: 2004, *Memorie della Societa Astronomica Italiana Supplement* **5**, 272

Chiosi, E., Vallenari, A., Held, E. V., Rizzi, L., and Moretti, A.: 2006, *A&A* **452**, 179

Cioni, M.-R. L., Habing, H. J., and Israel, F. P.: 2000, *A&A* **358**, L9

Cloutman, L. and Whitaker, R. W.: 1980a, *ApJ* **237**, 900

Cloutman, L. D. and Whitaker, R. W.: 1980b, *ApJ* **237**, 900

Cole, A. A.: 2005, *Bulletin of the American Astronomical Society* **37**, 1380

Cole, A. A., Smecker-Hane, T. A., Tolstoy, E., Bosler, T. L., and Gallagher, J. S.: 2004, *MNRAS* **347**, 367

Crowl, H. H., Sarajedini, A., Piatti, A. E., Geisler, D., Bica, E., Clariá, J. J., and Santos, J. F. C.: 2001, *AJ* **122**, 220

Da Costa, G. S. and Hatzidimitriou, D.: 1998, *AJ* **115**, 1934

de Grijs, R. and Anders, P.: 2006, *MNRAS* **366**, 295

de Grijs, R. and Goodwin, S. P.: 2008, *MNRAS* **383**, 1000

de La Fuente Marcos, R.: 1997, *A&A* **322**, 764

de La Fuente Marcos, R. and de La Fuente Marcos, C.: 2004, *New Astronomy* **10**, 53

Deardorff, J., Willis, G., and Lilly, D.: 1969, *Fluid Mech.* **35**, 7

Dib, S. and Burkert, A.: 2005, *ApJ* **630**, 238

Dirsch, B., Richtler, T., Gieren, W. P., and Hilker, M.: 2000, *A&A* **360**, 133

Dolphin, A. E.: 2000a, *PASP* **112**, 1397

Dolphin, A. E.: 2000b, *MNRAS* **313**, 281

Dolphin, A. E., Walker, A. R., Hodge, P. W., Mateo, M., Olszewski, E. W., Schommer, R. A., and Suntzeff, N. B.: 2001, *ApJ* **562**, 303

Dominguez, I., Chieffi, A., Limongi, M., and Straniero, O.: 1999, *ApJ* **524**, 226

Dopita, M. A., Wood, P. R., Meatheringham, S. J., Vassiliadis, E., Bohlin, R. C., Ford, H. C., Harrington, J. P., Stecher, T. P., and Maran, S. P.: 1997, in H. J. Habing and H. J. G. L. M. Lamers (eds.), *IAU Symp. 180: Planetary Nebulae*, p. 417

Dwek, E.: 1998, in E. P. Smith and A. Koratkar (eds.), *ASP Conf. Ser. 133: Science With The NGST*, p. 249

Dwek, E.: 2005, in R. Szczerba, G. Stasinska, and S. K. Gorny (eds.), *AIP Conf. Proc. 804: Planetary Nebulae as Astronomical Tools*, pp 197–203

Elmegreen, B. G.: 1997, *ApJ* **486**, 944

Elmegreen, B. G. and Lada, C. J.: 1977, *ApJ* **214**, 725

Elson, A., Sigurdsson, S., Davies, M., Hurley, J., and Gilmore, G.: 1998, *MNRAS* **300**, 857

Elson, R. A. W.: 1991, *APJs* **76**, 185

Elson, R. A. W., Fall, S. M., and Freeman, K. C.: 1987, *ApJ* **323**, 54

Elson, R. A. W., Gilmore, G. F., and Santiago, B. X.: 1997, *MNRAS* **289**, 157

Freytag, B., Ludwig, H., and Steffen, M.: 1996, *A&A* **313**, 497

Fujimoto, M. and Murai, T.: 1984, in S. van den Bergh and K. S. D. Boer (eds.), *IAU Symp. 108: Structure and Evolution of the Magellanic Clouds*, pp 115–123

Fukui, Y.: 2005, in C. Lidman and D. Alloin (eds.), *ASP Conf. Ser. 344: The Cool Universe: Observing Cosmic Dawn*, p. 155

Fukui, Y., Mizuno, N., Yamaguchi, R., Mizuno, A., Onishi, T., Ogawa, H., Yonekura, Y., Kawamura, A., Tachihara, K., Xiao, K., Yamaguchi, N., Hara, A., Hayakawa, T., Kato, S., Abe, R., Saito, H., Mano, S., Matsunaga, K., Mine, Y., Moriguchi, Y., Aoyama, H., Asayama, S., Yoshikawa, N., and Rubio, M.: 1999, *PASJ* **51**, 745

Gallagher, J. S., Mould, J. R., de Feijter, E., Holtzman, J., Stappers, B., Watson, A., Trauger, J., Ballester, G. E., Burrows, C. J., Casertano, S., Clarke, J. T., Crisp, D., Griffiths, R. E., Hester, J. J., Hoessel, J., Krist, J., Matthews, L. D., Scowen, P. A., Stapelfeld, K. R., and Westphal, J. A.: 1996, *ApJ* **466**, 732

García-Berro, E., Torres, S., Isern, J., and Burkert, A.: 1999, *MNRAS* **302**, 173

Gardiner, L. T. and Hatzidimitriou, D.: 1992, *MNRAS* **257**, 195

Gardiner, L. T., Sawa, T., and Fujimoto, M.: 1994, *MNRAS* **266**, 567

Geha, M. C., Holtzman, J. A., Mould, J. R., Gallagher, J. S., Watson, A. M., Cole, A. A., Grillmair, C. J., Stapelfeldt, K. R., Ballester, G. E., Burrows, C. J., Clarke, J. T., Crisp, D., Evans, R. W., Griffiths, R. E., Hester, J. J., Scowen, P. A., Trauger, J. T., and Westphal, J. A.: 1998, *AJ* **115**, 1045

Gieles, M., Lamers, H. J. G. L. M., and Portegies Zwart, S. F.: 2007, *ApJ* **668**, 268

Girardi, L., Bertelli, G., Bressan, A., Chiosi, C., Groenewegen, M. A. T., Marigo, P., Salasnich, B., and Weiss, A.: 2002, *A&A* **391**, 195

Girardi, L., Bressan, A., Bertelli, G., and Chiosi, C.: 2000, *A&AS* **141**, 371

Girardi, L., Chiosi, C., Bertelli, G., and Bressan, A.: 1995, *A&A* **298**, 87

Girardi, L., Chiosi, C., Bertelli, G., and Bressan, A.: 1996, in C. Leitherer, U. Fritze-von-Alvensleben, and J. Huchra (eds.), *ASP Conf. Ser. 98: From Stars to Galaxies: the Impact of Stellar Physics on Galaxy Evolution*, p. 195

Girardi, L., Grebel, E. K., Odenkirchen, M., and Chiosi, C.: 2004, *A&A* **422**, 205

Gizis, J. E., Reid, I. N., and Hawley, S. L.: 2002, *AJ* **123**, 3356

Glatt, K., Gallagher, III, J. S., Grebel, E. K., Nota, A., Sabbi, E., Sirianni, M., Clementini, G., Tosi, M., Harbeck, D., Koch, A., and Cracraft, M.: 2008, *AJ* **135**, 1106

Gouliermis, D., Brandner, W., and Henning, T.: 2006, *ApJl* **636**, L133

Gouliermis, D. A., Henning, T., Brandner, W., Dolphin, A. E., Rosa, M., and Brandl, B.: 2007, *ApJl* **665**, L27

Gratton, R. G., Bragaglia, A., Clementini, G., Carretta, E., Di Fabrizio, L., Maio, M., and Taribello, E.: 2004, *A&A* **421**, 937

Groenewegen, M. A. T.: 2000, *A&A* **363**, 901

Groenewegen, M. A. T. and Salaris, M.: 2001, *A&A* **366**, 752

Harris, H. C.: 1981, *AJ* **86**, 1192

Harris, J. and Zaritsky, D.: 1999, *AJ* **117**, 2831

Harris, J. and Zaritsky, D.: 2001, *ApJS* **136**, 25

Harris, J. and Zaritsky, D.: 2004, *AJ* **127**, 1531

Hatano, H., Kadowaki, R., Nakajima, Y., Tamura, M., Nagata, T., Sugitani, K., Tanabé, T., Kato, D., Kurita, M., Nishiyama, S., Baba, D., Ishihara, A., and Sato, S.: 2006, *AJ* **132**, 2653

Hatzidimitriou, D., Stanimirovic, S., Maragoudaki, F., Staveley-Smith, L., Dapergolas, A., and Bratsolis, E.: 2005, *MNRAS* **360**, 1171

Hernandez, X., Gilmore, G., and Valls-Gabaud, D.: 2000, *MNRAS* **317**, 831

Hill, A. and Zaritsky, D.: 2006, *AJ* **131**, 414

Hindman, J. V. and Balnaves, K. M.: 1967, *High resolution observations of neutral hydrogen in the small cloud of Magellan*, [Melbourne] 1967.

Hindman, J. V., Kerr, F. J., and McGee, R. X.: 1963, *Australian Journal of Physics* **16**, 570

Hodge, P.: 1986, *PASP* **98**, 1113

Hodge, P. W.: 1973, *AJ* **78**, 807

Hodge, P. W. and Lucke, P. B.: 1970, *AJ* **75**, 933

Holtzman, J. A., Mould, J. R., Gallagher, J. S., Watson, A. M., Grillmair, C. J., Ballester, G. E., Burrows, C. J., Clarke, J. T., Crisp, D., Evans, R. W., Griffiths, R. E., Hester, J. J., Hoessel, J. G., Scowen, P. A., Stapelfeldt, K. R., Trauger, J. T., and Westphal, J. A.: 1997, *AJ* **113**, 656

Hunter, D. A., Elmegreen, B. G., Dupuy, T. J., and Mortonson, M.: 2003, *AJ* **126**, 1836

Indebetouw, R., Robitaille, T. P., Whitney, B. A., Churchwell, E., Babler, B., Meade, M., Watson, C., and Wolfire, M.: 2007, *ApJ* **666**, 321

Isern, J., García-Berro, E., Hernanz, M., Mochkovitch, R., and Burkert, A.: 1995, *LNP Vol. 443: White Dwarfs* **443**, 19

Israel, F. P., de Graauw, T., Johansson, L. E. B., Booth, R. S., Boulanger, F., Garay, G., Kutner, M. L., Lequeux, J., Nyman, L.-A., and Rubio, M.: 2003a, *A&A* **401**, 99

Israel, F. P., Johansson, L. E. B., Rubio, M., Garay, G., de Graauw, T., Booth, R. S., Boulanger, F., Kutner, M. L., Lequeux, J., and Nyman, L.-A.: 2003b, *A&A* **406**, 817

Javiel, S. C., Santiago, B. X., and Kerber, L. O.: 2005, *A&A* **431**, 73

Just, A.: 2002, in E. Athanassoula, A. Bosma, and R. Mujica (eds.), *ASP Conf. Ser. 275: Disks of Galaxies: Kinematics, Dynamics and Peturbations*, pp 117–6

Just, A.: 2003, *AP&SS* **284**, 727

Kallivayalil, N., van der Marel, R. P., and Alcock, C.: 2006, *ApJ* **652**, 1213

Keller, S. C. and Wood, P. R.: 2006, *ApJ* **642**, 834

Kerber, L. O. and Santiago, B. X.: 2006, *A&A* **452**, 155

Kerr, F. J., Hindman, J. F., and Robinson, B. J.: 1954, *Australian Journal of Physics* **7**, 297

Kim, S., Dopita, M. A., Staveley-Smith, L., and Bessell, M. S.: 1999, *AJ* **118**, 2797

King, I.: 1962, *AJ* **67**, 471

Klessen, R. S.: 2003, in J. Makino and P. Hut (eds.), *Astrophysical Supercomputing using Particle Simulations*, Vol. 208 of *IAU Symposium*, pp 61–+

Kroupa, P.: 2000, in R. E. Schielicke (ed.), *Astronomische Gesellschaft Meeting Abstracts*, p. 11

Kroupa, P. and Boily, C. M.: 2002, *MNRAS* **336**, 1188

Kumai, Y., Hashi, Y., and Fujimoto, M.: 1993, *ApJ* **416**, 576

Kumar, B., Sagar, R., and Melnick, J.: 2008, *MNRAS* **386**, 1380

Lachaume, R., Dominik, C., Lanz, T., and Habing, H. J.: 1999, *A&A* **348**, 897

Lada, C. J.: 1987, in M. Peimbert and J. Jugaku (eds.), *Star Forming Regions*, Vol. 115 of *IAU Symposium*, pp 1–17

Lah, P., Kiss, L. L., and Bedding, T. R.: 2005, *MNRAS* **359**, L42

Larson, R. B.: 1993, in G. H. Smith and J. P. Brodie (eds.), *ASP Conf. Ser. 48: The Globular Cluster-Galaxy Connection*, p. 675

Larson, R. B.: 2003, in J. M. De Buizer and N. S. van der Bliek (eds.), *Galactic Star Formation Across the Stellar Mass Spectrum*, Vol. 287 of *Astronomical Society of the Pacific Conference Series*, pp 65–80

Lattanzio, J., Vallenari, A., Bertelli, G., and Chiosi, C.: 1991, *A&A* **250**, 340

Li, J. Z. and Smith, M.: 2005, *AJ* **130**, 721

Lisenfeld, U. and Ferrara, A.: 1998, *ApJ* **496**, 145

Lucke, P. B. and Hodge, P. W.: 1970, *AJ* **75**, 171

Mac Low, M.-M., Chang, T. H., Chu, Y.-H., Points, S. D., Smith, R. C., and Wakker, B. P.: 1998, *ApJ* **493**, 260

Mackey, A. D. and Gilmore, G. F.: 2003, *MNRAS* **338**, 120

Mackey, A. D. and Gilmore, G. F.: 2004, *MNRAS* **352**, 153

Maeder, A.: 1975, *A&A* **43**, 61

Maragoudaki, F., Kontizas, M., Morgan, D. H., Kontizas, E., Dapergolas, A., and Livanou, E.: 2001, *A&A* **379**, 864

Massey, P.: 2002, *VizieR Online Data Catalog* **2236**, 0

Mathewson, D. S., Ford, V. L., and Visvanathan, N.: 1986, *ApJ* **301**, 664

McCray, R. and Kafatos, M.: 1987, *ApJ* **317**, 190

McKee, C. F. and Tan, J. C.: 2003, *ApJ* **585**, 850

McLaughlin, D. E. and van der Marel, R. P.: 2005, *APJs* **161**, 304

Meixner, M., Gordon, K., Indebetouw, R., Whitney, B., Meade, M., Babler, B., Hora, J., Vijh, U., Srinivasan, S., Leitherer, C., Sewilo, M., Engelbracht, C., Block, M., For, B., Blum, R., Reach, W., Bernard, J.-P., and The SAGE Team: 2007, in A. Vazdekis and R. F. Peletier (eds.), *IAU Symposium*, Vol. 241 of *IAU Symposium*, pp 363–364

Meixner, M., Gordon, K. D., Indebetouw, R., Hora, J. L., Whitney, B., Blum, R., Reach, W., Bernard, J.-P., Meade, M., Babler, B., Engelbracht, C. W., For, B.-Q., Misselt, K., Vijh, U., Leitherer, C., Cohen, M., Churchwell, E. B., Boulanger, F., Frogel, J. A., Fukui, Y., Gallagher, J., Gorjian, V., Harris, J., Kelly, D., Kawamura, A., Kim, S., Latter, W. B., Madden, S., Markwick-Kemper, C., Mizuno, A., Mizuno, N., Mould, J., Nota, A., Oey, M. S., Olsen, K., Onishi, T., Paladini, R., Panagia, N., Perez-Gonzalez, P., Shibai, H., Sato, S., Smith, L., Staveley-Smith, L., Tielens, A. G. G. M., Ueta, T., Dyk, S. V., Volk, K., Werner, M., and Zaritsky, D.: 2006, *AJ* **132**, 2268

Mermilliod, J. and Mayor, M.: 1989, *A&A* **219**, 15

Micela, G., Sciortino, S., and Favata, F.: 1993, *ApJ* **412**, 618

Mizuno, N., Rubio, M., Mizuno, A., Yamaguchi, R., Onishi, T., and Fukui, Y.: 2001, *PASJ* **53**, L45

Mokiem, M. R., de Koter, A., Evans, C. J., Puls, J., Smartt, S. J., Crowther, P. A., Herrero, A., Langer, N., Lennon, D. J., Najarro, F., Villamariz, M. R., and Vink, J. S.: 2007, *A&A* **465**, 1003

Murai, T. and Fujimoto, M.: 1980, *PASJ* **32**, 581

Nazé, Y., Manfroid, J., Stevens, I. R., Corcoran, M. F., and Flores, A.: 2004, *ApJ* **608**, 208

Noel, N., Gallart, C., Costa, E., and Rene, M.: 2006, *Rev. Mex. Astronomia y Astrofizica* pp astro–ph/0603319

Noh, H.-R. and Scalo, J.: 1990, *ApJ* **352**, 605

Noyola, E. and Gebhardt, K.: 2007, *AJ* **134**, 912

Oey, M. S., Watson, A. M., Kern, K., and Walth, G. L.: 2005, *AJ* **129**, 393

Oh, K. S., Lin, D. N. C., and Aarseth, S. J.: 1995, *ApJ* **442**, 142

Olsen, K. A. G.: 1999, *AJ* **117**, 2244

Olsen, K. A. G., Hodge, P. W., Mateo, M., Olszewski, E. W., Schommer, R. A., Suntzeff, N. B., and Walker, A. R.: 1998, *MNRAS* **300**, 665

Olszewski, E. W., Suntzeff, N. B., and Mateo, M.: 1996, *ARA&A* **34**, 511

Pagel, B. E. J. and Tautvaisiene, G.: 1998, *MNRAS* **299**, 535

Pagel, B. E. J. and Tautvaišienė, G.: 1999, *Ap&SS* **265**, 461

Parker, J. W., Garmany, C. D., Massey, P., and Walborn, N. R.: 1992, *AJ* **103**, 1205

Parker, J. W., Hill, J. K., Bohlin, R. C., O'Connell, R. W., Neff, S. G., Roberts, M. S., Smith, A. M., and Stecher, T. P.: 1996, *ApJl* **472**, L29+

Pasetto, S., Chiosi, C., and Carraro, G.: 2003, *A&A* **405**, 931

Peebles, P. J. E.: 1980, *The large-scale structure of the universe*, Research supported by the National Science Foundation. Princeton, N.J., Princeton University Press, 1980. 435 p.

Piatti, A. E., Geisler, D., Sarajedini, A., Gallart, C., and Wischnjewsky, M.: 2008, *MNRAS* **389**, 429

Piatti, A. E., Santos, J. F. C., Clariá, J. J., Bica, E., Sarajedini, A., and Geisler, D.: 2001, *MNRAS* **325**, 792

Piatti, A. E., Santos, J. F. C., Clariá, J. J., Bica, E., Ahumada, A. V., and Parisi, M. C.: 2005, *A&A* **440**, 111

Pietrinferni, A., Cassisi, S., Salaris, M., and Castelli, F.: 2004, *ApJ* **612**, 168

Pietrzynski, G. and Udalski, A.: 1999, *Acta Astronomica* **49**, 157

Pietrzynski, G. and Udalski, A.: 2000, *Acta Astronomica* **50**, 337

Prather, M. J. and Demarque, P.: 1974, *ApJ* **193**, 109

Prim, R. C.: 1957, *Bell System Tech. J.* **36**, 1389

Rachford, B. L., Snow, T. P., Tumlinson, J., Shull, J. M., Blair, W. P., Ferlet, R., Friedman, S. D., Gry, C., Jenkins, E. B., Morton, D. C., Savage, B. D., Sonnentrucker, P., Vidal-Madjar, A., Welty, D. E., and York, D. G.: 2002, *ApJ* **577**, 221

Rafelski, M. and Zaritsky, D.: 2005, *AJ* **129**, 2701

Rhode, K. L., Salzer, J. J., Westpfahl, D. J., and Radice, L. A.: 1999, *AJ* **118**, 323

Rich, R. M., Shara, M., Fall, S. M., and Zurek, D.: 2000, *AJ* **119**, 197

Rizzi, L., Held, E., Bertelli, G., and et al.: 2002, in T. Lejeune and j. Fernandes (eds.), *ASP Conf. Ser. 274; Observed HR Diagrams and Stellar Evolution*, p. 490

Rizzi, L., Held, E. V., Momany, Y., Saviane, I., Bertelli, G., and Moretti, A.: 2003, *Memorie della Societa Astronomica Italiana* **74**, 510

Robitaille, T. P., Whitney, B. A., Indebetouw, R., Wood, K., and Denzmore, P.: 2006, *ApJS* **167**, 256

Rocha-Pinto, H. J. and Maciel, W. J.: 1997, *MNRAS* **289**, 882

Rocha-Pinto, H. J., Scalo, J., Maciel, W. J., and Flynn, C.: 2000, *A&A* **358**, 869

Rosado, M., Laval, A., Le Coarer, E., Georgelin, Y. P., Amram, P., Marcelin, M., Goldes, G., and Gach, J. L.: 1996, *A&A* **308**, 588

Rubio, M., Lequeux, J., and Boulanger, F.: 1993, *A&A* **271**, 9

Salaris, M., Percival, S., and Girardi, L.: 2003, *MNRAS* **345**, 1030

Sandage, A., Bell, R. A., and Tripicco, M. J.: 1999, *ApJ* **522**, 250

Scalo, J. M., Barry, D. C., and Sneden, C.: 1987, *BAAS* **19**, 1108

Schmeja, S. and Klessen, R. S.: 2006, *A&A* **449**, 151

Shaviv, G. and Salpeter, E. E.: 1973, *ApJ* **184**, 191

Siess, L., Dufour, E., and Forestini, M.: 2000, *A&A* **358**, 593

Sirianni, M., Jee, M. J., Benítez, N., Blakeslee, J. P., Martel, A. R., Meurer, G., Clampin, M., De Marchi, G., Ford, H. C., Gilliland, R., Hartig, G. F., Illingworth, G. D., Mack, J., and McCann, W. J.: 2005, *PASP* **117**, 1049

Smecker-Hane, T. A., Cole, A. A., Gallagher, J. S., and Stetson, P. B.: 2002, *ApJ* **566**, 239

Smith, H. A., Silbermann, N. A., Baird, S. R., and Graham, J. A.: 1992, *AJ* **104**, 1430

Smith, V. V., Hinkle, K. H., Cunha, K., Plez, B., Lambert, D. L., Pilachowski, C. A., Barbuy, B., Meléndez, J., Balachandran, S., Bessell, M. S., Geisler, D. P., Hesser, J. E., and Winge, C.: 2002, *AJ* **124**, 3241

Stanimirović, S., Staveley-Smith, L., and Jones, P. A.: 2004, *ApJ* **604**, 176

Stanimirovic, S., Staveley-Smith, L., Dickey, J. M., Sault, R. J., and Snowden, S. L.: 1999, *MNRAS* **302**, 417

Staveley-Smith, L., Sault, R. J., Hatzidimitriou, D., Kesteven, M. J., and McConnell, D.: 1997, *MNRAS* **289**, 225

Storm, J., Carney, B. W., Gieren, W. P., Fouqué, P., Latham, D. W., and Fry, A. M.: 2004, *A&A* **415**, 531

Stothers, R. and Chin, C.-W.: 1981, *ApJ* **247**, 1063

Stryker, L. L.: 1984, *ApJS* **55**, 127

Stryker, L. L., Da Costa, G. S., and Mould, J. R.: 1985, *ApJ* **298**, 544

Szewczyk, O., Pietrzyński, G., Gieren, W., Storm, J., Walker, A., Rizzi, L., Kinemuchi, K., Bresolin, F., Kudritzki, R.-P., and Dall'Ora, M.: 2008, *AJ* **136**, 272

Tenorio-Tagle, G. and Bodenheimer, P.: 1988, *ARA&A* **26**, 145

Testa, V., Ferraro, F., Chieffi, A., Straniero, O., Limongi, M., and Fusi Pecci, F.: 1999, *AJ* **118**, 2839

Tifft, W. G. and Snell, C. M.: 1971, *MNRAS* **151**, 365

Tosi, M., Gallagher, J., Sabbi, E., Glatt, K., Grebel, E. K., Christian, C., Cignoni, M., Clementini, G., Cole, A., Da Costa, G., Harbeck, D., Marconi, M., Meixner, M., Nota, A., Sirianni, M., and Smecker-Hane, T.: 2008, *ArXiv e-prints*

Udalski, A., Szymanski, M., Kubiak, M., Pietrzynski, G., Wozniak, P., and Zebrun, K.: 1998, *Acta Astronomica* **48**, 147

Unno, W. and Kondo, M.: 1989, *PASJ* **41**, 197

Vallenari, A., Chiosi, C., Bertelli, G., Meylan, G., and Ortolani, S.: 1992, *AJ* **104(3)**, 1100

Vallenari, A., Chiosi, C., Bertelli, G., Meylan, S., and Ortolani, S.: 1991, *A&AS* **87**, 517

Vallenari, A., Chiosi, C., Bertelli, G., and Ortolani, S.: 1996, *A&A* **309**, 358

van den Bergh, S.: 1991, *ApJ* **369**, 1

Walborn, N. R. and Parker, J. W.: 1992, *ApJ* **399**, L87

Weaver, R., McCray, R., Castor, J., Shapiro, P., and Moore, R.: 1977, *ApJ* **218**, 377

Weidner, C. and Kroupa, P.: 2004, *MNRAS* **348**, 187

Welch, D. L., McLaren, R. A., Madore, B. F., and McAlary, C. W.: 1987, *ApJ* **321**, 162

Weldrake, D. T. F., Sackett, P. D., Bridges, T. J., and Freeman, K. C.: 2004, *AJ* **128**, 736

Westerlund, B. E.: 1997, *The Magellanic Clouds*, Book,

Whitney, B. A., Indebetouw, R., Bjorkman, J. E., and Wood, K.: 2004, *ApJ* **617**, 1177

Wilson, C. P.: 1975, *AJ* **80**, 175

Wolfire, M. G., Hollenbach, D., McKee, C. F., Tielens, A. G. G. M., and Bakes, E. L. O.: 1995, *ApJ* **443**, 152

Wyse, R. F. G., Gilmore, G., Houdashelt, M. L., Feltzing, S., Hebb, L., Gallagher, III, J. S., and Smecker-Hane, T. A.: 2002, *New Astronomy* **7**, 395

Xiong, D. R.: 1980, *ChA* **4**, 234

Yoshizawa, A. M. and Noguchi, M.: 2003, *MNRAS* **339**, 1135

Zahn, J.: 1991, *A&A* **252**, 179

Zaritsky, D., Harris, J., Grebel, E. K., and Thompson, I. B.: 2000, *ApJL* **534**, L53

Zaritsky, D., Harris, J., Thompson, I. B., Grebel, E. K., and Massey, P.: 2002, *AJ* **123**, 855

Zhang, Q., Fall, S. M., and Whitmore, B. C.: 2001, *ApJ* **561**, 727